Université du Québec
Institut National de la Recherche Scientifique
Institut Armand-Frappier

TURNIP MOSAIC VIRUS MEMBRANE-ASSOCIATED REPLICATION COMPLEXES- ULTRASTRUCTURE AND ROLE IN VIRUS MOVEMENT

Par

Juan Wan

Thèse présentée pour l'obtention
du grade de Philosophiae doctor (Ph.D.)
en Immunologie et Virologie

Jury d'évaluation

Président du jury et examinateur interne	Prof. Peter Tijssen INRS – Institut Armand-Frappier
Examinateur externe	Prof. Peter Moffett Université de Sherbrooke
Examinateur externe	Prof. Hugo Germain Université du Québec à Trois-Rivières
Directeur de recherche	Prof. Jean-François Laliberté INRS – Institut Armand-Frappier

RÉSUMÉ

Les virus à ARN positifs [ARN(+)] remanient les membranes cellulaires pour faciliter la réplication de leur ARN viral (ARNv). Les complexes ribonucléoprotéiques viraux (RNPv) formés d'ARNv et de protéines du virus et de l'hôte sont associés aux membranes et se déplacent au travers des plasmodesmes (PD) pour atteindre les cellules avoisinantes. Une fois arrivé dans la nouvelle cellule, un nouveau cycle de synthèse d'ARNv est initié. Ces complexes RNPv peuvent à leur tour atteindre les tissus vasculaires et entreprendre leur déplacement sur une longue distance. Un nouveau concept émerge dans la communauté scientifique. Il consiste à considérer que la réplication de l'ARNv et le mouvement viral sont deux processus étroitement liés. Cependant, la nature du complexe RNPv demande encore à être définie.

La présente thèse se concentre sur l'étude des complexes associés aux membranes induits par le virus de la mosaïque du navet (*Turnip mosaic virus*, TuMV). Le TuMV est un virus à ARN (+) appartenant au genre viral *Potyvirus*. Ce dernier représente le plus grand genre des virus de plante. Ils sont responsables de plus de la moitié des pertes agricoles imputées aux virus.

La protéine virale $6K_2$ est membranaire et est responsable de la réorganisation du système endomembranaire pour former des vésicules mobiles. Ces dernières contiennent les complexes de réplication virale. Les complexes du TuMV associés aux membranes ont été largement étudiés par microscopie confocale essentiellement dans les cellules épidermiques.

Les deux objectifs de cette thèse ont été d'une part d'analyser la présence de complexes de réplication du TuMV associés aux membranes dans les tissus vasculaires et d'autre part de découvrir en détails l'ultrastructure de ces complexes dans plusieurs types cellulaires.

Le premier objectif a consisté à observer la présence de complexes de réplication associés aux membranes dans tous les types cellulaires présents dans les feuilles et les tiges de la plante. En faisant des coupes cryohistologiques, suivies

d'immuno-histolocalisations par microscopie confocale, il a pu être montré que les complexes de réplication associés aux membranes et induits par la protéine $6K_2$ étaient présents dans tous les types cellulaires y compris les tissus vasculaires tels que les tubes criblés du phloème et dans les vaisseaux du xylème. Des observations par microscopie électronique à transmission (MET) ont permis de montrer la présence de vésicules contenant l'ARNv en association avec des particules virales dans les vaisseaux du xylème. En menant des expériences de "girdling" sur tiges, où toutes les cellules meurent tout en maintenant l'intégrité des vaisseaux du xylème, il a été confirmé que le TuMV utilise les vaisseaux du xylème pour son infection systémique. Finalement, il a été démontré que des complexes RNPv du *Potato virus X* (PVX) associés à des membranes étaient aussi présents dans le phloème et le xylème de plantes infectées par ce virus.

Ces études indiquent que les usines de réplication virale peuvent se retrouver dans le phloème et le xylème, suggérant ainsi que la réplication virale et le mouvement à longue distance sont deux évènements étroitement liés.

Le second objectif a été dedéfinir par MET l'ultrastructure des réorganisations cellulaires induites par le TuMV. Une cinétique a été effectuée pour analyser le remodelage membranaire induit par le TuMV. À des étapes précoces de l'infection, il a été observé des amas de membranes ["convoluted membranes", (CM)] dérivant du réticulum endoplasmique rugueux (RER). À des étapes intermédiaires de l'infection, des vésicules à simple membrane (SMV) étaient observables. À des étapes plus tardives de l'infection, en plus d'agrégats de SMVs, des vésicules à double membrane (DMV) au cœur dense aux électrons étaient observables à proximité de corps denses aux électrons. Ensuite il a été montré par immuno-MET que les vésicules induites par le TuMV contenaient la protéine virale $6K_2$ et que seules les SMV constituaient les sites de réplication de l'ARNv. À des étapes tardives de l'infection, il a été aussi observé des corps dense aux électrons à proximité d'agglomérats de particules virales du TuMV qui pourraient être le site de leur assemblage. Par ailleurs, il a été aussi effectué de la tomographie électronique (TE) pour révéler en 3 dimensions (3D) l'accumulation de particules virales en association avec le tonoplaste dans la vacuole centrale.

Ces résultats contribuent d'une part à une meilleure compréhension de la nature des complexes RNPv impliqués dans le mouvement viral sur une longue distance et d'autre part, à avoir une vision plus fine de ce que sont les sites de réplication de l'ARNv du TuMV, ainsi que des sites d'assemblage et d'accumulation des particules virales.

---------- ----------

Juan Wan **Jean-François Laliberté**

Étudiante Directeur de recherche

ABSTRACT

Positive-strand RNA [(+) RNA] viruses remodel cellular membranes to facilitate viral RNA (vRNA) replication. Membrane-bound progeny viral ribonucleoprotein (vRNP) complexes then move through plasmodesmata (PDs) to adjacent cells to initiate new rounds of vRNA synthesis. These complexes ultimately reach the vascular tissues and are loaded into the vascular conducting tubes for long-distance trafficking. An emerging concept is that vRNA replication and movement are tightly linked processes. The moving vRNP complex, however, has yet to be defined.

This thesis focuses on *Turnip mosaic virus* (TuMV) -induced membrane-associated complexes. TuMV is a (+) RNA virus belonging to the genus *Potyvirus*, which is the largest genus of plant viruses, and is responsible for more than half of the viral crop damage in the world. The viral membrane protein $6K_2$ is responsible for membrane reorganization that leads to the formation of motile vesicles. These vesicles contain virus replication complexes. TuMV membrane-associated replication complexes dynamics have been widely studied by confocal microscopy in epidermal cells.

The two aims of this thesis were to investigate the presence of TuMV membrane-associated replication complexes in vascular tissues, and then to uncover the ultrastructure of the TuMV-induced membrane reorganization.

The first research objective consisted of looking at the presence of TuMV membrane-associated replication complexes in all types of plant leaf and stem cells. By using cryohistological preparation, immunohistolocalization and confocal microscopy, it was shown that $6K_2$-tagged membrane-associated replication complexes were present in all cell types, including the vascular conducting tubes, which were phloem sieve elements and xylem vessels. Transmission electron microcopy (TEM) observation results showed the presence of vRNA-containing vesicles that were associated with viral particles in xylem vessels. Then the stem girdling experiments confirmed that TuMV could establish a systemic infection of the plant by going through xylem vessels.

Finally, the presence of membrane-associated vRNP complexes was also demonstrated in the phloem and xylem of *Potato virus X* (PVX) infected plants.

Collectively, these studies indicate that viral replication factories could end up in the phloem and the xylem, suggesting that virus replication and long-distance trafficking are linked events.

The second objective was to define the ultrastructure of TuMV-induced cellular reorganization by TEM. A time course analysis of TuMV-induced membrane remodeling was initially performed.

Early during infection, rough endoplasmic reticulum (ER)-connected convoluted membrane (CM) structures were observed. Single-membrane vesicles (SMVs) were found at the mid stage of infection, while mixed aggregates containing SMVs, double-membrane vesicles (DMVs) with an electron-dense core, and electron-dense bodies were detected at a late stage of infection. Then the immuno-EM experiments showed that the vesicles are tagged with $6K_2$, and that only SMVs are the vRNA replication sites. I also observed electron-dense bodies associated TuMV particle bundles, which probably are the particle assembly site. Finally, with electron tomography (ET), it was shown that viral particles accumulating in the central vacuole as membrane-associated complexes.

Taken together, this work contributed to a better understanding of the nature of vRNP complexes for virus long-distance trafficking, of the ultrastructure of TuMV RNA replication sites, as well as particles assembly and accumulation sites.

---------- ----------

Juan Wan **Jean-François Laliberté**

Student Director of Research

SOMMAIRE RÉCAPITULATIF

Les virus à ARN positifs (ARN+) remodèlent les membranes cellulaires pour faciliter la réplication de leur ARN viral (ARNv). Ces réarrangements membranaires donnent naissance à ce qui est qualifié d'usines de réplication. Il est généralement admis que ces nouveaux compartiments constituent un environnement protégeant les facteurs viraux de la dégradation par les défenses de l'hôte. De plus, ces quasi-organites permettent de concentrer localement les éléments nécessaires à la réplication de l'ARNv, ce qui augmenterait l'efficacité de ce processus. Cependant différents virus à ARN+ induisent différentes structures membranaires pour la réplication de leur ARNv. Notamment, le nodavirus *Flock house virus* (FHV) qui en remodelant la membrane externe de la mitochondrie induit la formation de sphérules. Ces dernières n'étant pas totalement closes, elles laissent un canal d'environ 10 nm qui permet la connexion entre leur intérieur et le cytoplasme. Le flavivirus *Dengue virus* (DENV) quant à lui remodèle le réticulum endoplasmique (RE) pour former des amats de vésicules (vesicle packets, VPs) constituées de simples membranes (single-membrane vesicles, SMVs) dans le lumen de ce dernier. Les poliovirus remodèlent aussi le RE et/ou l'appareil de Golgi pour former des agrégats de SMVs. Le syndrome respiratoire aigu sévère (SRAS)-coronavirus remodèle aussi le RE mais en induisant la formation de vésicules doubles membranes.

Ces dernières années, quelques modèles en trois dimensions (3D) ont été générés pour des virus a ARN+ en faisant de la microscopie électronique a transmission couplée à de la tomographie électronique (MET-TE). La complexité des structures dévoilées a grandement amélioré notre compréhension sur la biogenèse et la fonction de ces structures membranaires. Les modèles 3D ont révélé que les virus à ARN+ induisent différentes structures membranaires pouvant coordonner divers processus de leur cycle infectieux. Par exemple, le SRAS-coronavirus induit la formation d'un complexe réarrangement membranaire ("convoluted membranes", CM) pour la synthèse et la maturation de la polyprotéine virale, de vésicules double membranes pour la réplication de l'ARNv et des VPs pour l'assemblage des particules virales et leur bourgeonnement à partir des cellules infectées.

Il existe très peu d'études par MET pour les virus de plante à ARN+. Les structures membranaires générées par ces derniers sont similaires à celles induites par les virus animaux à ARN+. Par exemple, le *Turnip yellow mosaic virus* (TYMV) induit la formation de sphérules à partir de la membrane externe des chloroplastes et leur intérieur est connecté au cytoplasme *via* un canal ouvert. Selon l'organisme hôte le *Brome mosaic virus* (BMV) induit soit la formation de sphérulesà partir des membranes du RE dans la levure et la formation de VPs dans le lumen du RE sous la forme d'une série de SMVs dans les cellules végétales.

Deux représentations 3D d'usines virales de virus de plantes ont été générées. Le *Melon necrotic spot virus* (MNSV) modifie les mitochondries pour former de larges dilatations internes interconnectées et semblablement connectées au cytoplasme par des pores et/ou d'autres structures plus complexes. Le *Beet black scorch virus* (BBSV) induit la formation de sphérules dans le lumen du RE.

En revanche nous avons peu de connaissances sur les détails architectureaux des usines virales induites par le virus de la mosaïque du navet (*Turnip Mosaic Virus,* TuMV). Le TuMV est un virus à ARN+ appartenant au genre *Potyvirus* dans la famille des *Potyviridae.* Les potivirus constituent le genre viral le plus important parmi les virus de plante et sont responsables de plus de la moitié des pertes agricoles induites par des virus dans le monde. Les particules virales sont flexibles et filamenteuses avec une longueur de 680 à 900 nm et un diamètre d'environ 11-15 nm. Ils ont un génome à ARN simple brin d'environ 10 kb. L'extrémité 5' du génome est liée de façon covalente à une protéine VPg (viral protein genome linked) et l'extrémité 3' comporte une queue poly(A). L'ARNv code pour une polyprotéine clivée par 3 protéinases virales pour générer au moins 12 protéines. La protéine membranaire $6K_2$ est responsable de la formation des usines de réplication virale du TuMV.

Les observations par microscopie optique ont montré que lors de l'infection par le TuMV de nombreuses vésicules induites par $6K_2$ prennent naissance à partir du RE. Les vésicules contiennent l'ARNv, et des protéines virales et de l'hôte impliquées dans la réplication virale. Ainsi, ces dernières sont considérées comme étant le lieu de la réplication de l'ARNv. Les analyses ultrastructurelles les plus récentes du

réarrangement cellulaire par les potyvirus se sont principalement concentrées sur des descriptions d'inclusions nucléaires et cytoplasmiques. Des images en MET de vésicules induites par le TuMV et le *Potato virus Y* (PVY) à partir de cellules infectées ont dévoilé d'une part la présence de nombreuses SMVs et parfois de SMVs directement connectés au RE rugueux (RER). Cependant aucune étude n'a été faite d'une part sur la biogenèse des usines virales au cours du temps durant l'infection et d'autre part sur la relation entre ces dernières et l'assemblage des particules virales.

La propagation d'un virus dans une plante implique des mouvements viraux de courte distance, de cellule à cellule au travers des plasmodesmes (PD), et de longue distance au travers des vaisseaux vasculaires notamment au travers des tubes criblés du phloème et des vaisseaux du xylème. Il est généralement entendu que les entités capables de se propager sont soit des particules virales soit des complexes ribonucléoprotéiques (RNP). Cependant, la nature exacte de ces complexes RNP n'a pas été définie. Un concept commence à émerger en mettant en avant le fait que la réplication de l'ARNv et le mouvement viral sont deux processus étroitement liés. Par exemple, il été proposé que le *Tobacco mosaic virus* (TMV) se déplace d'une cellule à l'autre en tant que complexes de réplication. La réplication et le trafic du *Potato virus X* (PVX) ont aussi été montrés comme étant couplés à l'entrée des PDs. Dans le cas du TuMV, il a été démontré par de l'imagerie cellulaire en temps réel que les complexes de réplication induits par $6K_2$ pouvaient se déplacer d'une cellule à l'autre. Cependant il est totalement inconnu si ces complexes de réplication avaient la capacité d'atteindre les tissus vasculaires et se déplacer sur une longue distance.

Les objectifs de ma recherche ont été:

1. de savoir si les usines de réplication induites par $6K_2$ pouvaient être impliquées dans le mouvement viral sur une longue distance ;
2. et de définir avec plus de précision l'ultrastructure du remodelage cellulaire induit par le TuMV.

Dans le cadre du premier objectif, une investigation a été mené mon sur la présence de structures contenant la protéine virale 6K2 étiqueté dans d'autres types cellulaires que les cellules de l'épiderme seules. Des plantes de *Nicotiana benthamiana*

ont été agroinfiltrées avec le clone infectieux TuMV/6k2:GFP qui permet d'avoir les usines de réplication étiquetées avec une étiquette fluorescente, ici la GFP. Des coupes transversales de feuilles systémiques au niveau de la nervure centrale, ainsi que des coupes longitudinales de tiges juste au dessus des feuilles inoculées (premier internode) ont été observées par microscopie confocale. Il a été observé que 6K2:GFP était présente dans tous les types cellulaires dans les tiges et feuilles de plantes infectées, notamment dans les tubes criblés du phloème et les vaisseaux du xylème. Ce dernier point suggère que le mouvement systémique du TuMV implique tous les vaisseaux vasculaires. Suite à une coloration au DioC6(3) lipophile il a été mis en évidence que les agrégats présentant la 6K2 étiquetée dans les vaisseaux vasculaires contiennaient des lipides. Il a été trouvé que ces agrégats contenaient de l'ARNv, l'ARN polymérase ARN dépendante virale (RdRpv). Ceci suggère que ces agrégats contiennent les complexes de réplication. Il a été aussi détecté la protéine de capside (CP) en association avec les agrégats contenant la 6K2 étiquetée, suggérant ainsi que des particules virales du TuMV ou de la CP associée aux complexes RNP sont aussi présentes.

Par ailleurs il a aussi été mené des analyses par des techniques conventionnelles de MET pour mieux caractériser l'ultrastructure des agrégats contenant la 6K2 étiquetée dans les vaisseaux vasculaires. Ces analyses ont permis de montrer la présence de vésicules contenant l'ARNv dans les vaisseaux du xylème en association avec des particules virales. Des analyses de sève xylémienne provenant de plantes infectées par microscopie confocale et Western blot ont montré qu'elle contenait des vésicules induites par 6K2, des éléments essentiels à la réplication du TuMV et l'assemblage de ses particules virales tels que la 6K2, la CP, la RdRpv ainsi qu'une protéine de l'hôte eIF(iso)4e. La sève xylémienne provenant de plantes infectées est infectieuse. Des expérimentations visant à détruire toute cellule vivante autour du xylème sur une portion de tige (stem girdling) a confirmé que le TuMV peut établir une infection systémique en exploitant les vaisseaux du xylème.

Les résultats des immunohistolocalisations ont montré que les tubes criblés du phloème et du xylème provenant de plantes infectées par le *Potato virus X* (PVX) contenaient aussi lipides associé à de l'ARNv non encapsidé. Ces éléments suggèrent

que la présence de complexes RNP associés aux membranes dans les vaisseaux vasculaires n'est pas une caractéristique limitée seulement au TuMV.

Pris ensembles, ces études indiquent que les usines virales peuvent aboutir dans le phloème et le xylème. D'après toutes ces observations, il a été proposé un modèle permettant d'expliquer le mouvement du TuMV dans les tubes criblés du phloème et les vaisseaux du xylème. Dans ce schéma, les vésicules induites par la 6K2 étiquetée et contenant l'ARNv et la RdRpv se déplacent depuis les cellules de l'épiderme vers les cellules compagnes en passant par les cellules du mésophile, de la gaine et du parenchyme vasculaire *via* les PDs. Une fois arrivées aux cellules compagnes les vésicules sont chargées dans les tubes criblés du phloème via des plasmodesmes particuliers appelés pore plasmodesmal unit (PPUs). Ces dernières pourraient soit voyager individuellement soit s'agglutiner pour former un support membranaire à l'assemblage des particules virales dans les tubes criblés du phloème suivant ainsi le flux de sève phloémienne à longue distance. Également, les usines virales du TuMV pourraient aussi entrer dans les cellules non différentiées du xylème, assurant ainsi la réplication virale avant que la mort cellulaire ne libère ces structures dans les vaisseaux matures du xylème.

Le second objectif a été d'obtenir l'ultrastructure du remodelage cellulaire induit par le TuMV. Différentes étapes de la préparation des échantillons ont été optimisé pour des analyses par MET, notamment afin d'améliorer le contraste des structures membranaires. Tout d'abord, en comparant des cellules provenant de feuilles agroinfiltrées et des feuilles systémiquement infectées par le TuMV, ces dernières ont été choisies pour faire mes analyses par MET du fait qu'il était bien plus facile de trouver les structures induites par le TuMV, ainsi que les inclusions cytoplasmiques. La zone autour de la nervure centrale de ces feuilles a été collectée à différents jours après l'infection (j.p.i) avec le clone TuMV/6K2:GFP. L'infection des tissus vasculaires a été décelée à 5 j.p.i et la colonisation des autres tissus à partir de 6 j.p.i.

Il a été observé des structures associées au RER ou celles connectées aux CM à des stades précoces de l'infection dans à la fois les cellules parenchymateuses et du mésophile. La présence d'agrégats de SMVs de différentes tailles a pu aussi être vue

à des stades intermédiaires de l'infection. La présence de SMVs et de vésicules double membranes (double-membrane vesicles, (DMVs)) avec un cœur dense aux électrons a été constatée en MET à des stades tardifs de l'infection. Le marquage par immunogold a révélé que les agrégats de vésicules contenaient la protéine 6K2 et que les SMV sont les sites de la réplication de l'ARNv.

Le remodelage cellulaire induit par le TuMV a été observé au niveau des cellules du mésophile par MET. Deux méthodes de traitement des échantillons ont été comparées l'une par fixation chimique et l'autre par congélation à haute pression et substitution par congélation (High-pressure freezing/freeze substitution (HPF/FS)). En utilisant ces deux méthodes des structures membranaires similaires ont été observées dans les tissus infectés. Cependant quelques différences ont pu être observées. Notamment, lors des observations menées dans les échantillons ayant subit le HPF/FS que les particules virales du TuMV étaient empaquetées en association avec des corps dense aux électron à proximité des vésicules induites par le TuMV. Ces structures et leur proximité suggèrent qu'elles seraient impliquées dans l'assemblage des particules virales. Une autre différence réside dans la taille, la forme et la densité aux électrons au cœur des SMV et des DMV. En effet, lors du traitement par HPF/FS les vésicules étaient plus petites, plus rondes et contenaient un cœur plus dense aux électrons. Par ailleurs, il a été détecté la présence de points denses aux électrons le long de la face cytoplasmique du tonoplaste. Ces mêmes structures étaient observables au centre de la vacuole. Par la suite, des analyses par MET-TE ont révélées que ces points alignés n'étaient autre que les particules virales du TuMV emprisonnées dans la partie centrale de la vacuole en étroite association avec le tonoplaste. Par un autre moyen, il a été confirmé que cette apparente présence de particules virales dans la vacuole avait bien lieu et non à côté de ce compartiment.

Pris ensemble, tous ces résultats ont permis de découvrir l'ultrastructure, la biogenèse et les fonctions de structures membranaires issues du remodelage induit par le TuMV au niveau cellulaire. En se basant sur ces observations, je propose un modèle qui lie les structures membranaires induites par le TuMV, la réplication de l'ARNv du TuMV et le stockage des particules virales au cœur de la vacuole. Ce modèle consiste en quatre étapes consécutives. Premièrement, le TuMV induit un remodelage du

système endomembranaire conduisant à une accumulation de CM connectées au RE. Ces CM pourraient être impliquées dans la maturation de la polyprotéine virale. Deuxièmement, à partir de ces CM des SMVs sont formées. Ces SMVs sont impliquées dans la réplication de l'ARNv. Troisièmement, une fois que suffisamment d'ARNv et de CP ont été produits l'assemblage des particules virales prendrait place à proximité des DMVs et des corps denses aux électrons. Quatrièmement, les particules virales seraient chargées dans la vacuole en étant protégées par le tonoplaste.

dcvPour conclure le travail effectué a permis de montrer que:

1. Le TuMv utilise à la fois le xylème et le phloème pour sont mouvement à longue distance dans la plante.
2. L'entité virale du TuMV se déplaçant à longue distance est un complexe de réplication associé aux membranes. Ceci souligne le lien étroit entre réplication et mouvement à longue distance.
3. Le TuMV induit différents types de structures membranaires dont une partie serait impliquée dans la réplication de l'ARNv, une autre dans l'assemblage des particules virales et une dernière pour le stockage de ces dernières.

Le travail réalisé ouvre de nouvelles perspectives de travail :

1. La collecte des usines virales induites 6K2 à partir de sève xylémienne de plantes infectées par le TuMV permettrait de faire des analyses protéomiques par spectrométrie de masse. Ceci permettrait de dévoiler une multitude de facteurs de l'hôte dans le complexe de réplication du TuMV.
2. Investiguer comment les usines virales arrivent dans les vaisseaux du xylème serait intéressant. La sève xylémienne étant connectée avec l'apoplaste dans la plante, il se pourrait que des complexes de réplication du TuMV y soient aussi présents. Il serait intéressant de vérifier si des exosomes pourraient être présent dans ce fluide extracellulaire afin de mieux comprendre le devenir des usines virales dans le xylème.
3. La génération de structures 3D à partir des usines virales du TuMV serait intéressante d'être menée en utilisant le protocole amélioré de MET/TE combiné

avec le HPF/FS. Ceci permettrait de mieux comprendre comment les particules virales du TuMV sont assemblées et comment elles s'accumulent dans la vacuole.

ACKNOWLEDGEMENTS

First and foremost, I want to thank my supervisor Professor Jean-François Laliberté. It was an honor to be his Ph.D student. I really appreciated all his time and ideas he devoted to me during my Ph.D. He provided unreserved support throughout the past four years, and guided me on the way of becoming a good research scientist. Without him, this Ph.D project would not have been possible. When my experiments did not work at the beginning, he kept on telling me “Don’t worry, you just need to practice and practice, the same as learning how to play the guitar.”

I would like to thank Professor Hugo Zheng from Mcgill University for his support and useful suggestions on my project.

I want to thank all the research group of the Facility for Electron Microscopy Research (FEMR) at Mcgill University, where I learned all the techniques and did all the experiments about transmission electron microscopy. I would like to thank especially the group leader Professor Hojatollah Vali for his support and suggestion about adding HA-tag for the immunogold labeling experiment, the EM coordinator Jeannie Mui who taught me all the techniques about conventional TEM sample preparation and electron microscope operation, the staff scientist Kaustuv Basu for helping me with HPF/FS sample preparation, the staff Scientist Mihnea Bostina for helping me with the electron tomography data collection and teaching me use the Linux operating system and the associated software for electron tomography data analyzing.

Many thanks to Jessy Tremblay who taught me how to operate the Zeiss LSM 780 confocal microscope, and who provided useful suggestions to decrease the background signal for the different dye staining and immunohistolocalization experiments, which resulted in the beautiful confocal images shown in my manuscripts. I also want to thank the different laboratory that shared equipments for my experiments, such as the cryostat and centrifuges.

I would like to acknowledge my former colleagues Romain Grangeon and Maxime Agbeci for their assistance and friendship. They helped me so much at the beginning of my Ph.D study. I am especially grateful to my current colleague Daniel

Garcia Cabanillas, who contributed the French translation of my thesis. He is also my co-author and we worked together on the xylem sap experiments. We also spend a lot of time together out of the laboratory. I very much appreciated his enthusiasm, wisdom, attention and amazing patience.

I would like to thank my family for their unconditional love and encouragement: my parents who raised me with freedom and supported me in all of my undertakings. Finally, my last thanks goes to my former classmate, current colleague and loving husband, Jun Jiang, for his patience and support through all these years.

TABLE OF CONTENTS

LIST OF FIGURES

CHAPTER 1: INTRODUCTION

CHAPTER 2: PUBLICATION NO. 1

CHAPTER 3: PUBLICATION NO. 2

CHAPTER 4: DISCUSSION

CHAPTER 5: OTHER CONTRIBUTIONS

Publication no. 3

LIST OF TABLES

LIST OF ABBREVIATIONS

(+) RNA	positive-strand RNA
2D	two-dimensional
3D	three-dimensional
Arf1	ADP ribosylation factor 1
AMV	*Alfalfa mosaic virus*
BBSV	*Beet black scorch virus*
BMV	*Brome mosaic virus*
BSA	bovine serum albumin
BSMV	*Barley stripe mosaic virus*
CC	companion cells
CFDA	5(6)-carboxyfluorescein diacetate
CGMMV	*Cucumber green mottle mosaic virus*
CI	cylindrical inclusion
CIRV	*Carnation Italian ringspot virus*
CLEM	correlative light electron microscopy
CM	convoluted membranes
CMV	*Cucumber mosaic virus*
COPI	coat protein complex I
COPII	coat protein complex II
CP	coat protein
CPMV	*Cowpea mosaic virus*
CRLV	*Carrot red leaf virus*
CVB3	*Coxsackievirus B3*
DENV	*Dengue virus*

$DiOC_6(3)$	3,3′-dihexyloxacarbocyanine iodide
DMVs	double-membrane vesicles
DPBS	Dulbecco's phosphate-buffered saline
dsRNA	double-stranded RNA
dpi	days post infection
EAV	*Equine arteritis virus*
EE	early endosome
eEF1A	eukaryotic elongation factor 1A
eIF(iso)4E	eukaryotic translation initiation factor iso4E
eIF4E	eukaryotic translation initiation factor 4E
EPTA	ethanolic phosphotungstic acid
ER	endoplasmic reticulum
ERES	ER exit sites
ERGIC	ER-Golgi intermediate compartment
ESCRT	endosomal sorting complexes required for transport
ET	electron tomography
EXPO	exocyst positive organelle
FHV	*Flock house virus*
FS	freeze-substitution
GFLV	*Grapevine fanleaf virus*
HAV	*Hepatitis A virus*
HC	helper component
HCpro	helper component proteinase
HCV	*Hepatitis C virus*
HPF	high-pressure freezing
HPF/FS	high-pressure freezing coupled with freeze substitution

Hsc70-3	heat shock cognate 70-3 protein
HSP70	heat shock protein 70
LE	late endosomes
LMV	*Lettuce mosaic virus*
LVs	lytic vacuoles
MAMPs/DAMPs	microbe/danger-associated molecular patterns
METTEM	Metal-Tagging TEM
miniSOG	mini singlet oxygen generator
MMVs	multi-membrane vesicles
MNSV	*Melon necrotic spot virus*
MOI	multiplicity of cellular infection
MPs	movement proteins
MTOC	microtubule organization center
MVB	multi vesicular bodies
MVB-PM	multivesiclular body-plasma membrane
MW	membranous web
NI	nuclear inclusions
NIa	nuclear inclusion protein a
NIa-pro	nuclear inclusion protein a protease
NIb	nuclear inclusion protein b
NLS	nuclear localization signals
NS	nonstructural
O-GlcNAc	O-linked N-acetylglucosamine
P3N-PIPO ORF	N-terminal half of P3 fused to the pretty interesting potyviridae
PABP	poly-A binding protein

PBS	phosphate-buffered saline
PD	plasmodesma
PDLP1	plasmodesmata located protein 1
PDs	plasmodesmata
PKR	protein kinase
PM	plasma membrane
PMMV	*Pepper mild mottle virus*
PMTV	*Potato mop-top virus*
pMVBs	peroxisomal multivesicular bodies
PPUs	pore plasmodesmal units
PPV	*Plum pox virus*
Pro	Proteinase
PRRs	pattern recognition receptors
PSbMV	*Pea seed-borne mosaic virus*
PSVs	protein storage vacuoles
PTB3	polypyrimidine tract-binding protein3
PVA	*Potato virus A*
PVBV	*Pepper vein banding virus*
PVC	prevacuolar compartments
PVX	*Potato virus X*
PVY	*Potato virus Y*
RCNMV	*Red clover necrotic mosaic virus*
RdRp	RNA-dependent RNA polymerase
RE	recycling endosomes
rER	rough ER
RHPs	reticulon homology proteins

RNP	ribonucleoprotein
RubisCO-LSU	ribulose-l,5-biphosphate carboxylase/oxygenase large subunit
RYMV	*Rice yellow mottle virus*
SARS	*Severe acute respiratory syndrome*
SBWMV	*Soilborne wheat mosaic virus*
SE	sieve elements
SEL	size-exclusion limit
SMTs	single-membrane tubules
SMV	*Soybean mosaic virus*
SMVs	single-membrane vesicles
SNARE receptors	soluble N-ethylmaleimide-sensitive-factor attachment protein
SUMO	small ubiquitin-like modifier
TAV	*Tomato aspermy virus*
TBSV	*Tomato bushy stunt virus*
TEM	transmission electron microscopy
TEM-ET	transmission electron microscopy coupled to electron tomography
TEV	*Tobacco etch virus*
TGBp	triple gene block protein
TGN	trans-Golgi network
TMV	*Tobacco mosaic virus*
ToMV	*Tomato mosaic virus*
TRSV	*Tobacco ringspot virus*
TRV	*Tobacco rattle virus*
TuMV	*Turnip mosaic virus*
TYMV	*Turnip yellow mosaic virus*

VPg	viral genome-linked protein
VPs	vesicle packets
vRdRp	viral RdRp
vRNA	viral RNA
vRNP	viral ribonucleoprotein
ZYMV	*Zucchini yellow mosaic virus*
γb	gamma b

CHAPTER 1: INTRODUCTION

1. The genus *Potyvirus*

1.1 Taxonomy and generality

The potyviruses [named after the type species *Potato virus Y* (PVY)] belong to the family *Potyviridae* in the picorna-like superfamily. Potyviruses are the largest genera of plant viruses (Hull 2002), and are responsible for more than half of the viral crop damage in the world (Shukla, Ward et al. 1994). Potyviruses affect the plant at different stages of its development: vegetative growth, flowering, fruiting and seedling stages. The disease symptoms that are observed on leaves are mosaics that are seen as yellow areas surrounded by normal green, healthy regions. The whole plants often show lighter coloring, stunting, leaf curling and ultimately decay.

Potyviruses are transmitted from plant to plant by aphids in a non-persistent manner. Each potyvirus may be transmitted by many different aphid species and each aphid species may transmit many different potyviruses (Gibbs, Ohshima et al. 2008). This increases the difficulty of preventing and controlling potyvirus infections by pesticides in crop plants. Some species are also transmitted through seeds, such as *Pea seed-borne mosaic virus* (PSbMV) and *Lettuce mosaic virus* (LMV).

1.2 Particles

Potyviruses are non-enveloped flexuous rod-shaped particles, of approximately 750 nm in length and 12 nm in diameter (Fig. 1A) (Varma, Gibbs et al. 1968). The three-dimensional (3D) structure of purified *Soybean mosaic virus* (SMV) particles has been determined (Kendall, McDonald et al. 2008) (Fig. 1B-D). The diameter of SMV is 14 nm, the helical symmetry is 8.8 subunits per turn, and the central hole has a radius of 1.5 nm. A potyvirus particle contains approximately 2000 copies of the coat protein (CP) monomer (Shukla, Ward et al. 1994). A model of the 3D structure of *Potato virus A* (PVA) CP has been determined (Baratova, Efimov et al. 2001). This model predicts three regions of tertiary structure: (i) a surface-exposed N-terminal region, comprising an unstructured N-terminus of 8 amino acids, four β-strands (β1 to β4) and an α1-helix, (ii) a C-terminal region including two α-helices (α7 and α8), as well as three β-strands (β5, β6, and β7) that organized in βαββα order, and (iii) a central region comprising a

bundle of four long α-helices (α2, α3, α4, and α6) in a fold similar to that found in *Tobacco mosaic virus* (TMV) CP and a short α5-helix (Fig. 1E) (Baratova, Efimov et al. 2001). The mechanism of particle assembly has been studied in vitro for PVY (McDonald and Bancroft 1977) and *Pepper vein banding virus* (PVBV) (Anindya and Savithri 2003), both of which show that the CP first forms ring-like intermediates, and then assemble into a helically constructed nucleoprotein. For PVBV, the formation of ring-like intermediates has been shown to be based on the interaction of N- and C-termini of CP subunits.

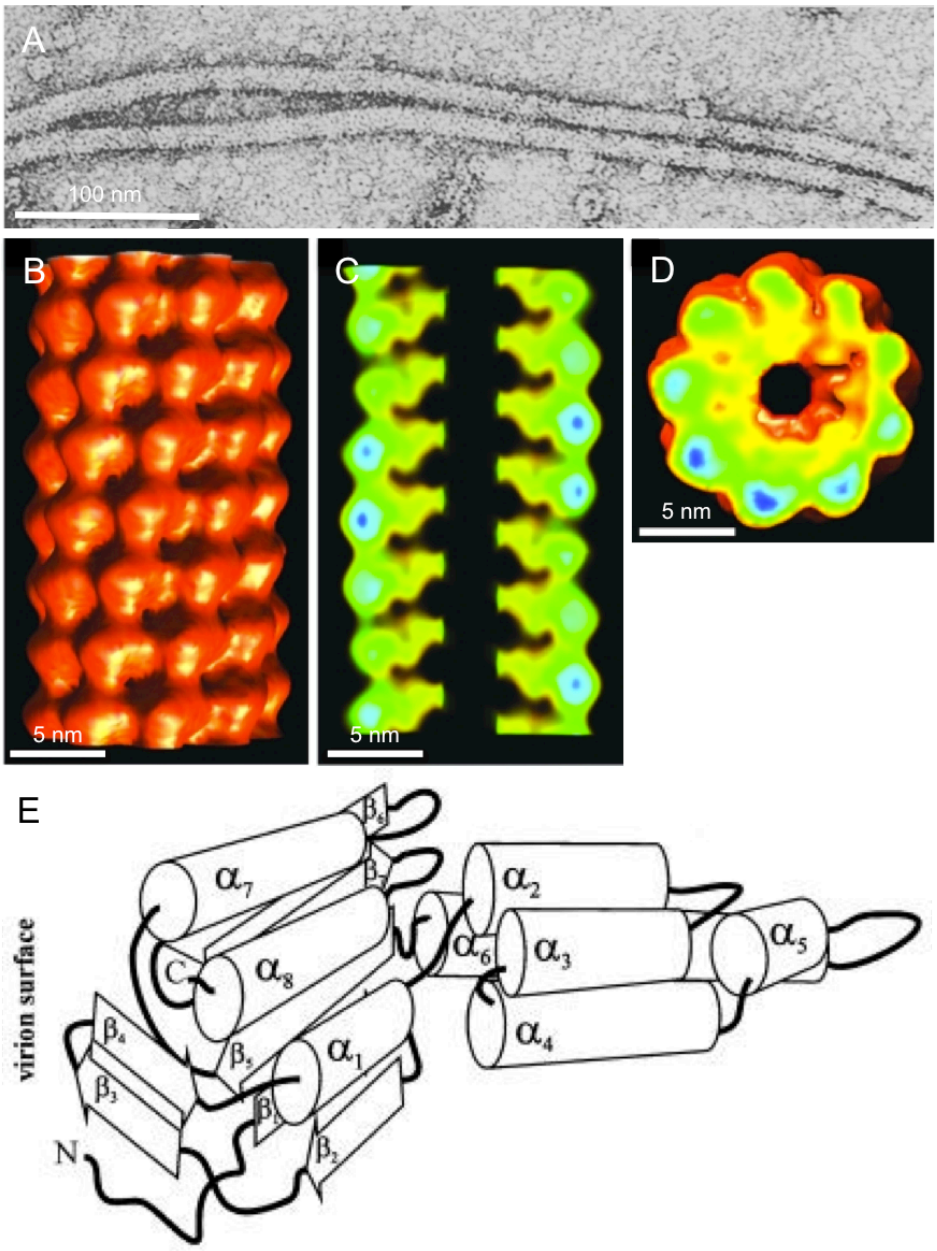

Figure 1. Ultrastructure of potyvirus particles and CP.

(A) Electron micrograph of PVY particles mounted in uranyl formate. (B to D) 3D representation shows, the outside surface view (B), a longitudinal cross-section (C) and a transverse cross-section (D) of SMV. (E) Schematic representation of the overall fold of the PVA CP. α-Helices are shown as cylinders, and β-strands are shown as angled open arrows, with thick solid lines indicating interconnecting loops and the N and C termini of the polypeptide chain. (A) is taken from (Varma, Gibbs et al. 1968), (B) to (D) are taken from (Kendall, McDonald et al. 2008), and (E) is taken from (Baratova, Efimov et al. 2001).

1.3 Genome organization

Potyviruses have a monopartite positive-strand RNA [(+) RNA] genome of approximately 10 kb in length. The 5' end of the viral RNA (vRNA) is covalently linked to a viral genome-linked protein (VPg) (Siaw, Shahabuddin et al. 1985) and the 3' end has a poly (A) tail (Puurand, Makinen et al. 1992) (Fig. 2). Once a potyviral particle enters into a plant cell, the genome is released into the cytoplasm and translated to produce a polyprotein, which is proteolytically processed into at least eleven mature proteins by three viral proteinases (Jiang and Laliberté 2011) (Fig. 2). The proteinases P1 and helper component proteinase (HCpro) are produced from the amino-terminus of the polyprotein, and they cleave themselves at their C-terminus (Carrington, Freed et al. 1989, Verchot, Koonin et al. 1991). The polyprotein from P3 to CP is processed by the proteinase "nuclear inclusion protein a (NIa)" (Adams, Antoniw et al. 2005).

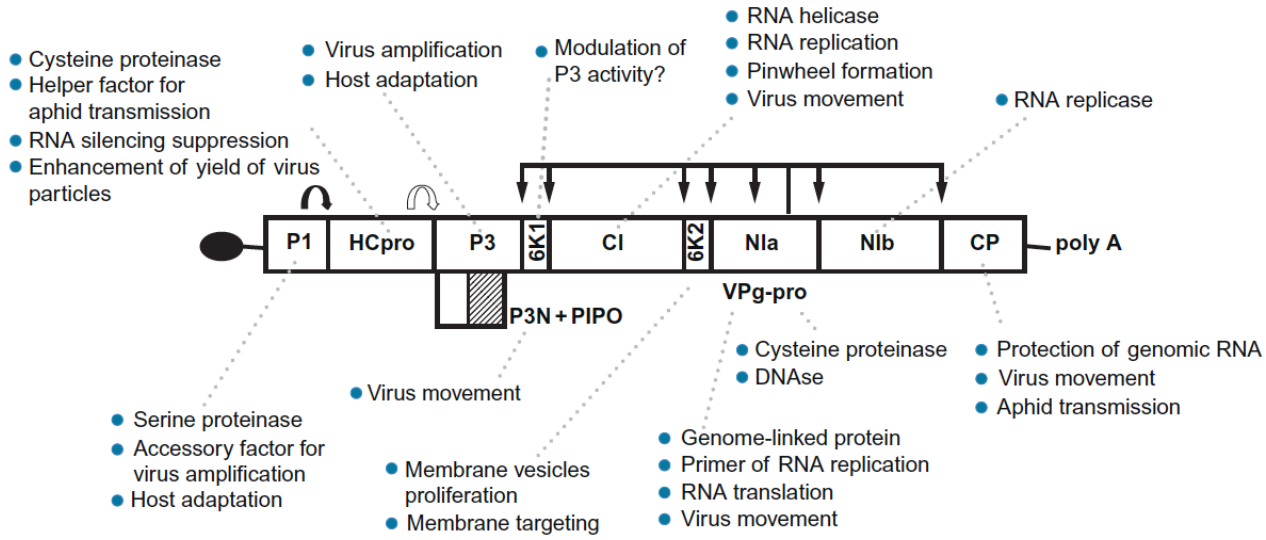

Figure 2. Potyvirus genome organization and functions of encoded proteins.

The viral genome-encoded polyprotein is represented as a rectangle in which individual proteins are divided by vertical lines. The overlapping PIPO ORF is indicated as a striped area below the P3 region. The terminal protein (VPg) is represented as a black ellipse. Arrows starting from the three proteases (P1, HCpro, and NIa) above the box indicate the cleavage sites in the polyprotein. All the known functions of each protein indicated with a blue dot are given at the end of the dotted lines starting from the given protein. P1, P1 proteinase; HCpro, helper component proteinase; P3, P3 protein; PIPO, pretty interesting potyviridae ORF; CI, cylindrical inclusion protein; NIa, nuclear inclusion protein a; VPg, viral genome-linked protein; Pro, Proteinase; NIb, nuclear inclusion protein b; CP, capsid protein. Taken from (Revers and Garcia 2015).

1.4 Function and localization of potyviral proteins

The eleven fully processed potyviral proteins are P1, HCpro, P3, N-terminal half of P3 fused to the pretty interesting potyviridae ORF (P3N-PIPO), $6K_1$, cylindrical inclusion (CI) protein, $6K_2$, VPg, nuclear inclusion protein a protease (NIa-pro), nuclear inclusion protein b (NIb)/RNA-dependent RNA polymerase (RdRp) and CP. Interactions between these potyviral proteins (including self-interactions), potyviral and plant proteins have been depicted as an elaborate protein-protein interaction network (Elena and Rodrigo 2012). Most of these mature potyviral proteins are multifunctional and their functions are summarized in Figure 2 (Revers and Garcia 2015). The detailed information (function and localization) of each potyviral proteins have been reviewed in (Revers and Garcia 2015) and (Sochor, Babula et al. 2012). Here, I will give detailed information concerning the proteins that were involved in this study.

1) HCpro

The name of the multifunctional protein HCpro (Maia, Haenni et al. 1996) is derived from its first discovered function of being an helper component (HC) for aphid transmission (Govier, Kassanis et al. 1977) and being a cysteine protease (pro) (Carrington, Freed et al. 1989). HCpro is also involved in suppression of RNA silencing (Llave, Kasschau et al. 2000), cell-to-cell (Rojas, Zerbini et al. 1997) and long-distance (Saenz, Salvador et al. 2002) movement, synergism between co-infecting viruses (Pruss, Ge et al. 1997) and symptom development (Redondo, Krause-Sakate et al. 2001). HCpro has also recently been shown to enhance CP stability, yield of viral particles and progeny infectivity (Valli, Gallo et al. 2014). HCpro has three structural domains: the N-terminal domain is essential for aphid transmission, the C-terminal domain is responsible for the proteinase activity, and the central region is involved in all the other functions (Plisson, Drucker et al. 2003). HCpro has been shown to interact with a large number of viral proteins: P1 (Merits, Guo et al. 1999), CI (Choi, Stenger et al. 2000), VPg (Yambao, Masuta et al. 2003), CP (Roudet-Tavert, German-Retana et al. 2002); and host proteins [See Table 1 of review (Revers and Garcia 2015)].

HCpro is located both in the cytoplasm and nucleus (Sahana, Kaur et al. 2014). HCpro has been shown to be a soluble protein in *Plum pox virus* (PPV) infected plants

(Ravelonandro, Peyruchaud et al. 1993), but also aggregates as cytoplasmic amorphous inclusions in some potyvirus-infected plants (de Mejia, Hiebert et al. 1985). The mutant HCpro^{N182L} is absent from the nucleus, and the amino acid N^{182} may regulate RNA silencing mechanisms (Sahana, Kaur et al. 2014). Moreover, HCpro has been detected at one end of the potyvirus particles, which may be associated with aphid transmission (Torrance, Andreev et al. 2006).

2) CI

The name of CI (Sorel, Garcia et al. 2014) derives from the ultrastructural observation that this protein forms cylindrical inclusions of different morphology (pinwheel, bundles and short curved laminated aggregates or scrolls) in the cytoplasm of potyvirus-infected cells (Edwardson, Christie et al. 1984). CI is an RNA helicase (Eagles, Balmori-Melian et al. 1994), and this activity plays an essential role in virus RNA replication (Fernandez, Guo et al. 1997). Mutation analysis results show that CI is involved in both cell-to-cell and long-distance movement (Carrington, Jensen et al. 1998). CI has been shown facilitating virus cell-to-cell movement by associating with P3N–PIPO (Wei, Zhang et al. 2010). Moreover, CI protein acts as an avirulence factor in gene-for-gene interactions with dominant-resistance host genes and as a recessive-resistance overcoming factor (Sorel, Garcia et al. 2014). Beside its self-interaction (Lopez, Urzainqui et al. 2001), CI has been shown to interact with three potyviral proteins: P1 and HCpro (Guo, Rajamaki et al. 2001), as well as P3N-PIPO (Wei, Zhang et al. 2010). CI has also been shown to interact with three host proteins: the plant ortholog of a dsRNA-activated protein kinase (PKR) inhibitor P58^{IPK} that is involved in viral pathogenesis (Bilgin, Liu et al. 2003), the chloroplastic photosystem I PSI-K protein that may be involved in antiviral defense (Jimenez, Lopez et al. 2006), the eukaryotic translation initiation factor 4E (eIF4E) that may be associated with overcoming the eIF4E-based resistance (Tavert-Roudet, Abdul-Razzak et al. 2012).

CI is located in cytoplasm and attached to plasmodesmata (PDs) (Sorel, Garcia et al. 2014). CI has also been found to be localized to one end of PVA particles, and may provide a molecular motor function both to disassemble and to translocate the viral genome through PDs (Gabrenaite-Verkhovskaya, Andreev et al. 2008).

3) $6K_2$

$6K_2$ is a 6 kDa membrane protein. It induces endoplasmic reticulum (ER) -derived membrane structures that contain virus replication complexes (Schaad, Jensen et al. 1997). $6K_2$-induced vesicles contain virus replication complexes that move intracellularly (Cotton, Grangeon et al. 2009) and intercellularly (Grangeon, Jiang et al. 2013). $6K_2$ protein is an avirulence determinant of systemic infection (Rajamaki and Valkonen 1999). It also affects viral long-distance movement and symptom induction independently and in a host-specific manner (Spetz and Valkonen 2004).

$6K_2$ is a very dynamic protein and localizes along the secretory pathway. It colocalizes with ER exit sites (ERES) markers Sar1, Sec23, and Sec24, and it thus has been suggested that biogenesis of $6K_2$ vesicles occurs at ERES in a coat protein complex I (COPI)- and coat protein complex II (COPII)- dependent manner (Wei and Wang 2008). $6K_2$ indirectly interacts with the SNARE (soluble N-ethylmaleimide-sensitive-factor attachment protein receptors) protein Syp71 via a third protein Vap27-1, which is essential for the fusing of $6K_2$ vesicles with chloroplasts during *Turnip mosaic virus* (TuMV) infection (Wei, Zhang et al. 2013).

The N-terminal soluble domain of $6K_2$ is required for ER export of the protein and for the formation of vesicles. ER export is not absolutely required for vRNA replication, but is necessary for virus cell-to-cell movement. Furthermore, $6K_2$ physically interacts with the COPII coatomer Sec24a and an Arabidopsis thaliana mutant line with a defective Sec24a shows a delay in the systemic infection by TuMV (Jiang, Patarroyo et al. 2015) .

4) NIb/RdRp

Certain potyviruses induce the accumulation of nuclear inclusions (NI) containing two proteins, designated as NIa and NIb (Knuhtsen, Hiebert et al. 1974, Domier, Shaw et al. 1987). The reason for the nuclear localization of NIb is not known. NIb contains two independent nuclear localization signals (NLS I and NLS II). Mutations within these NLS regions disrupt the nuclear translocation activity of NIb and also abolish vRNA amplification (Li, Valdez et al. 1997). In addition, NIb interacts with the small ubiquitin-

like modifier (SUMO) -conjugating enzyme SCE1 both in the nucleus and in the cytoplasm, and NIb SUMOylation is required for viral infection (Xiong and Wang 2013).

NIb is the RdRp for potyviral genome replication (Hong and Hunt 1996). RdRp uridylylates VPg, and the uridylylated VPg acts as primer for progeny RNA synthesis (Anindya, Chittori et al. 2005). It has been shown that RdRp directly interacts with three host proteins, the translation factor poly-A binding protein (PABP), the cellular chaperone heat shock cognate 70-3 protein (Hsc70-3), and the eukaryotic elongation factor 1A (eEF1A), which contribute to the formation of functional replication complexes (Beauchemin and Laliberté 2007, Dufresne, Thivierge et al. 2008, Thivierge, Cotton et al. 2008). RdRp is a soluble protein located in the nucleus (excluding nucleolus) and cytoplasm (Dufresne, Thivierge et al. 2008), and it is targeted to the membrane-bound replication complexes by interacting with VPg (Fellers, Wan et al. 1998) and Pro (Li, Valdez et al. 1997), domains of the $6K_2$-VPg-Pro intermediate (Dufresne, Thivierge et al. 2008).

5) CP

The main function of CP is the encapsidation of the viral genome. CP can be divided into three domains: the variable N- and C- terminal domains that are exposed on the surface of the potyvirus particle, and the conserved central core domain that is located inside of the potyvirus particle (Shukla, Ward et al. 1994). The N- and C-terminal domains are essential for CP inter-subunit interactions that are involved in the initiation of particle assembly (Anindya and Savithri 2003, Kang, Lim et al. 2006). The mutation studies of CP have shown that the central core domain of *Tobacco etch virus* (TEV) is essential for virus cell-to-cell movement, the N- and C-terminal domains being necessary for long-distance movement (Dolja, Haldeman et al. 1994, Dolja, Haldeman-Cahill et al. 1995). CP has also been shown to increase the size-exclusion limit (SEL) of PDs and to facilitate cell-to-cell movement of vRNA (Rojas, Zerbini et al. 1997). On the other hand, the N-terminal 'DAGX' motif of CP has a direct effect on aphid transmission of potyvirus particles by interacting with HCpro (Atreya, Lopez-Moya et al. 1995). CP is able to interact with the viral RdRp (vRdRp), which may involve regulation of vRNA synthesis (Hong, Levay et al. 1995).

Some posttranslational modifications, such as phosphorylation and O-GlcNAcylated, of CP have been described. CP was not phosphorylated when packaged into particles, and phosphorylated CP has reduced affinity for vRNA, suggesting CP phosphorylation may be involved in regulating formation and/or stability of viral ribonucleoproteins (Ivanov, Puustinen et al. 2001). The N-terminal domain of the PPV CP has been shown to be O-linked N-acetylglucosamine (O-GlcNAc) modified (Chen, Juarez et al. 2005). O-GlcNAcylation of PPV CP showed enhanced viral infection (Perez Jde, Udeshi et al. 2013). CP has been reported to interact with heat shock protein 70 (HSP70) and its cochaperone CPIP to regulate CP degradation (Hafren, Hofius et al. 2010). CP has also been reported to interact with tobacco ribulose-1,5-biphosphate carboxylase/oxygenase large subunit (RubisCO-LSU), which may be involved in the production of mosaic and yellowing symptoms of the plant (Feki, Loukili et al. 2005).

Immunohistolocalization result in TuMV-infected protoplast showed that some CP signal was located in close proximity to dsRNA punctate structures (a marker for replicating vRNA), suggesting that replication and encapsidation of vRNA are spatially separated (Cotton, Grangeon et al. 2009). During TuMV infection, CP was observed in the cytoplasm in close proximity to TuMV $6K_2$-tagged replication complexes or chloroplasts, and was associated with PD-localized structures of CI in the presence of P3N-PIPO (Wei, Zhang et al. 2010). This suggests that CP has a role in cell-to-cell movement of the virus.

2. Cellular remodeling during animal (+) RNA virus infection

(+) RNA viruses remodel intracellular membranes to generate organelle-like structures that are called replication factories. It is believed that these membrane organelles create an environment protecting viral components from a hostile degradative environment, and this environment also increases the local concentration of all necessary factors for vRNA replication thus ensuring high efficiency (Paul and Bartenschlager 2013). The ultrastructure and biogenesis of some animal (+) RNA virus replication factories have been studied by transmission electron microscopy coupled to electron tomography (TEM-ET). These rearranged sites contain distinct membrane structures that coordinate the different steps of the virus life cycle (polyprotein translation and processing, vRNA replication, virions assembly and release) in space and time to achieve efficient replication.

2.1 Ultrastructure of animal (+) RNA viruses vRNA replication sites

Different animal (+) RNA viruses generate distinct membrane structures as vRNA replication sites.

1) Spherules

The nodavirus *Flock house virus* (FHV) induces approximately 50-nm spherule formation by invagination of the outer mitochondrial membrane. The FHV RNA replication factor protein A and newly synthesized vRNA are localized in these spherules. The spherules have a neck region of approximately 10 nm in diameter connecting the interior of the spherules to the cytoplasm. This enables the import of ribonucleotides and export of progeny vRNA (Fig. 3A) (Kopek, Perkins et al. 2007).

2) Vesicle packets (VPs)

The flavivirus *Dengue virus* (DENV) remodels ER to form VPs, which are single-membrane vesicles (SMVs) enclosed within the ER lumen (Fig. 3B). These vesicles are labeled with nonstructural viral proteins- and dsRNA-specific gold particles, indicating they are the sites of vRNA replication (Welsch, Miller et al. 2009).

3) SMVs aggregate

Poliovirus remodels ER to form SMVs aggregate (Fig. 3C). Polioviral P2 proteins, which are nonstructural proteins associated with replication, induce rough ER (rER) membrane protrusions that ultimately form vesicles. These contain the replication complex that move away from the rER and that form a continuously growing vesiculated area in the center of the infected cell (Bienz, Egger et al. 1987).

4) Double-membrane vesicles (DMVs) aggregate

Severe acute respiratory syndrome (SARS)-coronavirus also remodels the ER to form a cluster of DMVs (Miller and Krijnse-Locker 2008) (Fig. 3D). SARS-coronavirus induced DMVs are labeled with replicase-specific antibodies, suggesting that they contain the viral replication complex (Snijder, van der Meer et al. 2006).

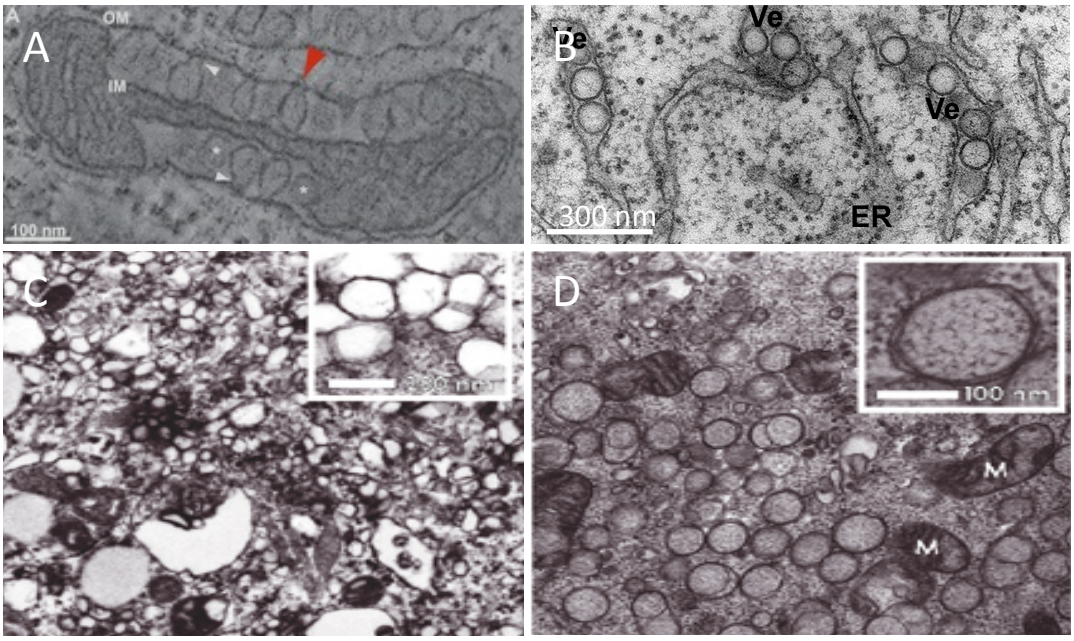

Figure 3. Transmission electron microscopy (TEM) images showing animal (+) RNA virus induced membrane structures for vRNA replication.

(A) FHV-induced spherules on mitochondria outer membrane. (B) DENV-induced VPs in ER lumen. (C) *Poliovirus*-indcued SMVs from ER membrane. (D) *SARS-coronavirus*-induced DMVs from ER membrane. (A) is taken from (Kopek, Perkins et al. 2007), (B) is taken from (Welsch, Miller et al. 2009), (C) and (D) are taken from (Miller and Krijnse-Locker 2008).

2.2 3D reconstitution of viral replication factories

In recent years, several 3D models of animal (+) RNA virus replication factories have been generated by TEM-ET. The sophisticated generated structural profile largely improves our understanding about the biogenesis and functions of these membrane structures.

2.2.1 Principle of TEM-ET

To reveal the high-resolution 3D structure of biological samples, electron tomography (ET) is the method of choice. The resolution of the 3D structures generated by ET reaches approximately 3 nm (Hoenger and McIntosh 2009), which allows the analyzing of their spatial distribution and their interactions in the native cellular context approaching the molecular level (Nickell, Kofler et al. 2006). Thus ET helps to bridge the gap between the cellular and molecular worlds.

The principle of ET has been fully described in two reviews (McIntosh, Nicastro et al. 2005, Barcena and Koster 2009). Briefly, TEM images give misleading information about the structural properties of biological samples. For example, in the 0° projection image of a sample, a small vesicle and a small tubule have a similar profile (Fig. 4A, blue ovals). One way to solve this problem is to collect a series of two-dimensional (2D) TEM images of these samples from different directions, which is the basic principle of ET.

There are several steps involved in ET: sample preparation, data collection, image alignment, tomographic reconstruction, post-processing and interpretation of the tomograms. Both chemical-fixation and high-pressure freezing coupled with freeze substitution [HPF/FS, including a fast-freezing (20–50 msec) step under high-pressure, a water substitution step (dehydration at −80°C to −90°C with organic solvent), and a subsequent resin embedding step.] prepared samples have been used for ET data collection. The thickness of the sections up to 300 nm that can be performed depends on the accelerating voltage of the electron microscope. To collect the raw data, the sections were put on a grid and placed into the tilt holder of an electron microscope (Fig. 4B). The holder is gradually tilted inside the microscope around an axis perpendicular to the electron beam, and the 2D images are recorded at different angles

(single axis tilt series) under the control of an automated data collection software (Fig. 4C, continuous arrows). The range of tilt angles that can be performed is limited (normally up to ±60° or ±70° with a 1-2° interval), because of the limited tilt available in most electron microscopes and the possible holder shadowing at high tilt. The missing image part of the sample can be partially compensated by a dual-axis tilt series sample collection (the second tilt series is taken by rotating the sample in 90°). Then, the recorded raw data is computationally aligned and reconstructed into a series of tomographic slices of the 3D structure, which are shown as serial “virtual sections” (each image shows a slice about 2–10 nm thick) of the sample. Finally, the 3D models are generated with special software. The key step is the segmentation, in which the different structures of interest are separated and masked in different colored surfaces.

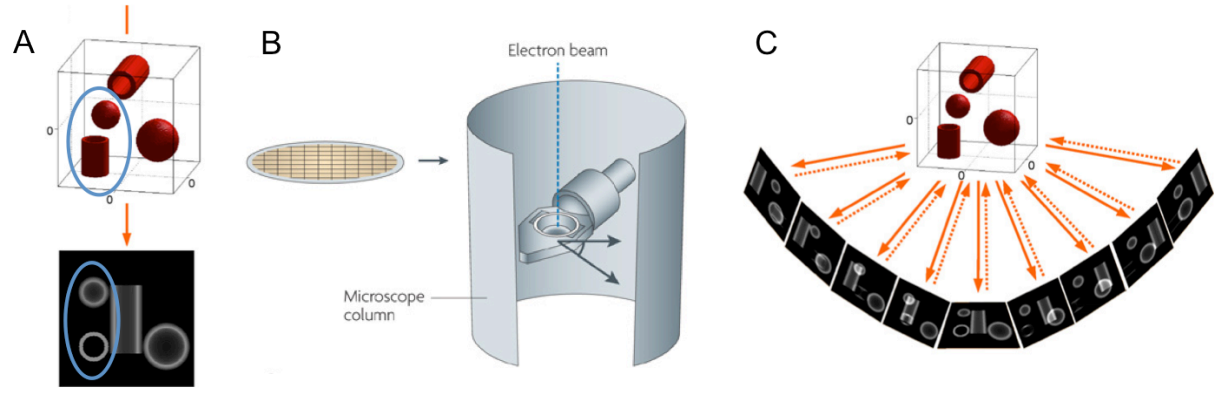

Figure 4. The principle of ET.

(A) The 0° projection of a sample results in a 2D image shown below. (B) The grid for the sections supporting, and the tilt holder in the column of an electron microscope. (C) For raw data collection, a series of 2D images are collected at different orientations of a sample (continuous arrows). For the back-projection, each recorded image is used to contribute to a 3D representation (discontinuous arrows). (A) and (C) are taken form (Barcena and Koster 2009), and (B) is taken from (Milne and Subramaniam 2009).

2.2.2 Distinct membrane structures support different steps in virus replication cycle

Distinct membrane structures can be simultaneously observed in one cell that is infected with some (+) RNA viruses, or they can be observed during the time course analysis and showed successive development. TEM-ET shows that these distinct membrane structures may contribute to different infectious steps, such as polyprotein translation and processing, vRNA replication, particles assembly, maturation and release.

1) DENV induced membrane structures.

Distinct membrane structures, including convoluted membranes (CM) and VPs can be found in DENV-infected cells. Immuno-EM studies indicated that CM may represent the site of DENV RNA translation/polyprotein processing (Mackenzie, Jones et al. 1996). The 3D architecture of VPs generated by ET shows a possible topological link between replication and assembly in infected cells (Welsch, Miller et al. 2009). As mentioned before the immuno-EM studies showed that the SMVs in the VPs are vRNA replication sites. The 3D model shows that the inter SMV membranes are continuous with the ER membrane (Fig. 5A, index of left panel), and there are pore-like openings that could enable release of newly synthesized vRNA (Fig. 5A, right panel). The viral particles are located on the nuclear envelope membrane just opposite of the pores, and this area might be for virus budding (Fig. 5A, index of left panel). The particles may travel in the ER and via secretory vesicles to the Golgi apparatus for maturation, since they can also be found in the ER lumen and Golgi apparatus (Fig. 5A, left panel) (Welsch, Miller et al. 2009).

2) SARS-coronavirus induced membrane structures.

The 3D model of SARS-coronavirus induced membrane structures is a unique reticulovesicular network of modified ER that integrates CM, numerous interconnected DMVs, and VPs (Fig. 5B) (Knoops, Kikkert et al. 2008). SARS-coronavirus replicase subunits are localized predominantly to CM, the dsRNA abundantly labels the interior of DMVs, and the particles are observed budding from VPs. Thus it was proposed that SARS-coronavirus induces CM for polyprotein synthesis and processing, DMVs for

vRNA replication, and VPs for virus assembly and budding (Knoops, Kikkert et al. 2008).

3) *Hepatitis C virus* (HCV) induced membrane structures

HCV is a *Hepacivirus* in the family *Flaviridae*. Expression of the entire HCV polyprotein induces the accumulation of vesicles that called membranous web (MW) (Egger, Wolk et al. 2002). Early in HCV infection, the main constituents of MW are SMVs and DMVs; the DMVs are predominating and are the vRNA replication sites, the role of SMVs is unknown (Fig. 5C, left panel) (Romero-Brey, Merz et al. 2012). Late in HCV infection, multi-membrane vesicles (MMVs) become more abundant. MMVs might be a result of a stress-induced reaction (Fig. 5C, right panel) (Romero-Brey, Merz et al. 2012). The 3D reconstructions show that the DMVs seem to be formed as ER protrusions connected to ER membranes via neck-like structures (Fig. 5C, index of the left panel). MMVs are likely to be formed by the extensive enwrapping and curling of membranes (Fig. 5C, index of the right panel) (Romero-Brey, Merz et al. 2012).

4) *Coxsackievirus B3* (CVB3) induced membrane structures

CVB3 is an *Enterovirus* in the family *Picornaviridae*. Conventional TEM images showed that enterovirus induces either heterogeneous SMVs (Bienz, Egger et al. 1983, Bienz, Egger et al. 1987) or DMVs (Schlegel, Giddings et al. 1996, Wong, Zhang et al. 2008, Kemball, Alirezaei et al. 2010) clustering in the perinuclear region and eventually occupying most of the cytoplasm. However, 3D models of enterovirus CVB3-induced membrane structures that were generated by ET showed different results (Limpens, van der Schaar et al. 2011). For example, the 3D architecture generated on HPF/FS-prepared CVB3-infected cells showed closed single-membrane tubules (SMTs) early in infection (Fig. 5D, left panel), DMVs and multilamellar structures at late stage (Fig. 5D, right panel). The SMTs are the sites of vRNA replication, but the functions of DMVs and multilamellar structures are not clear.

The transformation process of these different membrane structures has been proposed as follows. The membranes of the SMTs become more tightly apposed, resulting in flattened cisternae. Via an enwrapping mechanism, the cisterna curves into a vase-like configuration, and their membrane ends fuse, producing a closed, spherical

DMV. The DMVs then become enwrapped by other cisternae to form multilamellar structures (Limpens, van der Schaar et al. 2011, Belov, Nair et al. 2012).

In conclusion, the rearrangements of these four animal (+) RNA viruses correspond to either invaginations (DENV and SARS-coronavirus) or protrusions (HCV and CVB3) of membranes that are derived from ER.

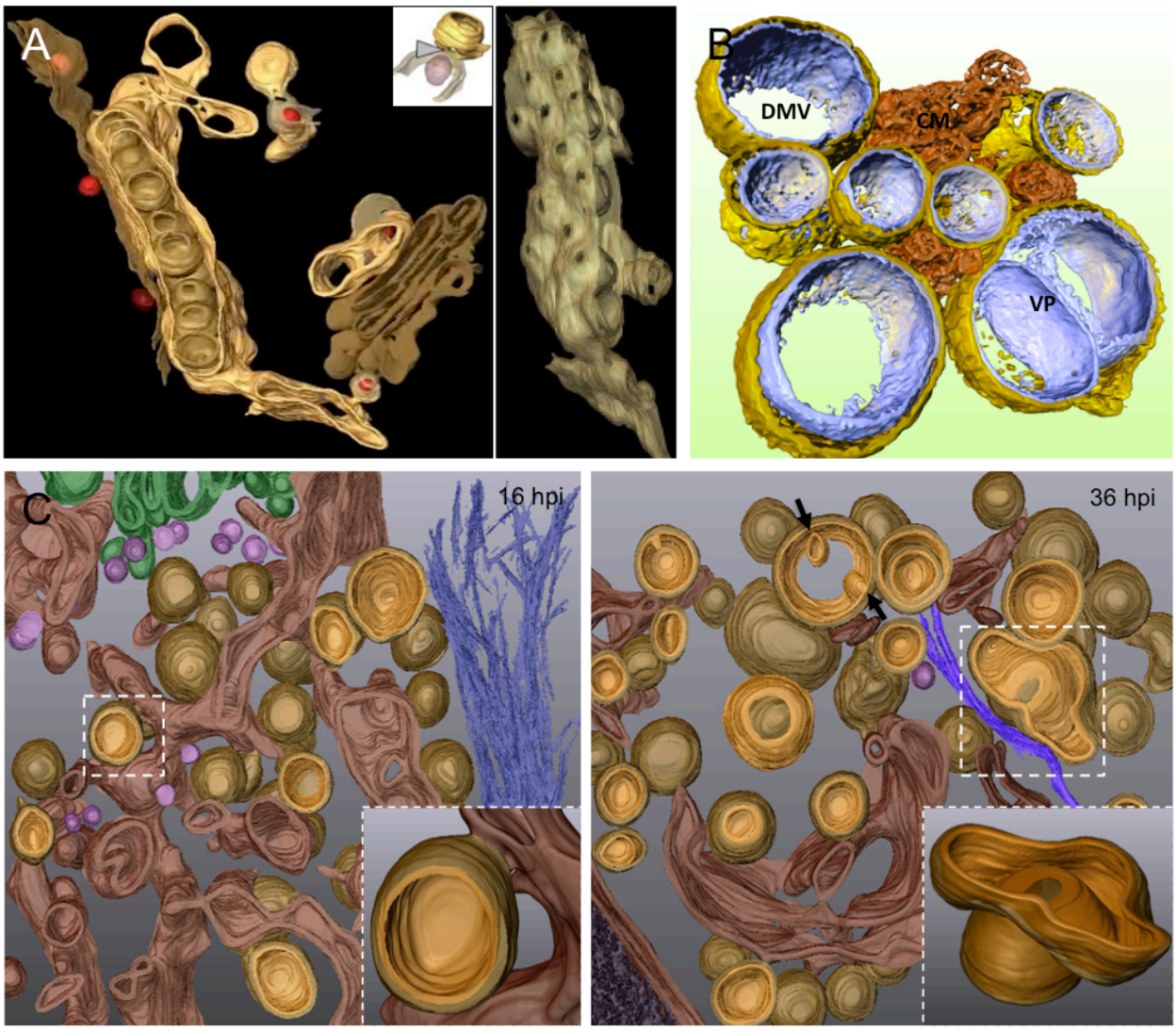

Exponential phase of RNA synthesis (mainly SMTs)

Late stage (SMT↓,DMVs↑, MMVs↑)

Figure 5. 3D models of animal (+) RNA virus induced membrane structures.

(A) 3D model shows the possible relation between DENV replication, assembly, and virion release. The left panel shows a 3D surface rendering of ER and Golgi membranes (yellow), outer nuclear envelope membrane (semitransparent), the vesicles in the ER (light brown) and virus particles (red). The index of left panel shows a 3D surface rendering of the ER/vesicle continuity (yellow) and the tightly apposed ER (semitransparent) containing a virus particle (red), where there is a putative virus budding site (arrow). The right panel shows the vesicle-containing ER segment (transparent), rotated by 90° around the y-axis, highlighting the vesicle openings. (B) 3D model shows the cluster of DMVs (outer membrane, gold; inner membrane, silver) with the outer membranes are connected to VPs and CM structure (bronze). (C) 3D architecture of HCV-induced membrane rearrangements. Left: Both SMVs (pink) and DMVs [inner membrane (yellowish brown), outer membrane (semi-transparent light brown)] are shown at early stage in infection, and the DMVs are primarily present. The index displays a connection between the outer membrane of a DMV and the ER (dark brown) membrane. Right: the MMVs are predominant at late stage in infection. Black arrows show invaginations of DMVs. The white star indicates a large MMV. The index highlights a double-membrane tubule enwrapping a DMV and presumably leading to the formation of a MMV. The intermediate filaments are colored in dark blue and the Golgi apparatus in green. hpi, hours post infection. (D) The left panel shows a surface rendering of SMTs (green), open (orange) and closed (yellow) DMVs, and ER (blue) at the exponential phase of CVB3 RNA synthesis. The right panel shows a surface rendering of DMVs (orange), multilamellar structures (red) and parts of the neighboring ER (blue) at late stage of CVB3 infection. (A) is adapted from (Welsch, Miller et al. 2009), (B) is adapted from (Knoops, Kikkert et al. 2008), (C) is adapted from (Romero-Brey, Merz et al. 2012), and (D) is adapted from (Limpens, van der Schaar et al. 2011).

3. Comparison between animal and plant cells

Animal and plant cells are both eukaryotic cells that contain membrane-bound organelles, such as nucleus, ER, Golgi apparatus, mitochondria and other organelles (Fig. 6). There are also basic differences between animal and plant cells. For instance, there are some special structures and organelles in a plant cell that are not present in an animal cell, such as the cell wall, chloroplasts, PDs and large vacuoles (Fig. 6). Different animal and plant (+) RNA viruses generate replication sites from distinct membrane-bound organelles [See Figure 2 of review (Netherton and Wileman 2011)]. The replication factories that are generated on different organelles by plant (+) RNA viruses will be discussed below. From another point of view, (+) RNA viruses hijack and modify different cellular pathways (secretory pathway, lipid synthesis pathway, autophagy pathway and so on) to facilitate their infectious cycle, and the modification of the secretory pathway has been reviewed (Belov and van Kuppeveld 2012, Patarroyo, Laliberté et al. 2012). How plant (+) RNA viruses subvert the secretory pathway will be detailed in the Discussion section of this thesis.

3.1 Special structures and organelles in plant cells

1) Cell wall

The cell wall is a layer of complex polysaccharide matrix that surrounds a plant cell (Fig. 6). The cell wall gives the plant cell most of its support and structure. Hence, plant cells are normally “squarish” or rectangular in shape. The cell wall also protects plant cells against pathogens, dehydration, and other stressful environmental factors, and play crucial roles in plant growth, cell differentiation, intercellular communication and water movement (Cosgrove 2005).

2) Plasmodesma (PD)

The structure and function of a PD have been fully described in the reviews of (Maule 2008, Lucas, Ham et al. 2009, Xu and Jackson 2010, Lee and Lu 2011, Maule, Benitez-Alfonso et al. 2011). Briefly, PD is a plasma membrane lined channel through the cell wall between adjacent cells (Fig. 6). It is formed during cytokinesis when a

component of the ER becomes trapped in the developing phragmoplast. PD has three major structural components: a membranous tube that establishes PM continuity between adjacent cells, a ER-derived central membranous rod called desmotubule, and the cell wall surrounding the PM that function as physical constraints on the channel through the deposition of callose at the neck regions.

PDs are gateways for symplastic communication. They control the trafficking of small molecules as well as of a wide spectrum of endogenous proteins and ribonucleoprotein (RNP) complexes. It is thus important for the fundamental processes of plant growth, development and defense (Heinlein and Epel 2004). The conductivity of PD is regulated in response to developmental and physiological cues. Thus, PD can exist in different states, closed, open or dilated, and therefore either restrict or allow the trafficking of molecules based on their molecular size (Crawford and Zambryski 2001).

3) Chloroplast

The chloroplast is a lens-shaped double membrane (the outer and the inner envelope membrane) organelle (Fig. 6). Photosynthetic fixation of CO_2 occurs in the chloroplasts. The *de novo* synthesis of fatty acids in plants occurs primarily in the plastids (including chloroplasts that are able to generate the reducing power and ATP required for fatty acid synthesis by capture of light energy in the reactions of photosynthetic electron transport). These fatty acids are used for the synthesis of plastidial and other cellular membranes in all cells (Rawsthorne 2002). Association between the ER and chloroplasts as well as stromules that connect different chloroplasts have been regularly reported (Schattat, Barton et al. 2011). The direct ER-to-chloroplast association has been thought to be one of the possible transport routes for lipid transfer from the ER to the chloroplast membrane (Xu, Fan et al. 2008).

4) Large vacuole

Plant vacuoles are multifunctional organelles bound by a single membrane, which is called the tonoplast (Fig. 6). Plant vacuoles participate in maintenance of turgor pressure and homeostasis, storage of proteins, ions, and secondary metabolites (i.e. pigments and toxic compounds), degradation of proteins and old organelles (autophagy), defense responses, programmed cell death via auto-lysis (reviewed in

(Marty 1999, Oda, Higaki et al. 2009)). There are at least two types of plant vacuoles, the lytic vacuoles (LVs) of acidic pH with lysosome-like properties and protein storage vacuoles (PSVs) of neutral pH mainly in seeds for reserve accumulation (Oda, Higaki et al. 2009).

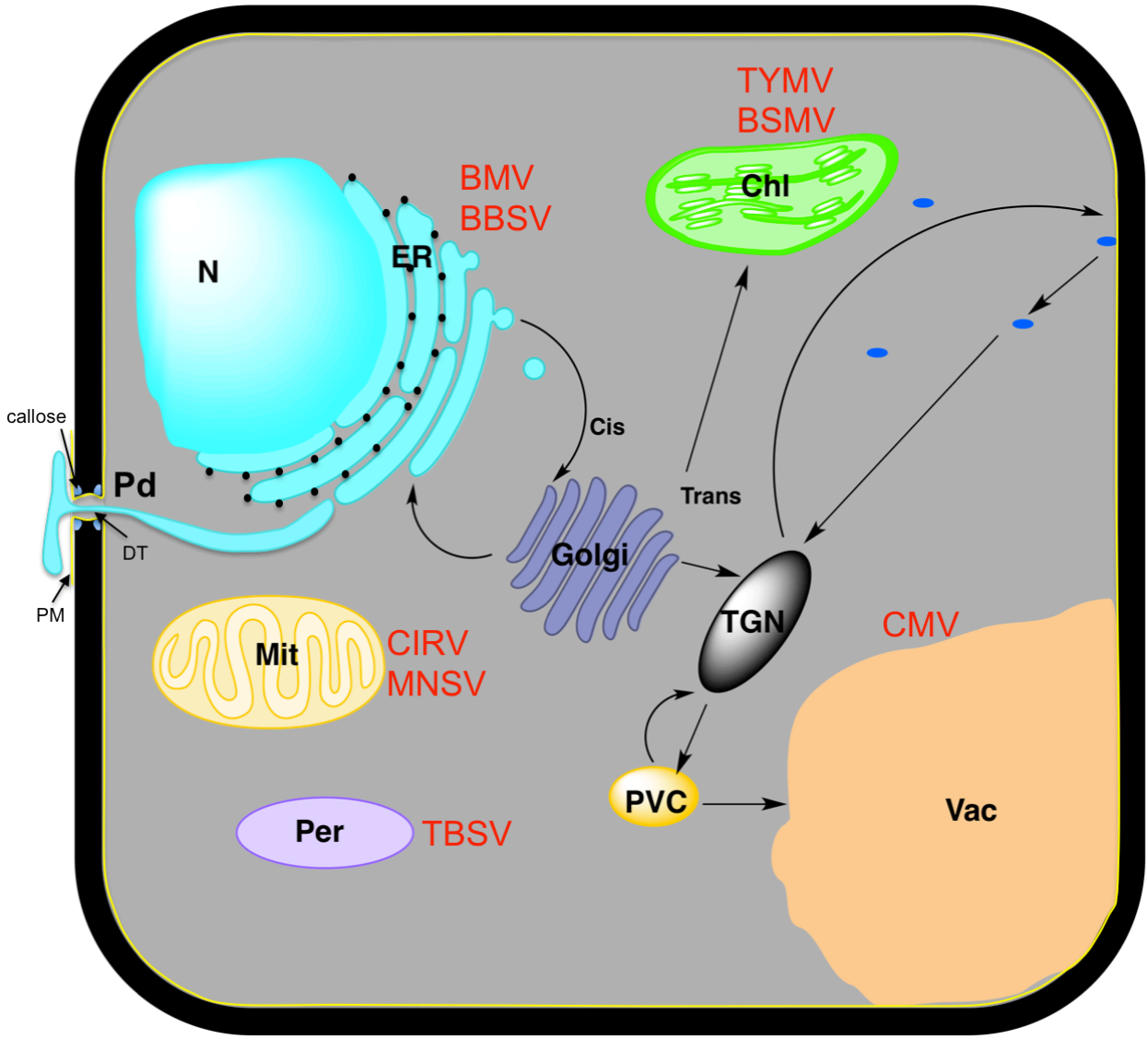

Figure 6. Schematic representation of a plant cell.

The black border indicates the cell wall, and the gray presents the cytoplasm. The small dark blue ellipses present the endosomes. Plant viruses (in red) remodel different organelle membranes for replication are placed beside the organelles. N, nucleus; ER, endoplasmic reticulum; Chl, chloroplast; Mit, mitochondrion; Per, peroxisome; TGN, trans-Golgi network; PVC, pre-vacuolar compartment; Vac, vacuole; Pd, plasmodesma; PM, plasma membrane; DT, desmotubule.

3.2 Secretory pathway

The secretory pathway contains a complex network of organelles including ER, Golgi apparatus, trans-Golgi network (TGN), various endosomes, and lysosome/vacuole (in plant cells). Proteins and lipids are synthesized and modified in ER, and then delivered to Golgi apparatus for further modification and sorting. Cargo molecules that are modified in the Golgi apparatus are usually delivered to the TGN where they are translocated to the plasma membrane (and cell wall in plant cell), or to the endosomes and then the lysosome/vacuole (Fig. 6).

1) Similarity and differences

The similarity and differences of secretory pathway between animal and plant cells have been fully described in a review (Patarroyo, Laliberté et al. 2012). Briefly, the morphology of ER in plant and animal cells is similar, and both of them exhibit a labyrinth-like morphology composed of membranous tubules and cisternae. However, in animal cells the ER is mainly aligned with microtubules and in plant cells with microfilaments. The molecular mechanisms underlying protein transport in the ER–Golgi interface are very conserved between animal and plant cells. Protein transport is linked by the ER-Golgi intermediate compartment (ERGIC) in animal cells, but no such intermediate has been revealed in plant cells. The organization of the Golgi apparatus in plant and animal cells is quite different. In animal cells, Golgi stacks form a single large perinuclear ribbon at the microtubule organization center (MTOC). In plant cells, the Golgi apparatus is present in the form of numerous individual cisternal stacks that move rapidly along the actin/ER cable in the cytoplasm. Although it is not well studied, the protein transport in post-Golgi traffic network appears quite different between animal and plant cells. In plant cells (Fig. 6), the TGN may also have a similar function as an early endosome (EE) in animal cells. At the TGN/EE, proteins can be either recycled back to the plasma membrane, or further transported to multi vesicular bodies (MVB) or prevacuolar compartments (PVC), a compartment equivalent to the late endosomes (LE) in animal cells, to vacuole. In animal cells, proteins can be recycled back to the plasma membrane via recycling endosomes (RE), but no RE has been identified in plant cells.

2) ER

ER is the largest membrane-bound organelle in eukaryotic cells, and many (+) RNA viruses have been reported to remodel ER membranes to facilitate their replication (Schwartz, Chen et al. 2002, Knoops, Kikkert et al. 2008, Welsch, Miller et al. 2009, Bamunusinghe, Seo et al. 2011, Limpens, van der Schaar et al. 2011, Belov, Nair et al. 2012, Cao, Jin et al. 2015). ER is an interconnected network comprised of rER and smooth ER (Fig. 6). rER is continuous with the nuclear envelope, studded with millions of ribosomes, and is involved in protein synthesis, folding, quality control and dispatch. Smooth ER is not associated with ribosomes, and is involved in lipid production and metabolism and steroid hormones production. The morphology of the ER is actively shaped, and undergoes continuous rearrangement to properly execute its function. The ER is frequently connected to various organelles including the plasma membrane, peroxisomes, mitochondria, Golgi apparatus, and in plant cells, chloroplasts (see the review (Chen, Doyle et al. 2012)).

4. Plant (+) RNA viruses replication factories

Plant (+) RNA viruses also remodel different membrane-bound organelles to generate replication factories that are similar to those of animal (+) RNA viruses induced membrane structures. In recent years, the understanding of plant (+) RNA virus induced replication factories has been greatly improved.

4.1 Ultrastructure of plant (+) RNA viruses replication factories

Limited TEM studies for plant (+) RNA virus replication factories have been generated. Interestingly, plant (+) RNA viruses that belong to the same genus or same family may target different organelles to generate their replication factories.

In the case of the family *Bromoviridae,* it has been shown that in surrogate yeast cells *Brome mosaic virus* (BMV) nonstructural protein 1a (containing RNA helicase-like and capping domains) localizes to ER membranes, recruits BMV nonstructural protein 2a (containing an RdRp domain) and vRNA templates, induces the formation of 60- to 75-nm spherules in the ER lumen for vRNA replication (Schwartz, Chen et al. 2002). But in *N. benthamiana* plant leaf cells, the structural protein CP induces VPs that are observed as a series of SMVs within the ER lumen for vRNA replication (Bamunusinghe, Seo et al. 2011) (Fig. 7A). Whereas, the related *Cucumber mosaic virus* (CMV) induces spherules on the tonoplast, and the viral particles are located in the cytoplasm close to the spherules (Fig. 7B) (Hatta and Francki 1981).

In the case of the genus *Tombusvirus* in the Family *Tombusviridae, Tomato bushy stunt virus* (TBSV) induces extensive membrane invaginations on the boundary of peroxisome to form peroxisomal multivesicular bodies (pMVBs) (Fig. 7C), which contain protein components of the viral membrane-bound RNA replication complex (Scholthof, Scholthof et al. 1995, McCartney, Greenwood et al. 2005). Whereas, *Carnation Italian ringspot virus* (CIRV) modifies mitochondrial outer membrane to form pMVBs, which are seen as numerous internal vesicles/spherules. These serve as the sites for vRNA replication (Di Franco, Russo et al. 1984, Hwang, McCartney et al. 2008) (Fig. 7D). The tombusviruses show remarkable flexibility in utilizing various subcellular membranes for replication under different conditions. For instance, TBSV replication

could switch to the ER in the absence of peroxisomes (Jonczyk, Pathak et al. 2007), and chimeric tombusviruses have been generated that carried sequences to retarget them to the alternative organelles (Xu and Nagy 2014).

As mentioned above, 3D reconstructions of numerous animal (+) RNA viruses replication factories have been characterized. However, 3D architecture of plant (+) RNA virus replication factories is limited. Only in recent years, 3D representations of two plant virus (in the family *Tombusviridae*) replication factories have been generated. The carmovirus *Melon necrotic spot virus* (MNSV) infection modifies mitochondria, which show large, interconnected, internal dilations that appeared to be connected with the cytoplasm by pores and/or complex structures (Gomez-Aix, Garcia-Garcia et al. 2014). The necrovirus *Beet black scorch virus* (BBSV) infection induces spherules in the ER lumen (Cao, Jin et al. 2015) (Fig. 7E). Despite their different genome organization and host cells, these two plant (+) RNA viruses generate replication factories that have similarities to some animal (+) RNA virus induced membrane structures, such as the membrane invagination and the pore-like opening allowing exchange of materials between the lumen of the spherules and the cytoplasm. These common features indicates that these viruses may use similar strategies to build the viral factories, such as hijacking the same cellular pathway or same host proteins.

Turnip yellow mosaic virus (TYMV, *Tymovirus, Tymoviridae*) also induces spherule formation from the membrane of chloroplasts. The interior of the spherules is connected to the cytoplasm through a neck region about 15 to 22 nm in diameter (Hatta, Bullivant et al. 1973, Hatta and Matthews 1974) (Fig. 7F). TYMV 66K protein, carrying the RdRp domain, has been shown to be at the edge of the spherules by immunogold labeling, suggesting that the spherules are likely to be TYMV replication sites (Prod'homme, Le Panse et al. 2001). TYMV particles can be found in the electron-lucent zone in the cytoplasm over the spherules of chloroplast (Hatta, Bullivant et al. 1973, Hatta and Matthews 1974, Hatta and Matthews 1976), and it has been proposed that TYMV particles are assembled at the necks of the spherules (Hatta and Matthews 1976). *Barley stripe mosaic virus* (BSMV, *Hordeivirus, Virgaviridae*) induces membrane invaginations in chloroplasts (Fig. 7G), which contain dsRNA (Lin and Langenberg 1985), viral triple gene block protein (TGBp) 2 and gamma b [γb, a 17 kDa cysteine-rich

protein has RNA-binding (Donald and Jackson 1996) and silencing suppression activities (Bragg, Lawrence et al. 2004)] (Torrance, Cowan et al. 2006), as well as viral-like particles (McMullen, Gardner et al. 1978), indicating that these invaginations may be the sites of BSMV RNA replication and particles assembly.

4.2 Morphology conservation of viral replication structures

(+) RNA viruses can be divided into three superfamilies: flavi-like, alpha-like and picorna-like viruses. For animal (+) RNA viruses, except HCV, all the other studied flavi-like and alpha-like viruses induce formation of discrete membrane invaginations with negative membrane curvature (the membranes are curved directionality toward to the compartment of the organelles) (Romero-Brey and Bartenschlager 2014). Whereas, picorna-like viruses, such as poliovirus and CBV3 rely on positively curved (the membranes are budded toward the outside medium of the organelles) convoluted tubular–vesicular membrane networks (Limpens, van der Schaar et al. 2011, Belov, Nair et al. 2012). Viruses in the family *Bromoviridae, Tymoviridae* and *Virgaviridae* are in the alpha-like superfamily. Viruses in the family *Tombusviridae* are in the flavi-like superfamily. As shown in the 2D images above, these plant (+) RNA virus induced replication factories are formed by negative membrane curvature. Not much is known about the finer details of potyvirus induced replication factories. Potyviruses belong to the picorna-like superfamily, and may induce replication factory formation by positive membrane curvature.

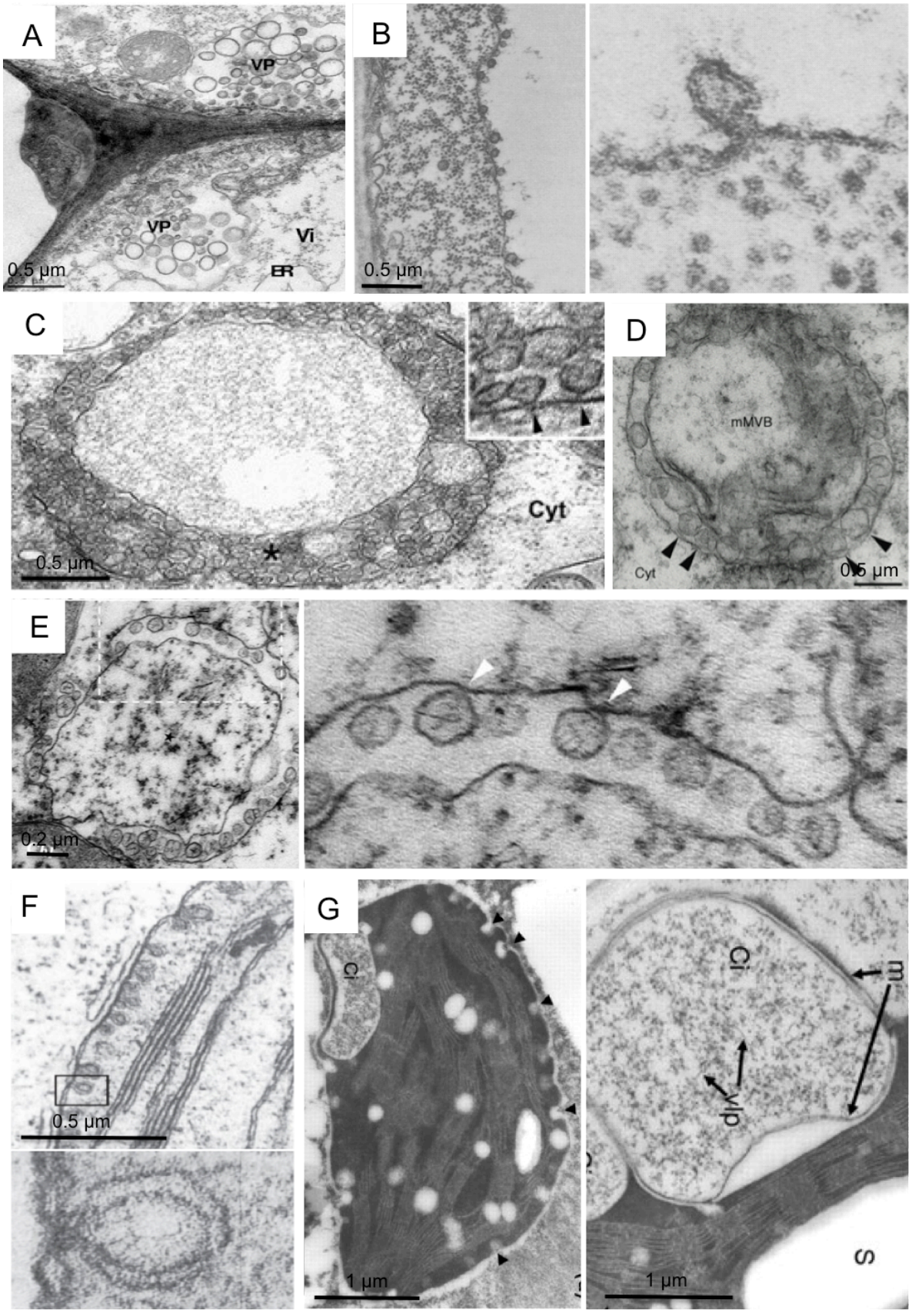
A
VP
VP
Vi
ER
0.5 µm
B
0.5 µm
C
Cyt
0.5 µm
D
mMVB
Cyt
0.5 µm
E
0.2 µm
F
0.5 µm
G
1 µm
Ci
m
vlp
1 µm
S

Figure 7. TEM images of plant (+) RNA virus replication factories.

(A) BMV-induced VPs are shown as a collection of vesicles in the ER lumen of two neighboring cells. Assembled virions (Vi) are found close to the VPs. (B) CMV-induced spherules on the tonoplast. The right panel is a higher magnification showing the extension of a spherule membrane with the tonoplast. (C) TBSV-induced pMVB in a peroxisome. The inset is the higher magnification of the area indicated by the asterisk. Arrowheads denote two distinct vesicle-like structures located within the lumen of the pMVB that appear to be connected by a neck to the pMVB boundary membrane. Cyt, cytosol. (D) CIRV-induced MVB in mitochondria. Arrowheads denote examples of vesicle/spherule-like structures in MVB. Cyt, cytosol; mMVB, mitochondria-derived multivesicular body. (E) BBSV-induced spherules in ER lumen. Right panel is the higher magnification of the dashed rectangle in left panel. White arrowheads point to potential connections between spherules and the outer ER membrane. (F) TYMV-induced spherules at the chloroplast periphery. The lower panel is the higher magnification of the black rectangle in the upper panel, which shows the open channel on a spherule. (G) BSMV-induced cytoplasmic invaginations at the chloroplast periphery, which is highlighted by arrowheads in the left panel (not post-fixed with osmium tetroxide). BSMV-induced membrane-bound cytoplasmic inclusions (Ci) in the deformed chloroplasts of both the left and right panels (post-fixed with osmium tretroxide). The Ci in the lower panel contains virus-like particles. Ci, cytoplasmic inclusion; m, membrane; S, Starch granule; vlp, virus-like particles. (A) is taken from (Bamunusinghe, Seo et al. 2011), (B) is taken from (Hatta and Francki 1981), (C) is taken from (McCartney, Greenwood et al. 2005), (D) is taken from (Hwang, McCartney et al. 2008), (E) is taken from (Cao, Jin et al. 2015), (F) is taken from (Hatta and Matthews 1974) and (G) is taken from (Torrance, Cowan et al. 2006).

5. Viral and host proteins involved in the biogenesis of replication factories

After the ultrastructural characterization of (+) RNA virus replication factories, it is essential to uncover the mechanism behind their formation. It is thus important to know which viral proteins are responsible for their induction, and which cellular pathway or host proteins are hijacked during these processes?

5.1 Viral proteins responsible for membrane remodeling

The role of viral proteins in the formation of animal (+) RNA virus replication factories has been reviewed in (Romero-Brey and Bartenschlager 2014). The molecular mechanism for replication factory formation is poorly understood. It is, however, clear that generally one or a few membrane-associated viral proteins play key roles in the membrane remodeling, since ectopic expression of these viral proteins can induce similar membrane structures as in virus infected cells. For few (+) RNA virus, those proteins are nonstructural (NS) proteins. For instance, FHV protein A is the only protein needed for vRNA replication and are found to accumulate in the spherules (Kopek, Perkins et al. 2007). However, expressing protein A alone induced only “zippering” of the surfaces of adjacent mitochondria but did not induce spherule formation, indicating that protein A is necessary, but not sufficient for spherule formation (Kopek, Settles et al. 2010). Interestingly, both the protein A and replication competent vRNA are required for the formation of spherules (Kopek, Settles et al. 2010). On the other hand, coexpression of two *Equine arteritis virus* (EAV; family *Arteriviridae*, order *Nidovirales*) putative transmembrane nonstructural proteins (nsp2 and nsp3) are sufficient to induce the formation of DMVs that strikingly resemble those found in infected cells (Snijder, van Tol et al. 2001). In the case of SARS-coronavirus, the three transmembrane nonstructural proteins (nsp3, nsp4 and nsp6) coexpressed together can induce the formation of DMVs that are similar to those observed in virus-infected cells (Angelini, Akhlaghpour et al. 2013).

The role of viral proteins in the formation of plant (+) RNA virus replication factories has been reviewed in (Laliberté and Sanfaçon 2010, Laliberté and Zheng

2014). Similarly, the membrane remodeling is attributed to the action of one or two viral proteins. As mentioned above, the sole expression of the BMV NS protein 1a in yeast cells is sufficient to induce the formation of spherules (Schwartz, Chen et al. 2002). Expression of BMV structural protein CP alone could induce ER membrane vesiculation similar to those VPs formed during BMV infection (Schwartz, Chen et al. 2002, Bamunusinghe, Seo et al. 2011). In the case of TBSV, the membrane-associated 33-kD replication protein (p33) is essential for the formation of pMVBs, but the sole expression of p33 targets peroxisomes, causing their progressive aggregation and eventually the formation of peroxisomal ghosts, which are not the same as the pMVBs (lacking the internal vesicles that appear to be derived from peroxisomal boundary membrane invagination) (McCartney, Greenwood et al. 2005). This indicates that the TBSV encoded membrane-associated 92-kD replication protein (p92), which interacts with p33, and possibly with other viral and/or host cell factors, is also needed for the formation of pMVBs.

5.2 Host proteins hijacked for replication factories formation

In recent years, more and more research has focused on the role of host factors during virus replication. Several host proteins that play key roles in the replication factories formation have been identified. These host proteins are normally involved in membrane bending, fusion or reshaping, such as the reticulon homology proteins (RHPs), the proteins from the early secretory pathway (COPI or COPII components involved in ER-Golgi transporting) or the late secretory pathway [endosomal sorting complexes required for transport (ESCRT) proteins involved in endosomal/ MVB protein-sorting].

1) RHPs

RHPs are a family of proteins involved in shaping the ER by inducing and stabilizing highly positively curved ER tubules (Voeltz, Prinz et al. 2006, Yang and Strittmatter 2007, Hu, Shibata et al. 2008). Reticulon 3 has been shown to directly interact with the enterovirus 2C protein and is thus likely engaged in induction and/or stabilization of positive membrane curvature of enterovirus replication factories (Tang,

Yang et al. 2007). BMV replicase protein 1a directly binds to and recruits reticulon proteins to spherules, and might stabilize positive membrane curvature in neck-like openings to the cytoplasm or facilitate expansion of the spherule volume by partially neutralizing overall negative membrane curvature (Diaz, Wang et al. 2010).

2) COPI or COPII components

GBF1, a guanine nucleotide exchange factor for Arf1, coordinates the formation and fusion of COPI vesicles in trafficking between ER and early Golgi (Bui, Golinelli-Cohen et al. 2009), was recognized as an essential factor for replication of enteroviruses such as poliovirus (Belov, Feng et al. 2008) and CVB3 (Lanke, van der Schaar et al. 2009), and was also implicated in replication of mouse hepatitis coronavirus (Verheije, Raaben et al. 2008) and HCV (Goueslain, Alsaleh et al. 2010). ADP ribosylation factor 1 (Arf1), a highly conserved small GTPase that is implicated in the formation of COPI vesicles (Brandizzi and Barlowe 2013), interacts with the *Red clover necrotic mosaic virus* (RCNMV) replication protein p27 within the virus-induced large punctate structures of the ER membrane (Hyodo, Mine et al. 2013).

Sar1, a small GTPase that regulates assembly of COPII at ER exit sites (Hanton, Chatre et al. 2008), was relocalized with p27 in p27-induced large aggregate structures of ER membranes (Hyodo, Mine et al. 2013). The expression of a dominant negative mutant, which inhibits COPII vesicle formation in plant cells, also inhibits RCNMV RNA accumulation (Hyodo, Mine et al. 2013).

3) ESCRT proteins

The ESCRT machinery plays major role in the sorting of cargo proteins from the endosomal limiting membrane to the lumen via membrane invagination and vesicle formation. TBSV replication protein p33 interacts with the vacuolar sorting protein Vps4p and three other ESCRT-III proteins and Vps4p is essential for the formation of spherules (Barajas, Martin et al. 2014).

6. Plant virus movement

Plant systemic infection involves cell-to-cell and long-distance movement of the virus (Fig. 8A). For cell-to-cell movement, the infectious viral unit moves through PDs from the initially infected cell to neighboring non-infected cells. Following multiple rounds of vRNA replication and cell-to-cell movement, the viral unit reaches vascular tissues and is downloaded into the vascular conducting tubes (phloem sieve elements and xylem vessel elements) (Fig. 8B). Once in the conducting tubes, the viral unit follows the flow of water and photoassimilates and is uploaded to distal parts of the plant, thus achieving systemic infection.

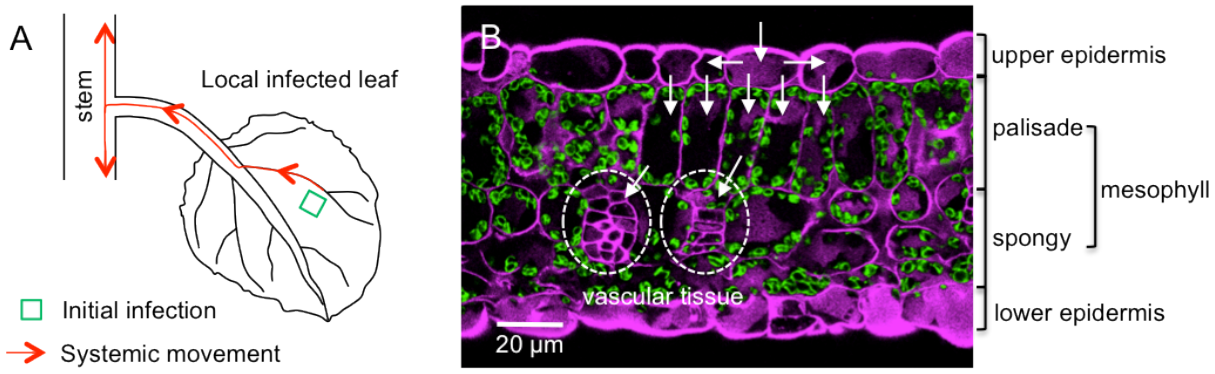

Figure 8. Plant virus movement.

(A) To establish systemic infection, plant viruses have to move cell-to-cell in the initially infected area (green square) to the vascular tissues (veins), and then move through vascular tissues to the rest part of the plant (red arrows). (B) Viruses normally enter and replicate in epidermal cells, then move cell-to-cell through PDs along the mesophyll cells to the vascular tissues. Once in the vascular tissue, they load into the vascular conducting tubes (the phloem sieve elements and xylem vessels) for long-distance movement. The cell wall is shown in magenta, and the chloroplasts are shown in green.

6.1 Cell-to-cell movement

6.1.1 Modification of PD by plant viruses

PDs are tightly controlled channels that normally allow the passive diffusion of small, soluble molecules. Plant virus particles or the free folded viral genomes are too large to pass through unmodified PD (Fig. 9A). Hence, plant viruses normally encode movement proteins (MPs) that increase the SEL of PD to facilitate their cell-to-cell movement. There are two types of MPs based on their functional properties. The first type is the nontubule forming MP that shows RNA-binding properties and mediates the translocation of viral ribonucleoprotein (vRNP) complexes without obvious structural reorganization of PD (e.g., TMV 30K (Meshi, Watanabe et al. 1987, Wolf, Deom et al. 1989)). The second type is the tubule forming MP that brings about a structural reorganization of the PD channel through the formation of tubules that provide the conduit for the movement of virus particles or vRNP from cell to cell (e.g., *Cowpea mosaic virus* [CPMV] MP (Wellink, van Lent et al. 1993)).

The potyviral genome does not code for any specific MP, but several multifunctional viral proteins are involved in cell-to-cell movement. The core domains of CP is involved in cell-to-cell movement (Dolja, Haldeman-Cahill et al. 1995). HCpro is also implicated in cell-to-cell movement, and both HCpro and CP modify SEL and promote vRNA movement from cell to cell (Rojas, Zerbini et al. 1997). Mutational analysis showed that CI protein is critical for cell-to-cell movement (Carrington, Jensen et al. 1998). It is suggested that the CI protein is anchored by the PD-located P3N-PIPO and positions the vRNP complex over the PD (Wei, Zhang et al. 2010).

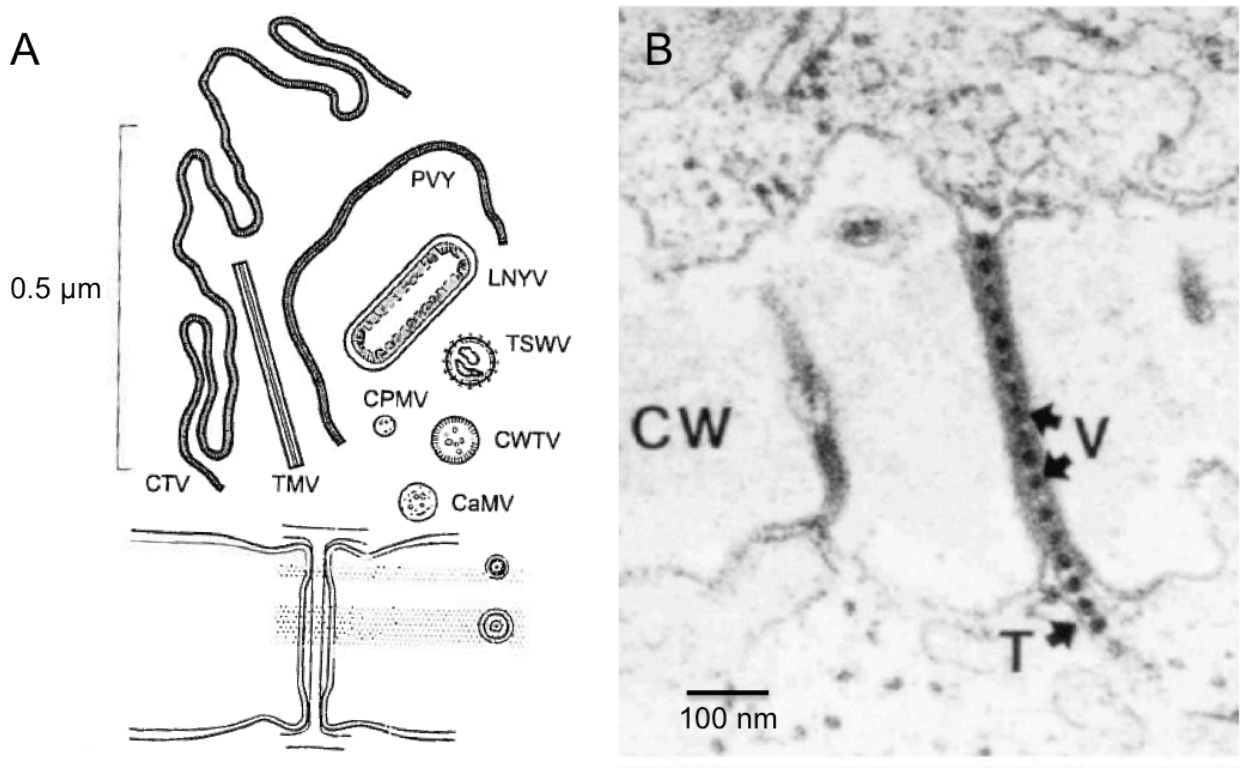

Figure 9. Plant viruses and PD.

(A) The relative size of some plant virus particles (above) compared with the size of a PD (below): CaMV, *Cauliflower mosaic virus*; CPMV, *Cowpea mosaic virus*; CTV, *Citrus tristeza virus*; LNYV, *Lettuce necrotic yellows virus*; TSWV, *Tomato spotted wilt virus*; WTV, *Wound tumor virus*. (B) Electron micrograph of *Strawberry mottle virus* (SMoV) systemically infected leaf of *C. quinoa* showing a tubular structure (T) with virus particles (V) in a plasmodesmata between adjacent mesophyll cells. CW, cell wall. (A) is taken from (Gibbs 1976) and (B) is taken from (Thompson, Leone et al. 2002).

6.1.2 The entity for plant virus cell-to-cell movement

The moving entities for cell-to-cell movement are thought to be viral particles or vRNP complexes. For some icosahedral plant viruses, particles have been detected within modified PD under TEM (Fig. 9B), indicating that they move their genome to the adjacent cells in a CP-encapsidated form (Ritzenthaler, Schmit et al. 1995, Thompson, Leone et al. 2002). However, the CP of some plant viruses is not required for cell-to-cell movement, or the CP is essential for cell-to-cell movement but particle formation is not required, suggesting that they move cell-to-cell as vRNP complexes. For instance, although the CP of TMV is essential for long-distance movement, it is not required for cell-to-cell movement (Carrington, Kasschau et al. 1996). The 30K MP of TMV increases the SEL of PD (Wolf, Deom et al. 1989) and possesses ssRNA-binding activity to form a transferable complex with vRNA (Wolf, Deom et al. 1989). In the case of CMV, both the MP and CP are essential for cell-to-cell movement (Canto, Prior et al. 1997), but the formation of virus particles is not required for its cell-to-cell movement (Kaplan, Zhang et al. 1998). The 3a MP of CMV increases the penetration capacity of the PDs (Ding, Li et al. 1995) and binds to ssRNA cooperatively (Li and Palukaitis 1996). Deletion of the C-terminal 33 amino acids of the CMV 3a MP resulted in CP-independent cell-to-cell movement, but not long-distance movement (Kim, Kalinina et al. 2004). However, the exact nature of the trafficking vRNP complexes is still not defined.

An emerging concept is that vRNA replication and movement are tightly linked processes. For example, it has been proposed that TMV moves from cell to cell as intact replication complexes (Kawakami, Watanabe et al. 2004). Replication and trafficking of *Potato virus X* (PVX) have also been shown to be coupled at the entrance of PD (Tilsner, Linnik et al. 2013). Furthermore, TuMV-induced membrane-bound replication complexes have been observed by live-cell imaging to move from one cell to another (Grangeon, Jiang et al. 2013). The vRNP complex may then be the viral replication complex.

6.2 Long-distance movement

6.2.1 Vascular tissue differentiation and the conducting tubes

Mature vascular tissue consists of highly specialized cell types that generally arise from discrete populations of undifferentiated progenitor cells located in meristem niches (Schuetz, Smith et al. 2013). The *de novo* differentiation of parenchyma cells could result in the formation of procambial cells (Fig. 10A, a), which are vascular precursor cells. Once formed, individual procambial cells can undergo periclinal divisions (parallel to the plane of cell elongation) (Fig. 10A, b), ultimately giving rise to the procambium tissue, from which specialized xylem and phloem cells are subsequently formed. However, a subset of cells within the procambium remains in an undifferentiated state, positioned between the differentiating xylem and phloem tissues (Fig. 10A, c). These cells function as vascular stem cells and enable the prolonged formation of vascular tissues in rapidly elongating or expanding organs such as young stems and leaves during primary plant growth (Fig. 10A, c). The procambium provides a source of vascular stem cells during primary growth (Fig. 10A, d), while the vascular cambium and associated cambial cells perform an analogous role during secondary growth as the plant continues to grow and mature (Fig. 10A, c). Differentiation of vascular tissues from the procambium/vascular cambium follows two different developmental pathways to produce xylem and phloem (Fig. 10A, e and f).

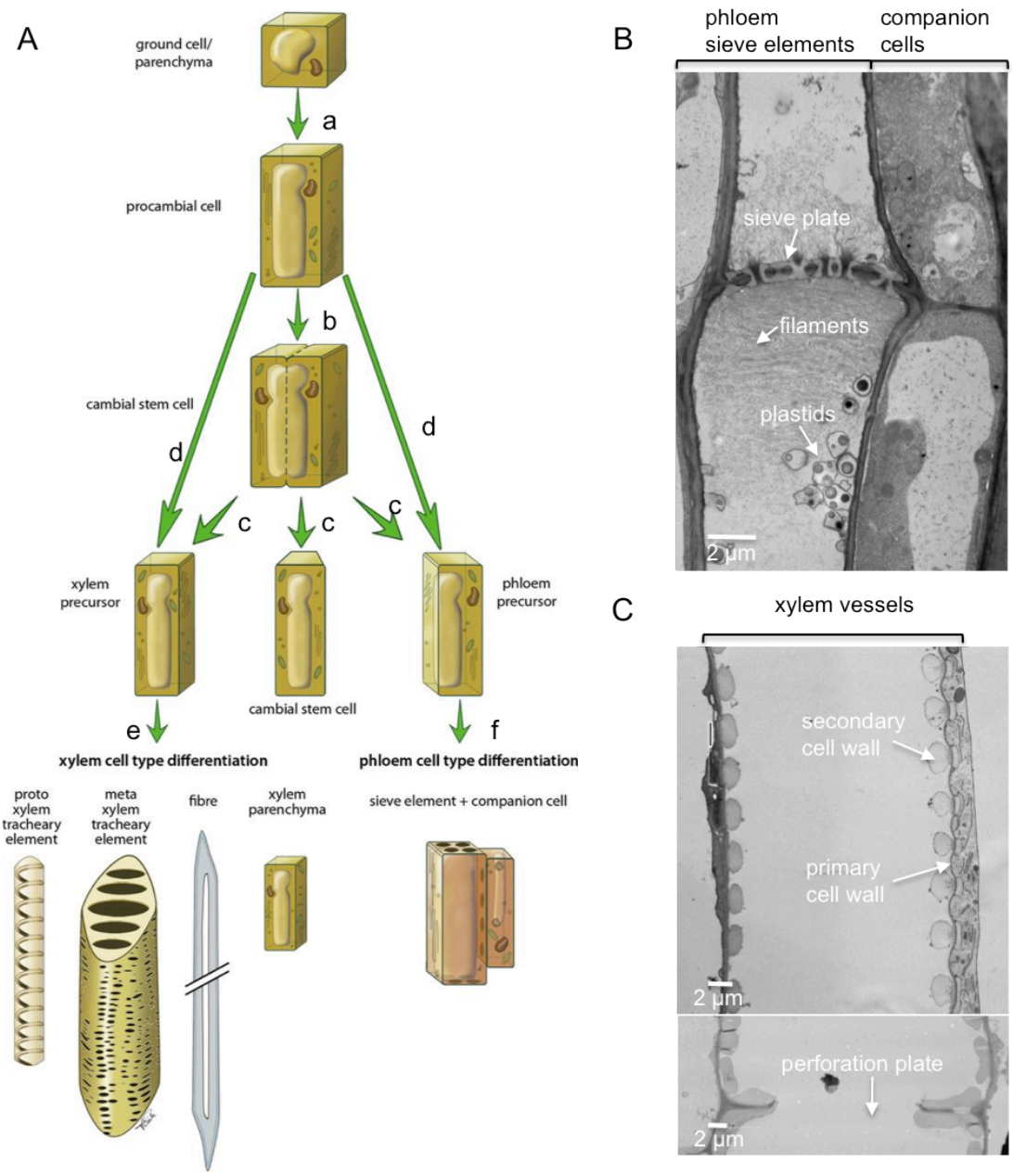

Figure 10. Differentiation and structure of plant vascular tissue.

(A) Overview of procambial/cambial cell specification and xylem/phloem cell differentiation. Procambial cells can form by the *de novo* differentiation of parenchyma cells (a), or by division of existing procambial cells during primary growth, thereby forming the procambium. The vascular cambium and associated cambial cells are derived from the procambium during the transition to secondary growth, at which point the nomenclature of 'procambial' cells no longer applies and 'cambial' cells is used instead (b). Cambial/procambial cells differentiate into either xylem or phloem cell types (c to f). (B) Ultrastructure of phloem sieve elements and xylem vessels. (A) is taken from (Schuetz, Smith et al. 2013).

1) Phloem

Mature phloem tissues of angiosperms consist of sieve elements, phloem companion cells and parenchyma cells. The conducting tubes of the phloem are the sieve elements, which assemble into sieve tubes to form a continuous microfluidics network throughout the plant body (Fig. 10B). Sieve tubes function to transport photoassimilates and signals from source to sink tissues, such as leaves, roots and seeds. Many of the organelles, such as the nucleus, the vacuole, ribosomes, Golgi, and the cytoskeleton are lost during sieve elements differentiation. But sieve elements are not empty tubes, since they still contain smooth ER, mitochondria and sieve element plastids that are appressed against the sieve elements wall, as well as phloem protein [p proteins (Knoblauch and Peters 2010)] filaments located at the margins and also clotted in the lumen of sieve elements (Froelich, Mullendore et al. 2011) (Fig. 10B). The mature sieve element relies on the associated companion cells for maintenance of its physiological function (Fisher, Wu et al. 1992). The specialized PD connecting one sieve element with one companion cell is called pore plasmodesmal units (PPUs). Different from the other PDs, PPUs are always branched on the companion cell side, but have only one channel on the sieve element side (Oparka and Turgeon 1999).

2) Xylem

Mature xylem tissues are composed of three main cell types: xylem tracheary (vessel) elements, xylary fibres, and xylem parenchyma cells (Fig. 10A). The conducting tubes of the xylem are the xylem vessels. Vessel elements are the building blocks of xylem vessels, which constitute the major part of the water and solute upward transporting system in a plant. The side walls of mature vessel elements contain pits, which are areas lacking a secondary cell wall; the end walls of the mature vessel elements are removed, and the openings are called perforation plates (Roberts and McCann 2000) (Fig. 10C).

Vessel elements that are formed during early and later stages of plant and vascular development are structurally distinguished as protoxylem and metaxylem (Fig. 10A) (Schuetz, Smith et al. 2013). Protoxylem vessel elements form during primary plant growth and deposit localized annular or helical secondary cell wall thickenings,

reinforcement patterns that allow these cells to continue to elongate within actively growing areas of the plant. As vascular tissues mature and primary growth ceases, relatively larger metaxylem vessel elements are formed. These are marked by a distinctive pitted or reticulate pattern of secondary cell wall deposition. Unlike the protoxylem wall thickenings, this pattern of secondary cell wall deposition does not allow continued cell elongation, and thus the shape of the metaxylem precursor cells is reflected in the radial and axial dimensions of the mature metaxylem vessels. As a final stage of differentiation, both protoxylem and metaxylem vessel elements undergo programmed cell death, resulting in a continuous system of adjoining hollow cells.

6.2.2 Modification of vascular conducting tubes by plant viruses

1) Phloem loading and unloading of viral materials

Most plant viruses move systemically through the phloem along the source-to-sink flow of photoassimilates for long-distance movement [reviewed in (Hipper, Brault et al. 2013)]. It is believed that the loading and uploading of viral material during phloem transport are through PPUs. Even though the SEL of PPUs (Kempers and Bel 1997) is larger than that of the other PDs (Wolf, Lucas et al. 1989, Derrick, Barker et al. 1990), PPUs should not allow, in their native state, viral particles or vRNP complexes to pass through. It is thus believed that specific interactions between virus and host factors are required to allow the viral entity to go through. For instance, the MP of CMV is targeted to PPUs and enter the sieve elements (Blackman, Boevink et al. 1998), suggesting that this viral protein modifies the SEL of PPUs and helps viral entry into sieve elements.

The viral entity loads into phloem sieve elements through PPUs in all vein classes of source leaves (Cheng, Su et al. 2000, Silva, Wellink et al. 2002). The viral phloem unloading pattern is similar to the phloem-mobile dye 5(6)-carboxyfluorescein diacetate (CFDA), which is limited to major veins of sink leaves (Roberts, Cruz et al. 1997, Cheng, Su et al. 2000, Silva, Wellink et al. 2002).

2) Xylem loading and unloading of viral materials

CP or viral particles of some viruses have also been observed in xylem vessels and/or guttation fluid, suggesting that these viruses may move systemically through

xylem vessels. It has been proposed that replicating viruses enter into immature xylem vessel elements. Upon programmed cell death, these become hollow vessels, thereby releasing viruses into the water flow (Opalka, Brugidou et al. 1998). Colocalization of anti- *Rice yellow mottle virus* (RYMV) antibodies and a cell wall marker for cellulosic β-(1–4)-D-glucans over vessel pit membranes suggests that the pit membranes might be a pathway for virus migration between vessels (Opalka, Brugidou et al. 1998). Viral uploading into xylem parenchymal cells would also take place through pit membranes (Opalka, Brugidou et al. 1998, Verchot, Driskel et al. 2001).

6.2.3 The entity for plant virus long-distance movement

Both viral particles and yet-to-be-defined vRNP complexes have been implicated as the unit for plant virus long-distance movement.

Some viruses are believed to move systemically as viral particles since CP deletions debilitating virus assembly prevent systemic infection (Brault, Bergdoll et al. 2003, Zhang, Zhao et al. 2013, Hipper, Monsion et al. 2014), and some virus particles are observed in the vascular conducting tubes or their sap. For instance, some investigations showed the actual presence of viral particles in sieve elements. This is the case for the icosahedral *Tobacco ringspot virus* (TRSV) (Halk and McGuire 1973) and *Carrot red leaf virus* (CRLV) (Murant and Roberts 1979) (Fig. 11A). In addition, viral particles were also observed in phloem sap, such as the icosahedral CMV (Requena, Simón-Buela et al. 2006) and the rigid rod-shaped *Cucumber green mottle mosaic virus* (CGMMV) (Simón-Buela and García-Arenal 1999). For the xylem, icosahedral RYMV particles were found in xylem vessels (Fig. 11B) (Opalka, Brugidou et al. 1998). Flexuous rod-shaped viral particles of *Zucchini yellow mosaic virus* (ZYMV) were found in both xylem vessels of root tissue and the guttation fluid (French and Elder 1999) (Fig. 11C). Moreover, icosahedral BMV (Ding, Boydston et al. 2001), and rigid rod-shaped *Tomato mosaic virus* (ToMV) and *Pepper mild mottle virus* (PMMV) (French, Elder et al. 1993) particles were found in guttation fluid. Guttation fluid originates from xylem exudate, indicating that these plant viruses can move through xylem within the infected plant.

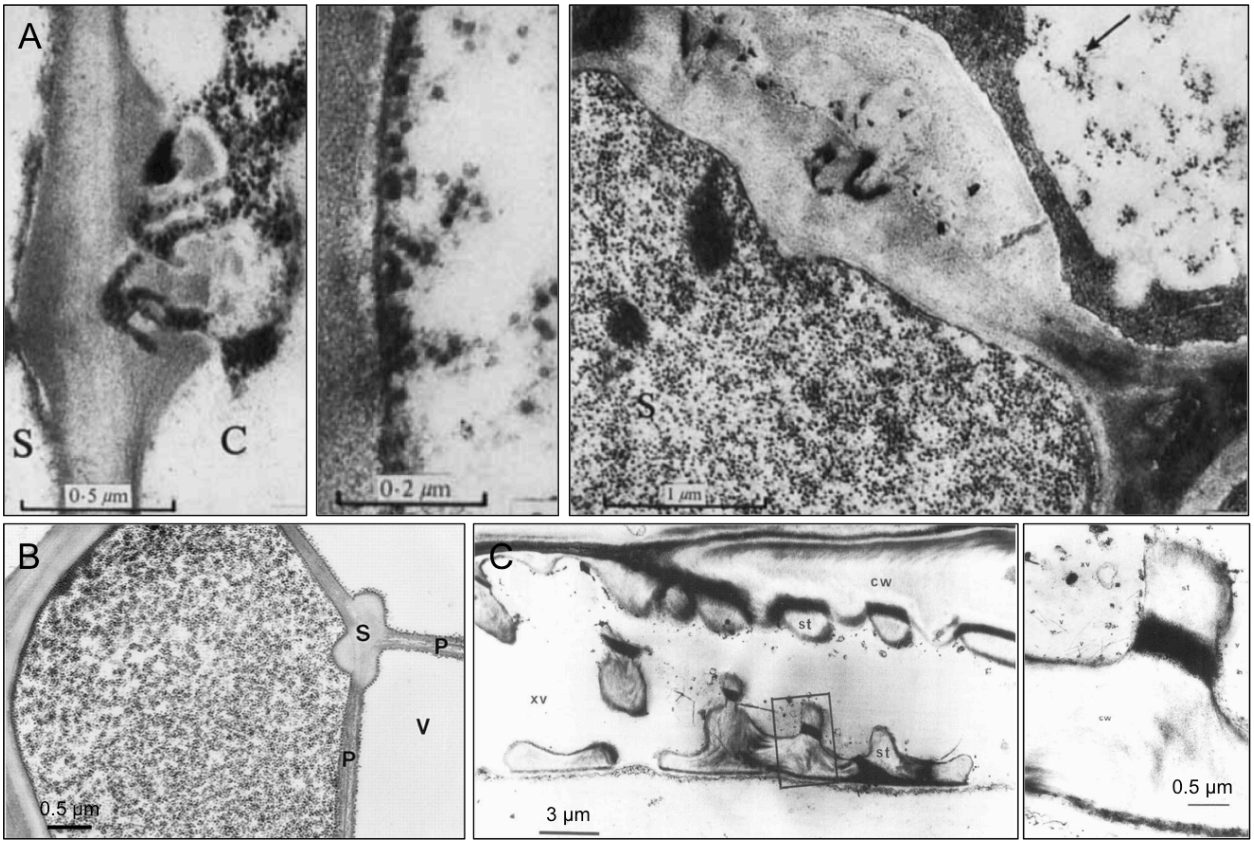

Figure 11. Plant virus particles are associated with vascular conducting tubes.

(A) In CRLV infected chervil (*Anthriscus cerefolium*), particles were found in the branched PD linking companion cells and sieve elements (left panel), usually sparsely distributed and occurred in the parietal region of the sieve elements (middle panel), and sometimes appeared entirely filling the sieve elements (right panel). (B) A xylem vessel of RYMV-infected plants with virus particles. S, secondary walls; P, pit membrane; V, vessel. (C) ZYMV particles in longitudinal-section of fully differentiated xylem vessel from *Cucumis sativus* L.root. XV, xylem vessel; st, secondary thickening; CW, cell wall; V, virus particles. (A) is taken from (Murant and Roberts 1979), (B) is taken from (Opalka, Brugidou et al. 1998) and (C) is taken from (French and Elder 1999).

Alternatively, some viruses are believed to move as vRNP complexes since systemic movement was still observed when the CP gene has been deleted from the viral genome (Swanson, Barker et al. 2002, Savenkov, Germundsson et al. 2003, Gopinath and Kao 2007, Manabayeva, Shamekova et al. 2013), such as *Tobacco rattle virus* (TRV), *Potato mop-top virus* (PMTV), BMV and TBSV. The CP of the icosahedral TBSV (Manabayeva, Shamekova et al. 2013) and RYMV (Opalka, Brugidou et al. 1998), the CP of the rigid rod-shaped *Soilborne wheat mosaic virus* (SBWMV) (Verchot, Driskel et al. 2001) and the flexuous rod-shaped PVX (Betti, Lico et al. 2012) were detected in xylem vessels, but it was not clear if the moving entities were particles or CP-associated vRNP complexes.

The above studies, however, mainly relied on electron microscopy and infections assays, and may have missed the presence of other viral components that might be involved in transport.

For potyviruses, it is still not clear if long-distance transport involves exclusively viral particles or if vRNP complexes are also implicated (Dolja, Haldeman et al. 1994, Cronin, Verchot et al. 1995, Dolja, Haldeman-Cahill et al. 1995, Schaad, Lellis et al. 1997, Kasschau and Carrington 2001, Rajamaki and Valkonen 2002). But whether viral particles or vRNP complexes are involved in viral movement, the full nature of the viral entity being implicated has not been defined.

7. Cellular remodeling during potyvirus infection

7.1 TuMV replication factories

TuMV infection induces the formation of numerous motile vesicles that originate from the ER (Fig. 12A). Many accumulates near the nucleus, forming a perinuclear globular structure (Fig. 12A) containing ER, Golgi, COPII membranes and chloroplasts (Grangeon, Agbeci et al. 2012). This globular structure maintains a dynamic connection with cortical ER and Golgi apparatus. Additionally the motile vesicles (see below) are functionally linked to the perinuclear globular structure, suggesting the globular structure could provide an extended platform for viral replication and protein synthesis (Grangeon, Agbeci et al. 2012). These vesicles move rapidly along microfilaments (Beauchemin, Boutet et al. 2007, Cotton, Grangeon et al. 2009, Grangeon, Agbeci et al. 2012) and use the secretory pathway and myosin motors (Agbeci, Grangeon et al. 2013) to ultimately reach PDs for delivery into adjacent cells for cell-to-cell infection (Grangeon, Jiang et al. 2013).

TuMV induced-vesicles contain vRNA as well as several replication-related viral proteins (VPg-Pro, vRdRp, CI) and host proteins [eukaryotic translation initiation factor iso4E (eIF(iso)4E), PABP, Hsc70-3, and eEF1A], and are thus considered to be the site of vRNA replication (Beauchemin, Boutet et al. 2007, Beauchemin and Laliberté 2007, Dufresne, Thivierge et al. 2008, Cotton, Grangeon et al. 2009, Agbeci, Grangeon et al. 2013). Among these proteins, the viral protein VPg, which is covalently linked to the 5' end of the vRNA, functions as a hub protein that interacts with itself, several viral and host proteins, thus controlling many processes leading to virus production and spread (Fig. 12B) (Jiang and Laliberté 2011).

The viral membrane protein $6K_2$ is responsible for vesicle formation (Schaad, Jensen et al. 1997, Beauchemin, Boutet et al. 2007). Recently, the molecular mechanisms of $6K_2$ functioning during the biogenesis of TuMV vesicles has been studied in our laboratory. The N-terminal deletion mutant of $6K_2$ shows ER retention, indicating the presence of ER export signal in the N-terminal of $6K_2$, and the N-terminal single amino-acid mutation $6K_2$W15A mutation reduces TuMV replication level and abolishes the cell-to-cell movement (Jiang, Patarroyo et al. 2015). $6K_2$ can physically

intact with the COPII coatomer component Sec24a, and both cell-to-cell and systemic movements are slowed down in a Sec24a dysfunctional *Arabidopsis thaliana* plant, (Jiang, Patarroyo et al. 2015). Thus, $6K_2$ interacts with the early secretory pathway component Sec24a for membrane remodeling and virus movement.

Furthermore, TuMV exploits multiple subcellular membranes for replication, since in addition to ER membranes, the chloroplast membrane is also important for TuMV infection. TuMV $6K_2$ was observed to fuse with the chloroplast envelope (Wei, Huang et al. 2010). Vesicle fusion is apparently controlled by the Syp71 SNARE protein (Wei, Zhang et al. 2013).

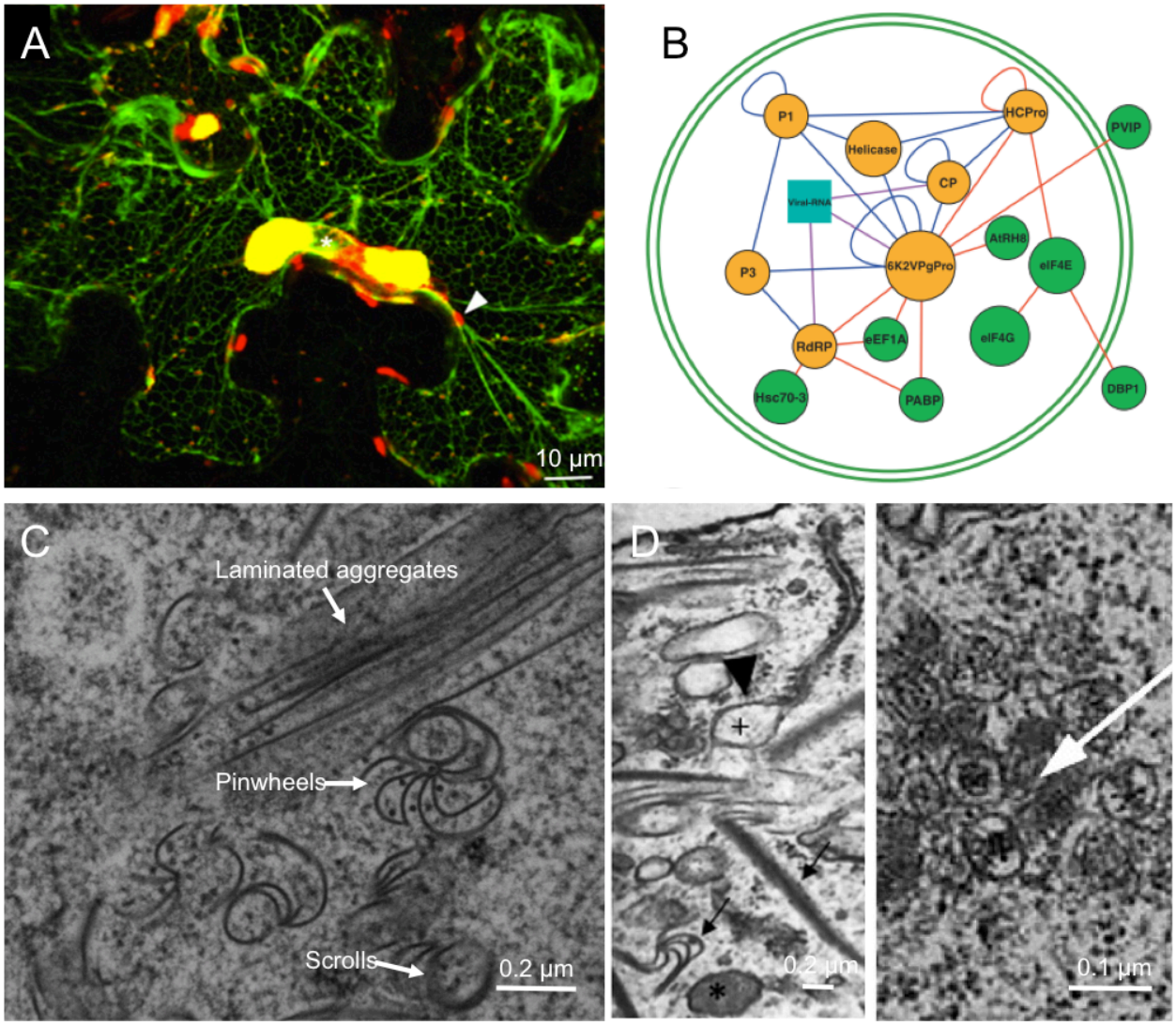
A
10 µm
B
P1
HCPro
PVIP
Helicase
CP
Viral-RNA
AtRH8
P3
6K2VPgPro
eIF4E
RdRP
eEF1A
eIF4G
Hsc70-3
PABP
DBP1
C
Laminated aggregates
Pinwheels
Scrolls
0.2 µm
D
0.2 µm
0.1 µm

Figure 12. Potyvirus induced cellular remodeling.

(A) Three-dimensional confocal microscopy images of leaf epidermal cells of *N. benthamiana* showing GFP-HDEL (green) in TuMV-infected cells expressing $6K_2$:mCherry (red) 4 days after agroinfiltration. White arrowhead indicates the linkage between the globular structure and the cortical ER through transvacuolar strands. (B) Interaction map of the potyvirus VPg. Circles depicted in orange are viral proteins and in green are plant proteins. Interactions connecting the protein nodes are represented by color-coded lines: in blue are interactions uncovered by one assay; in red are interactions supported by two or more assays; in black are interactions reported in the predicted Arabidopsis Interaction Resource (PAIR) database; in magenta are protein-RNA interaction. Interactions taking place within viral replication factories are shown within the green circle. (C) TEM image shows 3 types of TuMV-induced CI: pinwheels, scrolls, laminated aggregates. (D) Ultrastructure of potyvirus induced vesicles. Left: TuMV-induced electron-translucent (+) and -opaque (*) vesicles, the black arrowhead denote vesicle closely associated with tubular ER, black arrows point CI close to the vesicles. Right: PVY-induced vesicles with an electron-dense content (white arrow). (A) is taken from (Grangeon, Agbeci et al. 2012), (B) is taken from (Jiang and Laliberté 2011) and (D) is taken from (Grangeon, Agbeci et al. 2012) (left) and (Otulak and Garbaczewska 2012) (right).

7.2 Ultrastructure of TuMV induced cellular remodeling

The above studies about potyvirus relied mainly on light microscopy observations. The most recent ultrastructural analyses of cellular reorganization during potyvirus infections have focused on the description of nuclear and cytoplasmic inclusions (Fig. 12C) (Edwardson, Christie et al. 1984, Achon, Pinner et al. 1996, Otulak and Garbaczewska 2010, Otulak and Garbaczewska 2012). TEM images of virus-induced vesicles have also been reported for TuMV- (Grangeon, Agbeci et al. 2012) and PVY- infected cells (Otulak and Garbaczewska 2012) (Fig. 12D). These images showed the presence of numerous SMVs, and on some occasions, the vesicles were found to be in direct continuity with the rough ER. There have been, however, no studies looking at the biogenesis of these vesicles over the time course of viral infection, and their relationship with viral particle assembly.

8. Problematic and research objectives

TuMV is one of the widely studied potyviruses, and it has a very wide host range infecting most cruciferous plants. TuMV infected plants are stunted, the leaves are distorted, with black spots. Early infection of cabbage by TuMV in the seedbed or soon after transplanting can reduce yield by 75%. Understanding the cell and molecular biology of how TuMV takes over the host cell is a prerequisite to develop new resistance strategies.

As mentioned above, TuMV induces $6K_2$-tagged replication factories, and the $6K_2$-tagged membrane-associated replication complexes are also involved in TuMV intracellular and intercellular movement. My first research objective was to investigate if $6K_2$-tagged replication factories could be involved in virus long-distance movement. Therefore, my specific objectives to achieve this goal were to:

1) Observe the appearance and distribution of $6K_2$-tagged structures in TuMV-infected leaf and stem sections prepared by cryosectioning, focusing especially on the vascular conducting tubes (phloem sieve elements and xylem vessels).

2) Test if those $6K_2$-tagged structures in the other cell types contain the replication complexes by immunohistolocalization.

Although electron-translucent and electron-opaque SMVs, which are occasionally connected with rough ER, have been observed in TuMV-infected cells under TEM, the exact functions of these vesicles are not clear. In addition, (+) RNA virus particles assembly sites are generally shown close to the replication factories, but TuMV particles assembly sites are still not known. Therefore, the second research objective was to better define the ultrastructure of TuMV-induced cellular reorganization. My specific objectives to achieve this goal were to:

1) Perform time course analysis of TuMV-induced cellular reorganization under TEM.

2) Determine the localization of vRNA, viral and host proteins in TuMV-induced membrane structures, and to confirm their exact functions during the infectious cycle by immunogold labeling;

3) Conduct TEM-ET to generate a 3D model of TuMV-induced membrane structures to better understand the biogenesis of those structures.

CHAPTER 2: PUBLICATION NO. 1

Turnip mosaic virus moves systemically through both phloem and xylem as membrane-associated complexes

Plant Physiology

April 2015, Vol. 167, No. 4, p.1374-1388.

Juan Wan[1], Daniel Garcia Cabanillas[1], Huanquan Zheng[2],

and Jean-François Laliberté[1*]

1. INRS-Institut Armand-Frappier, Laval, Québec, Canada
2. Department of Biology, McGill University, Montréal, Québec, Canada

*** Author for correspondence**: Prof. Jean-François Laliberté

Address : INRS-Institut Armand Frappier

531, boulevard des Prairies, Laval, Québec, Canada, H7V 1B7

Tel: 1.450.687.5010

Email: jean-francois.laliberte@iaf.inrs.ca

Contribution of student

This manuscript has been published in *Plant Physiology*. I designed and performed almost all of the experimental work and analysed data with advice from my supervisor Professor Jean-François Laliberté. I prepared the first draft of this manuscript, and Jean-Francois Laliberté helped me improve the writing. My colleague Daniel Garcia Cabanillas did some experimental work, which is showed in Figure 7. He also helped in correcting the manuscript.

Résumé

Les virus de plante se déplacent systémiquement dans une plante au travers du phloème. Ils se déplacent sous forme de virions ou sous forme de complexes ribonucléoprotéiques. Cependant, la nature exacte de ces complexes n'est absolument pas claire. Le génome d'ARN du virus de la mosaïque du navet (*Turnip mosaic virus*, TuMV) d'environ 10 kb code entre autre pour une protéine membranaire appelée $6K_2$. Cette dernière réaménage le système endomembranaire de l'hôte pour induire la formation d'usines de replication virale. Les usines virales du TuMV sont des vésicules qui contiennent l'ARN viral (ARNv) et des protéines virales impliquées dans la réplication. Dans cette étude, nous démontrons la présence de vésicules contenant la $6K_2$, l'ARNv et l'ARN polymérase ARN dépendante virale (vRdRp) dans les tubes criblés du phloème et les vaisseaux du xylème. Les observations menées par microscopie électronique ont dévoilé la présence de vésicules contenant l'ARNv en étroite association avec des particules virales. Des expérimentations visant à détruire toute cellule vivante autour du xylème sur une portion de la tige (stem girdling) a confirmé que le TuMV peut établir une infection systémique en passant au travers des vaisseaux du xylème. Des plantes infectées par le *Potato virus X* présentaient elles aussi de l'ARNv non encapsidé en association avec des membranes à la fois dans les tubes criblés du phloème et les vaisseaux du xylème. Ceci suggère que la présence de complexes ribonucléoprotéiques en association avec des membranes dans le phloème et le xylème n'est pas une caractéristique limitée au TuMV seul. Pris ensemble ces études indiquent que les usines virales peuvent se retrouver dans le phloème et le xylème.

Abstract

Plant viruses move systemically in plants through the phloem. They move as virions or as ribonucleic protein complexes, although it is not clear what these complexes are made of. The approximately 10-kb RNA genome of *Turnip mosaic virus* (TuMV) encodes a membrane protein, known as $6K_2$, that induces endomembrane rearrangements for the formation of viral replication factories. These factories take the form of vesicles that contain viral RNA (vRNA) and viral replication proteins. In this study, we report the presence of $6K_2$-tagged vesicles containing vRNA and the vRNA-dependent RNA polymerase in phloem sieve elements and in xylem vessels. Transmission electron microscopy observations showed the presence in the xylem vessels of vRNA-containing vesicles that were associated with viral particles. Stem-girdling experiments, which leave xylem vessels intact but destroy the surrounding tissues, confirmed that TuMV could establish a systemic infection of the plant by going through xylem vessels. Phloem sieve elements and xylem vessels from *Potato virus X*-infected plants also contained lipid-associated nonencapsidated vRNA, indicating that the presence of membrane-associated ribonucleic protein complexes in the phloem and xylem may not be limited to TuMV. Collectively, these studies indicate that viral replication factories could end up in the phloem and the xylem.

Introduction

Plant viruses use the host preexisting transport routes to propagate infection to the whole plant. After replication in the initially infected cells, viruses move cell to cell through plasmodesmata (PDs) and start a new round of replication in the newly infected cells. This cycle is repeated until viruses reach vascular tissues, where they enter into the conducting tubes for systemic movement. Several studies have indicated that plant viruses are passively transported along the source-to-sink flow of photoassimilates and thus are believed to move systemically through the phloem (for review, see Hipper et al., 2013).

The conducting tube of the phloem is the sieve element. The mature sieve element is enucleated and relies on the associated companion cells for the maintenance of its physiological function (Fisher et al., 1992). The specialized PD connecting one sieve element with one companion cell is called the pore plasmodesmal unit (PPU). Different from the other PDs, PPUs are always branched on the companion cell side but have only one channel on the sieve element side (Oparka and Turgeon, 1999). It is believed that the loading and uploading of viral material during phloem transport are through PPUs. Even though the size exclusion limit of PPUs (Kempers and Bel, 1997) is larger than that of the other PDs (Wolf et al., 1989; Derrick et al., 1990), PPUs should not allow, in their native state, virions or viral ribonucleoprotein (vRNP) complexes to pass through. It is thus believed that specific interactions between virus and host factors are required to allow the viral entity to go through. For instance, the movement protein of *Cucumber mosaic virus* (CMV) is targeted to PPUs (Blackman et al., 1998), suggesting that this viral protein modifies the size exclusion limit of PPUs and helps viral entry into sieve elements.

Most plant viruses are assumed to move systemically through the phloem as virions. This assumption is based on the observation that Coat Protein (CP) deletions debilitating virus assembly prevent systemic infection (Brault et al., 2003; Zhang et al., 2013; Hipper et al., 2014). Some investigations showed the actual presence of virions in sieve elements. This is the case for the icosahedral *Tobacco ringspot virus* (Halk and McGuire, 1973), *Carrot red leaf virus* (Murant and Roberts, 1979), *Potato leaf roll virus*

(Shepardson et al., 1980), and *Beet western yellows virus* (Hoefert, 1984). In addition, virions also were observed in phloem sap, such as the icosahedral CMV (Requena et al., 2006) and the rigid rod-shaped Cucumber green mottle mosaic virus (Simón-Buela and García-Arenal, 1999). Some viruses also are believed to move as ribonucleic protein (RNP) complexes, since systemic movement was observed in CP mutants where virion assembly was hindered. For instance, *Tobacco rattle virus*, *Potato mop-top virus*, *Brome mosaic virus*, and *Tomato bushy stunt virus* can still move systemically when the CP gene has been deleted from the viral genome (Swanson et al., 2002; Savenkov et al., 2003; Gopinath and Kao, 2007; Manabayeva et al., 2013). For potyviruses, it is still not clear if long-distance transport involves exclusively viral particles or if vRNP complexes also are implicated (Dolja et al., 1994, 1995; Cronin et al., 1995; Schaad et al., 1997; Kasschau and Carrington, 2001; Rajamaki and Valkonen, 2002). But whether virions or vRNP complexes are involved in viral movement, the full nature of the viral entity being implicated has not been defined.

Xylem also is used for systemic infection of viruses, but its importance in viral transport generally has been overlooked. Vessel elements are the building blocks of xylem vessels, which constitute the major part of the water-upward-transporting system in a plant. The side walls of mature vessel elements contain pits, which are areas lacking a secondary cell wall; the end walls of the mature vessel elements are removed, and the openings are called perforation plates (Roberts and McCann, 2000). CP or virions of some plant viruses of all different shapes have been detected in the xylem vessels and/or guttation fluid, suggesting that these viruses may move systemically through xylem vessels. For example, the CP of the icosahedral *Tomato bushy stunt virus* (Manabayeva et al., 2013) and *Rice yellow mottle virus* (Opalka et al., 1998), the CP of the rigid rod-shaped *Soilborne wheat mosaic virus* (Verchot et al., 2001) and *Cucumber green mottle mosaic virus* (Moreno et al., 2004), and the flexuous rod-shaped *Potato virus X* (PVX; Betti et al., 2012) were detected in xylem vessels. Colocalization of anti-*Rice yellow mottle virus* antibodies and a cell wall marker for cellulosic β-(1-4)-D-glucans over vessel pit membranes suggests that the pit membranes might be a pathway for virus migration between vessels (Opalka et al., 1998). Moreover, flexuous rod-shaped virions of *Zucchini yellow mosaic virus* were

found in both xylem vessels of root tissue and the guttation fluid (French and Elder, 1999). Finally, icosahedral *Brome mosaic virus* (Ding et al., 2001) and rigid rod-shaped *Tomato mosaic virus* and *Pepper mild mottle virus* (French et al., 1993) virions were found in guttation fluid. Guttation fluid originates from xylem exudate, indicating that these plant viruses can move through xylem within the infected plant. The above studies, however, mainly relied on electron microscopy and infection assays and may have missed the presence of other viral components that might be involved in transport.

Turnip mosaic virus (TuMV) is a positive-strand RNA virus belonging to the family Potyviridae, genus Potyvirus, which contains around 30% of the currently known plant viruses and causes serious diseases in numerous crops (Shukla et al., 1994). Potyviruses are nonenveloped, flexuous rod-shaped particles of 680 to 900 nm in length and 11 to 13 nm in diameter. The genomic approximately 10-kb RNA encodes a polyprotein, which is processed into at least 11 mature proteins. TuMV remodels cellular membranes into viral factories, which are intracellular compartments involved in viral replication and movement. These compartments take the form of vesicles of approximately 100 nm in diameter originating from the endoplasmic reticulum (Grangeon et al., 2012). These vesicles contain viral RNA (vRNA) and viral and host proteins involved in vRNA replication (Beauchemin et al., 2007; Beauchemin and Laliberté, 2007; Dufresne et al., 2008; Huang et al., 2010; Grangeon et al., 2012). The viral membrane $6K_2$ protein is involved in the membrane alterations and vesicle production (Beauchemin et al., 2007). The membrane-bound replication complexes can move intracellularly and cell to cell (Grangeon et al., 2013) at a rate of one cell being infected every 3 h (Agbeci et al., 2013). Intercellular trafficking of the replication complex is likely mediated by the PD-localized potyviral proteins Cytoplasmic Inclusion (CI) and P3N-PIPO (for N-terminal Half of P3 fused to the Pretty Interesting Potyviridae ORF; Carrington et al., 1998; Wei et al., 2010; Vijayapalani et al., 2012) as well as CP (Dolja et al., 1994, 1995), Viral Protein genome-linked (VPg; Nicolas et al., 1997; Rajamaki and Valkonen, 1999, 2002), and Helper Component-Proteinase (HC-Pro; Cronin et al., 1995; Kasschau et al., 1997; Rojas et al., 1997; Kasschau and Carrington, 2001), which are involved in both cell-to-cell and vascular movement.

It is expected that, ultimately, TuMV reaches the vascular tissues of the plant, but how and under what form it is released into the conducting tubes are not known. To further understand viral spread and systemic movement, we investigated the distribution of $6K_2$-tagged TuMV factories in all of the leaf and stem tissues other than the epidermal cells. We found TuMV factories in all tissues. Interestingly, we observed $6K_2$-tagged vesicles, containing vRNA and viral replication proteins, in both phloem sieve elements and xylem vessels. We confirmed that TuMV could move systemically through xylem by a so-called stem-girdling assay, which induces cell death of the phloem without affecting xylem integrity. Hence, our study indicates that membrane-associated TuMV replication complexes are involved in the systemic movement of the virus.

Materials and Methods

Plasmid DNA and Plant Inoculation

Turnip mosaic virus infectious clone was engineered to coproduce $6K_2$ as a fluorescence protein fusion at its C-terminal end to form the plasmids pCambiaTuMV/$6K_2$:GFP and pCambiaTuMV/$6K_2$:mCherry (Cotton et al., 2009). The $6K_2$:GFP or $6K_2$:mCherry coding region was inserted between P1 and HC-Pro cistrons of the TuMV genome. The junctions flanking P1 and HC-Pro contained residues recognized by the P1 and Pro proteinases, respectively. $6K_2$:GFP or $6K_2$:mCherry is thus released from the polyprotein when the latter is processed during infection. TuMV infectious clones and the mock empty vector pCambia 0390 were electroporated into Agrobacterium tumefaciens strain AGL1 and selected on Luria-Bertani ampicillin-kanamycin plates. The pellet of an overnight culture was resuspended in water supplemented with 10 mM $MgCl_2$ and 150 µM acetosyringone and kept at room temperature for 2 to 4 h. The solution was then diluted to an optical density at 600 nm of 0.2. Agroinfiltration was performed in 4-week-old *N. benthamiana* plants, which were grown under a 16-h-light/8-h-dark photoperiod with 22°C day/20°C night temperatures.

Antibodies

The mouse monoclonal anti-dsRNA J2 antibody (stock solution is 1 mg mL^{-1}; English and Scientific Consulting) was used at the following dilutions: for immunohistolocalization, 1:500; and for immunogold labeling, 1:40. The rabbit polyclonal antibodies were used at the following dilutions for immunolocalization: for anti-vRdRp (Dufresne et al., 2008), 1:50; and for anti-CP (Cotton et al., 2009), 1:50. The dilutions for western-blot analysis were as follows: anti-GFP, 1:20,000; anti-vRdRp, 1:6,000; anti-eIF(iso)4E (Léonard et al., 2004), 1:1,000; anti-CP, 1:2,500; and anti-PTB3 (Rühl et al., 2012), 1:5,000.

For immunohistolocalization, goat anti-mouse and goat anti-rabbit conjugated to Alexa Fluor 568 secondary antibodies (Molecular Probes) were used at a dilution of 1:500. For immunogold labeling, secondary goat anti-mouse antibodies conjugated to 10-nm gold particles (Sigma-Aldrich) were used at a dilution of 1:20. For western-blot

analysis, the secondary goat anti-rabbit antibodies conjugated to horseradish peroxidase (Kirkegaard & Perry Laboratories) were used at a dilution of 1:20,000.

Cryohistological Preparation and Immunohistolocalization

Histological preparation and immunohistolocalization were done as described previously (Grangeon et al., 2013). Briefly, one *N. benthamiana* leaf was agroinfiltrated with mock empty vector or TuMV infectious clones or PVX-GFP (Peart et al., 2002). Systemically infected leaves and stems were fixed at 6 d postinoculation followed by a sucrose gradient and cryosectioning as described (Knapp et al., 2012). In addition, before sucrose gradient treatment, the samples were treated with 100 mM Gly in phosphate-buffered saline (PBS) for 1 h to reduce the background fluorescence. The sections were collected on Superfrost Plus Microscope Slides (Fisher Scientific) pretreated with 0.01% (w/v) poly-L-Lys (Sigma-Aldrich). After drying for 2 h, the sections were incubated in PBS for 20 min. They were then incubated for 1 h in a blocking solution of 5% (w/v) bovine serum albumin (BSA) and 0.3% (v/v) Triton X-100 in PBS. Thereafter, the sections were incubated for 1 h with the primary antibody in an incubation solution containing 5% (w/v) BSA and 0.05% (v/v) Tween 20 in PBS, washed three times with a washing solution of 0.05% (v/v) Tween 20 in PBS for 10 min, incubated for 1 h with secondary antibody, followed by washing three times with washing solution for 10 min. Both the primary and secondary antibodies were pretreated with mock sections for 1 h to reduce the nonspecific binding. SlowFade Gold (Molecular Probes) was mounted on the sections after they dried, and cover glasses (VWR) were sealed with nail polish.

Fluorescent Brightener 28, Aniline Blue, and $DiOC_6(3)$ Staining

Fluorescent Brightener 28 (Calcofluor White M2R; Sigma-Aldrich) staining was done as described previously (Knapp et al., 2012). For staining sieve plate callose with Aniline Blue (Methyl Blue; Sigma-Aldrich), sections were incubated for 15 min in 0.05% (w/v) Aniline Blue in 50 mM sodium phosphate, pH 7.2, and then washed three times with PBS for 10 min. The stock solution and the buffer were mixed just before use. For $DiOC_6(3)$ staining (Molecular Probes), $DiOC_6(3)$ was used at a final concentration of 1

μM in PBS. Sections were incubated for 30 min in $DiOC_6(3)$ solution and washed three times with PBS for 10 min. When Aniline Blue and $DiOC_6(3)$ staining were coupled with immunohistolocalization, $DiOC_6(3)$ staining was processed after immunohistolocalization, and Aniline Blue staining was the last step. All of the staining steps were performed in the dark.

Confocal Microscopy

The sections were observed using a 20× (numerical aperture = 0.8) objective and a 63× (numerical aperture = 1.4) oil-immersion objective on an LSM-780 confocal microscope (Zeiss). Zen 2011 (Zeiss) was used for image acquisition. Solid-state and argon ion lasers were used for LSM-780 microscope experiments. Excitation/emission wavelengths were 405/410 to 440 nm for Fluorescent Brightener 28 and Aniline Blue, 488/490 to 560 nm for GFP and CFDA, 561/600 to 630 nm for mCherry, 561/570 to 640 nm for Alexa Fluor 568 goat anti-mouse and anti-rabbit IgG, and 561/650 to 700 nm for chloroplasts. Data from blue, green, and red channels were collected separately.

TEM

For TEM, the stems at 6 d postinoculation were fixed in 2.5% (w/v) glutaraldehyde in 0.1 M sodium cacodylate buffer, pH 7.4, postfixed in 1% (w/v) osmium tetroxide with 1.5% (w/v) potassium ferrocyanide in sodium cacodylate buffer, stained with 2% (w/v) tannic acid, dehydrated in a graded series of acetone, and embedded in Epon resin. After polymerization, 90- to 100-nm ultrathin sections were obtained and stained with 4% (w/v) uranyl acetate for 8 min and Reynolds lead citrate for 5 min. Then, the sections were examined in a Tecnai T12 transmission electron microscope (FEI) operating at 120 kV. Images were recorded using an AMT XR80C CCD camera system (FEI).

Immunogold Labeling

The stems obtained at 6 d postinoculation were fixed in 4% (w/v) formaldehyde and 0.25% (w/v) glutaraldehyde in 0.1 M Sorensen’s phosphate buffer, pH 7.4,

dehydrated in a graded series of alcohol, and embedded in LR White resin. Ninety- to 100-nm sections were treated with 0.02 M Gly in Dulbecco's phosphate-buffered saline (DPBS; 137 mM NaCl, 2.7 mM KCl, 1.5 mM KH_2PO_4, 6.5 mM Na_2HPO_4, 1 mM $CaCl_2$, and 0.5 mM $MgCl_2$, pH 7.4) to inactivate residual aldehyde groups for 10 min, blocked with DPBS plus 2% (w/v) BSA, 2% (w/v) casein, and 0.5% (w/v) ovalbumin (DPBS-BCO) for 5 min, and then incubated for 1 h with the primary antibody that was diluted in DPBS-BCO. Grids were washed six times for 5 min in DPBS, incubated for 1 h with the secondary antibody that was diluted in DPBS-BCO, and washed six times for 5 min in DPBS and then six times for 5 min in water. The sections were stained with 4% (w/v) uranyl acetate for 5 min and Reynolds lead citrate for 3 min. Background labeling was determined using mock-infected stem sections. Quantification of the distribution of gold particles per μm^2 and relative labeling distribution were performed over mock-infected and TuMV-infected sections according to Lucocq et al. (2004).

Xylem Sap Collection and Western-Blot Analysis

The collection of xylem sap was based on a protocol that was described previously (Metzner et al., 2010). Briefly, stems from *N. benthamiana* were harvested 7 d postinoculation by agroinfiltration with pCambiaTuMV/6K_2:GFP. The stems were then cut, washed under water to avoid sampling contamination from injured cells, and dried on tissue papers. They were next placed in different 3-mL syringes that were connected with centrifugation tubes following by centrifugation at 3,000 rpm for 10 min at 4°C. Western-blot analysis was done as described previously (Cotton et al., 2009).

Surface Application of CFDA

The dye CFDA (Sigma-Aldrich) was made up as a 6 mg mL^{-1} stock in acetone and diluted with water to 60 µg mL^{-1} for use. Approximately 1 cm^2 of adaxial mature source leaf surfaces was gently abraded with fine sandpaper, and 20 µL of CFDA was applied to both steam-treated and control non-steam-treated *N. benthamiana* leaf surfaces. The treated leaves were then covered with a thin polyethylene film to ensure an even coverage of the dye across the leaf surface and to prevent evaporation. After 6 and 24 h, young sink leaves were observed with a confocal microscope.

Results

TuMV Factories Are Present in All Types of *N. benthamiana* Leaf and Stem Cells

TuMV factories in *N. benthamiana* epidermal cells are characterized by the presence of numerous 100-nm $6K_2$-tagged vesicles containing replication complexes, many of them aggregating to form a large irregularly shaped globe-like structure near the nucleus (Grangeon et al., 2012). Different types of cells have different structures and functions. Hence, it is of interest to investigate how TuMV factories appear in the other types of plant cells in addition to epidermal cells. To do this, we improved a cryohistological protocol (Knapp et al., 2012) to view TuMV factories in different types of cells. Instead of vacuum infiltration, the fixative was infiltrated in the leaf with a 3-mL syringe. Additionally, glutaraldehyde autofluorescence was quenched with Gly, allowing the glutaraldehyde concentration to be increased from 0.1% to 1%. This increase helped to maintain the integrity of the sections, especially for the fragile and large longitudinal stem sections.

N. benthamiana plants were agroinfiltrated with the TuMV infectious clone pCambiaTuMV/$6K_2$:GFP or with the mock empty vector pCambia 0390, and 6 d later the systemically infected and mock-infected leaf tissues were cryosectioned into 30-µm-thick cross-section samples and processed for confocal microscopy observation. To distinguish the different types of cells, the cell wall was labeled with Fluorescent Brightener 28 dye, which binds (1→4)-β-linked D-glucopyranosyl units (Wood, 1980). As shown in Figure 1A (left), the lower and upper epidermal cells, mesophyll cells, angular collenchyma cells, and vascular tissue were easily distinguishable. Notably, the chloroplasts (shown in red) are predominantly located in the mesophyll cells. At higher magnification (right), we could also distinguish the xylem and phloem easily. $6K_2$:GFP was present in all types of leaf cells of infected plants (Fig. 1B). We also detected $6K_2$:GFP-tagged signals in xylem vessels (Fig. 1B, right, dashed circle), suggesting that TuMV systemic movement involves these conducting tube elements. A closeup view of two vascular parenchyma cells (Fig. 1B, right, bottom dashed rectangle) showed that $6K_2$:GFP-tagged structures are approximately 0.5-µm vesicles. This is consistent with

what is observed in live epidermal cells (Grangeon et al., 2012), which indicates that tissue fixation did not produce any apparent artifactual structures.

To further investigate if $6K_2$:GFP-tagged TuMV factories are found in vascular conducting tubes, we processed stem internodes just above the inoculated leaf at 6 d postinoculation to obtain 30-µm longitudinal section samples for confocal microscopy observation. In TuMV-infected stem, the $6K_2$:GFP-tagged TuMV factories were distributed in trichomes, epidermal cells, cortex, vascular tissue, and pith cells (Fig. 1C, arrows). As for leaf cross sections, we detected $6K_2$:GFP-tagged signals in xylem vessels (Fig. 1C, dashed circle; see below).

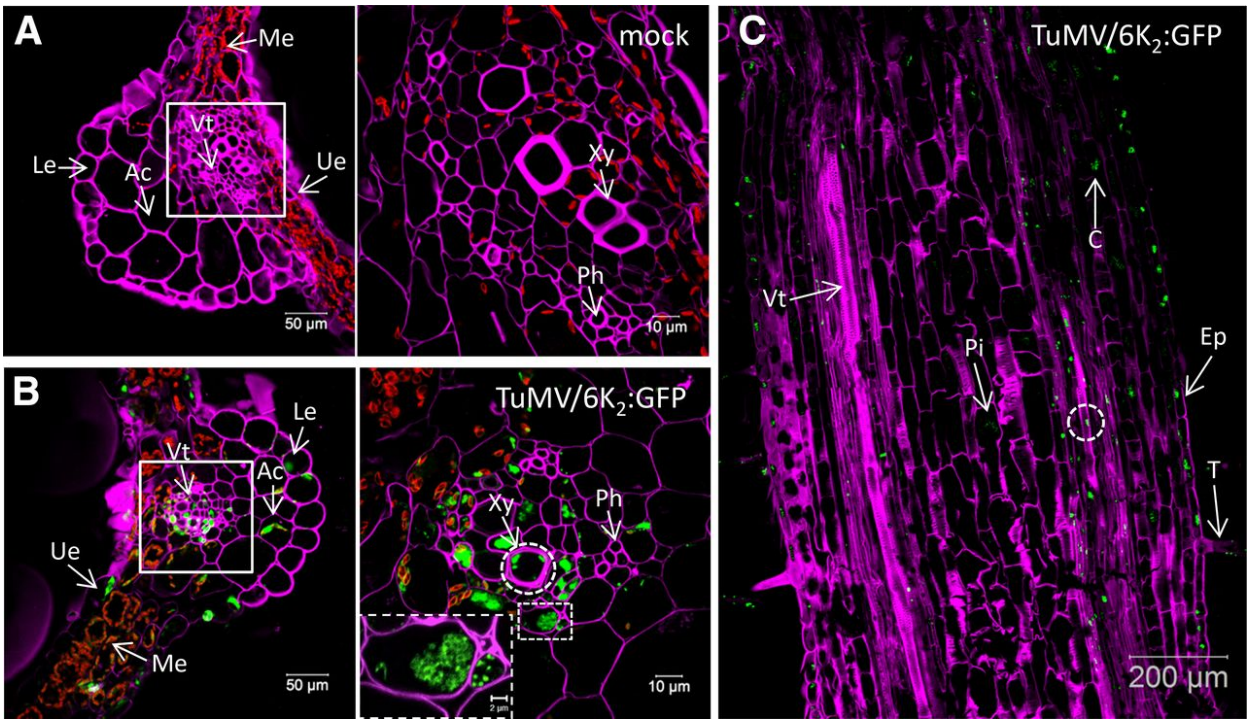

Figure 1. Distribution of TuMV 6K_2:GFP in *N. benthamiana* leaf and stem tissues.

A and B, Cross sections of mock-infected (A) and TuMV/6K_2:GFP systemically infected (B) *N. benthamiana* leaf midrib were observed by confocal microscopy. Samples were analyzed with a Zeiss LSM-780 confocal microscope using a 20× objective (left). White squares indicate the vascular tissue region observed with a 63× objective shown at right. The dashed rectangle at right in B shows a closeup view of two vascular parenchyma cells. C, Longitudinal section of a TuMV/6K_2:GFP-infected *N. benthamiana* stem internode above the inoculated leaf imaged by confocal tile scanning. The tile scan was carried out by assembly two × four images with a 20× objective. The dashed circles indicate the presence of 6K_2:GFP in xylem vessels. The Fluorescent Brightener 28-stained cell wall is shown in false-color magenta, 6K_2:GFP is shown in green, and chloroplasts are shown in red. All of the images are single optical slices. Ac, Angular collenchyma cells; C, cortex; Ep, epidermal cells; Le, lower epidermis; Me, mesophyll cells; Ph, phloem; Pi, pith cells; T, trichome; Ue, upper epidermis; Vt, vascular tissue; Xy, xylem.

$6K_2$-Associated Membrane Complexes Are Present in Sieve Elements

To examine more specifically the presence of $6K_2$:GFP in the phloem, sieve elements were highlighted by staining callose in the sieve plates with Aniline Blue (Evert, 1977; Koh et al., 2012). As shown in Figure 2A, the mock-infected stem longitudinal section was stained with Aniline Blue and the lipophilic dye 3,3′-dihexyloxacarbocyanine iodide [$DiOC_6(3)$], which at high concentration stains all intracellular membranes in fixed cells (Terasaki and Reese, 1992). The Aniline Blue staining (shown in false-colored magenta) clearly highlighted the sieve plate (Fig. 2A, arrow) and labeled PPUs (Fig. 2A, dashed arrow) of one sieve element. $DiOC_6(3)$-stained ring-like structures of about 1 µm in diameter were located at the parietal layer of sieve elements (Fig. 2A, arrowheads), which are sieve element plastids (Froelich et al., 2011). In TuMV-infected stems, $6K_2$:mCherry (shown in false-colored green) was observed as large aggregates (dashed ovals) throughout the sieve tube elements, and the aggregates contained lipids, as they were labeled with the lipophilic dye $DiOC_6(3)$ (Fig. 2B, shown in false-colored red). $6K_2$-labeled ring-like structures also were observed (Fig. 2B, arrowheads), and these may represent sieve element plastids whose membrane had incorporated the viral protein.

To test whether the $6K_2$ aggregates might be replication complexes, we performed immunohistolocalization with the double-stranded RNA (dsRNA)-specific monoclonal antibody J2, which specifically recognizes dsRNA of more than 40 bp in length in a sequence-nonspecific manner (Schönborn et al., 1991). No dsRNA signal was observed in noninfected samples (Fig. 2C). In infected samples, dsRNA was detected in the $6K_2$ aggregates (Fig. 2D, dashed oval) but not within the sieve element plastids (Fig. 2D, arrowheads). We also performed immunohistolocalization with a rabbit serum against the TuMV viral RNA-dependent RNA polymerase (vRdRp; Dufresne et al., 2008). No vRdRp signal was observed in mock samples (Fig. 2E). In the sieve elements of infected samples, vRdRp was associated with $6K_2$ aggregates (Fig. 2F, dashed ovals) but not with the $6K_2$-tagged sieve element plastids (Fig. 2F, arrowheads). Thus, $6K_2$-associated membrane complexes were present in phloem sieve elements

and contained vRNA and vRdRp, suggesting that viral replication complexes were present in these conducting vessels.

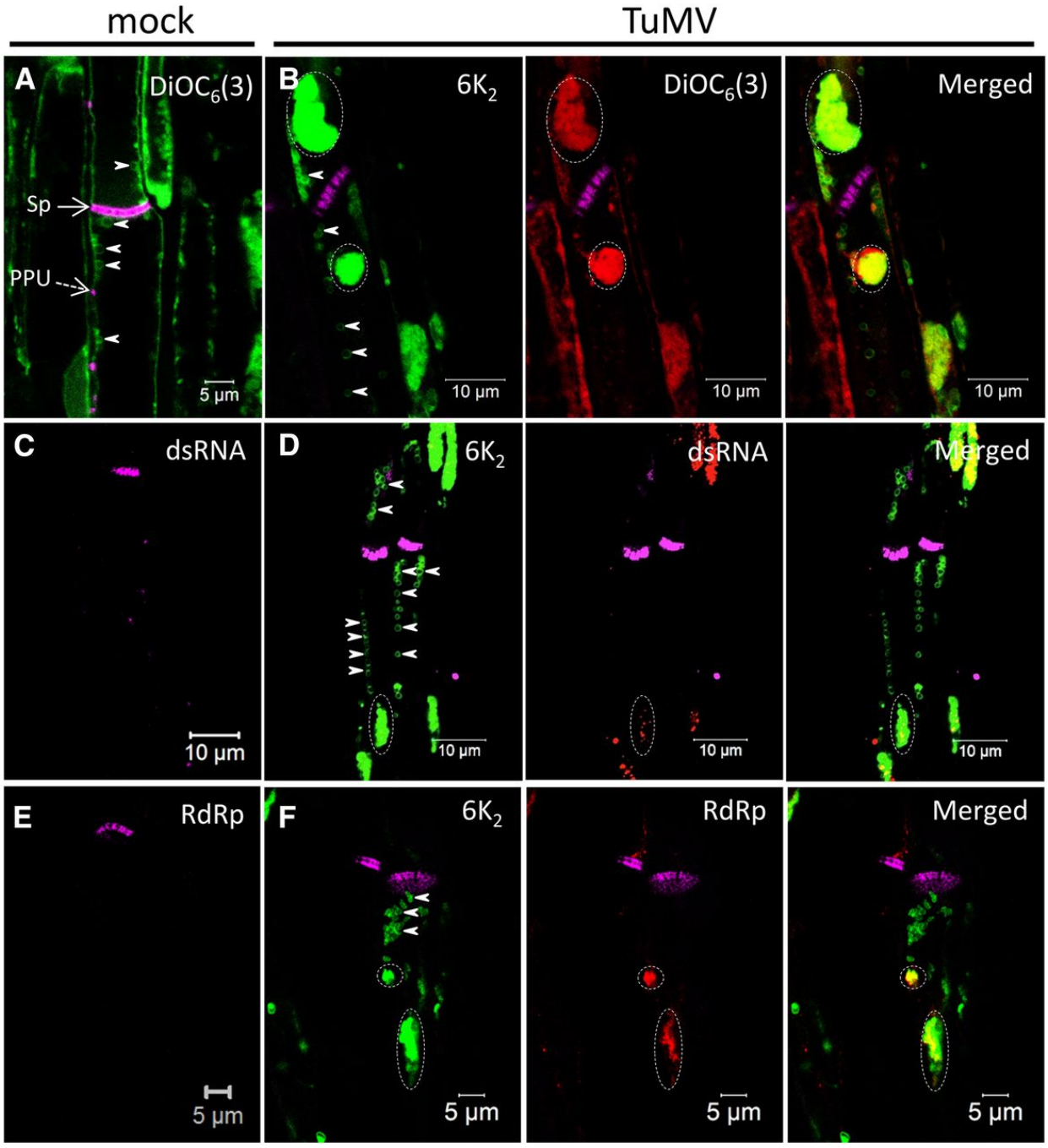
mock
TuMV
A
DiOC6(3)
Sp
PPU
5 µm
B
6K2
10 µm
DiOC6(3)
10 µm
Merged
10 µm
C
dsRNA
10 µm
D
6K2
10 µm
dsRNA
10 µm
Merged
10 µm
E
RdRp
5 µm
F
6K2
5 µm
RdRp
5 µm
Merged
5 µm

Figure 2. Phloem membrane aggregates contain viral replication complexes.

Longitudinal sections of mock-infected (A, C, and E), TuMV/$6K_2$:mCherry-infected (B), and TuMV/$6K_2$:GFP-infected (D and F) *N. benthamiana* stem internodes above the inoculated leaf were observed with a Zeiss LSM-780 confocal microscope using a 63× objective. Aniline Blue-stained sieve plates are shown in false-color magenta, $DiOC_6(3)$-stained lipids are shown in green in A and in red in the middle and right parts of B, and $6K_2$:mCherry has been false colored in green. Immunohistolocalization of dsRNA (C and D) and vRdRp (E and F) was performed on mock-infected (C and E) and TuMV/$6K_2$:GFP-infected (D and F) longitudinal sections. $6K_2$:GFP is shown in green, and dsRNA and vRdRp are shown in red. Dashed ovals highlight the presence of $6K_2$ vesicle aggregates, and arrowheads point to the ring-like structures in sieve elements. Images are single optical slices. Sp, Sieve plate.

Moreover, we performed immunohistolocalization with a rabbit serum against TuMV CP (Cotton et al., 2009). No CP signal was observed in noninfected samples (Fig. 3A). TuMV CP has been shown not to localize with dsRNA punctate structures in infected *N. benthamiana* protoplasts (Cotton et al., 2009). Likewise, CP was localized mainly at the periphery of $6K_2$ aggregates, as punctate and sometimes elongated structures, and was not associated with cortical $6K_2$ vesicles, as shown here for cells of the pith cell area (Fig. 3B, bottom left rectangle). These CP signals are likely TuMV virions, which have been observed adjacent to vesicle aggregates by transmission electron microscopy (TEM; J. Wan, unpublished data). We also detected CP in sieve elements (Fig. 3D), but it was not associated with $6K_2$ aggregates (dashed oval) or with sieve element plastids (arrowhead). Thus, the CP signal in sieve elements likely represents TuMV virions.

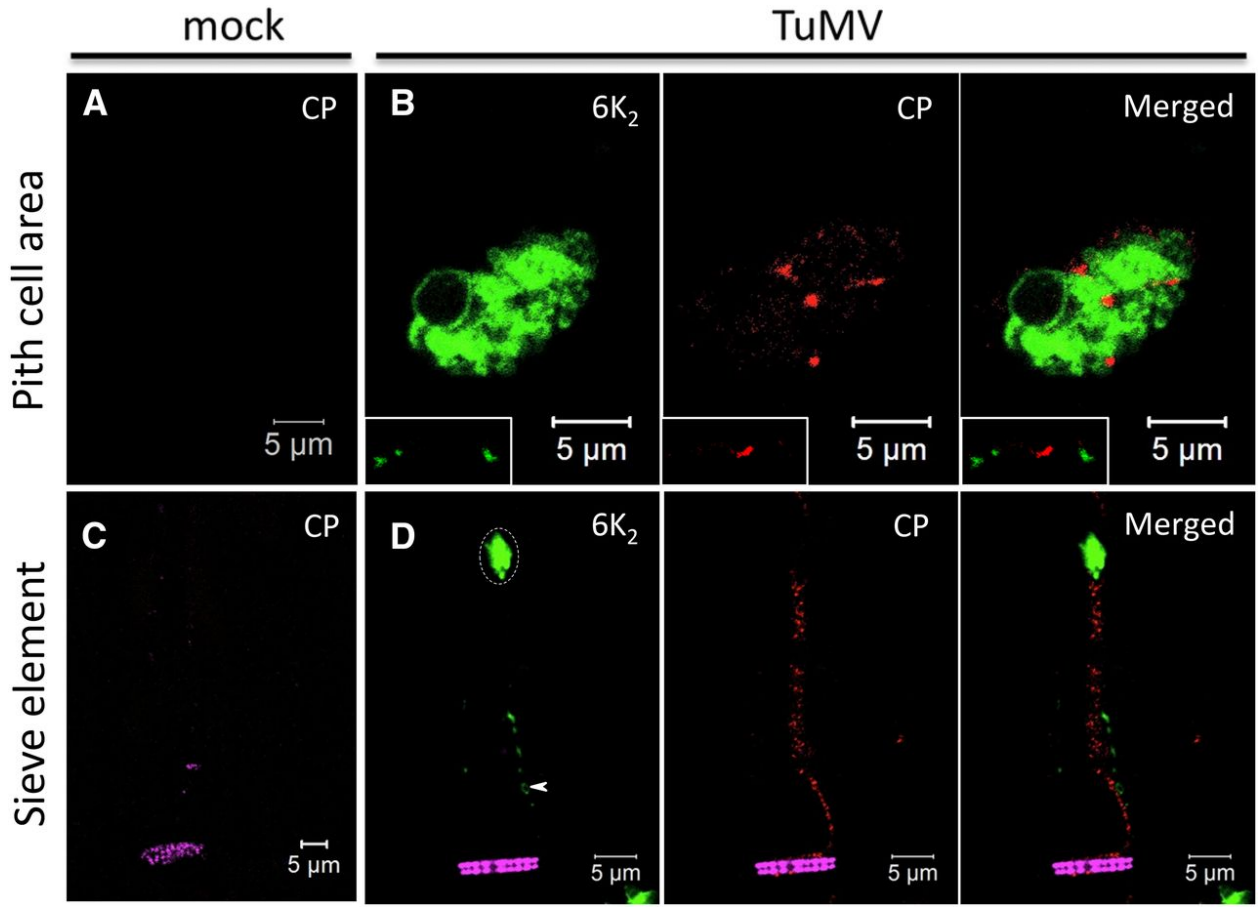

Figure 3. CP distribution in TuMV-infected cells.

Immunohistolocalization of CP was performed on mock-infected (A and C) and TuMV/$6K_2$:GFP-infected (B and D) longitudinal sections of *N. benthamiana* stem internodes. Sections were observed with a Zeiss LSM-780 confocal microscope using a 63× objective. CP signal was detected in TuMV-infected pith cell area (B) as well as in sieve elements (D). The rectangles in B show $6K_2$ and CP at the cell periphery. Aniline Blue-stained sieve plates are shown in false-color magenta, $6K_2$:GFP is shown in green, and CP is shown in red. The images are single optical slices. The dashed oval highlights the presence of $6K_2$ vesicle aggregates, and the arrowhead points to the ring-like structures in sieve elements.

$6K_2$-Associated Membrane Complexes Are Present in Xylem Vessels

As described above, leaf cross sections pointed to the possible presence of $6K_2$:GFP in xylem vessels (Fig. 1B). Longitudinal sections of stem internodes just above the inoculated leaf confirmed the presence of $6K_2$:GFP in xylem vessels (Fig. 4A). Xylem vessels were easily discernible due to their characteristic perforated cell wall. The presence of $6K_2$:GFP within xylem vessels was not an experimental spillover contamination resulting from tissue damage during the sectioning process, as optical sectioning showed that $6K_2$:GFP-tagged aggregates were truly located inside the xylem vessels (see the three-dimensional reconstruction of an infected xylem vessel in Supplemental Movie S1). Moreover, $6K_2$:mCherry-tagged aggregates contained lipids, as they were labeled with the lipophilic dye DiOC6(3) (Fig. 4B).

Xylem vessels are dead cells normally used for water transportation. This raises the question of whether the $6K_2$:GFP aggregates are active for viral infection. To answer this question, we looked for the presence of dsRNA/vRNA, vRdRp, and CP via immunohistolocalization in the $6K_2$:GFP aggregates. dsRNA, vRdRp, and CP (Fig. 4, C–E) were detected in the $6K_2$:GFP aggregates. As for sieve elements (Figs. 2, C and E, and 3, A and C), no signal for the presence of dsRNA, vRdRp, and CP was observed in mock samples (data not shown). Taken together, these observations indicate that $6K_2$-associated membrane complexes in xylem vessels contain vRNA and viral replication and movement proteins (i.e. CP).

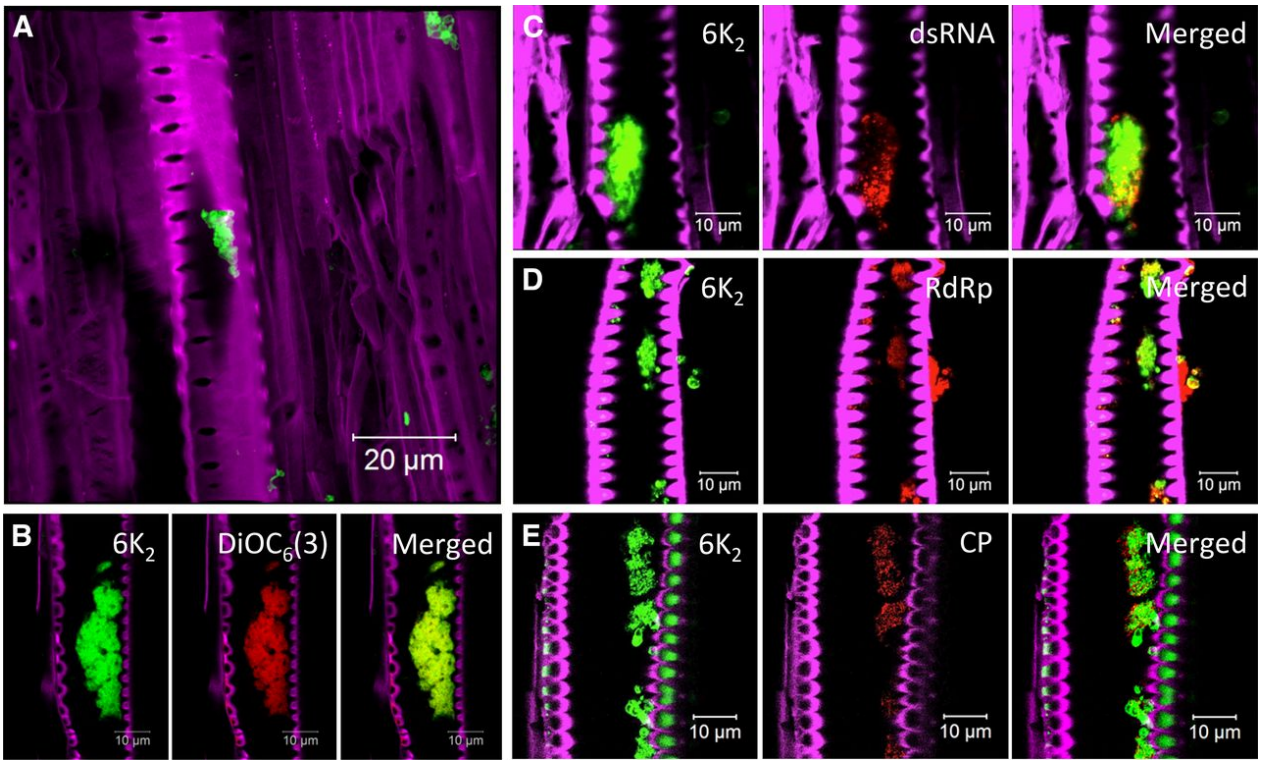

Figure 4. TuMV replication complexes in xylem vessel.

Longitudinal sections of *N. benthamiana* stem internodes infected with TuMV expressing $6K_2$ fused to either GFP (A and C–E) or mCherry (B) were observed with a Zeiss LSM-780 confocal microscope with a 63× objective. Lipids were stained with the membrane dye $DiOC_6(3)$ (B). Immunohistolocalization of dsRNA (C), vRdRp (D), and CP (E) was performed as described in Figure 3. The Fluorescent Brightener 28-stained cell wall is shown in false-color magenta, $6K_2$:GFP is shown in green, $6K_2$:mCherry has been false colored in green, and $DiOC_6(3)$ has been false colored in red. dsRNA, vRdRp, and CP are shown in red. A is a three-dimensional image; the other confocal images are single optical slices.

We then examined the ultrastructure of TuMV aggregates in xylem vessels by TEM. At 6 d postinoculation, TuMV-infected and mock-infected stem internodes just above the inoculated leaf were fixed, dehydrated, and embedded in Epon for structure observation or in LR White for immunogold labeling. In mock-infected stem, the xylem vessels contained only a few electron-opaque materials (Fig. 5A). In contrast, in TuMV-infected stem, the xylem vessels were full of vesicular structures, especially in the perforation plates between two xylem vessel elements (Fig. 5B), indicating that the vesicles might be moving through these pore structures. Interestingly, under higher magnification, we detected TuMV virion-like structures that were associated with the membrane vesicles (Fig. 5C, arrow). The presence of TuMV particles was confirmed by negative staining with 2% (w/v) phosphotungstate of the collected xylem sap (Fig. 5D, arrows).

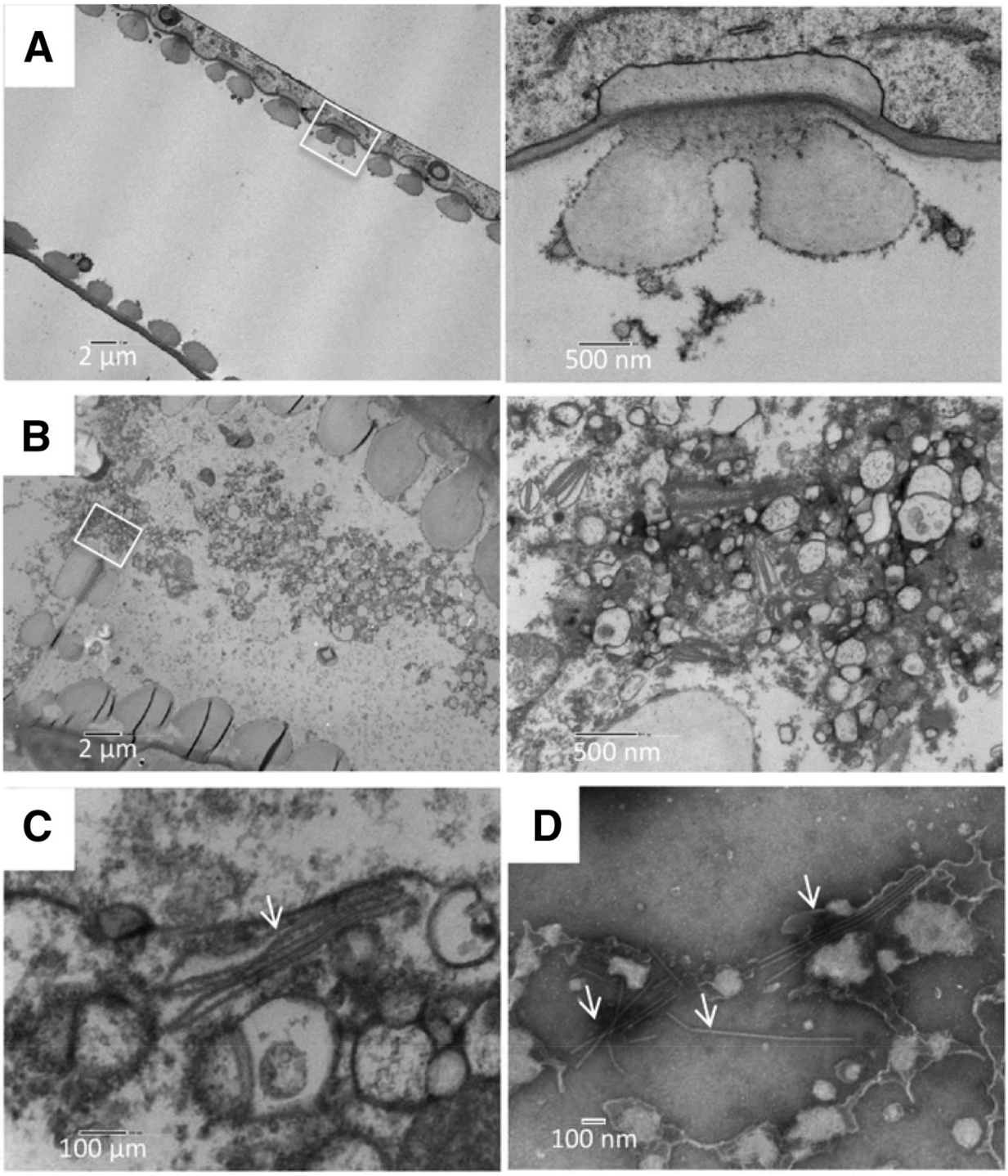
A
2 µm
500 nm
B
2 µm
500 nm
C
100 µm
D
100 nm

Figure 5. Ultrastructure of TuMV-induced membrane alterations in xylem vessels.

A and B, Longitudinal sections of mock-infected (A) and TuMV-infected (B) *N. benthamiana* stem internodes above the inoculated leaf were collected and observed by TEM. White squares indicate the areas that are shown at higher magnification at right. The higher magnification of the white square in B shows TuMV viral factories located in the perforation plate between two xylem vessel elements. C, TuMV virions (arrow) associated with vesicles. D, Xylem sap from TuMV-infected *N. benthamiana* was collected and observed by TEM following negative staining. TuMV virions are highlighted by arrows.

To further confirm the content of the membrane structures in xylem vessels, we performed immunogold labeling using the anti-dsRNA monoclonal antibody. Very few gold particles were found in xylem parenchyma cells (Fig. 6A) and xylem vessels (Fig. 6B) on a mock-infected section treated with primary antibody J2 and secondary antibodies. The detection of inclusion bodies and membrane vesicles in partially differentiated xylem vessels indicated that this cell was infected by TuMV (Fig. 6C). Under higher magnification, we detected gold particles (arrows) in the membrane vesicles in partially differentiated (Fig. 6C) and also in fully differentiated xylem vessels (Fig. 6D). Quantification of the gold particles per μm^2 and relative labeling distribution were performed over mock-infected and TuMV-infected sections. The results revealed that, compared with TuMV-infected sections (0.42 ± 0.04 particles μm^{-2}), the mock-infected sections did not show any significant labeling (0.07 ± 0.03 particles μm^{-2}; Fig. 6E). In TuMV-infected sections, the gold particles were mainly found decorating TuMV-induced vesicles (76.25%). Only a few gold particles were found over the rest of the cytoplasm, corresponding to the nonspecific background signal from the antibody (Fig. 6F). Thus, TuMV virions in xylem vessels are associated with vesicular complexes that contain TuMV RNA.

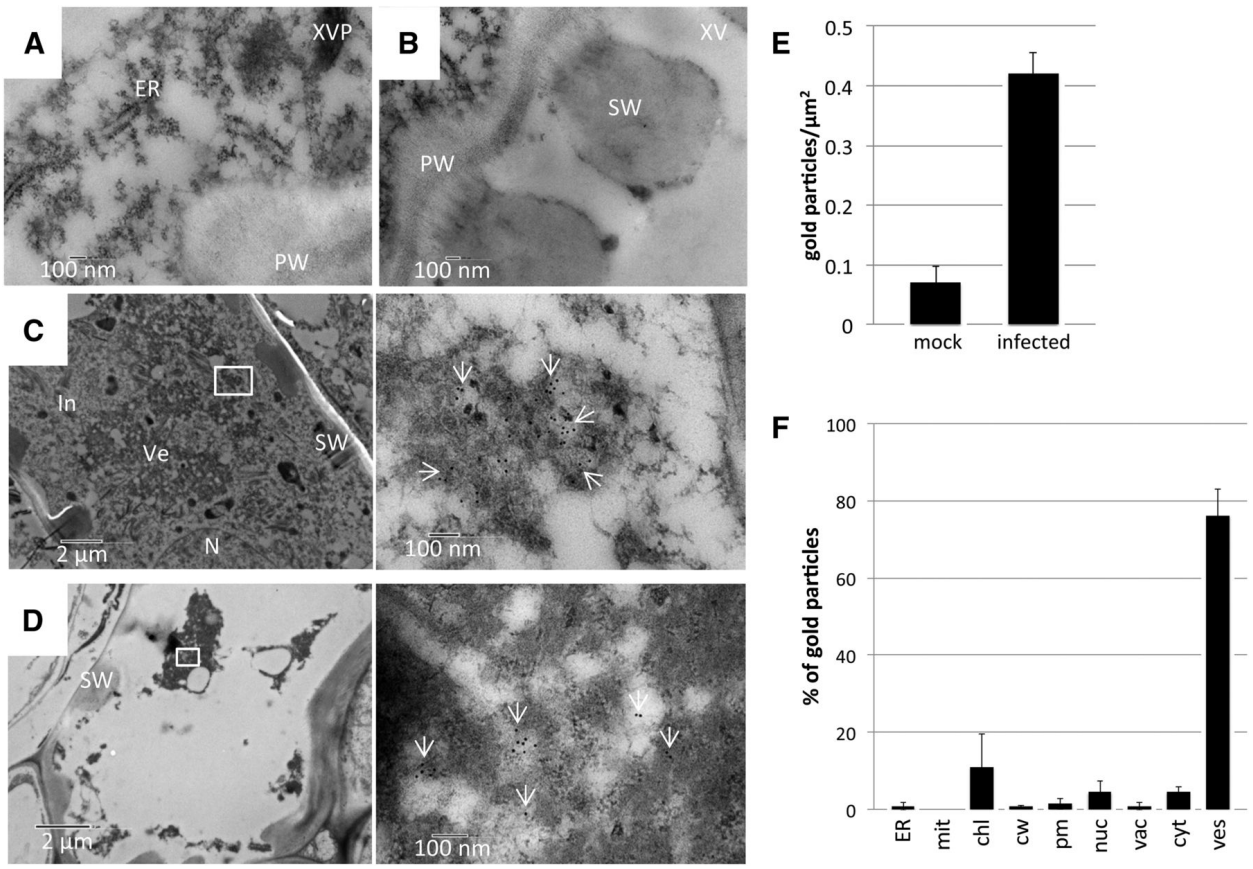

Figure 6. Immunoelectron microscopy localization of dsRNA in TuMV-infected xylem vessels.

A to D, Labeling was performed by using the anti-dsRNA monoclonal antibody J2 on longitudinal sections of mock-infected (A and B) and TuMV-infected (C and D) *N. benthamiana* stem internodes. White squares indicate the areas that are shown at higher magnification at right. Arrows point to gold particles in vesicles. E and F, Number of gold particles per μm^2 in mock-infected versus TuMV-infected cells (E) and relative labeling distribution in infected cells (F). Two different labeling experiments were considered, and 200 gold particles were counted per experiment. chl, Chloroplast; cw, cell wall; cyt, cytosol; ER, endoplasmic reticulum; In, inclusion bodies; mit, mitochondrion; N and nuc, nucleus; pm, plasma membrane; PW, primary cell wall; SW, secondary cell wall; vac, vacuole; Ve and ves, vesicles; XV, xylem vessel; XVP, xylem parenchymal cell.

Xylem Sap from TuMV-Infected Plants Contains Eukaryotic Initiation Factor (iso)4E and Is Infectious

Analysis of xylem sap by confocal microscopy confirmed our previous finding in the fixed stem tissues. Using phase contrast, the xylem sap from mock-infected plants was essentially devoid of cellular material (Fig. 7A). In contrast, the xylem sap from TuMV-infected plants contained a large number of what appears to be vesicles, many of which were positively labeled with $6K_2$:GFP (Fig. 7B). We then looked for the presence of viral proteins and for the host translation eukaryotic initiation factor (iso)4E [eIF(iso)4E] in xylem sap by western-blot analysis. eIF(iso)4E was chosen because it has been shown to be part of the TuMV replication complex (Beauchemin et al., 2007). As expected, the viral proteins $6K_2$:GFP, CP, and vRdRp, as well as eIF(iso)4E, were detected in the xylem sap from TuMV-infected plants but not from mock-infected plants (Fig. 7C). Since eIF(iso)4E is an intracellular protein, its absence in mock-infected xylem sap indicates that the presence of the above proteins in infected xylem sap was not the consequence of contaminating cellular breakage during sap collection. As an indicator of phloem contamination in the collected xylem sap, we looked for the presence of Polypyrimidine Tract-Binding Protein3 (PTB3), a homolog to the pumpkin (Cucurbita maxima) phloem-mobile ribonucleoprotein complex RBP50 (Ham et al., 2009). This protein was detected in a total protein extract but not in an infected xylem sap from TuMV-infected plants (Fig. 7D), suggesting that there was no apparent contamination from companion cells and phloem exudates. The xylem sap from TuMV-infected plants also was tested for the infection of healthy *N. benthamiana* plants by mechanical inoculation. After 5 d, we detected TuMV systemic infection under UV light (data not shown), which indicated that the xylem sap was infectious. In conclusion, the xylem sap from TuMV-infected plants contains $6K_2$ vesicles and viral as well as host protein that are essential for TuMV replication and assembly.

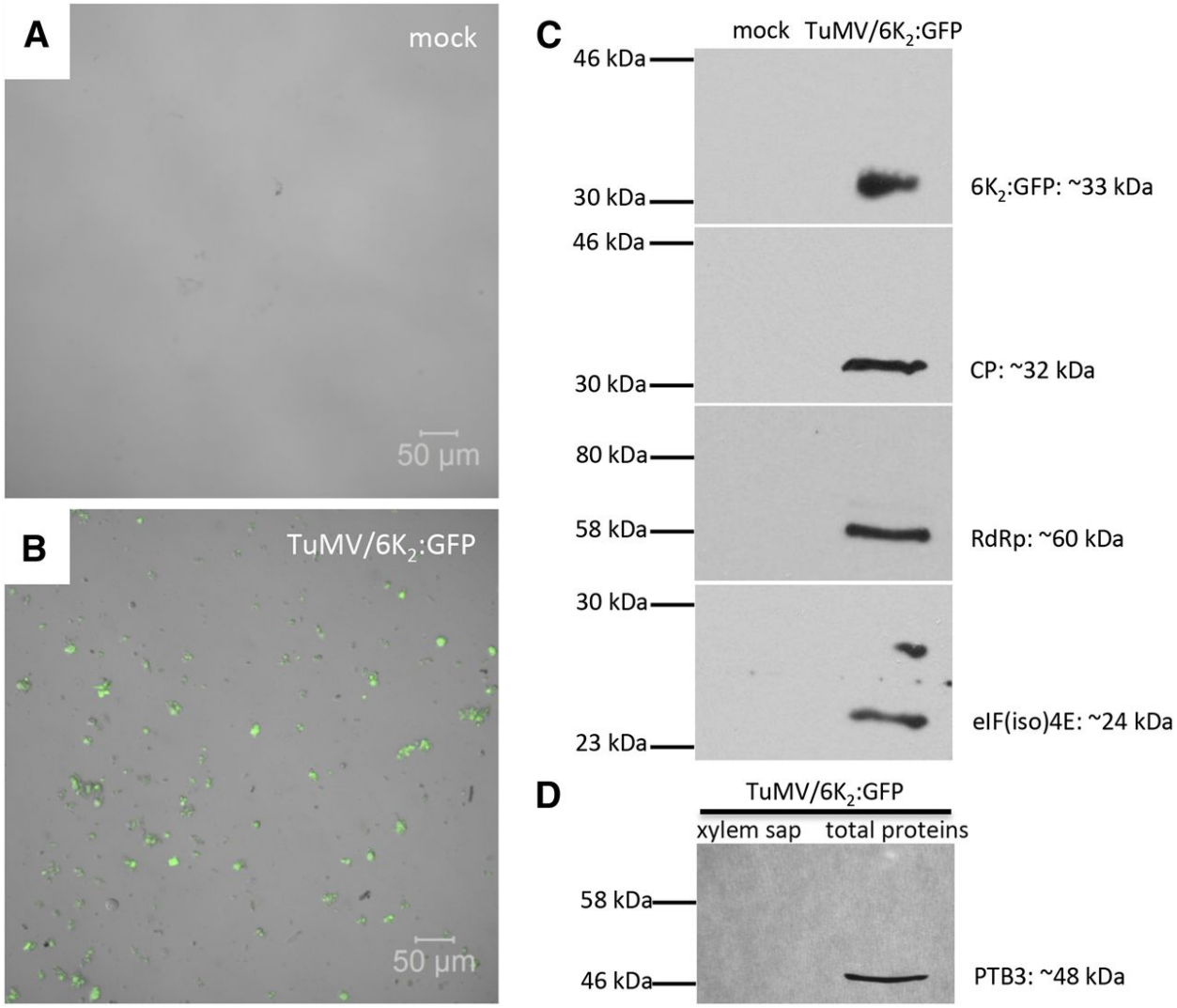

Figure 7. Western-blot protein analysis of xylem sap.

A and B, Xylem sap was collected from mock-infected (A) and TuMV/6K_2:GFP-infected (B) *N. benthamiana* plants and was observed by confocal microscopy. 6K_2:GFP is shown in green. C, Western-blot analysis of xylem sap from mock- and TuMV-infected plants using rabbit sera against GFP, CP, vRdRp, or eIF(iso)4E. D, Western-blot analysis of xylem sap and total protein leaf extract from TuMV-infected plants using a rabbit serum against the phloem-specific PTB3 protein.

Stem Girdling Confirms That TuMV Can Spread Systemically through the Xylem

To further substantiate that xylem vessels are involved in TuMV systemic movement, we performed a stem-girdling experiment. *N. benthamiana* plants were agroinfiltrated with pCambiaTuMV/6K_2:GFP. At 1 h following agroinfiltration with pCambiaTuMV/6K2:GFP, the stem internode just above the agroinfiltrated leaf was treated with a jet of steam for 15 s, until water soaking became apparent (Moreno et al., 2004). As a consequence, a segment of about 5 to 10 mm long was reduced to a very thin strand within 1 h and showed dry necrosis 1 d later (Fig. 8A). Since xylem vessels are dead tissues surrounded by a thick cell wall, their structural integrity should not be affected by the steam treatment. To confirm that this was the case, cross and longitudinal sections of girdled stems were examined by confocal microscopy, which showed that all cells had collapsed except for the xylem vessels (Fig. 8B). To further confirm that the phloem was totally destroyed after steam treatment, we used the phloem-loading dye 5-(and 6)-carboxyfluorescein diacetate (CFDA). It was reported previously that the phloem transport of CFDA was interrupted when phloem was destroyed following stem girdling (Grignon et al., 1989). Thus, CFDA was applied to an abraded source leaf below the girdled stem section, and its movement into upper sink leaves was assessed 6 and 24 h later by confocal microscopy. As expected for phloem movement, CFDA clearly marked the class I, II, and III vein network of a young sink leaf of nongirdled plants 6 h after CFDA application (Fig. 8C, left). On the other hand, no CFDA labeling was observed in young sink leaves of girdled plants (n = 10) 6 and 24 h after CFDA application (Fig. 8C, right). Normally, in TuMV-agroinfiltrated leaves, cell-to-cell movement starts at 3 d postinoculation and systemic infection is detected at 5 d postinoculation. Here, TuMV/6K_2:GFP infection was observed above the steam-treated section by UV light between 7 and 10 d (Fig. 8D; Table I), suggesting that xylem vessels also are used by TuMV for its systemic infection, although at a slower rate. At the first indication of systemic infection taking place in girdled plants, we collected stem cross sections just above the girdled part for histological analysis. Figure 8E shows that 6K_2:GFP was found only in vascular tissues at this early stage. Under higher magnification, we observed the 6K_2:GFP-tagged vesicles in xylem vessels and xylem parenchymal cells (arrowhead) as well as other xylem-associated cells, indicating that

once TuMV passed the girdled stem through xylem vessels, it can be unloaded in the xylem parenchymal cells just above the girdled stem.

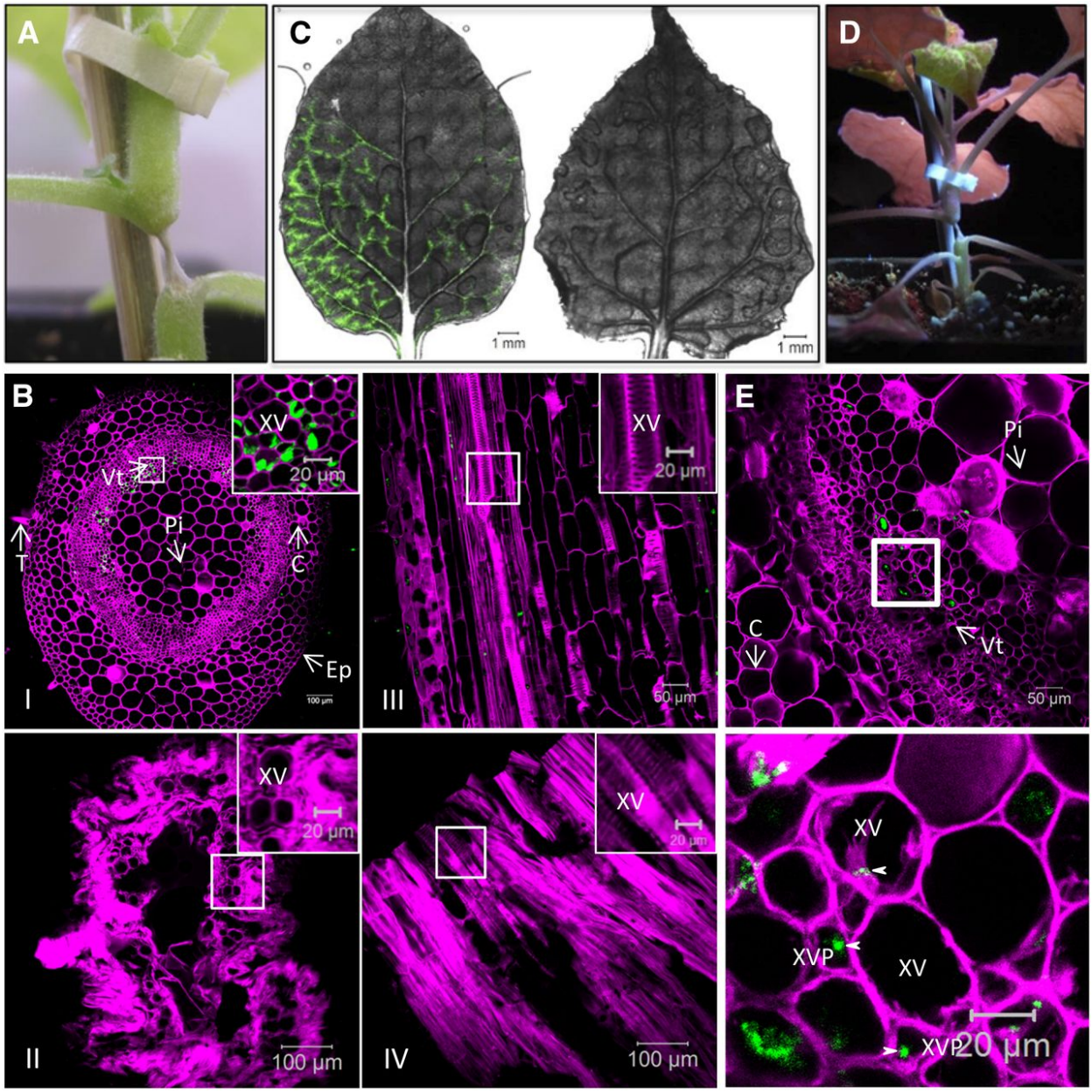
A
C
D
1 mm
1 mm
B
XV
20 µm
Vt
Pi
T
C
Ep
100 µm
I
III
XV
20 µm
50 µm
E
Pi
C
Vt
50 µm
II
XV
20 µm
100 µm
IV
XV
20 µm
100 µm
XV
XVP
XV
XVP
20 µm

Figure 8. TuMV infection following the stem-girdling experiment.

A, Closeup view of an *N. benthamiana* stem internode that was treated with steam for 15 s the day before. The internode is above the leaf that was infiltrated with A. tumefaciens containing pCambiaTuMV/6K_2:GFP 1 h before the steam treatment. B, Cross sections and longitudinal sections of TuMV-infected stem internode above the inoculated leaf were collected by cryosectioning and observed by confocal microscopy. Cross-sections of TuMV-infected stem internode are shown before (I) and after (II) steam treatment. Longitudinal sections of TuMV-infected stem internode are shown before (III) and after (IV) steam treatment. Top right squares show at a high magnification the xylem vessels and surrounding cells before steam treatment (I and III) and intact xylem vessels and dead surrounding cells after steam treatment (II and IV). C, Upper young leaves of stem nongirdled (left) and girdled (right) plants in which the source leaves were treated with CFDA. D, The steam-treated plant from A shows TuMV systemic infection under UV light at 10 d after agroinoculation. E, A stem cross-section just above the girdled stem section at a very early stage of systemic infection. The white square indicates the area of higher magnification shown at bottom. C, Cortex; Ep, epidermal cell; Pi, pith cells; T, trichome; Vt, vascular tissue; XV, xylem vessel; XVP, xylem parenchymal cell.

Table 1. Analysis of TuMV infection in steam-treated *N. benthamiana* plants.

Treatment	Inoculated Leaves (5 d p.i.)		Upper Leaves (10 d p.i.)	
	N	Infected	N	Infected
		%		%
TuMV nonsteamed	15	15 (100)	15	15 (100)
TuMV steamed 1	8	8 (100)	8	3 (38)
TuMV steamed 2	15	15 (100)	15	1 (6)
TuMV steamed 3	15	15 (100)	15	4 (26.7)
TuMV steamed 4	15	15 (100)	15	3 (20)

N, Number of inoculated plants; p.i., days postinoculation; TuMV steamed 1/2/3/4, four separate experiments.

Membrane-Associated vRNA of PVX Is Present in Both Phloem and Xylem

The observations that TuMV factories are present in both phloem and xylem led us to ask whether this is a unique feature of potyviruses. PVX virions can enter, move through, and exit the phloem, as demonstrated by grafting experiments (Cruz et al., 1998). In addition, the CP of PVX was detected in xylem vessels (Betti et al., 2012). We thus analyzed the vascular tissues of PVX-infected plants. *N. benthamiana* plants were agroinfiltrated with the PVX infectious clone PVX-GFP (Peart et al., 2002), and 8 d later the stem internodes just above the inoculated leaf were processed to collect 30-µm longitudinal section samples for confocal microscopy observation. Sieve elements were stained with Aniline Blue and xylem vessels were stained with Fluorescent Brightener 28, and both are shown in magenta. We detected dsRNA in the sieve elements via immunohistolocalization, which was associated with lipids (Fig. 9A), suggesting that those structures could be PVX replication complexes. A similar pattern was observed in the xylem vessels of PVX-infected plants (Fig. 9B). Thus, PVX RNA was present in both phloem and xylem and was associated with lipids.

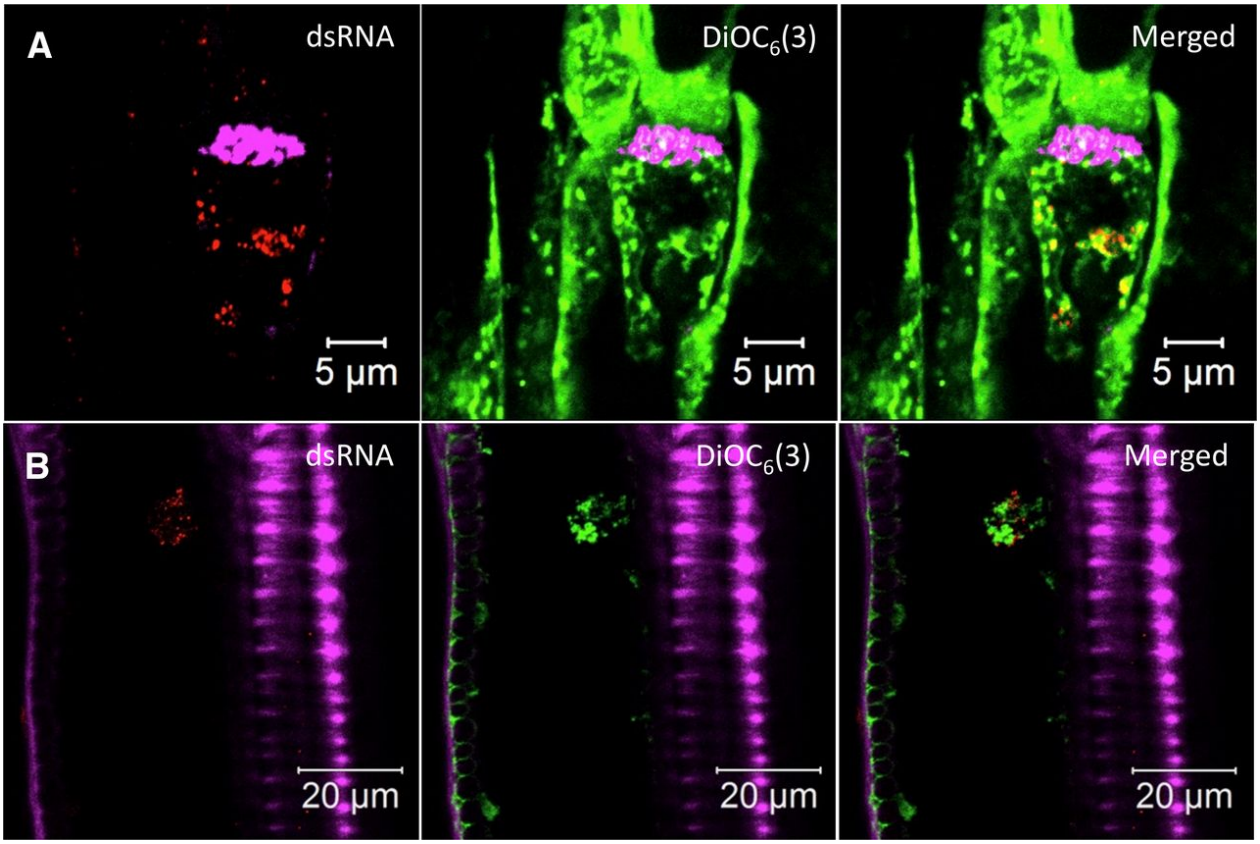

Figure 9. Membrane-associated vRNA in PVX-infected sieve elements and xylem vessels.

Longitudinal sections of PVX-infected *N. benthamiana* stem internode above the inoculated leaf were collected by cryosectioning and observed by confocal microscopy. Immunohistolocalization of dsRNA and lipid staining with $DiOC_6(3)$ in one sieve element (A) and one xylem vessel (B) of a PVX-infected plant are shown. Aniline Blue-stained callose and Fluorescent Brightener 28-stained cell wall are shown in false-color magenta, $DiOC_6(3)$ is shown in green, and dsRNA is shown in red. All images are single optical slices.

Discussion

Viruses use the vascular tissues, in particular the phloem, for the systemic infection of plants. Viral particles are apparently the transmission agent responsible for transmitting the disease in the whole plant, but vRNP complexes also have been implicated. The nature of this trafficking vRNA complex, however, has not been defined.

In this study, we showed the presence of membrane-associated complexes centered on the $6K_2$ protein of TuMV, which also contained vRNA and vRdRp, in sieve elements and xylem vessels. Since $6K_2$ is detected as a $6K_2$-VPg-Proteinase (Pro) fusion in infected cells (Léonard et al., 2004), it is likely that VPg and Pro also are present. The vRNA associated with the $6K_2$:GFP aggregates is probably the replicative form of the vRNA, since the dsRNA punctate structures observed in xylem vessels are identical to those observed in the cytoplasm of infected epidermal cells. Moreover, the dsRNA recognized by the monoclonal antibody is not likely to be encapsidated vRNA, since the immunohistolocalization protocol does not involve protease treatment, and gold particles are associated with vesicles and not viral particles in immunogold electron microscopy images following incubation with the dsRNA monoclonal antibody. The vesicles in sieve elements and xylem vessels are reminiscent to those found in the cytoplasm of TuMV (Grangeon et al., 2012) and are very similar to other plant and mammalian virus-infected cells (for review, see Miller and Krijnse-Locker, 2008; Laliberté and Sanfaçon, 2010). These intracellular vesicles are the building blocks of viral factories, which contain viral replication complexes. In the case of TuMV, these same vesicles also are the vehicles for the intracellular and intercellular movement of vRNA (Grangeon et al., 2012, 2013). It thus appears that the TuMV RNP complexes found in vascular conducting tubes are, in fact, membrane-associated viral replication complexes. The observation that the host translation initiation factor eIF(iso)4E, which is part of the potyvirus replication complex (Beauchemin et al., 2007), was found in infected xylem sap supports the idea that viral factories end up in vascular conducting tubes. It will be interesting to see if CI and P3N-PIPO are involved in phloem loading from the companion cells and if they are associated with the $6K_2$ structures found in sieve elements and xylem vessels. Consequently, the long-distance transducing agent

for TuMV is likely to contain membrane-bound replication complexes closely associated with particles. The presence of viral factories in the phloem and xylem may not be limited to TuMV, since membrane-associated, nonencapsidated vRNA also was observed in PVX-infected plants.

To our knowledge, the possibility that viral replication complexes could end up in, and could travel through, the phloem and the xylem has never been considered. Limited evidence for their presence, on the other hand, can be found in some previous investigations. For instance, the membrane association of *Turnip yellow mosaic virus* and CMV particles in xylem has been reported (Hitchborn and Hills, 1965). Likewise, *Potato virus Y* particles along with cytoplasmic inclusions as well as vesicles were documented in xylem vessels (Otulak and Garbaczewska, 2009, 2012). Finally, large aggregates of Triple Gene Block Protein 3 (TGBp3) of CMV were found in sieve elements and were associated with CMV particles (Blackman et al., 1998). Recently, TGBp2 and TGBp3 of PVX were shown to induce the formation of endoplasmic reticulum-derived vesicles at PD orifices. These vesicles contained the vRdRp and nonencapsidated vRNA (Tilsner et al., 2013). So, it may well be that the TGBp3 aggregates are, in fact, CMV replication complexes associated with viral particles.

Traditionally, the phloem has been considered as a canal for distributing water, nutrients, and hormones essential for the growth and development of various organs of the plant. Recent studies have shown, however, that the phloem has more elaborate functions (for review, see Lucas et al., 2013). For instance, it has been demonstrated that PDs and the phloem sieve tube system function cooperatively for the long-distance delivery of proteins (Xoconostle-Cázares et al., 2000; Aoki et al., 2002; Gómez et al., 2005), mRNA (Sasaki et al., 1998; Ruiz-Medrano et al., 1999; Xoconostle-Cázares et al., 1999; Haywood et al., 2005; Roney et al., 2007), and small RNA (Yoo et al., 2004; Buhtz et al., 2008; Lin et al., 2008; Pant et al., 2008). Furthermore, the identification of ribosomal and associated components involved in mRNA translation in the sieve tube system of the cucurbits (Lin et al., 2009; Ma et al., 2010) is challenging the general belief that mature sieve elements lack the capacity for protein synthesis (Ham and Lucas, 2014). Sieve elements thus have the capacity of enclosing intricate structures such as membrane-bound vRNP complexes that might be active in RNA synthesis, as

evidenced by the presence of dsRNA, a marker for vRNA replication, in the $6K_2$ aggregates. This hypothesis could be tested by collecting phloem exudate and subjecting it to in vitro metabolic labeling to see if vRNA synthesis and translation are indeed taking place.

Based on our observation, we suggest a schematic model for the movement of TuMV into small vein sieve elements (Fig. 10A). In this scheme, $6K_2$-tagged vesicles, which contain vRNA and vRdRp, move from epidermal cells to mesophyll cells, bundle sheath, vascular parenchyma, and companion cells through PDs. Once in companion cells, the $6K_2$-tagged vesicles are loaded into sieve elements through PPUs. Either individual $6K_2$ vesicles move through sieve elements or they amalgamate to form a membrane support for virion assembly, which would be released for phloem transport, as proposed by Blackman et al. (1998) for CMV.

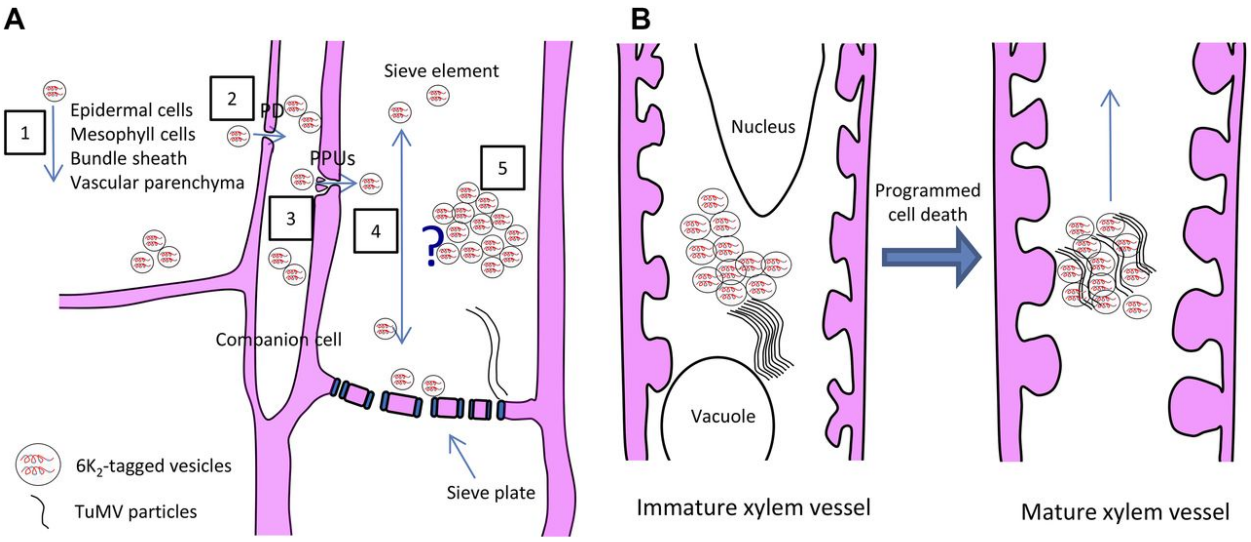

Figure 10. Model for TuMV long-distance movement.

A, Schematic model for TuMV moving into small vein sieve elements. First, $6K_2$-tagged vesicles, which contain vRNA and vRdRp, move from epidermal cells to mesophyll cells, bundle sheath, vascular parenchyma (1), and companion cells through PDs (2). Then, the $6K_2$-tagged vesicles are loaded into sieve elements through PPUs (3). Once in the sieve element, there are two possibilities. One possibility is that individual $6K_2$ vesicles move through sieve elements (4). Another possibility is that the $6K_2$ vesicles amalgamate together to form membrane aggregates, which stay in sieve elements for virion assembly, and the assembled virions are then released for phloem transport (5). B, Schematic model for TuMV movement into xylem vessels. $6K_2$-tagged vesicles enter into the immature xylem elements through pit membranes and replicate in the cytoplasm before programmed cell death occurs and then move upward in the plant after xylem becomes a hollow vessel.

CP or particles for some viruses have been found in the xylem (French et al., 1993; Andrianifahanana et al., 1997; Opalka et al., 1998; French and Elder, 1999; Ding et al., 2001; Verchot et al., 2001; Moreno et al., 2004; Betti et al., 2012; Manabayeva et al., 2013). This conducting vessel would not be a dead end for infection, since the stem-girdling experiment (Fig. 8) demonstrated that TuMV spreading through xylem vessels caused systemic infection. This investigation has shown that, in addition to viral particles, membrane-bound replication complexes also end up in xylem vessels. TuMV vesicles containing dsRNA were found in immature xylem vessels. This suggests that TuMV replication vesicles may enter into immature xylem vessels and replicate in the cytoplasm before programmed cell death occurs and then move upward in the plant after the xylem becomes a hollow vessel (Fig. 10B), as proposed by Opalka et al. (1998) for *Rice yellow mosaic virus*. The question that follows is how the replication complex is unloaded from xylem vessels. The fluid and content that are exchanged between xylem vessels and xylem parenchymal cells move through pit membranes. Small and large solutes, such as the membrane-impermeant fluorophores CFDA and Texas Red-labeled dextran (10 kD), are unloaded from xylem via the xylem vessel-xylem parenchyma pit membranes, likely by endocytosis. They are then symplasmically transported through PDs to other parenchyma elements and ultimately to sieve elements (Botha et al., 2008). This may also be the case for TuMV, since $6K_2$ is observed in xylem parenchymal cells just above the girdled stem section in which only xylem vessels are intact. This has been suggested for *Soilborne wheat mosaic virus*, which enters and moves systemically through xylem vessels and also laterally between adjacent xylem vessels through pit membranes (Verchot et al., 2001). Displacement of the Ca^{2+} from pit membranes by some viral factors may contribute to the disruption of the pit membranes and may facilitate systemic virus transport (Opalka et al., 1998).

Acknowledgments

We thank Dr. Andreas Wachter (University of Tübingen) for the serum against PTB3, Dr. Peter Moffett (Université de Sherbrooke) for the plasmid PVX-GFP and critical reading of the article, Dr. Hojatollah Vali and Jeannie Mui (Facility of Electron Microscopy Research, McGill University) for TEM technical support, and Jessy Tremblay (Institut National de la Recherche Scientifique-Institut Armand-Frappier) for support with the Zeiss LSM-780 confocal microscope.

References

Agbeci M, Grangeon R, Nelson RS, Zheng H, Laliberté J-F (2013) Contribution of host intracellular transport machineries to intercellular movement of turnip mosaic virus. PLoS Pathog **9:** e1003683

Andrianifahanana M, Lovins K, Dute R, Sikora E, Murphy JF (1997) Pathway for phloem-dependent movement of pepper mottle potyvirus in the stem of capsicum annuum. Phytopathology **87:** 892-898

Aoki K, Kragler F, Xoconostle-Cázares B, Lucas WJ (2002) A subclass of plant heat shock cognate 70 chaperones carries a motif that facilitates trafficking through plasmodesmata. Proceedings of the National Academy of Sciences **99:** 16342-16347

Beauchemin C, Boutet N, Laliberté J-F (2007) Visualization of the Interaction between the Precursors of VPg, the Viral Protein Linked to the Genome of Turnip Mosaic Virus, and the Translation Eukaryotic Initiation Factor iso 4E In Planta. Journal of Virology **81:** 775-782

Beauchemin C, Laliberté J-F (2007) The poly(a) binding protein is internalized in virus-induced vesicles or redistributed to the nucleolus during turnip mosaic virus infection. Journal of Virology **81:** 10905-10913

Betti C, Lico C, Maffi D, D'Angeli S, Altamura MM, Benvenuto E, Faoro F, Baschieri S (2012) Potato virus X movement in Nicotiana benthamiana: new details revealed by chimeric coat protein variants. Molecular Plant Pathology **13:** 198-203

Blackman LM, Boevink P, Cruz SS, Palukaitis P, Oparka KJ (1998) The movement protein of cucumber mosaic virus traffics into sieve elements in minor veins of nicotiana clevelandii. The Plant Cell Online **10:** 525-537

Botha CE, Aoki N, Scofield GN, Liu L, Furbank RT, White RG (2008) A xylem sap retrieval pathway in rice leaf blades: evidence of a role for endocytosis? J Exp Bot **59:** 2945-2954

Brault V, Bergdoll M, Mutterer J, Prasad V, Pfeffer S, Erdinger M, Richards KE, Ziegler-Graff V (2003) Effects of point mutations in the major capsid protein of beet

western yellows virus on capsid formation, virus accumulation, and aphid transmission. Journal of Virology **77:** 3247-3256

Buhtz A, Springer F, Chappell L, Baulcombe DC, Kehr J (2008) Identification and characterization of small RNAs from the phloem of Brassica napus. The Plant Journal **53:** 739-749

Carrington JC, Jensen PE, Schaad MC (1998) Genetic evidence for an essential role for potyvirus CI protein in cell-to-cell movement. Plant J **14:** 393-400

Cotton S, Grangeon R, Thivierge K, Mathieu I, Ide C, Wei T, Wang A, Laliberté J-F (2009) Turnip mosaic virus rna replication complex vesicles are mobile, align with microfilaments, and are each derived from a single viral genome. Journal of Virology **83:** 10460-10471

Cronin S, Verchot J, Haldeman-Cahill R, Schaad MC, Carrington JC (1995) Long-distance movement factor: a transport function of the potyvirus helper component proteinase. Plant Cell **7:** 549-559

Cronin S, Verchot J, Haldemancahill R, Schaad MC, Carrington JC (1995) Long-distance movement factor - a transport function of the potyvirus helper component proteinase. Plant Cell **7:** 549-559

Cruz SS, Roberts AG, Prior DAM, Chapman S, Oparka KJ (1998) Cell-to-cell and phloem-mediated transport of potato virus x: The role of virions. The Plant Cell Online **10:** 495-510

Derrick PM, Barker H, Oparka KJ (1990) Effect of virus infection on symplastic transport of fluorescent tracers in Nicotiana clevelandii leaf epidermis. Planta **181:** 555-559

Ding XS, Boydston CM, Nelson RS (2001) Presence of brome mosaic virus in barley guttation fluid and its association with localized cell death response. Phytopathology **91:** 440-448

Dolja VV, Haldeman R, Robertson NL, Dougherty WG, Carrington JC (1994) Distinct functions of capsid protein in assembly and movement of tobacco etch potyvirus in plants. The EMBO journal **13:** 1482-1491

Dolja VV, Haldeman-Cahill R, Montgomery AE, Vandenbosch KA, Carrington JC (1995) Capsid protein determinants involved in cell-to-cell and long distance movement of tobacco etch potyvirus. Virology **206:** 1007-1016

Dufresne PJ, Thivierge K, Cotton S, Beauchemin C, Ide C, Ubalijoro E, Laliberté J-F, Fortin MG (2008) Heat shock 70 protein interaction with Turnip mosaic virus RNA-dependent RNA polymerase within virus-induced membrane vesicles. Virology **374:** 217-227

Evert RF (1977) Phloem structure and histochemistry. Annual Review of Plant Physiology **28:** 199-222

Fisher DB, Wu Y, Ku MSB (1992) Turnover of soluble proteins in the wheat sieve tube. Plant Physiology **100:** 1433-1441

French CJ, Elder M (1999) Virus particles in guttate and xylem of infected cucumber (Cucumis sativus L.). Annals of Applied Biology **134:** 81-87

French CJ, Elder M, Skelton F (1993) Recovering and identifying infectious plant viruses in guttation fluid. HortScience **28:** 746-747

Froelich DR, Mullendore DL, Jensen KH, Ross-Elliott TJ, Anstead JA, Thompson GA, Pélissier HC, Knoblauch M (2011) Phloem ultrastructure and pressure flow: Sieve-element-occlusion-related agglomerations do not affect translocation. The Plant Cell Online **23:** 4428-4445

Gómez G, Torres H, Pallás V (2005) Identification of translocatable RNA-binding phloem proteins from melon, potential components of the long-distance RNA transport system. The Plant Journal **41:** 107-116

Gopinath K, Kao CC (2007) Replication-independent long-distance trafficking by viral rnas in nicotiana benthamiana. The Plant Cell **19:** 1179-1191

Grangeon R, Agbeci M, Chen J, Grondin G, Zheng H, Laliberté J-F (2012) Impact on the endoplasmic reticulum and golgi apparatus of turnip mosaic virus infection. Journal of Virology **86:** 9255-9265

Grangeon R, Jiang J, Wan J, Agbeci M, Zheng H, Laliberte JF (2013) 6K2-induced vesicles can move cell to cell during turnip mosaic virus infection. Front Microbiol **4:** 351

Grignon N, Touraine B, Durand M (1989) 6(5) Carboxyfluorescein as a tracer of phloem sap translocation. American Journal of Botany **76:** 871-877

Ham BK, Brandom JL, Xoconostle-Cazares B, Ringgold V, Lough TJ, Lucas WJ (2009) A polypyrimidine tract binding protein, pumpkin RBP50, forms the basis of a phloem-mobile ribonucleoprotein complex. Plant Cell **21:** 197-215

Ham BK, Lucas WJ (2014) The angiosperm phloem sieve tube system: a role in mediating traits important to modern agriculture. J Exp Bot **65:** 1799-1816

Haywood V, Yu T-S, Huang N-C, Lucas WJ (2005) Phloem long-distance trafficking of GIBBERELLIC ACID-INSENSITIVE RNA regulates leaf development. The Plant Journal **42:** 49-68

Hipper C, Brault V, Ziegler-Graff V, Revers F (2013) Viral and cellular factors involved in phloem transport of plant viruses. Frontiers in Plant Science **4**

Hipper C, Monsion B, Bortolamiol-Bécet D, Ziegler-Graff V, Brault V (2014) Formation of virions is strictly required for turnip yellows virus long-distance movement in plants. Journal of General Virology **95:** 496-505

Hitchborn JH, Hills GJ (1965) The use of negative staining in the electron microscopic examination of plant viruses in crude extracts. Virology **27:** 528-540

Hoefert LL (1984) Beet western yellows virus in phloem of pennycress. Journal of Ultrastructure Research **88:** 44-54

Huang T-S, Wei T, Laliberté J-F, Wang A (2010) A Host RNA Helicase-Like Protein, AtRH8, Interacts with the Potyviral Genome-Linked Protein, VPg, Associates with the Virus Accumulation Complex, and Is Essential for Infection. Plant Physiology **152:** 255-266

Kasschau KD, Carrington JC (2001) Long-distance movement and replication maintenance functions correlate with silencing suppression activity of potyviral HC-Pro. Virology **285:** 71-81

Kasschau KD, Cronin S, Carrington JC (1997) Genome amplification and long-distance movement functions associated with the central domain of tobacco etch potyvirus helper component-proteinase. Virology **228:** 251-262

Kempers R, Bel AE (1997) Symplasmic connections between sieve element and companion cell in the stem phloem ofVicia faba L. have a molecular exclusion limit of at least 10 kDa. Planta **201:** 195-201

Knapp E, Flores R, Scheiblin D, Scheiblin D, Modla S, Czymmek K, Czymmek K, Yusibov V (2012) A cryohistological protocol for preparation of large plant tissue sections for screening intracellular fluorescent protein expression. Biotechniques **52:** 31-37

Koh E-J, Zhou L, Williams D, Park J, Ding N, Duan Y-P, Kang B-H (2012) Callose deposition in the phloem plasmodesmata and inhibition of phloem transport in citrus leaves infected with “Candidatus Liberibacter asiaticus”. Protoplasma **249:** 687-697

Laliberté J-F, Sanfaçon H (2010) Cellular remodeling during plant virus infection. Annual Review of Phytopathology **48:** 69-91

Leonard S, Viel C, Beauchemin C, Daigneault N, Fortin MG, Laliberte JF (2004) Interaction of VPg-Pro of Turnip mosaic virus with the translation initiation factor 4E and the poly(A)-binding protein in planta. Journal of General Virology **85:** 1055-1063

Lin M-K, Lee Y-J, Lough TJ, Phinney BS, Lucas WJ (2009) Analysis of the Pumpkin Phloem Proteome Provides Insights into Angiosperm Sieve Tube Function. Molecular & Cellular Proteomics **8:** 343-356

Lin S-I, Chiang S-F, Lin W-Y, Chen J-W, Tseng C-Y, Wu P-C, Chiou T-J (2008) Regulatory network of microrna399 and pho2 by systemic signaling. Plant Physiology **147:** 732-746

Lucas WJ, Groover A, Lichtenberger R, Furuta K, Yadav SR, Helariutta Y, He XQ, Fukuda H, Kang J, Brady SM, Patrick JW, Sperry J, Yoshida A, Lopez-Millan AF, Grusak MA, Kachroo P (2013) The plant vascular system: evolution, development and functions. J Integr Plant Biol **55:** 294-388

Lucocq JM, Habermann A, Watt S, Backer JM, Mayhew TM, Griffiths G (2004) A Rapid Method for Assessing the Distribution of Gold Labeling on Thin Sections. Journal of Histochemistry & Cytochemistry **52:** 991-1000

Ma Y, Miura E, Ham BK, Cheng HW, Lee YJ, Lucas WJ (2010) Pumpkin eIF5A isoforms interact with components of the translational machinery in the cucurbit sieve tube system. Plant J **64:** 536-550

Manabayeva SA, Shamekova M, Park J-W, Ding XS, Nelson RS, Hsieh Y-C, Omarov RT, Scholthof HB (2013) Differential requirements for Tombusvirus coat protein and P19 in plants following leaf versus root inoculation. Virology **439:** 89-96

McGuire ELHJM (1973) Translocation of tobacco ringspot virus in soybean. Phytopathology **63:** 1291-1300

Metzner R, Schneider HU, Breuer U, Thorpe MR, Schurr U, Schroeder WH (2010) Tracing cationic nutrients from xylem into stem tissue of French bean by stable isotope tracers and cryo-secondary ion mass spectrometry. Plant Physiol **152:** 1030-1043

Miller S, Krijnse-Locker J (2008) Modification of intracellular membrane structures for virus replication. Nat Rev Micro **6:** 363-374

Moreno IM, Thompson JR, García-Arenal F (2004) Analysis of the systemic colonization of cucumber plants by Cucumber green mottle mosaic virus. Journal of General Virology **85:** 749-759

Murant AF, Roberts IM (1979) Virus-like particles in phloem tissue of chervil (Anthriscus cerefolium) infected with carrot red leaf virus. Annals of Applied Biology **92:** 343-346

Nicolas O, Dunnington SW, Gotow LF, Pirone TP, Hellmann GM (1997) Variations in the VPg protein allow a potyvirus to overcome va gene resistance in tobacco. Virology **237:** 452-459

Opalka N, Brugidou C, Bonneau C, Nicole M, Beachy RN, Yeager M, Fauquet C (1998) Movement of rice yellow mottle virus between xylem cells through pit membranes. Proceedings of the National Academy of Sciences **95:** 3323-3328

Oparka KJ, Turgeon R (1999) Sieve elements and companion cells—traffic control centers of the phloem. The Plant Cell **11:** 739-750

Otulak K, Garbaczewska G (2009) Ultrastructural events during hypersensitive response of potato cv. Rywal infected with necrotic strains of potato virus Y. Acta Physiologiae Plantarum **32:** 635-644

Otulak K, Garbaczewska G (2012) Cytopathological potato virus Y structures during Solanaceous plants infection. Micron **43:** 839-850

Pant BD, Buhtz A, Kehr J, Scheible W-R (2008) MicroRNA399 is a long-distance signal for the regulation of plant phosphate homeostasis. The Plant Journal **53:** 731-738

Peart JR, Cook G, Feys BJ, Parker JE, Baulcombe DC (2002) An EDS1 orthologue is required for N-mediated resistance against tobacco mosaic virus. The Plant Journal **29:** 569-579

Rajamaki ML, Valkonen JP (1999) The 6K2 protein and the VPg of potato virus A are determinants of systemic infection in Nicandra physaloides. Mol Plant Microbe Interact **12:** 1074-1081

Rajamaki ML, Valkonen JP (2002) Viral genome-linked protein (VPg) controls accumulation and phloem-loading of a potyvirus in inoculated potato leaves. Mol Plant Microbe Interact **15:** 138-149

Rajamaki ML, Valkonen JPT (2002) Viral genome-linked protein (VPg) controls accumulation and phloem-loading of a potyvirus in inoculated potato leaves. Molecular Plant-Microbe Interactions **15:** 138-149

Requena A, Simón-Buela L, Salcedo G, García-Arenal F (2006) Potential involvement of a cucumber homolog of phloem protein 1 in the long-distance movement of cucumber mosaic virus particles. Molecular Plant-Microbe Interactions **19:** 734-746

Roberts K, McCann MC (2000) Xylogenesis: the birth of a corpse. Current Opinion in Plant Biology **3:** 517-522

Rojas MR, Zerbini FM, Allison RF, Gilbertson RL, Lucas WJ (1997) Capsid protein and helper component-proteinase function as potyvirus cell-to-cell movement proteins. Virology **237:** 283-295

Roney JK, Khatibi PA, Westwood JH (2007) Cross-species translocation of mrna from host plants into the parasitic plant dodder. Plant Physiology **143:** 1037-1043

Rühl C, Stauffer E, Kahles A, Wagner G, Drechsel G, Rätsch G, Wachter A (2012) Polypyrimidine tract binding protein homologs from arabidopsis are key regulators of alternative splicing with implications in fundamental developmental processes. The Plant Cell Online **24:** 4360-4375

Ruiz-Medrano R, Xoconostle-Cazares B, Lucas WJ (1999) Phloem long-distance transport of CmNACP mRNA: implications for supracellular regulation in plants. Development **126:** 4405-4419

Sasaki T, Chino M, Hayashi H, Fujiwara T (1998) Detection of several mrna species in rice phloem sap. Plant and Cell Physiology **39:** 895-897

Savenkov EI, Germundsson A, Zamyatnin AA, Sandgren M, Valkonen JPT (2003) Potato mop-top virus: the coat protein-encoding RNA and the gene for cysteine-rich protein are dispensable for systemic virus movement in Nicotiana benthamiana. Journal of General Virology **84:** 1001-1005

Schaad MC, Lellis AD, Carrington JC (1997) VPg of tobacco etch potyvirus is a host genotype-specific determinant for long-distance movement. Journal of Virology **71:** 8624-8631

Schonborn J, Oberstraβ J, Breyel E, Tittgen J, Schumacher J, Lukacs N (1991) Monoclonal antibodies to double-stranded RNA as probes of RNA structure in crude nucleic acid extracts. Nucleic Acids Research **19:** 2993-3000

Shepardson S, Esau K, McCrum R (1980) Ultrastructure of potato leaf phloem infected with potato leafroll virus. Virology **105:** 379-392

Shukla DD, Ward CW, Brunt AA (1994) The Potyviridae. CAB international, Wallingford, United kingdom

Simón-Buela L, García-Arenal F (1999) Virus particles of cucumber green mottle mosaic tobamovirus move systemically in the phloem of infected cucumber plants. Molecular Plant-Microbe Interactions **12:** 112-118

Swanson M, Barker H, Macfarlane SA (2002) Rapid vascular movement of tobraviruses does not require coat protein: evidence from mutated and wild-type viruses. Annals of Applied Biology **141:** 259-266

Terasaki M, Reese TS (1992) Characterization of endoplasmic reticulum by co-localization of BiP and dicarbocyanine dyes. Journal of Cell Science **101:** 315-322

Tilsner J, Linnik O, Louveaux M, Roberts IM, Chapman SN, Oparka KJ (2013) Replication and trafficking of a plant virus are coupled at the entrances of plasmodesmata. The Journal of Cell Biology **201:** 981-995

Verchot J, Driskel BA, Zhu Y, Hunger RM, Littlefield LJ (2001) Evidence that soilborne wheat mosaic virus moves long distance through the xylem in wheat. Protoplasma **218:** 57-66

Vijayapalani P, Maeshima M, Nagasaki-Takekuchi N, Miller WA (2012) Interaction of the trans-frame potyvirus protein P3N-PIPO with host protein PCaP1 facilitates potyvirus movement. PLoS Pathog **8:** e1002639

Wei T, Zhang C, Hong J, Xiong R, Kasschau KD, Zhou X, Carrington JC, Wang A (2010) Formation of complexes at plasmodesmata for potyvirus intercellular movement is mediated by the viral protein P3N-PIPO. PLoS Pathog **6:** e1000962

Wolf S, Lucas WJ, Deom CM, Beachy RN (1989) Movement protein of tobacco mosaic virus modifies plasmodesmatal size exclusion limit. Science **246:** 377-379

Wood PJ (1980) Specificity in the interaction of direct dyes with polysaccharides. Carbohydrate Research **85:** 271-287

Xoconostle-Cázares B, Ruiz-Medrano R, Lucas WJ (2000) Proteolytic processing of CmPP36, a protein from the cytochrome b5 reductase family, is required for entry into the phloem translocation pathway. The Plant Journal **24:** 735-747

Xoconostle-Cázares B, Xiang Y, Ruiz-Medrano R, Wang H-L, Monzer J, Yoo B-C, McFarland KC, Franceschi VR, Lucas WJ (1999) Plant paralog to viral movement protein that potentiates transport of mrna into the phloem. Science **283:** 94-98

Yoo B-C, Kragler F, Varkonyi-Gasic E, Haywood V, Archer-Evans S, Lee YM, Lough TJ, Lucas WJ (2004) A systemic small rna signaling system in plants. The Plant Cell **16:** 1979-2000

Zhang X, Zhao X, Zhang Y, Niu S, Qu F, Zhang Y, Han C, Yu J, Li D (2013) N-terminal basic amino acid residues of Beet black scorch virus capsid protein play a critical role in virion assembly and systemic movement. Virol J **10:** 200

CHAPTER 3: PUBLICATION NO. 2

Ultrastructural characterization of *Turnip mosaic virus* induced cellular rearrangements reveal membrane-bound viral particles accumulating in vacuoles

Submitted to Journal of virology

Juan Wan[1], Kaustuv Basu[2], Jeannie Mui [2], Hojatollah Vali [2,3],

Huanquan Zheng[4], and Jean-François Laliberté[1#]

1. INRS-Institut Armand-Frappier, Laval, Québec, Canada
2. Facility for Electron Microscopy Research, McGill University, Montréal, Québec, Canada
3. Department of Anatomy & Cell Biology, Montréal, Québec, Canada
4. Department of Biology, McGill University, Montréal, Québec, Canada

 # Correspondence should be sent to:

Jean-François Laliberté

INRS-Institut Armand-Frappier

531, boulevard des Prairies

Laval, Québec, Canada H7V 1B7

Telephone number: 1-450-687-5010, ext. 4445

email address: jean-francois.laliberte@iaf.inrs.ca

Contribution of student

This manuscript has been submitted to *Journal of Virology*. I designed and performed almost all of the experimental work and analysed data with advice from my supervisor Professor Jean-François Laliberté. Jeannie Mui, Kaustuv Basu and Mihnea Bostina of FEMR team at McGill University helped me improve the conventional TEM sample preparation protocol, the HPF/FS sample preparation, and collect the electron tomography data. I prepared the first draft of this manuscript, and Jean-Francois Laliberté helped me improve the writing.

Résumé

Les virus à ARN positif [ARN(+)] remanient les membranes cellulaires pour faciliter leur réplication et leur assemblage. Dans le cas du virus de la mosaïque du navet [*Turnip mosaic virus*, (TuMV)] la protéine virale membranaire $6K_2$ joue un rôle essentiel dans l'altération du système endomembranaire. Même si les structures dynamiques induites par $6K_2$ ont été largement étudiées par microscopie confocale, la caractérisation détaillée de leur ultrastructure n'a pas encore été examinée. Dans cette étude, nous avons investigué sur la formation des structures membranaires induites par le TuMV au cours du temps par deux méthodes de fixation, la fixation chimique et la fixation par congélation à haute pression et substitution par congélation (high-pressure freezing/freezing substitution, HPF/FS) pour faire de la microscopie électronique à transmission a différents temps au cours de l'infection. Lors des étapes précoces de l'infection, nous avons observé la formation d'agrégats de membranes sans forme définie (convoluted membranes, CM) et connectés au réticulum endoplasmique rugueux (RER). Puis à des étapes intermédiaires de l'infection, nous avons découvert des agrégats hétérogènes de ce qui semblerait être des vésicules à simple membrane (SMVL, single membrane vesicle-like). À des stades tardifs de l'infection, nous avons observé des SMVLs, des vésicules à double membrane (DMVLs, double membrane vesicle-like) avec un cœur dense aux électrons, ainsi que des corps denses aux électrons. Un marquage à l'immunogold a montré que les vésicules induites par le TuMV contiennent la protéine $6K_2$ et que seules les vésicules à simple membrane (SMVL) sont les sites de réplication de l'ARN viral. Nous avons effectué de la tomographie électronique (TE) pour générer un modèle en 3 dimensions de ces vésicules, ceci a révélé qu'il s'agissait de tubules. Plus tardivement lors de l'infection nous avons observé des paquets de particules filamenteuses en association avec des corps denses aux électrons ce qui suggère qu'il s'agirait des sites d'assemblage des particules virales du TuMV. De plus, il a été observé une accumulation de particules virales du TuMV au sein de la vacuole sous forme d'un réseau linéaire associé aux membranes. Nos travaux dévoilent l'apparition séquentielle des différentes structures

membranaires induites par le TuMV pour assurer la réplication virale, l'assemblage de des particules virales et de leur accumulation.

Abstract

Positive-strand RNA [(+) RNA] viruses remodel cellular membranes to facilitate virus replication and assembly. In the case of *Turnip mosaic virus* (TuMV), the viral membrane protein $6K_2$ plays an essential role in endomembrane alterations. Although $6K_2$-induced membrane dynamics have been widely studied by confocal microscopy, the ultrastructure of this remodeling has not been extensively examined. In this study, we investigated the formation of TuMV-induced membrane changes by chemical fixation and high-pressure freezing/freeze substitution (HPF/FS) for transmission electron microscopy at different times of infection. We observed the formation of convoluted membranes connected to rough endoplasmic reticulum (rER) early in the infection process, followed by the production of single-membrane vesicle-like (SMVL) structures at mid stage of infection. Both SMVL and double-membrane vesicle-like structures with electron-dense cores, as well as electron-dense bodies, were found late in the infection process. Immunogold labeling results showed that the vesicle-like structures were $6K_2$ tagged, and only the SMVL structures were viral RNA replication sites. Electron tomography (ET) was used to regenerate a three-dimensional model of these vesicle-like structures, which showed they were in fact tubules. Late in infection, we observed filamentous particle bundles associated with electron-dense bodies, which suggests that these are sites for viral particle assembly. In addition, TuMV particles were observed to accumulate in the central vacuole as membrane-associated linear arrays. Our work thus unravels the sequential appearance of distinct TuMV-induced membrane structures for viral RNA replication, viral particle assembly and accumulation.

Introduction

Positive-strand RNA [(+) RNA] viruses remodel cellular membranes for different stages of the infectious process, such as protein translation and processing, viral RNA (vRNA) synthesis, particle assembly, and virus transmission. Ultrastructural studies showed distinct membrane structures could be simultaneously generated in one cell that was infected with animal (+) RNA viruses. For instance, *severe acute respiratory syndrome* (SARS) coronavirus-induced membrane structures are a unique reticulovesicular network of modified endoplasmic reticulum (ER) that integrates convoluted membranes (CM) for polyprotein synthesis and processing, numerous interconnected double-membrane vesicles (DMVs) for vRNA synthesis, and vesicle packets (VPs) for virus assembly and budding (1). (+) RNA virus-induced distinct membrane structures can be also observed during the time course of infection. *Coxsackievirus B3* (CVB3) induces single-membrane tubules (SMTs) at an early stage of infection for vRNA synthesis, followed by the formation of DMVs and multilamellar structures late in infection (2).

Plant (+) RNA viruses also manipulate host membranes for their replication [reviewed in (3)]. However, limited transmission electron microscopy (TEM) data have been generated on the remodeling of cellular membrane during vRNA replication and encapsidation. Several plant (+) RNA viruses have been observed to produce spherule-like structures on different membrane-bound organelles such as ER [*Brome mosaic virus* (BMV) (4)], vacuole [*Cucumber mosaic virus* (CMV) (5)], peroxisome [*Tomato bushy stunt virus* (TBSV) (6, 7)], mitochondrion [*Carnation Italian ringspot virus* (CIRV) (8, 9)] and chloroplast [*Turnip yellow mosaic virus* (TYMV, *Tymovirus, Tymoviridae*) (10, 11)]. These spherule-like structures are similar to those induced by some animal (+) RNA viruses for vRNA synthesis, as they are all formed by membrane invagination of the outer organelle membrane and have a pore-like opening allowing exchange of materials between the lumen of the spherule and the cytoplasm. These spherule-like structures are static and reside inside the different membrane-bound organelles. Conversely, another type of plant (+) RNA virus-induced membrane structures are ER-derived vesicles, which are highly motile and morphologically dynamic, such as in

Cowpea mosaic virus (CPMV) (12), *Grapevine fanleaf virus* (GFLV) (13), *Potato virus X* (PVX) (14, 15) and *Turnip mosaic virus* (TuMV) (16) infected cells. However, not much is known about the ultrastructure of these ER-derived vesicles.

TuMV is a (+) RNA virus that belongs to the genus *Potyvirus* in the family *Potyviridae*. Potyviruses are the largest genera of plant viruses and are responsible for more than half of the viral crop damage in the world [reviewed in (17)]. Potyviral particles are flexuous rods of approximately 680 to 900 nm in length and 11 to 15 nm in diameter. The viral genome is a single RNA molecule of approximately 10 kb. The 5' end is covalently linked to a protein VPg (for viral protein genome-linked) and the 3' end has a poly (A) tail. The vRNA codes for a polyprotein that is processed by three viral proteinases into at least 12 proteins.

TuMV infection leads to the formation of numerous vesicles that originate from the ER (16, 18, 19). The viral membrane protein $6K_2$ is responsible for vesicle formation (18). $6K_2$-induced vesicles contain vRNA and several replication-related viral and host proteins (18-21), and are thus considered to be the site of vRNA replication. These vesicles also participate in cell-to-cell movement of the vRNA. They are motile (19), traffic through the secretory pathway and use myosin motors (22). Ultimately, the vesicles associate with plasmodesmata (PD) and are then released into neighboring cells (23) for a new round of infection. They are also involved in long distance virus movement as they are present in phloem sieve elements and xylem vessels (Wan et al. 2015).

The above studies relied mainly on observations in light microscopy. TEM images of virus-induced vesicles have also been reported for TuMV- (16), and *Potato virus Y* (PVY)-infected cells (24). These images showed the presence of numerous single-membrane vesicles (SMVs), or what appeared to be vesicles, and on some occasions, the vesicles were found to be in direct continuity with the rough endoplasmic reticulum (rER). There has been, however, no study looking at the biogenesis of these apparent vesicles over the time course of infection, and their relationship with viral particle assembly.

In this study, we investigated the formation and maturation of the TuMV-induced membrane remodeling that took place over several days of infection. The first change that was observed involved rER-connected convoluted membrane accumulation. This was followed by the formation of SMV-like (SMVL) structures, which were shown to be vRNA replication sites. Later in the infection process, double-membrane vesicle-like (DMVL) structures having an electron-dense core were observed, along with electron-dense bodies associated with viral particle bundles. Electron tomography (ET) showed that the vesicle-like structures were in fact tubules. In addition, TuMV particles were observed to accumulate in the central vacuole as membrane-associated linear arrays.

Materials and Methods

Plasmid DNA and plant inoculation

The infectious clone pCambiaTuMV/6K_2:GFP has been described previously (25). The plasmid pCambiaTuMV/6K_2:GFP:HA was constructed as follow. The GFP fragment was amplified by PCR from pGreen/PABP:GFP (26) by using the forward primer 5'-CGGGATCCATGGTGAGCAAGGGCGA-3' and the reverse primer 5'-CGGAATTCTTACTTGTACAGCTCGTCCA-3' (the restriction sites are underlined), and digested with BamHI and EcoRI. The digested GFP fragment was then used to replace the mCherry fragment of pCambia/6K2:mCherry (23), and the resulting construct was named pCambia/6K2:GFP. The 6K_2:GFP:HA-coding region was amplified by PCR from pCambia/6K_2:GFP by using the forward primer 5'-GCTCTAGAATGAACACCAGCGACATGAGC-3' and the reverse primer 5'-CGGAATTCTTA***AGCGTAGTCTGGAACGTCGTATGGGTA***CTTGTACAGCTCGTCCA TGCC-3' (the restriction sites are underlined, the HA tag cording sequence are highlighted in bold italics), and digested with XbaI and EcoRI. The digested 6K_2:GFP-HA fragment was then used to replace 6K_2:GFP fragment of pCambia/6K_2:GFP, and the resulting construct was named pCambia/6K_2:GFP:HA. The 6K_2:GFP:HA-coding region was amplified again by PCR from pCambia/6K_2:GFP:HA by using the forward primer 5'-TCCCCGCGGGAAACACCAGCGACATGAGC-3' and the reverse primer 5'-TCCCCGCGG***CTGCCTGGTGATAGACACAAGC***AGCGTAGTCTGGAACGTC-3' (the restriction sites are underlined, the proteinase cleavage site cording sequence are highlighted in bold italics). The PCR product was digested with SacII and introduced into SacII site of p35Tunos/SacII (27) to obtain p35Tunos/6K_2:GFP:HA. This plasmid was then cut with SmaI and KpnI, and ligated in pCambiaTunos (23) that was cut with the same enzymes. Kanamycin-resistant *E. coli* colonies were screened for plasmids containing the fragment encoding 6K_2:GFP:HA, and the resulting construct is pCambiaTuMV/ 6K_2:GFP:HA. All plasmid constructs were verified by sequencing.

TuMV infectious clones and the mock empty vector pCambia 0390 were electroporated into *Agrobacterium tumefaciens* strain AGL1 and selected on Luria broth (LB) ampicillin-kanamycin plates. The pellet of an overnight culture was resuspended in

water supplemented with 10 mM $MgCl_2$ and 150 µM acetosyringone and kept at room temperature (RT) for 2 to 4 h. The solution was then diluted to an OD_{600} of 0.3. Agroinfiltration was performed with 4-week-old *N. benthamiana* plants, which were grown under a 16 h light/8 h dark photoperiod, 22°C day /20°C night temperatures.

Histological preparation and confocal microscopy

The midrib area of TuMV/6K_2:GFP systemically infected *N. benthamiana* leaves were cut and fixed in 4% (w/v) paraformaldehyde plus 0.5% (w/v) glutaraldehyde at different dpi for more than 24 h at 4°C. The air between the intercellular spaces was removed by infiltrating with the fixative before the cutting. The fixed samples were treated with 100 mM glycine in phosphate-buffered saline (PBS) for 1h to reduce the background fluorescence, followed by sucrose gradient and cryosectioning as described (28). The sections were observed using a 20× (N.A.=0.8) objective on an LSM-780 confocal microscope (Carl Zeiss Microscopy). Zen 2011 (Carl Zeiss Microscopy) was used for image acquisition. Excitation/emission wavelengths were 405/410–440 nm for Fluorescent Brightener 28, 488/490–560 nm for GFP.

Chemical fixation

Small pieces (1.5 mm x 2 mm) of mock- and TuMV- infected leaf midrib were cut and fixed in 2.5% (w/v) glutaraldehyde in 0.1 M sodium cacodylate buffer, pH 7.4 for 24 h at 4°C. After rinsing 3 times for 10 min each in washing buffer at RT, the samples were post-fixed in 1% (w/v) osmium tetroxide with 1.5% (w/v) potassium ferrocyanide in sodium cacodylate buffer for 2 h at 4°C. The samples were then rinsed in washing buffer at RT (3 times for 10 min each) and stained with 1% (w/v) tannic acid for 1 h at 4°C. After rinsing 3 times in water at RT, the samples were dehydrated in a graded acetone series (30, 50, 70, 80, 90 and 100%) for 20 min at each step at RT. 100% acetone rinsing was repeated two more times. The samples were then gradually infiltrated with increasing concentrations of Epon 812 resin (50, 66, 75 and 100%) mixed with acetone for a minimum of 8 h for each step. 25-psi vacuum was applied, when the samples were in pure Epon 812 resin. Samples were finally embedded in pure, fresh Epon 812 resin and polymerized at 60°C for 48 h. After polymerization, the 90-100 nm

ultrathin sections were obtained and stained with 4% (w/v) uranyl acetate for 8 min and Reynolds lead citrate for 5 min. Sections were examined in a Tecnai T12 transmission electron microscope (FEI) operating at 120 kV. Images were recorded using an AMT XR80C charge-coupled-device (CCD) camera system (Advanced Microscopy Techniques, Corp.).

Immunogold labeling

Large pieces (1.5 mm x 5 mm) of mock- and TuMV- infected leaf midrib were cut and fixed in 4% (w/v) formaldehyde and 0.25% (w/v) glutaraldehyde in 0.1 M Sorensen's phosphate buffer, pH 7.4 for 4 h at 4°C. After rinsing the samples 3 times for 10 min each in washing buffer at RT. For anti-dsRNA antibody treated samples, samples were post-fixed in 0.1% (w/v) reduced osmium tetroxide for 15 min at 4°C (29). The samples were then rinsed in water at RT (3 times for 10 min each) and dehydrated in a graded alcohol series (30, 50, 70, 80, 90, 95 and 100%) for 20 min at each step at 4°C on a rotator. Rinsing in 100% alcohol was repeated one more time. The samples were then gradually infiltrated with increasing concentrations of LR white resin (50, 75 and 100%) mixed with alcohol for a minimum of 8 h for each step at 4°C on a rotator. The samples were finally embedded in pure LR White resin and polymerized at 50°C for 48 h. 90 -100 nm sections were incubated in 20 mM glycine in Dulbecco's phosphate buffered saline [DPBS (137 mM NaCl, 2.7 mM KCl, 1.5 mM KH_2PO_4, 6.5 mM Na_2HPO_4, 1 mM $CaCl_2$, 0.5 mM $MgCl_2$, pH 7.4)] for 10 min to inactivate residual aldehyde groups, and then in blocking solution (DPBS-BCO: 2% (w/v) BSA, 2% (w/v) casein, and 0.5% (w/v) ovalbumin in DPBS) for 5 min. Sections were then incubated with primary antibody diluted in DPBS-BCO for 1 h at RT. After 6 washings (5 min each) in DPBS, sections were incubated with secondary antibodies diluted in DPBS-BCO. After washing with DPBS and distilled water, grids were stained with 4% (w/v) uranyl acetate for 5 min and Reynolds lead citrate for 3 min. Background labeling was determined using mock-infected leaf cross-sections. Quantification of the distribution of the gold particles per μm^2 and relative labeling distribution were performed over mock-infected and TuMV-infected sections according to (30).

For the primary antibodies, the mouse monoclonal anti-dsRNA antibody J2 (stock solution is 1 mg ml^{-1}) (English and Scientific Consulting Bt.) was diluted in DPBS-BCO to 1:40, the rat monoclonal anti-HA antibody 3F10 (stock solution is 0.1 mg ml^{-1}) (Roche) was diluted in DPBS-BCO to 1:10, the rabbit polyclonal anti-RdRp antibodies (Dufresne et al., 2008) were diluted in DPBS-BCO to 1:20. For the secondary antibodies, the goat anti-mouse and anti-rat antibodies conjugated to 10 nm gold particles (Sigma-Aldrich), as well as the goat anti-rabbit antibodies conjugated to 12 nm gold particles (Jackson ImmunoResearch) were used at a dilution of 1:20.

High-pressure freezing and freeze substitution (HPF/FS)

For HPF, discs with a diameter of 1.2 mm of mock- and TuMV- infected leaf tissues (avoidimg rib tissue) were punched out with a punching device for flat specimen carriers (Leica Microsystems) in a drop of 1-hexadecene on a soft piece of rubber. Subsequently the samples were transferred into the cavity (1.2 mm in diameter) of gold-plated flat specimen carriers that were 200 µm in depth and pre-filled with 1-hexadecene as a cryoprotectant. The samples were frozen immediately in a high-pressure freezer (Leica EM PACT2; Leica Microsystems). Platelets containing frozen samples were then transferred and stored under liquid nitrogen conditions in transfer boxes.

FS was carried out using an automatic FS system (Leica EM AFS2; Leica Microsystems) at −80°C (72 h), −65°C (24 h), −40°C (12 h), −20°C (12 h), 0°C (6 h) and RT (2 h) in anhydrous acetone containing 2% osmium tetroxide and 0.2% uranyl acetate. After the samples were rinsed three times in anhydrous acetone for 15 min, they were infiltrated with increasing concentrations of Epon 812 resin [5 (4 h), 10 (8 h), 25 (8 h), 50 (18 h), 75 (24 h), 100% (24 h)] mixed with acetone at RT. The embedded samples were then polymerized in pure, fresh Epon 812 resin for 48 h at 60°C. Ultrathin sections were cut, post-stained, as described above, and observed in the TEM.

Electron tomography

90-nm-thick and 200-nm-thick chemical-fixed sections were collected on formvar-coated copper grids. A series of single-axis tilt images were collected with a Tecnai G^2 F20 Cryo-S/TEM (FEI) operated at an accelerating voltage of 200 kV, and these images were recorded with a Gatan Ultrascan 4000 4k x 4k Digital CCD Camera System Model 895. Images captured over a tilt range of ± 64° (1° increments) on the 90-nm-thick section, and the resulting images had a pixel size of 0.5 nm. Images captured over a tilt range of ± 60° [2° increments in low tilts (up to tilt angle ±30°) and 1° increments at high tilts (from tilt angles ±30° to ±60°)] on the 200-nm-thick sections, and the resulting images had a pixel size of 1.0 nm (Fig. 6) and 0.78 nm (Fig. 7). The images from the tilt series were aligned and reconstructed into a series of tomographic slices using the IMOD software package (31). The 3-D surface models were created with the Amira (ver. 6.0) visualization package (FEI Visualization Sciences Group), by manually selecting areas of interest.

Vacuole isolation

The vacuole isolation was done as described previously (32) with some modifications. 4-week-old *N.benthamiana* plants were agroinfiltrated with the infectious clone TuMV/6K_2:GFP or mock empty vector pCambia 0390. TuMV systemically infected leaves or mock-infected young leaves were collected at 9 dpi, and sliced into 1-mm stripes using a razor blade. The processed leaves were placed in protoplast enzyme solution (0.4 M mannitol, 20 mM Mes, pH 5.7. 20 mM KCl, 1.5% (w/v) Cellulase R-10, 0.2% (w/v) Macerozyme R-10, 0.1% (w/v) BSA, 10 mM $CaCl_2$). Vacuum was applied for 20 minutes to remove the air within the leaf tissues, and then the vacuum was slowly released for about 10 minutes to allow the protoplast enzyme solution to enter into the leaf tissues. The leaf stripes were kept in dark at RT for another 3.5 hours. The released protoplasts were filtered with a 41-μm filter, and centrifuged at 100g for 3 min at 4 °C. Protoplasts were washed two times in washing buffer (0.4 M mannitol, 20 mM Mes, pH 5.7), and then resuspended in 10 ml prewarmed (37 °C) lysis buffer (0.2 M mannitol, 10% (w/v) Ficoll, 10 mM EDTA, pH 8.0, 5 mM sodium phosphate, pH 8.0). After 5

minutes, 5 ml of the solution was overlayed with 3 ml 4% (w/v) Ficoll solution and 1 ml ice-cold vacuole buffer (0.2 M mannitol, 2 mM EDTA, pH 8.0, 5 mM sodium phosphate, pH 7.5). The gradient was centrifuged at 1,500 g for 20 min at 10 °C, and the vacuoles were located at the interface between 0 and 4% Ficoll.

Results

TEM protocol for improved membrane contrast

To obtain a well-defined description of TuMV-induced cellular reorganization, we optimized several steps in sample preparation to enhance membrane structure contrast in TEM. Different fixatives (2.5% glutaraldehyde or 4% paraformaldehyde plus 2% glutaraldehyde), post-fixation solutions (1% osmium tetroxide, or reduced osmium - 1% osmium tetroxide plus 1.5% potassium ferrocyanide), dehydration solutions (ethanol or acetone) and embedding mediums (Epon or Spurr) were tested. Tannic acid was also added before dehydration, since tannic acid-treated samples showed increased contrast and better delineation of cell membranes (33). Epon tended to give higher image contrast than Spurr, but its penetration into the sample was inhibited because of its higher viscosity (34). To solve this problem, the time period for each Epon embedding step was increased and vacuum was applied during pure Epon embedding to improve solute penetration into the dense cell wall (see Materials and Methods).

Cells from either agroinfiltrated leaf or upper TuMV systemically infected leaf were analyzed by TEM. The cytoplasm of mesophyll cells from agroinfiltrated leaf was pushed to the periphery of the cell owing to the presence of the large central vacuole (Fig. 1, A upper panel). Although it was easy to find organelles, such as nucleus, chloroplasts, mitochondria and peroxisomes, TuMV cytoplasmic inclusions and virus-induced membrane structures were more difficult to observe, likely due to the compacted cytosol (Fig. 1A, lower panel). On the other hand, TuMV cytoplasmic inclusions (arrows) and virus-induced membrane structures (arrowheads) (Fig. 1B, lower panel) were more apparent in the relatively more abundant cytoplasm of younger mesophyll cells from the systemically infected leaves (Fig. 1B, upper panel). Finally, choosing systemically infected leaves over agroinfiltrated leaves for TEM characterization avoided unknown bacterium-induced negative effects, since Agrobacteria were frequently found in the intercellular space of the infiltrated leaf (Fig. 1C, arrow).

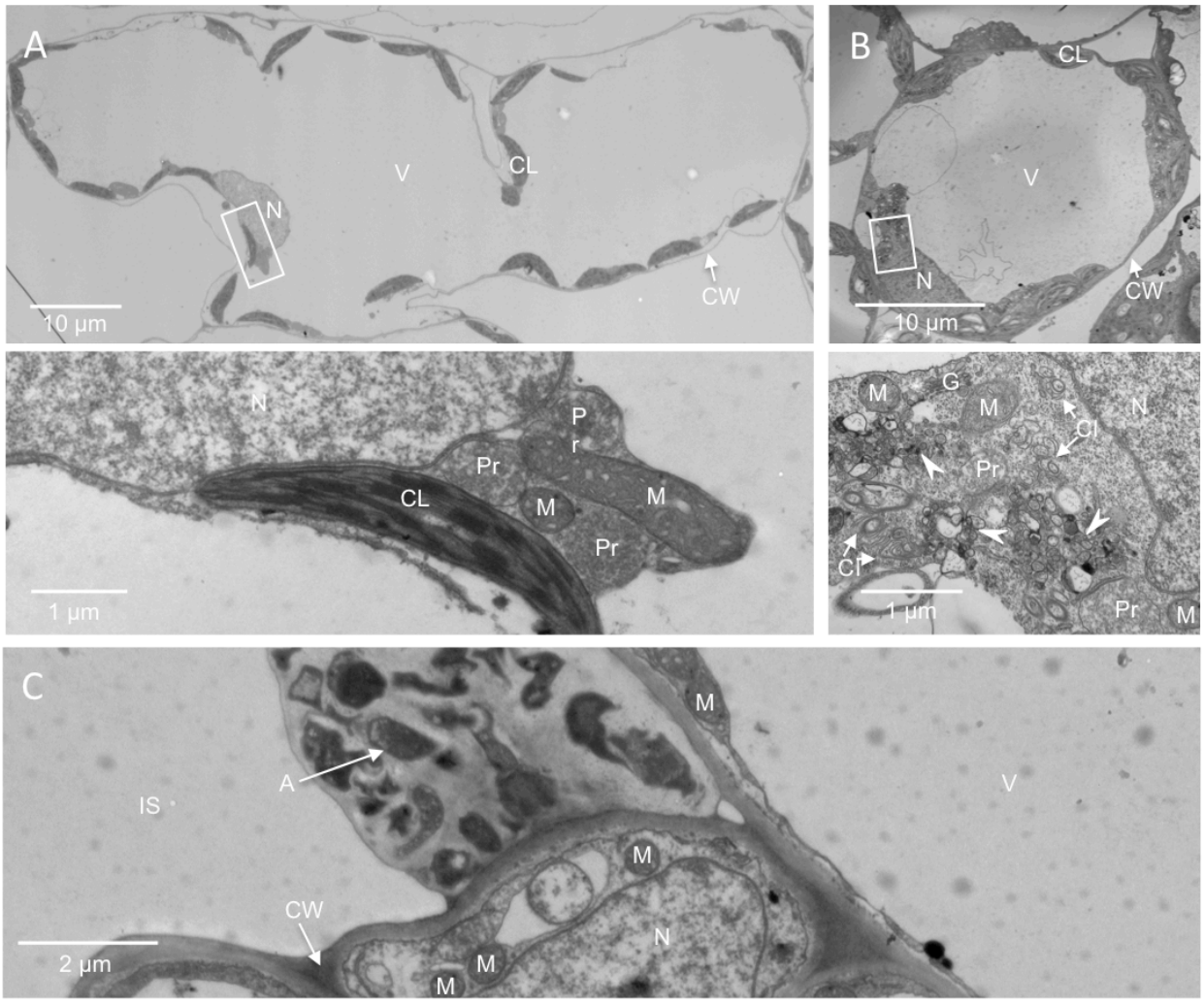

Figure 1. Comparison of agroinfiltrated and systemically TuMV-infected leaves.

Cross-sections of TuMV agroinfiltrated (A, C) and systemically infected (B) *N. benthamiana* leaves were collected and observed by TEM. Overview of mesophyll cells in TuMV agroinfiltrated (A) and systemically infected (B) leaves, with higher magnification of the rectangle-delineated area shown in the panel below, with highlighted organelles and TuMV-induced membranous aggregates and cytoplasmic inclusion bodies. Arrowheads indicate TuMV-induced membranous aggregates. (C) Agrobacteria in the intercellular space of the TuMV agroinfiltrated leaf. N, nucleus; V, vacuole; CL, chloroplast; CW, cell wall; Pr, peroxisome; M, mitochondrion; G, Golgi apparatus; CI, cytoplasmic inclusion body; IS, intercellular space; A, Agrobacterium.

Time course analysis of TuMV-induced cellular reorganization

The midrib area of systemically infected leaves was collected at different days post infection (dpi) with the infectious clone TuMV/6K_2:GFP, which produces GFP fluorescing 6K_2-tagged vesicles during infection (Fig. 2, A white rectangle). No 6K_2:GFP signal was observed by confocal microscopy in the cross sections of the midrib area at 4 dpi (n=8), suggesting that infection has not yet reached the upper non-infiltrated leaves (Fig. 2B, left panel). Infection of vascular tissues, however, was noted at 5 dpi (Fig. 2B, middle panel), which then spread to all the other tissues (e.g. angular collenchyma cells, epidermal cells and mesophyll cells) at 6 dpi (Fig. 2B, right panel). This time frame was thus chosen to observe the progression of TuMV cellular reorganization by TEM.

Since TuMV reached the vascular tissues first and then moved to the rest of systemically infected leaf tissues, we initially focused on vascular parenchymal cells. Cells were scored positive for TuMV infection by the presence of cytoplasmic inclusions of different morphology (e.g. pinwheel, bundles and short curved laminated aggregates or scrolls) (35). Infected cells were characterized by the accumulation of CM structures that were adjacent to the rER at 5 dpi (Fig. 2C). Few SMVL structures were present at the periphery of CM amalgams (Fig. 2C, lower panel). We then observed the presence of numerous heterogeneously sized SMVL structures at 6 dpi in most of the vascular parenchymal cells (Fig. 2D). The shape of the SMVL structures was round or oval, and the size was estimated to be 113 nm ± 38 nm (n=56) in diameter or in length. Finally, we observed both SMVL structures and DMVL structures with an electron-dense core in most of the cells at 7 dpi (Fig. 2E). The shape of DMVL structures was also round or oval, the outer membrane diameter or length being 244 nm ± 60 nm (n = 52) and the inner membrane diameter or length being 162 nm ± 48 nm (n = 52).

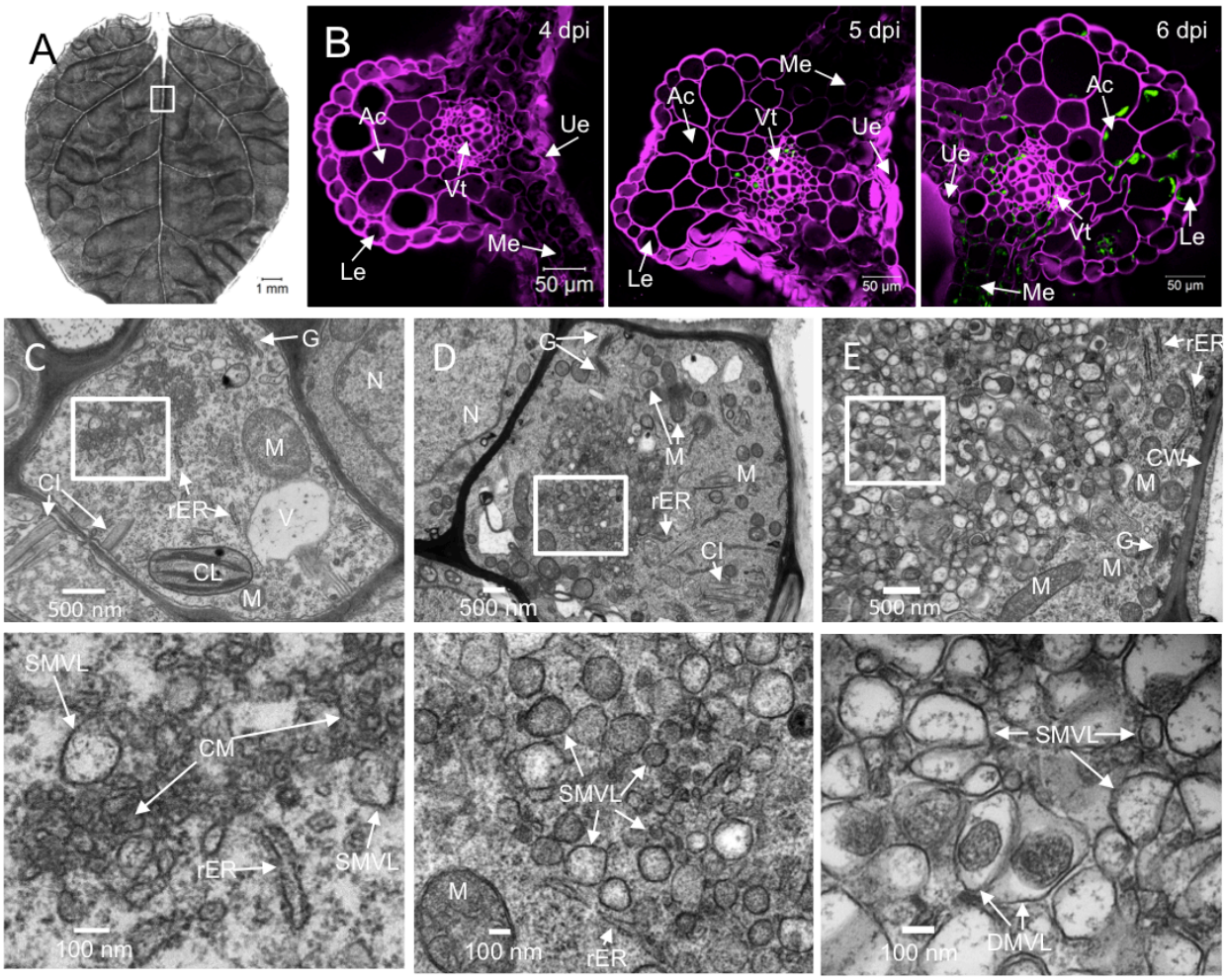
A
1 mm
B
4 dpi
Ac
Ue
Vt
Me
Le
50 µm
5 dpi
Me
Ac
Vt
Ue
Le
50 µm
6 dpi
Ac
Ue
Vt
Le
Me
50 µm
C
G
N
M
Cl
rER
V
CL
M
500 nm
D
G
N
M
M
rER
Cl
500 nm
E
rER
CW
M
G
M
M
500 nm
SMVL
CM
rER
SMVL
100 nm
SMVL
M
100 nm
rER
SMVL
DMVL
100 nm

Figure 2. Time course analysis of TuMV-induced membranous aggregates in *N.benthamiana* leaf midrib.

(A) An upper young leaf of *N. benthamiana* plant was imaged by tile scanning with a Zeiss LSM-780 confocal microscope using a 10× objective. The tile-scan was carried out by assembling 11×13 images. (B) Cross-sections of TuMV/$6K_2$:GFP systemically infected leaf midrib area (marked with rectangle in panel A) were imaged in confocal microscopy using a 20× objective at the indicated dpi in upper right corner. Fluorescent brightener 28-stained cell wall is shown in false-color magenta. $6K_2$:GFP is shown in green. All images are single optical slices. (C to E) Time course analysis of TuMV-induced membranous aggregates in vascular parenchymal cells. TuMV/$6K_2$:GFP systemically infected *N. benthamiana* leaf midribs were chemically fixed, processed, and observed by TEM. The lower panels show the higher magnification of the areas in the rectangles in the upper panels. (C) TuMV-induced CM structures, which were associated with SMVL structures, were located close to rER in a vascular parenchymal cell at 5 dpi. (D) TuMV-induced heterogeneous SMVL structures in a vascular parenchymal cell at 6 dpi. (E) TuMV-induced aggregates contain both SMVL structures and DMVL structures with an electron-dense core in a vascular parenchymal cell at 7 dpi. Ue, upper epidermis; Le, lower epidermis; Ac, angular collenchyma cells; Vt, vascular tissue; Me, mesophyll cells; N, nucleus; G, Golgi apparatus; M, mitochondrion; V, vacuole; CL, chloroplast; CW, cell wall; rER, rough endoplasmic reticulum; CI, cytoplasmic inclusion body; CM, convoluted membranes; SMVL, single-membrane vesicle-like structure; DMVL, double-membrane vesicle-like structure.

As expected, a one-day delay in membrane modification took place in mesophyll cells compared to vascular parenchymal cells. At 6 dpi, the CM structures were either closely located near, or connected with, the rER, and some SMVL structures were associated with the CM structures (Fig. 3, A). At 7 dpi, aggregations of heterogeneously sized SMVL structures of 111 nm ± 42 nm (n=72) in diameter or in length were observed (Fig. 3B). At 8 dpi, both SMVL structures and DMVL structures with an electron-dense core were observed (Fig. 3C). DMVL structures had an outer membrane diameter or length of 172 nm ± 56 nm (n = 40), and electron-dense core diameter or length of 114 nm ± 45 nm (n = 40).

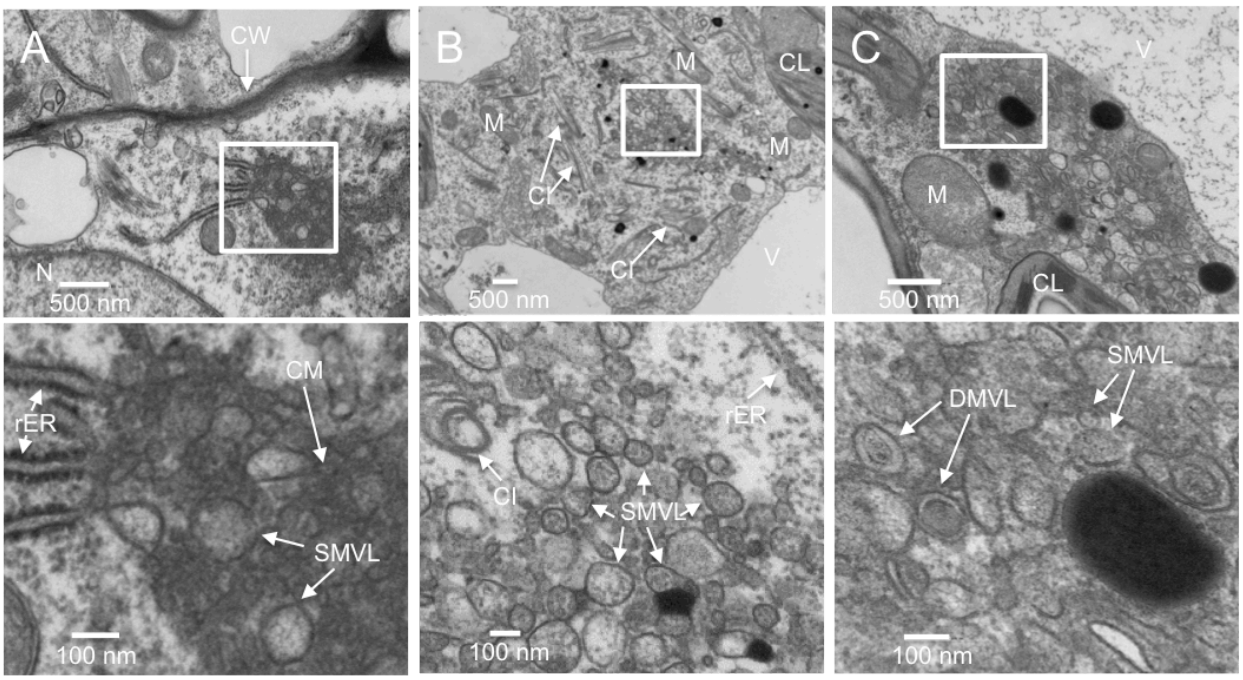

Figure 3. Time course analysis of TuMV-induced membranous aggregates in mesophyll cells.

(A to C) TuMV/6K_2:GFP systemically infected *N. benthamiana* leaf midribs were chemically fixed, processed, and observed by TEM. The higher magnification image of the areas in the white rectangles is shown in the panels below. (A) TuMV-induced CM structures, amid SMVL structures, were connected with several rER in a mesophyll cell at 6 dpi. (B) TuMV-induced heterogeneous SMVL structures close to the rER in a mesophyll cell at 7 dpi. (C) TuMV-induced aggregates contain both SMVL structures and DMVL structures with an electron-dense core in a mesophyll cell at 8 dpi. CW, cell wall; M, mitochondrion; CL, chloroplast; V, vacuole; CI, cytoplasmic inclusion body; rER, rough endoplasmic reticulum; CM, convoluted membranes; SMVL, single-membrane vesicle-like structure; DMVL, double-membrane vesicle-like structure.

SMVL structures are RNA replication sites of TuMV

To confirm if TuMV-induced membranous aggregates were $6K_2$-containing structures (Figs. 2 and 3), an HA tag was fused to the C-terminal of $6K_2$:GFP ($6K_2$:GFP:HA). The $6K_2$:GFP:HA coding sequence was thus introduced into the TuMV infectious clone pCambiaTuMV to produce pCambiaTuMV/$6K_2$:GFP:HA (Fig. 4A). Introduction of the $6K_2$:GFP:HA in the polyprotein produced the expected protein with the right molecular weight as shown by western blot analysis using an anti-HA monoclonal antibody (Fig. 4B). TuMV infection was not compromised as analyzed by western blot analysis using a rabbit serum raised against the coat protein (CP) of TuMV (Fig. 4B), nor the morphology of $6K_2$ vesicles when observed under the confocal microscope (data not shown). Immunogold labeling using an anti-HA monoclonal antibody confirmed that the TuMV-induced membranous aggregates were truly tagged with $6K_2$ (Fig. 4C, arrowheads). Immunogold labeling using anti-RNA dependent RNA polymerase (RdRp) polyclonal antibodies also showed the vesicle aggregates contained RdRp (Fig. 4D, arrowheads).

To better differentiate between the distinctive TuMV-induced membrane structures (i.e. CM, SMVL and DMVL structures), a 15-min post-fixation incubation period with 0.1% reduced osmium tetroxide was added before the dehydration step. This step increased the membrane contrast, but also decreased the antigenicity of the tested proteins. For instance, anti-HA and anti-RdRp labeling was weak with osmium-treated samples, since only a few gold particles were found on the sections (data not shown). However, the anti-dsRNA monoclonal antibody J2 worked well on the reduced osmium-treated samples (Fig. 4E). In mesophyll cells at 8 dpi, when SMVL structures were distinguishable from DMVL structures on osmium-treated samples, anti-dsRNA specific gold particles mainly decorated the SMVL structures (Fig. 4E).

Quantification of the number of gold particles per μm^2 and relative labeling distribution were performed over mock-infected and TuMV-infected sections. For each of the three different antibodies, at least 10 sections were observed. Practically no labeling with the anti-HA and anti-dsRNA monoclonal antibodies was observed in mock-infected samples (Fig. 4F). On the other hand, anti-HA and anti-dsRNA labeling were

specifically associated with TuMV-induced membranous aggregates, and were essentially absent from the rest of the cell (Fig. 4G). Background labeling was detected with the polyclonal anti-RdRp antiserum in mock-infected samples (Fig. 4F), but higher labeling was observed on TuMV-induced membranous aggregates (Fig. 4G). Quantification of anti-dsRNA gold particle distribution on SMVL and DMVL structures in mesophyll cells was performed on TuMV-infected sections at 8 dpi. The results showed that the gold particles were mainly associated with SMVL structures (98.5%) with few gold particles found on the DMVL structures (Fig. 4H). No gold particles decorated CM structures (data not shown). These data suggest that SMVL structures are TuMV RNA replication sites.

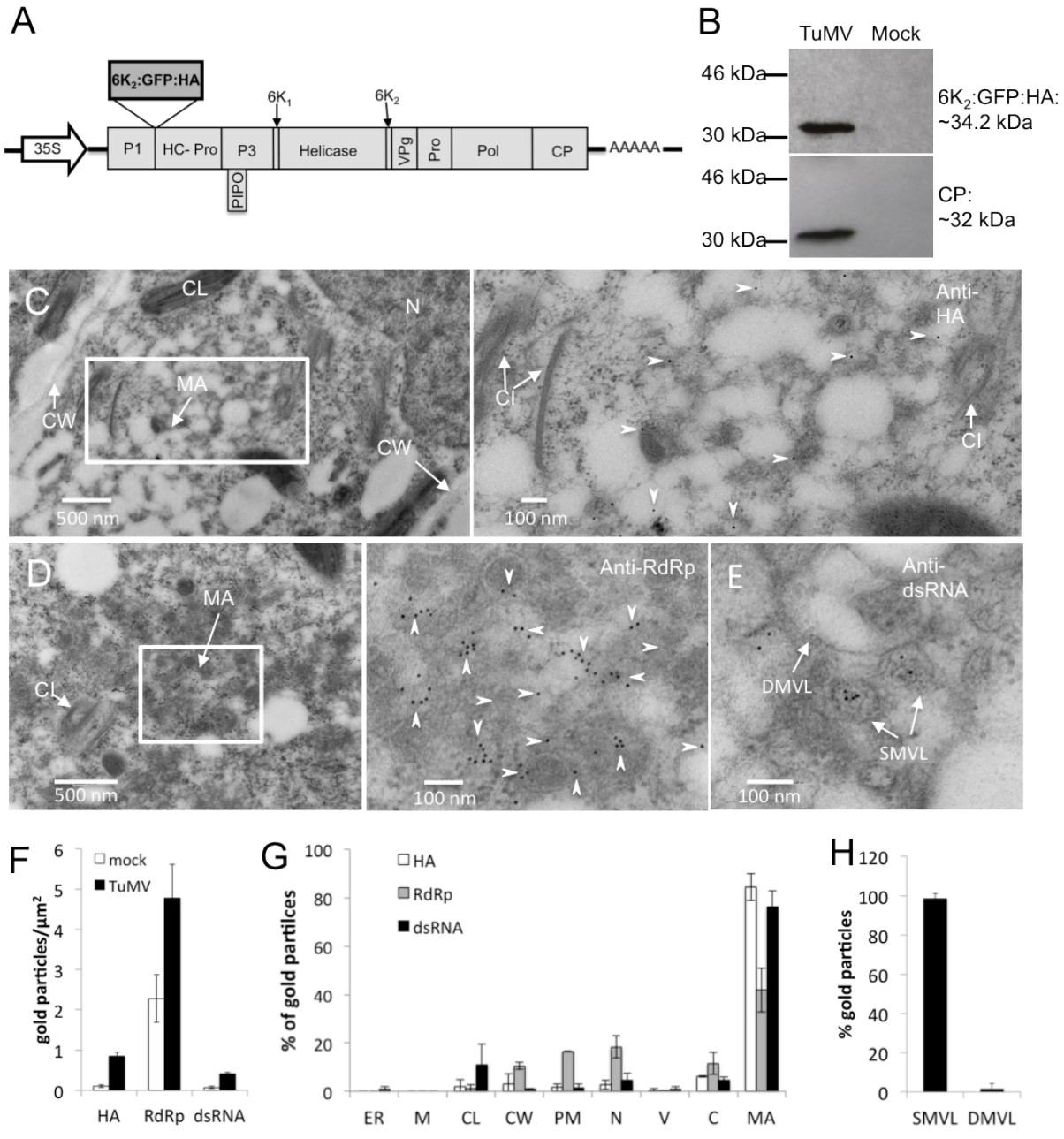
A
6K2:GFP:HA
6K1
6K2
35S
P1
HC- Pro
P3
Helicase
VPg
Pro
Pol
CP
AAAAA
PIPO
B
TuMV
Mock
46 kDa
30 kDa
6K2:GFP:HA:
~34.2 kDa
46 kDa
30 kDa
CP:
~32 kDa
C
CL
N
MA
CW
CW
500 nm
Anti-
HA
CI
CI
100 nm
D
MA
CL
500 nm
Anti-RdRp
100 nm
E
Anti-
dsRNA
DMVL
SMVL
100 nm
F
mock
TuMV
gold particles/µm²
HA
RdRp
dsRNA
G
HA
RdRp
dsRNA
% of gold partilces
ER
M
CL
CW
PM
N
V
C
MA
H
% gold particles
SMVL
DMVL

Figure 4. Subcellular localization of TuMV RNA replication sites.

(A) Schematic representation of the infectious clone TuMV/$6K_2$:GFP:HA that coexpresses $6K_2$ as a GFP:HA protein fusion. Black lines show the plasmid backbone, arrow indicates the CaMV 35S promoter, and AAAAA indicates the position of the polyadenylated tail. Rectangles represent TuMV proteins. $6K_2$:GFP:HA is inserted between P1 and HC-Pro. (B) Western blot analysis of $6K_2$:GFP:HA and CP expression in *N. benthamiana* plants after TuMV/$6K_2$:GFP:HA infection. (C to E) Immunogold labeling was performed on the cross-sections of mock- and TuMV- infected *N. benthamiana* leaf tissues by using anti-HA, anti-RdRp and anti-dsRNA antibodies. The higher magnification image of the areas in the white rectangles is shown on the right of each subpanel. Arrowheads indicate HA-specific (C) and RdRp-specific (D) gold particles, which are located in TuMV-induced membranous aggregates. (E) The dsRNA-specific gold particles are mainly localized to TuMV-induced SMVL structures. (F to H) Number of gold particles per μm^2 in mock-infected versus TuMV-infected cells (F), relative labeling distribution in infected cells (G) and relative labeling distribution in TuMV-induced membranous aggregates (H) are shown. Two different labeling experiments were considered and 200 gold particles were counted for each experiment. N, nucleus; CL, chloroplast; CW, cell wall; MA, membranous aggregate; CI, cytoplasmic inclusion body; SMVL, single-membrane vesicle-like structure; DMVL, double-membrane vesicle-like structure; ER, endoplasmic reticulum; M, mitochondrion; PM, plasma membrane; C, cytosol; V, vacuole.

Comparison of TuMV-induced cellular reorganization in chemically fixed and HPF/FS prepared samples

Chemical fixation may induce ultrastructural artifacts owing to the slow diffusion of chemical fixatives that results in non-synchronized immobilization of cellular macromolecular components, and to the selective cross-linking reactions of chemical fixatives, such as aqueous aldehydes and osmium tetroxide. High-pressure freezing (HPF) is widely regarded as the optimal fixation method for TEM (36). HPF is complete within milliseconds and ensures simultaneous immobilization of all macromolecular components (37). Subsequent processing for morphological studies is predominantly achieved by freeze-substitution (FS), where ice is removed by organic solvents at around −90°C. Freeze-substituted samples appear similar to materials prepared for TEM by conventional chemical fixation methods, but they have a greater likelihood of displaying structures in their native state (38). Since HPF/FS leads to an improved ultrastructural preservation, we also conducted HPF/FS for sample preparation.

Currently, HPF allows for a depth of 200 μm thick without detectable ice crystallization damage (39). In *N. benthamiana* systemically infected leaves, the thickness of the midrib is 356 μm ± 64 μm (n = 35), while it is 97 μm ± 23 μm (n = 35) for the other leaf area. To avoid ice crystallization damage, the leaf area without the rib tissue was consequently chosen. Consistent with what we observed in chemically fixed samples, HPF/FS-prepared mesophyll cells showed similar membrane remodeling. CM structures were observed at 6 dpi (Fig. 5, A) and SMVL structures of 74 nm ± 22 nm (n=48) in diameter were observed at 7 dpi (Fig. 5B) in mesophyll cells. However, instead of only SMVL structures and DMVL structures with an electron-dense core being observed in chemically fixed mesophyll cells (Fig. 5D, E), electron-dense bodies of 172 nm ± 59 nm (n = 20) in diameter were also frequently observed in HPF/FS-prepared mesophyll cells at 8 dpi (Fig, 5C, I-III). DMVL structures had an outer vesicle diameter of 138 nm ± 20 nm (n = 48), and electron-dense core diameter of 93 nm ± 19 nm (n = 48). Thus, the sizes of SMVL and DMVL structures in HPF/FS-prepared samples were smaller than that in chemically fixed samples. Another noticeable difference is that HPF/FS-prepared vesicles were largely rounded and had more electron dense materials within them (Fig. 5C-E).

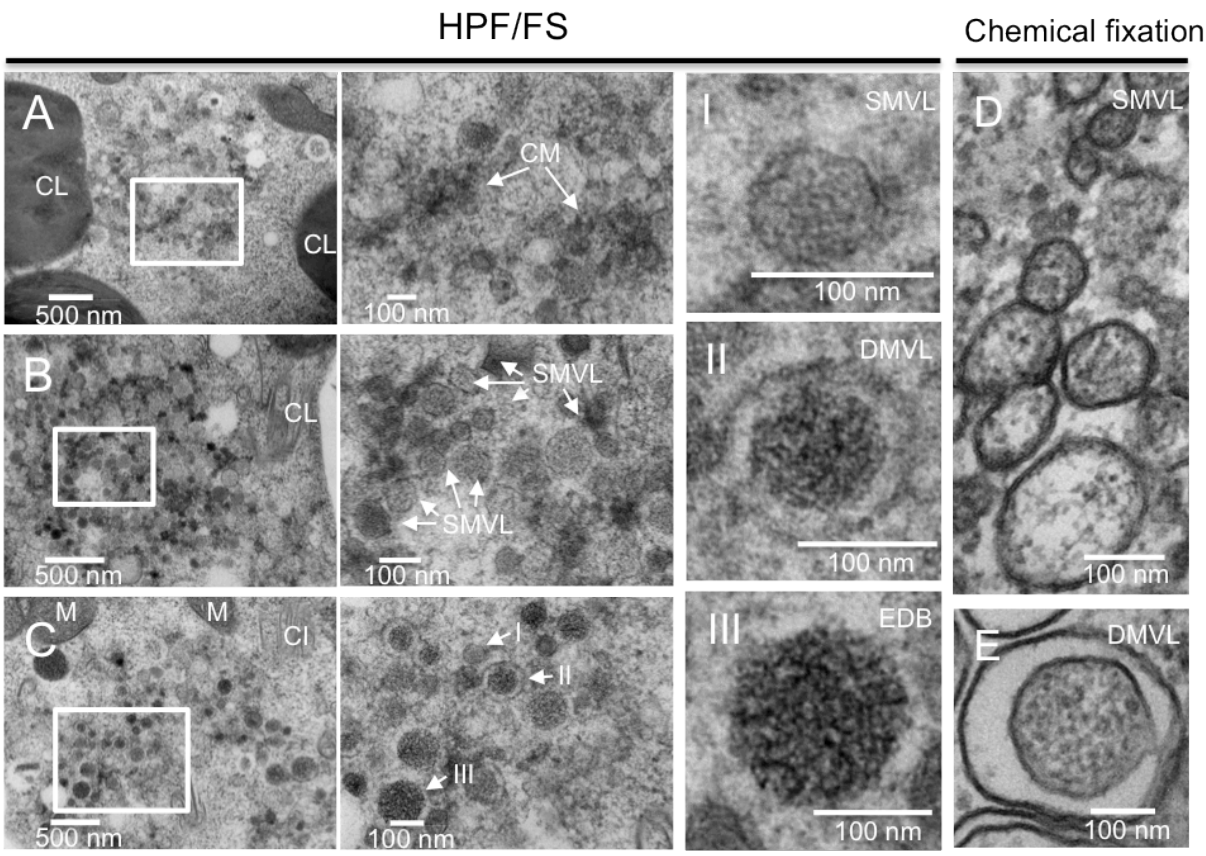

Figure 5. Comparison of TuMV-induced membranous aggregates in HPF/FS prepared and chemically fixed samples.

(A to C) Time course analysis of TuMV-induced membranous aggregates in mesophyll cells. TuMV/6K_2:GFP systemically infected *N. benthamiana* leaf without rib tissues were fixed by HPF, processed by FS and observed by TEM. The higher magnification image of the areas in the white rectangles is shown in the right panels. (A) TuMV-induced CM structures in a mesophyll cell at 6 dpi. (B) TuMV-induced heterogeneous SMVL structures in a mesophyll cell at 7 dpi. (C) TuMV-induced aggregate contain SMVL structures (I), DMVL structures with an electron-dense core (II) and electron-dense bodies (III) in a mesophyll cell at 8 dpi. (D and E) TuMV-induced heterogeneous SMVL structures (D) and a DMVL structure (E) in chemically fixed mesophyll cells. CL, chloroplast; M, mitochondrion; CM, convoluted membranes; SMVL, single-membrane vesicle-like structure; DMVL, double-membrane vesicle-like structure; EDB, electron-dense body.

Three-dimensional (3-D) architecture of TuMV-induced membrane reorganization

We performed ET on semithin (200 nm) sections to generate the 3-D representation of the numerous heterogeneously sized SMVL structures that were observed in vascular parenchymal cells at 6 dpi (Fig. 2D). Panels I to IV of Figure 6 show the representative tomograms that were generated from a single-axis tilt series. SMVL structures associated with rER were clearly observed, along with three closely associated cytoplasmic inclusions having a pinwheel configuration. Panels V and VI show the 3-D surface rendering generated from tilted images over a range of ± 60° (1° increments in high tilts and 2° increments in low tilts), and indicate that the SMVL structures were actually SMTs (represented in yellow), similar to those observed in CVB3 (2) and poliovirus (40) infected cells (see also Movie S1). The 3-D surface rendering shows that most SMTs are closely packed together and have a similar orientation. The SMTs were touching one another, but no holes or connections were observed. Cytoplasmic inclusions (represented in magenta) and rER were often found in close proximity to TuMV modified membranes, and some dilated rER (represented sky blue, including ER membranes and the associated ribosomes) were physically connected with the SMTs (Fig. 6, red arrows).

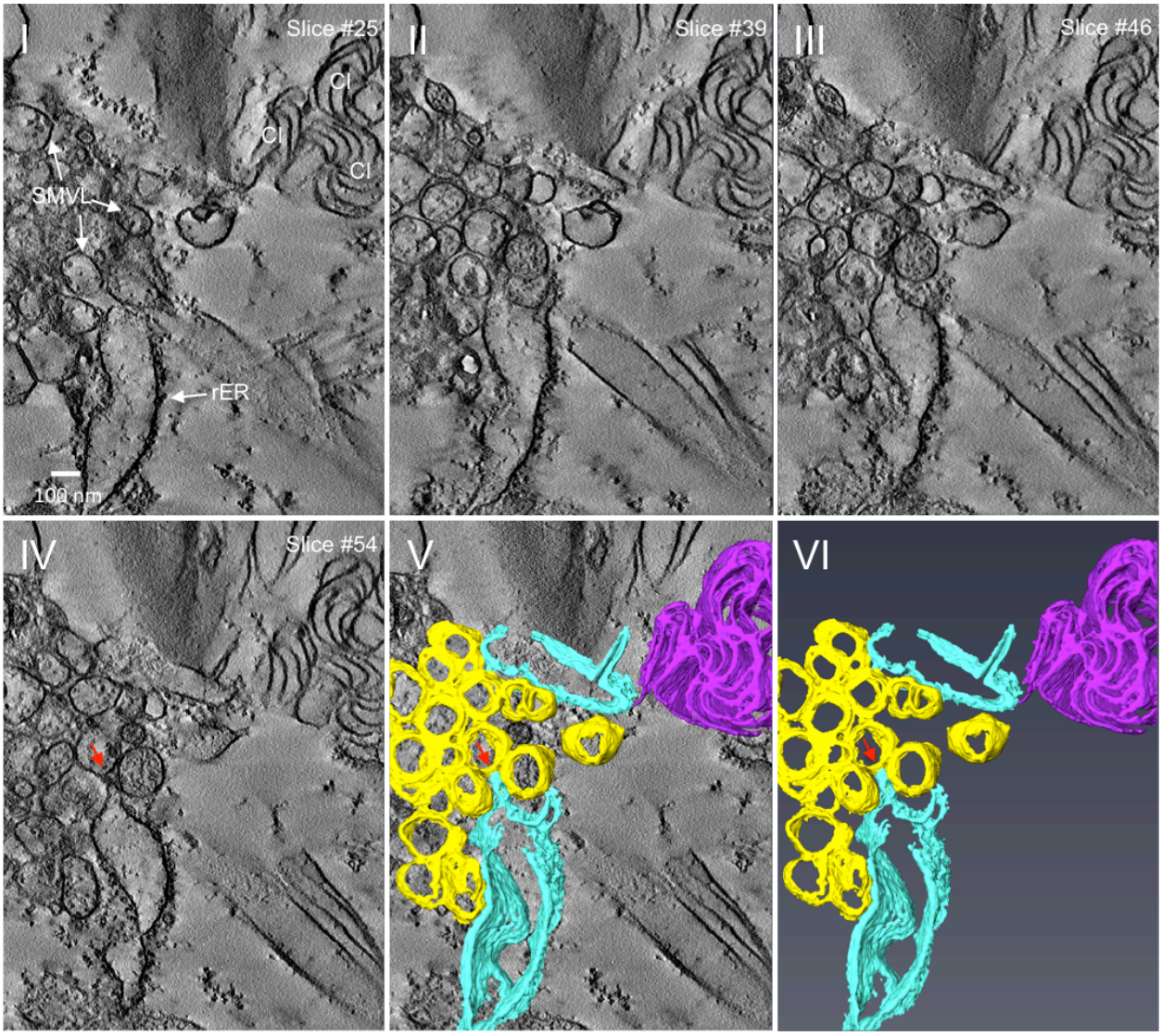

Figure 6. 3-D reconstruction of TuMV-induced membrane rearrangement at mid stage of infection.

Panel I to IV are representative tomogram slices generated on a 200-nm-thick section from TuMV-infected vascular parenchymal cell at 6 dpi, which show the SMVL structures in close proximity of dilated rER and CI. Panel V and VI show a 3-D surface rendering of the closely packed SMTs, dilated rER and CI. The red arrows indicate the connection between a SMT and the rER membrane. The SMTs are colored yellow, rER sky blue and CI magenta. CI, cytoplasmic inclusion body; rER, rough endoplasmic reticulum; SMVL, single-membrane vesicle-like structure.

We next investigated the 3-D architecture of the membrane structures at 7 dpi in TuMV-infected vascular parenchymal cells (Fig. 7 and Movie S2). At this stage, the membrane structures had various shapes and complexities (Fig. 7A), and 3-D renderings were generated from selected membrane structures (boxed areas). Figure 7B is a close-up view of a SMVL structure (left panel) along with its 3-D surface rendering (right two panels), which shows its tubular nature (represented in yellow). The 3-D rendering of the electron-dense fibrillar materials inside this SMT was also regenerated (represented in light red). These fibrillar materials could be the replication complexes containing vRNA, as proposed for *Beet black scorch virus (BBSV)* induced replication factories (41), which is consistent with our observation that SMVL structures contain dsRNA (Fig. 4E). Adjacent to the SMT is an irregularly shaped tubule (represented in green) that might represent an intermediate structure leading to the formation of DMTs (see below).

The left panel of Figure 7C is a close-up of the square areas depicted in Figure 7A, and the two right panels are the 3-D surface rendering for some of the membrane structures. These membrane structures are SMTs (in yellow) along with double-membrane tubules (DMTs) (outer membrane is represented in light blue, and inner membrane in dark blue), interspersed between them with irregularly shaped tubules (represented in green), with frequent membrane pairing (Fig. 7C, white arrowheads) or curving (Fig. 7C, red arrowheads) (see also Movie S2). Figure 7D also shows tubule bending. Finally, the left panel of Figure 7E is a close-up view of a DMVL structure (left panel), along with its 3-D surface rendering (right two panels). The DMT contents (represented in dark red) did not have a fibrillar profile, but almost fill the inner core of the DMT.

In conclusion, the SMVL and DMVL structures that were observed in the two-dimensional (2-D) TEM images of TuMV-infected cells were in fact tubules. These SMTs and DMTs were also interspersed with irregularly shaped tubules, which might be intermediate forms leading to the transformation of SMTs into DMTs.

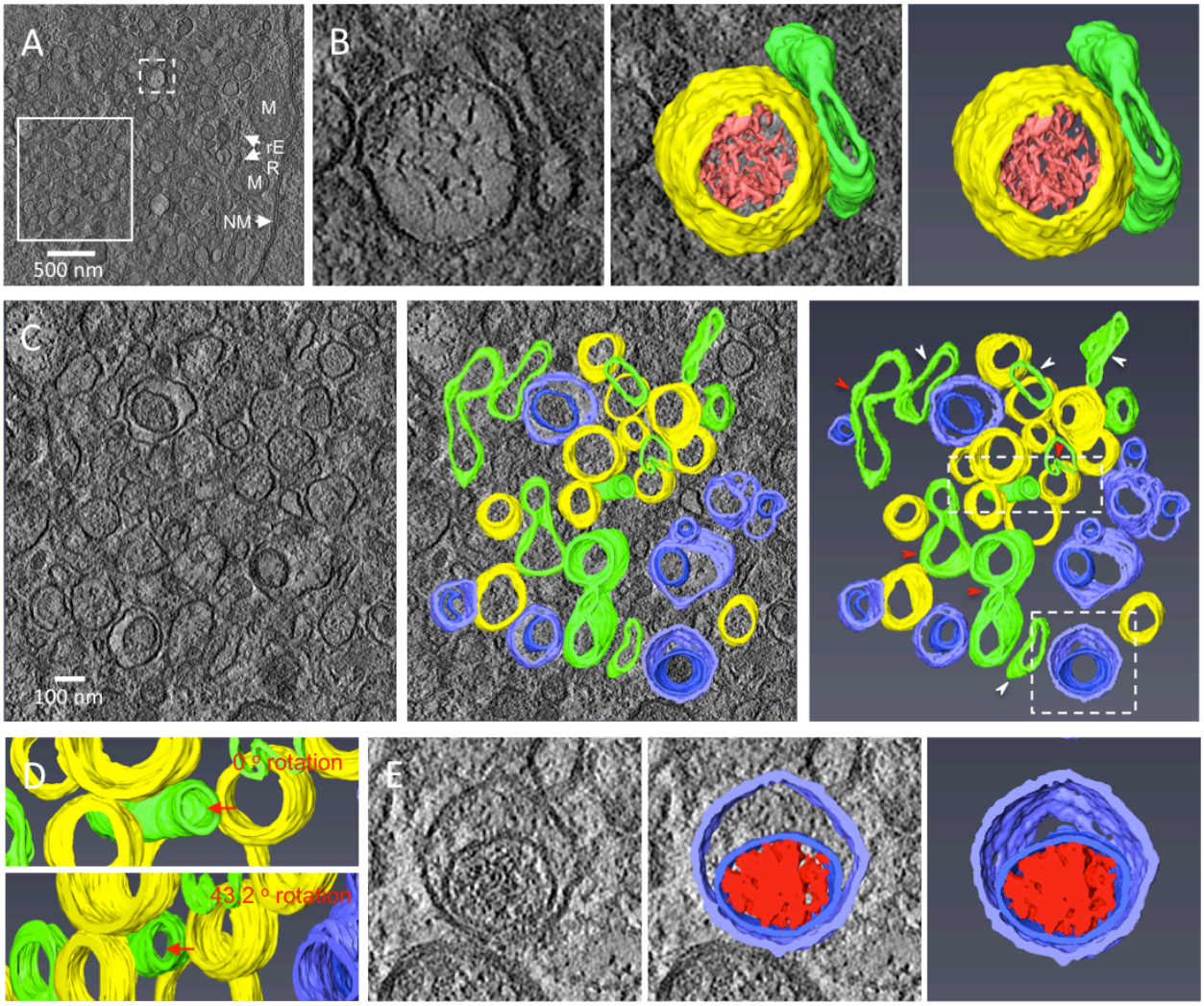
A
M
rER
M
NM
500 nm
B
C
100 nm
D
0° rotation
43.2° rotation
E

Figure 7. 3-D architecture of TuMV-induced complex membrane structures at late stage of infection.

(A) Overview of a single slice of a tomogram generated on a 200-nm-thick section in the perinuclear region of TuMV-infected vascular parenchymal cell at 7 dpi. (B) A higher magnification image (left panel) of the area in the dashed white square of panel A, and the 3-D model (middle and right panels) shows a SMT with fibrillar material inside and with adjacent intermediate tubular structure. (C) A higher magnification image (left panel) of area in the white rectangle of panel A, and the 3-D model (middle and right panels) shows SMTs, intermediate tubular structures and DMTs. White arrowheads indicate the intermediate SMTs that paired into flattened cisternae, and red arrowheads indicate the intermediate SMTs with slightly negative curvature that may result in the wrapping of cytoplasm to form DMTs. (D) A higher magnification image of the area in the dashed white rectangle in the right panel of C. The red arrow in the upper panel indicates a slightly bent, intermediate tubular structure (green) located among several SMTs (yellow) with similar orientation. The red arrow in the lower panel indicates a view rotated 43.2^{o} around the Y-axis, highlighting its tubular nature. (E) A higher magnification image of the area in the dashed white square in the right panel of C. The left panel shows a DMVL structure and its electron-dense materials. The middle and right panels show the 3-D model of the DMT with a core of electron-dense materials. The SMTs are colored yellow and electron-dense materials are colored light red. The intermediate tubular structures are colored green. The outer membranes of DMTs are colored light blue and inner membranes dark blue. The electron-dense materials inside DMTs are colored dark red. rER, rough endoplasmic reticulum; M, mitochondrion; NM, nuclear membrane.

Viral particle bundles associated with electron-dense bodies

At 8 dpi, filament bundles in association with electron-dense bodies in the vicinity of TuMV-induced membranous aggregates were frequently observed in HPF/FS-prepared mesophyll cells (Fig. 8, A). Individual filaments were 13 nm ± 1 nm (n=30) in width, which corresponds to the thickness of TuMV particles. The electron-dense bodies had diameters of 64 nm ± 13 nm (n=44), and DMVL structures with similar intensity of the electron-dense content were found close to them (Fig. 8A, B). These structures were also seen in chemically fixed samples, although less frequently (Fig. 8C). These data suggest that these bodies are involved in viral particle assembly.

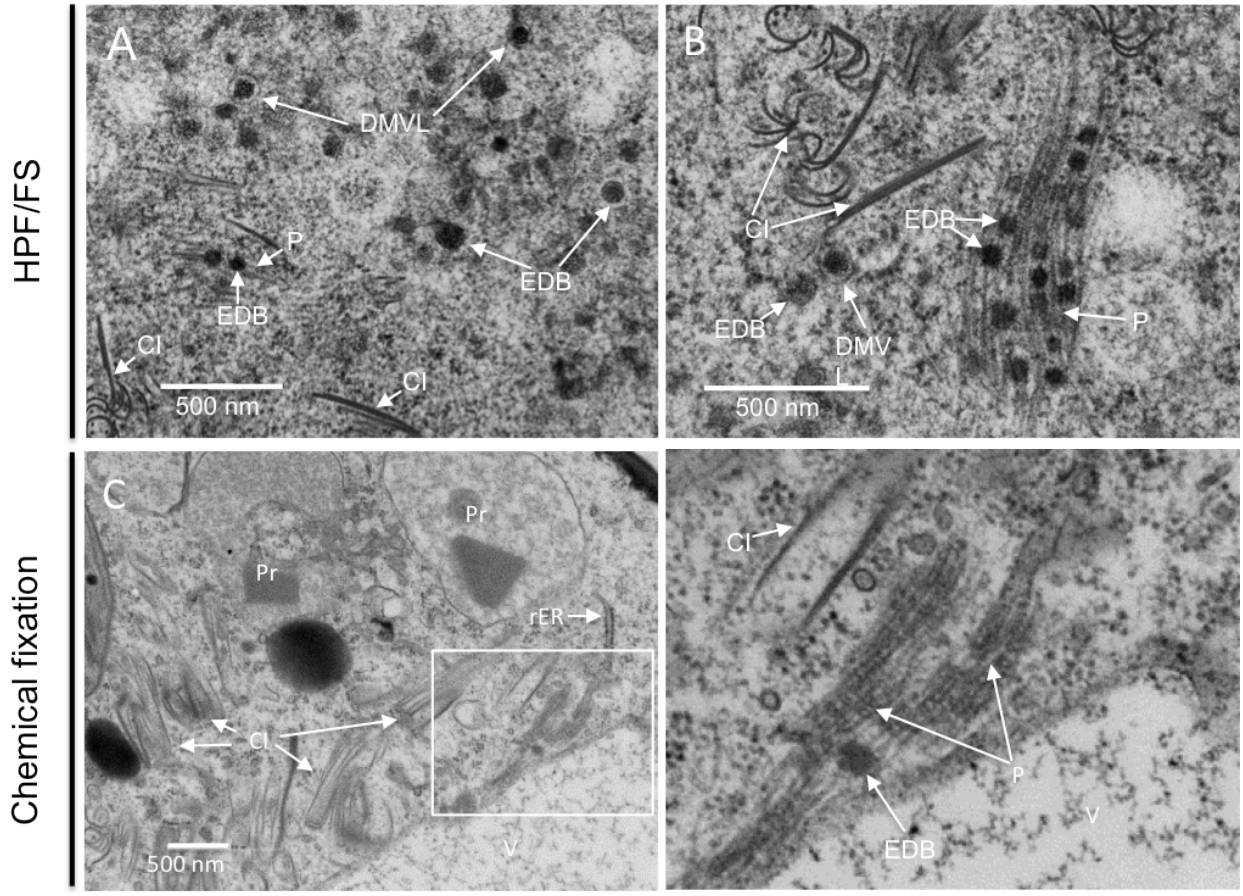

Figure 8. TuMV particles are associated with electron-dense bodies.

(A and B) In HPF/FS-prepared samples, viral-like particles are found as filament bundles associated with electron-dense bodies in the vicinity of TuMV-induced membranous aggregates at a late stage of infection (A), and the DMVL structures are found close to these filament bundle structures (B). (C) In chemically fixed samples, the filament bundles associated with electron-dense bodies are found in the cytoplasm near the tonoplast. CI, cytoplasmic inclusion body; DMVL, double-membrane vesicle-like structure; EDB, electron-dense body; P, particles; Pr, peroxisome; V, vacuole; rER, rough endoplasmic reticulum.

TuMV particles accumulate in vacuoles

In addition to the above described vesicle-like structures, linear arrays of dot-like structures with a diameter of 15 nm ± 1 nm (n=30) were seen juxtaposing the cytoplasmic face of the tonoplast, and frequently protruding into the vacuole (Fig. 9, A, I). Figure 9A (Panel II) shows that the aligned dots were enclosed in a membrane sac within the central vacuole. These structures were also found in HPF/FS-prepared samples, although the vacuole showed more electron-dense material (Fig. 9B).

The diameter of the dot-like structures is consistent with the diameter of viral particles. These structures may then represent the top view of vertically aligned viral particles. To confirm that this was the case, a 3-D representation was generated by ET. A series of single-axis tilt 2-D images were collected on a 90-nm-thick ultrathin section (Fig. 9C and Movie S3) over a tilt range of ± 64° (1° increments). Images were aligned and reconstructed to generate a 3-D representation of this structure. The middle and right panels of Figure 9C showed the 3-D reconstruction of the complete tomogram of the image of the left panels. 3-D surface rendering of the aligned dot-like structures clearly showed that they were a cross section of a monolayer of TuMV particles aligned along the same axis, and that they were enclosed with a membrane envelope, likely derived from the tonoplast.

Vacuoles from mock and TuMV systemically infected leaves were isolated to confirm that viral particles accumulated in these organelles. Vacuoles were released from protoplasts and isolated by Ficoll gradient centrifugation (Fig. 9D). We then performed western blot analysis with anti-CP and anti-helper component proteinase (HCpro) polyclonal antibodies. The western blot analysis results showed that the vacuoles isolated from TuMV infected leaves contained CP (Fig. 9E), supporting the tomography data showing that TuMV particles are loaded into the vacuoles. HCpro, which is involved in aphid transmission of viral particles, was also detected in purified vacuoles (Fig. 9E).

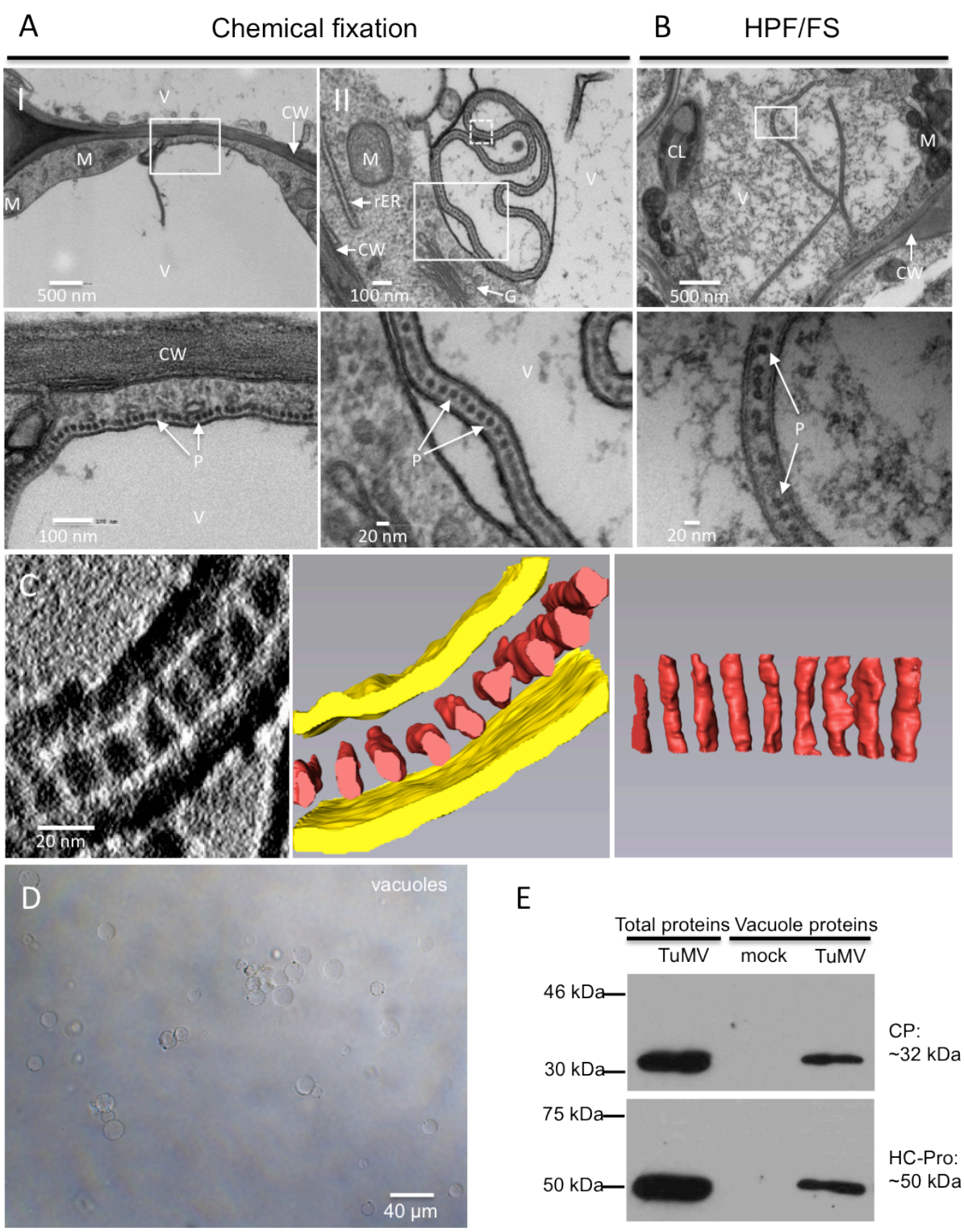
A
Chemical fixation
B
HPF/FS
I
V
CW
M
M
V
500 nm
II
M
V
rER
CW
100 nm
G
CL
M
V
CW
500 nm
CW
P
V
100 nm
V
P
20 nm
P
20 nm
C
20 nm
D
vacuoles
40 µm
E
Total proteins
Vacuole proteins
TuMV
mock
TuMV
46 kDa
30 kDa
CP:
~32 kDa
75 kDa
50 kDa
HC-Pro:
~50 kDa

Figure 9. TuMV acquires an envelope by hijacking the tonoplast.

(A, B) TuMV/6K_2:GFP systemically infected *N. benthamiana* leaf midribs were fixed by chemical fixation (A) or HPF (B), processed, and observed by TEM. The higher magnification image of the area in the white rectangle is shown in the panel below. Monolayer dot-like structures are aligned along the tonoplast (A, panel I), and loaded into the vacuole from the cytoplasm (A, panel II and B). (C) 3-D reconstruction of enveloped TuMV particles by ET. Left panel is the higher magnification of the area in the white square in panel A (II) with a 180° rotation, and it is a single slice of the tomogram generated from the 90-nm-thick section and showing enveloped dot-like structures in the vacuole. Middle panel is the 3-D model generated from the whole tomogram of the left panel, and right panel is the 90° rotation of dot-like structures of the middle panel. Tonoplast is colored yellow and dot-like structures are colored red. (D, E) CP and HCpro are present in purified vacuoles. Vacuoles were isolated from systemically TuMV-infected *N. benthamiana* leaves by Ficoll gradient centrifugation (D). Western blot analysis of viral proteins CP and HCpro in vacuoles purified from mock-infected and TuMV systemically infected *N. benthamiana* leaves (E). The total proteins of TuMV systemically infected *N. benthamiana* leaves are used as a positive control. V, vacuole; CW, cell wall; M, mitochondrion; rER, rough endoplasmic reticulum; G, Golgi apparatus; CL, chloroplast; P, particles.

Discussion

We have looked in this study at the cellular remodeling that takes place during TuMV infection using a time course ultrastructural analysis. The very first event that was observed in the infected cells was the accumulation of CM structures close to or connected to the rER (Fig. 2C and 3A). These CM collections are reminiscent of those induced during infection by *Dengue virus* (DENV, flavivirus) (42) and SARS-coronavirus (1). CM structures have been proposed to be sites of viral polyprotein processing and storage for proteins and lipids involved in vRNA replication (42). Based on the morphological similarities between the CM structures induced by TuMV and by flavivirus, and their observation early in the infection process, we propose that TuMV-induced CM structures are also sites for polyprotein processing, and/or for storage of proteins and lipids required for vesicle-like structures biogenesis. Indeed, large accumulation of lipids have been observed to be associated with TuMV replication complexes (43) and for other plant viruses as well (44).

Few SMVL structures were observed amidst CM structures in vascular parenchymal and mesophyll cells (Fig. 2C and 3A), but SMVL structures became prevalent one day later in these cells (Fig. 2D and 3B). The SMVL structures scored positive by immunogold labeling for $6K_2$ and RdRp, as well as for dsRNA (Fig. 4C-E), suggesting these structures are the sites for vRNA replication. TuMV-induced SMVL structures are similar to the membrane structures induced during infection by enteroviruses CVB3 (2) and poliovirus (45). Conventional 2-D TEM images of enteroviruses CVB3 and poliovirus induced membrane structures have been described as either SMVs (46, 47) or DMVs (48-50). Whereas for both viruses, ET generated 3-D models revealed the SMVs observed by TEM are SMTs that originated from the anterograde membrane traffic system early during infection (2, 51). Both potyviruses and enteroviruses belong to the picorna-like virus superfamily, suggesting they might share similar membrane modification mechanisms. Similarly in this study, the 3-D model showed TuMV-induced SMVL structures are SMTs (Figs. 6 and 7). Polioviral replication proteins were localized on the external cytoplasmic surface of the single-membrane tubule/vesicle. This apparently was not the case for TuMV. vRNA replication probably

occurs inside the SMVL structures since dsRNA-specific gold particles were located within the SMVL structures (Fig. 4E). In addition, the electron-dense fibrillar materials inside the SMT that were generated by ET might represent replication complexes (Fig. 7B). Intratubular localization of the replication complex is further supported by previous membrane fractionation data that showed the replication-associated soluble viral and host proteins (VPg-Pro, RdRp and PABP2) were trapped within the lumen of $6K_2$ vesicles (26).

DMVL structures were observed rather late in the infection cycle (Fig. 2E and 3C), and were characterized by having an electron-dense core, which was particularly apparent when samples were processed by HPF/FS (Fig. 5C). Poliovirus induced DMTs may result from a transformation process of membrane apposition, enwrapping, and fusion of SMTs (40). The 3-D model generated at the late stage of TuMV infection also suggested that the DMVL structures are DMTs and that they were formed by enwrapping of the SMTs, which resulted in the engulfment of cytoplasm (Fig. 7). Electron-dense bodies of similar size and intensity as the electron-dense core found within DMVL structures were associated with filament bundles (Fig. 8). These bodies may derive from DMVL structures and may be associated with TuMV particle assembly. It is important to note that no SMVL structures were found near these assembly sites. This fits our confocal microscopy observations that CP did not colocalize with membrane-bound viral replication complexes (19, 43), suggesting vRNA encapsidation occurs at a site adjacent to membrane-bound vRNA replication complexes. These tubules are likely the ultrastructure underlying the peri-nuclear ER amalgam observed by confocal microscopy during TuMV infection (16). However, the ultrastructure of the TuMV-induced small motile vesicles still needs to be defined.

We observed the accumulation of TuMV particles as a linear array in the central vacuole with the tonoplast forming an envelope around them (Fig. 9, A-C). Similar aligned dot-like structures were observed for the potyviruses *Pokeweed mosaic virus* (52) and *Carnation vein mottle virus* (53) infected cells, but their exact nature was not explained. The tonoplast has also been shown to be remodeled during several plant virus infections. TEM images showed tonoplast-associated vesicles protruded into the vacuole in cucumovirus *Cucumber mosaic virus* (CMV) and *Tomato aspermy virus*

(TAV) (5), and alfamovirus *Alfalfa mosaic virus* (AMV) (54) infected cells. Owing to the presence of replicase proteins, the authors concluded these were sites of vRNA synthesis (55). On the other hand, the icosahedral sobimovirus *Rice yellow mottle virus* (RYMV) particles have been found in vacuoles as crystalline arrays (56). The authors proposed the acidic pH and the presence of Ca^{+} could facilitate crystal formation and thus stabilize RYMV particles, which may allow the virus to accumulate to high levels without having deleterious effects on cellular viability and integrity. The highly stable and compact RYMV particles would ultimately be released from the vacuole during xylem vessel differentiation and trafficking along the water flow for long-distance movement (56). The membrane envelope around TuMV particles would thus provide a protective shield against the harsh environmental conditions prevalent in the central for subsequent long-distance movement during xylem vessel differentiation (43).

Potyviruses are transmitted plant-to-plant by aphids in a non-persistent manner (57). The interaction between CP and the receptor in the cuticle of the aphid stylet tip is mediated by the viral protein HCpro (58). HCpro was detected in purified vacuoles from TuMV-infected cells (Fig. 9E). The accumulation of TuMV particles in the vacuole may have something to do with virus plant-to-plant transmission by aphids. Aphids are phloem feeders, since phloem sap is rich in key nutrients, such as carbohydrates (sucrose), amino acids and minerals (59). Before the phloem nutrient source is sampled, the aphid performs host plant selection by probing the peripheral plant tissues. Potyviruses have been suggested to be acquired and inoculated during brief (<1 min) and superficial stylet penetrations in the peripheral plant tissues (epidermal and mesophyll cells) (60). Once the suitable host plant is detected, the aphid ultimately inserts the stylet along the cell wall of parenchymatous cells into the phloem sieve element for nutrient acquisition. The aphid recognizes the phloem sap by sensing pH (7.0-7.5) and high sucrose concentration (about 400 $mmol^{-1}$; (61). During the search for phloem sap, the stylet tip is observed inserting into the vacuole of parenchymatous and owing to the acidic pH (5.0-5.5) and low sucrose concentration, the stylet is withdrawn and changes direction until the sieve element is reached (61). This brief probing of the aphid stylet in the central vacuole may be sufficient to acquire the membrane-bound TuMV.

On the basis of the above observations, we propose the following model that links the TuMV-induced membrane remodeling for vRNA replication with virus storage in the central vacuole (Fig. 10). Membrane remodeling starts with the accumulation of ER-connected CM structures. This leads to the formation of SMTs that are involved in vRNA replication. As infection proceeds, the number of SMTs decreases, and DMTs with an electron-dense core and electron-dense bodies are generated. Possibly at this stage, vRNA and CP have been produced in sufficient quantities for particle assembly to take place in the vicinity of DMTs and electron-dense bodies. Finally, TuMV particles accumulate in a linear array along the same axis in the central vacuole, being enveloped by the tonoplast.

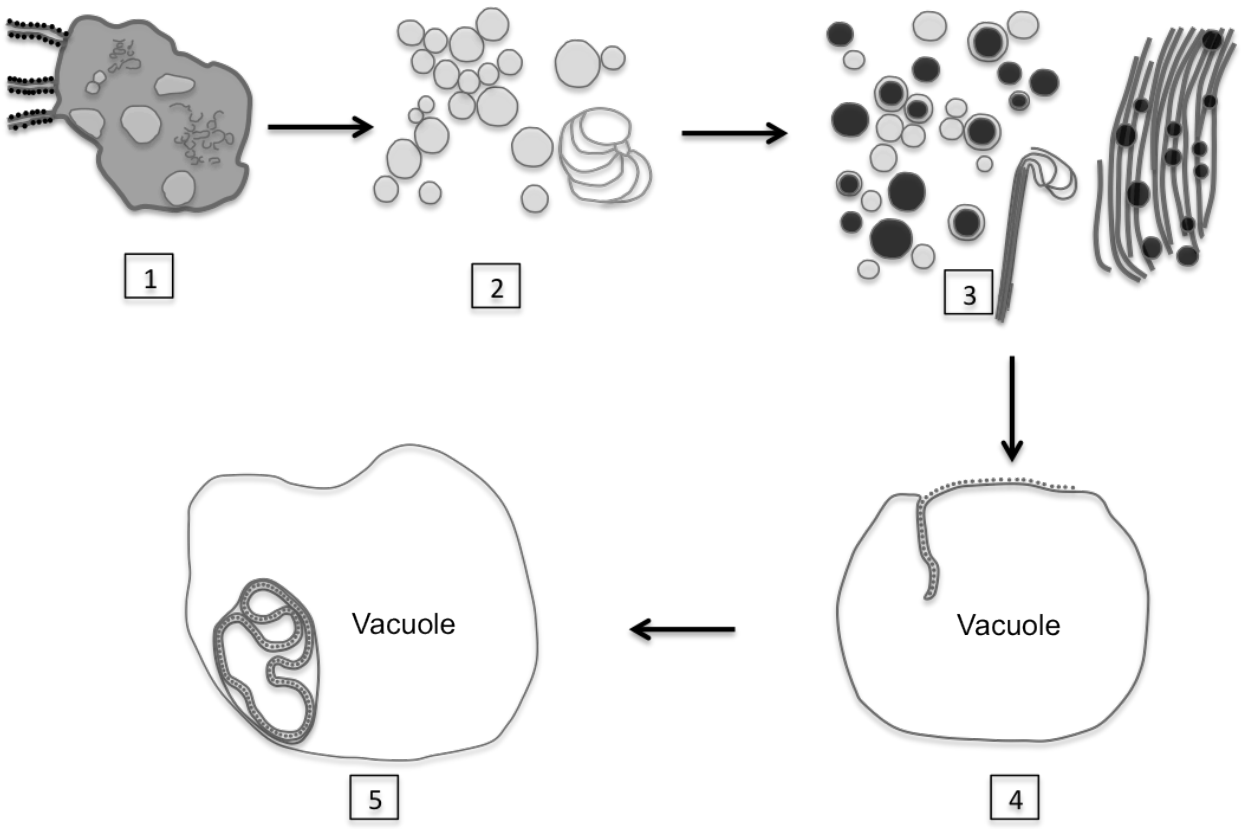

Figure 10. Model for TuMV-induced membrane structures formation.

Accumulation of ER-connected CM structures, which may be involved in polyprotein processing, are observed at an early stage of TuMV infection (1). At mid stage of TuMV infection, SMTs are produced, which are transformed from CM structures and are involved in vRNA replication (2). In addition to SMTs, DMTs and electron-dense bodies are produced at late stage of TuMV infection. Electron-dense bodies associated with viral-like particles filament bundles are present in the vicinity of this mixed aggregate. Possibly at this point, vRNA and CP have been produced in sufficient quantities for particle assembly to take place (3). Finally, the assembled viral particles are loaded in the central vacuole (4) and enclosed by a modified tonoplast (5).

Acknowledgments

This research was supported by grants from the Natural Science and Engineering Research Council (NSERC) of Canada and from Le Fonds de recherche du Québec sur la nature et les technologies (FRQNT) to HZ and JFL. We thank Jessy Tremblay (INRS-Institut Armand-Frappier) for Zeiss LSM 780 confocal microscope assistance. We thank Olivier Voinnet (ETH Zürich) for the anti-HCpro serum.

References

1. **Knoops K, Kikkert M, Worm SH, Zevenhoven-Dobbe JC, van der Meer Y, Koster AJ, Mommaas AM, Snijder EJ.** 2008. SARS-coronavirus replication is supported by a reticulovesicular network of modified endoplasmic reticulum. PLoS Biol **6:**e226.

2. **Limpens RW, van der Schaar HM, Kumar D, Koster AJ, Snijder EJ, van Kuppeveld FJ, Barcena M.** 2011. The transformation of enterovirus replication structures: a three-dimensional study of single- and double-membrane compartments. MBio **2**.

3. **Laliberté J-F, Zheng H.** 2014. Viral Manipulation of Plant Host Membranes. Annual Review of Virology **1:**237-259.

4. **Schwartz M, Chen J, Janda M, Sullivan M, den Boon J, Ahlquist P.** 2002. A positive-strand RNA virus replication complex parallels form and function of retrovirus capsids. Molecular cell **9:**505-514.

5. **Hatta T, Francki RIB.** 1981. Cytopathic Structures Associated with Tonoplasts of Plant Cells Infected with Cucumber Mosaic and Tomato Aspermy Viruses. Journal of General Virology **53:**343-346.

6. **Scholthof KB, Scholthof HB, Jackson AO.** 1995. The tomato bushy stunt virus replicase proteins are coordinately expressed and membrane associated. Virology **208:**365-369.

7. **McCartney AW, Greenwood JS, Fabian MR, White KA, Mullen RT.** 2005. Localization of the tomato bushy stunt virus replication protein p33 reveals a peroxisome-to-endoplasmic reticulum sorting pathway. The Plant cell **17:**3513-3531.

8. **Di Franco A, Russo M, Martelli GP.** 1984. Ultrastructure and Origin of Cytoplasmic Multivesicular Bodies Induced by Carnation Italian Ringspot Virus. Journal of General Virology **65:**1233-1237.

9. **Hwang YT, McCartney AW, Gidda SK, Mullen RT.** 2008. Localization of the Carnation Italian ringspot virus replication protein p36 to the mitochondrial outer

membrane is mediated by an internal targeting signal and the TOM complex. BMC cell biology **9:**54.

10. **Hatta T, Bullivant S, Matthews RE.** 1973. Fine structure of vesicles induced in chloroplasts of Chinese cabbage leaves by infection with turnip yellow mosaic virus. J Gen Virol **20:**37-50.

11. **Hatta T, Matthews RE.** 1974. The sequence of early cytological changes in Chinese cabbage leaf cells following systemic infection with turnip yellow mosaic virus. Virology **59:**383-396.

12. **Carette JE, Stuiver M, Van Lent J, Wellink J, Van Kammen A.** 2000. Cowpea mosaic virus infection induces a massive proliferation of endoplasmic reticulum but not Golgi membranes and is dependent on de novo membrane synthesis. J Virol **74:**6556-6563.

13. **Ritzenthaler C, Laporte C, Gaire F, Dunoyer P, Schmitt C, Duval S, Piequet A, Loudes AM, Rohfritsch O, Stussi-Garaud C, Pfeiffer P.** 2002. Grapevine fanleaf virus replication occurs on endoplasmic reticulum-derived membranes. Journal of virology **76:**8808-8819.

14. **Mitra R, Krishnamurthy K, Blancaflor E, Payton M, Nelson RS, Verchot-Lubicz J.** 2003. The potato virus X TGBp2 protein association with the endoplasmic reticulum plays a role in but is not sufficient for viral cell-to-cell movement. Virology **312:**35-48.

15. **Bamunusinghe D, Hemenway CL, Nelson RS, Sanderfoot AA, Ye CM, Silva MA, Payton M, Verchot-Lubicz J.** 2009. Analysis of potato virus X replicase and TGBp3 subcellular locations. Virology **393:**272-285.

16. **Grangeon R, Agbeci M, Chen J, Grondin G, Zheng H, Laliberte JF.** 2012. Impact on the endoplasmic reticulum and Golgi apparatus of turnip mosaic virus infection. Journal of virology **86:**9255-9265.

17. **Revers F, Garcia JA.** 2015. Molecular biology of potyviruses. Adv Virus Res **92:**101-199.

18. **Beauchemin C, Boutet N, Laliberté J-F.** 2007. Visualization of the Interaction between the Precursors of VPg, the Viral Protein Linked to the Genome of Turnip Mosaic Virus, and the Translation Eukaryotic Initiation Factor iso 4E In Planta. Journal of virology **81:**775-782.

19. **Cotton S, Grangeon R, Thivierge K, Mathieu I, Ide C, Wei T, Wang A, Laliberté J-F.** 2009. Turnip Mosaic Virus RNA Replication Complex Vesicles Are Mobile, Align with Microfilaments, and Are Each Derived from a Single Viral Genome. Journal of virology **83:**10460-10471.

20. **Beauchemin C, Laliberté J-F.** 2007. The Poly(A) Binding Protein Is Internalized in Virus-Induced Vesicles or Redistributed to the Nucleolus during Turnip Mosaic Virus Infection. Journal of virology **81:**10905-10913.

21. **Dufresne PJ, Thivierge K, Cotton S, Beauchemin C, Ide C, Ubalijoro E, Laliberté J-F, Fortin MG.** 2008. Heat shock 70 protein interaction with Turnip mosaic virus RNA-dependent RNA polymerase within virus-induced membrane vesicles. Virology **374:**217-227.

22. **Agbeci M, Grangeon R, Nelson RS, Zheng H, Laliberte JF.** 2013. Contribution of host intracellular transport machineries to intercellular movement of turnip mosaic virus. PLoS Pathog **9:**e1003683.

23. **Grangeon R, Jiang J, Wan J, Agbeci M, Zheng H, Laliberte JF.** 2013. 6K2-induced vesicles can move cell to cell during turnip mosaic virus infection. Frontiers in microbiology **4:**351.

24. **Otulak K, Garbaczewska G.** 2012. Cytopathological potato virus Y structures during Solanaceous plants infection. Micron **43:**839-850.

25. **Thivierge K, Cotton S, Dufresne PJ, Mathieu I, Beauchemin C, Ide C, Fortin MG, Laliberte JF.** 2008. Eukaryotic elongation factor 1A interacts with Turnip mosaic virus RNA-dependent RNA polymerase and VPg-Pro in virus-induced vesicles. Virology **377:**216-225.

26. **Beauchemin C, Laliberte JF.** 2007. The poly(A) binding protein is internalized in virus-induced vesicles or redistributed to the nucleolus during turnip mosaic virus infection. Journal of virology **81:**10905-10913.

27. **Beauchemin C, Bougie V, Laliberte JF.** 2005. Simultaneous production of two foreign proteins from a polyvirus-based vector. Virus Res **112:**1-8.

28. **Knapp E, Flores R, Scheiblin D, Scheiblin D, Modla S, Czymmek K, Czymmek K, Yusibov V.** 2012. A cryohistological protocol for preparation of large plant tissue sections for screening intracellular fluorescent protein expression. BioTechniques **52:**31-37.

29. **Kopek BG, Perkins G, Miller DJ, Ellisman MH, Ahlquist P.** 2007. Three-dimensional analysis of a viral RNA replication complex reveals a virus-induced mini-organelle. PLoS Biol **5:**e220.

30. **Lucocq JM, Habermann A, Watt S, Backer JM, Mayhew TM, Griffiths G.** 2004. A rapid method for assessing the distribution of gold labeling on thin sections. J Histochem Cytochem **52:**991-1000.

31. **Kremer JR, Mastronarde DN, McIntosh JR.** 1996. Computer visualization of three-dimensional image data using IMOD. J Struct Biol **116:**71-76.

32. **Robert S, Zouhar J, Carter C, Raikhel N.** 2007. Isolation of intact vacuoles from Arabidopsis rosette leaf-derived protoplasts. Nat Protoc **2:**259-262.

33. **Kalina M, Pease DC.** 1977. The probable role of phosphatidyl cholines in the tannic acid enhancement of cytomembrane electron contrast. J Cell Biol **74:**742-746.

34. **Wu S, Baskin TI, Gallagher KL.** 2012. Mechanical fixation techniques for processing and orienting delicate samples, such as the root of Arabidopsis thaliana, for light or electron microscopy. Nat Protoc **7:**1113-1124.

35. **Edwardson JR, Christie RG, Ko NJ.** 1984. Potyvirus Cylindrical Inclusions—Subdivision—IV. phytopathology **74:**1111-1114.

36. **Studer D, Michel M, Muller M.** 1989. High pressure freezing comes of age. Scanning Microsc Suppl **3:**253-268; discussion 268-259.

37. **Gilkey JC, Staehelin LA.** 1986. Advances in ultrarapid freezing for the preservation of cellular ultrastructure. Journal of Electron Microscopy Technique **3:**177-210.

38. **McDonald K, Morphew MK.** 1993. Improved preservation of ultrastructure in difficult-to-fix organisms by high pressure freezing and freeze substitution: I. Drosophila melanogaster and Strongylocentrotus purpuratus embryos. Microsc Res Tech **24:**465-473.

39. **Vanhecke D, Graber W, Studer D.** 2008. Close-to-native ultrastructural preservation by high pressure freezing. Methods Cell Biol **88:**151-164.

40. **Belov GA, Nair V, Hansen BT, Hoyt FH, Fischer ER, Ehrenfeld E.** 2012. Complex Dynamic Development of Poliovirus Membranous Replication Complexes. Journal of Virology **86:**302-312.

41. **Cao X, Jin X, Zhang X, Li Y, Wang C, Wang X, Hong J, Wang X, Li D, Zhang Y.** 2015. Morphogenesis of the ER membrane-invaginated vesicles during Beet black scorch virus infection: The role of auxiliary replication protein and new implications of three-dimensional architecture. Journal of virology.

42. **Welsch S, Miller S, Romero-Brey I, Merz A, Bleck CK, Walther P, Fuller SD, Antony C, Krijnse-Locker J, Bartenschlager R.** 2009. Composition and three-dimensional architecture of the dengue virus replication and assembly sites. Cell Host Microbe **5:**365-375.

43. **Wan J, Cabanillas DG, Zheng H, Laliberte JF.** 2015. Turnip mosaic virus Moves Systemically through Both Phloem and Xylem as Membrane-Associated Complexes. Plant physiology **167:**1374-1388.

44. **Lee WM, Ahlquist P.** 2003. Membrane synthesis, specific lipid requirements, and localized lipid composition changes associated with a positive-strand RNA virus RNA replication protein. Journal of virology **77:**12819-12828.

45. **Bienz K, Egger D, Pfister T, Troxler M.** 1992. Structural and functional characterization of the poliovirus replication complex. Journal of virology **66:**2740-2747.

46. **Bienz K, Egger D, Rasser Y, Bossart W.** 1983. Intracellular distribution of poliovirus proteins and the induction of virus-specific cytoplasmic structures. Virology **131:**39-48.

47. **Bienz K, Egger D, Pasamontes L.** 1987. Association of polioviral proteins of the P2 genomic region with the viral replication complex and virus-induced membrane synthesis as visualized by electron microscopic immunocytochemistry and autoradiography. Virology **160:**220-226.

48. **Schlegel A, Giddings TH, Jr., Ladinsky MS, Kirkegaard K.** 1996. Cellular origin and ultrastructure of membranes induced during poliovirus infection. J Virol **70:**6576-6588.

49. **Wong J, Zhang J, Si X, Gao G, Mao I, McManus BM, Luo H.** 2008. Autophagosome supports coxsackievirus B3 replication in host cells. J Virol **82:**9143-9153.

50. **Kemball CC, Alirezaei M, Flynn CT, Wood MR, Harkins S, Kiosses WB, Whitton JL.** 2010. Coxsackievirus infection induces autophagy-like vesicles and megaphagosomes in pancreatic acinar cells in vivo. J Virol **84:**12110-12124.

51. **Belov GA, Nair V, Hansen BT, Hoyt FH, Fischer ER, Ehrenfeld E.** 2012. Complex dynamic development of poliovirus membranous replication complexes. Journal of virology **86:**302-312.

52. **Kim KS, Fulton JP.** 1969. Electron microscopy of pokeweed leaf cells infected with pokeweed mosaic virus. Virology **37:**297-308.

53. **Weintraub M, Ragetli HW.** 1970. Distribution of viruslike particles in leaf cells of Dianthus barbatus infected with carnation vein mottle virus. Virology **40:**868-881.

54. **Martelli G, Russo M.** 1985. Virus-Host Relationships, p. 163-205. *In* Francki RIB (ed.), The Plant Viruses. Springer US.

55. **Ibrahim A, Hutchens HM, Berg RH, Loesch-Fries LS.** 2012. Alfalfa mosaic virus replicase proteins, P1 and P2, localize to the tonoplast in the presence of virus RNA. Virology **433:**449-461.

56. **Brugidou C, Opalka N, Yeager M, Beachy RN, Fauquet C.** 2002. Stability of rice yellow mottle virus and cellular compartmentalization during the infection process in Oryza sativa (L.). Virology **297:**98-108.

57. **Ng JC, Falk BW.** 2006. Virus-vector interactions mediating nonpersistent and semipersistent transmission of plant viruses. Annu Rev Phytopathol **44:**183-212.

58. **Syller J.** 2005. The roles and mechanisms of helper component proteins encoded by potyviruses and caulimoviruses. Physiological and Molecular Plant Pathology **67:**119-130.

59. **Dinant S, Bonnemain JL, Girousse C, Kehr J.** 2010. Phloem sap intricacy and interplay with aphid feeding. Comptes rendus biologies **333:**504-515.

60. **Powell G.** 1991. Cell membrane punctures during epidermal penetrations by aphids: consequences for the transmission of two potyviruses. Annals of Applied Biology **119:**313-321.

61. **Hewer A, Becker A, van Bel AJ.** 2011. An aphid's Odyssey--the cortical quest for the vascular bundle. The Journal of experimental biology **214:**3868-3879.

CHAPTER 4: DISCUSSION

1. Overview

The work accomplished during my Ph.D studies has contributed to the general understanding of the involvement of TuMV-induced membrane-associated complexes in long-distance movement and the ultrastructure of TuMV-induced cellular reorganization.

Through cryohistological and immunohistolocalization observations of TuMV-infected plants, this study showed that $6K_2$-tagged TuMV membrane-associated replication complexes were distributed in all the different types of leaf and stem cells, including the vascular conducting tubes: phloem sieve elements and xylem vessels. It was confirmed that those membrane-bound replication complexes could move through xylem vessels and establish systemic infection. it was also demonstrated that PVX membrane-associated replication complexes could also end up in the phloem and the xylem. These findings show that the infectious entities for TuMV long-distance movement could be membrane-bound RNP complexes that contain vRNA, replication-associated viral and host proteins, thus supporting the concept that vRNA replication and movement are tightly linked processes. Furthermore, these findings also suggest the presence of viral components in the apoplast.

Using TEM on TuMV-infected leaf tissue, rough ER -associated or -connected CM structures were observed early in the infection process. SMVs were then found at the mid stage of infection, and mixed aggregates containing SMVs, DMVs with an electron-dense core, and electron-dense bodies at the late stage of infection. The immunogold labeling experiments then showed that the aggregated vesicles are $6K_2$-tagged and that SMVs are the vRNA replication sites. I also observed that TuMV particle bundles associated with electron-dense bodies are likely involved in viral particle assembly. Finally, viral particles accumulating in the central vacuole were detected as membrane-associated complexes. These findings show that $6K_2$-tagged membrane structures undergo continuous modifications to properly execute their function during TuMV infection. These findings confirm that TuMV can subvert several different cellular pathways to profit its infection.

2. Virus replication and movement are linked events

Previously, plant virus replication and movement were considered separate events. Consequently, studies were either focused on viral replication complex formation or MP-mediated trafficking. However, there is accumulating evidence showing that these two processes are linked events. The connection of vRNA replication and movement could then facilitate the efficient and fast delivery of viruses throughout the plant.

Plant virus movement involves intracellular movement, cell-to-cell movement and long-distance movement. Connection between intracellular and cell-to-cell movement has been demonstrated by the recruitment of MPs to viral replication complexes, locating virus replication complexes at PDs, and virus replication complexes moving directly across PDs. For instance, it has been proposed that membrane-bound TMV replication complexes, which contain vRNA, viral replicase components and 30-kDa MPs, form in the perinuclear region, then move along microfilaments to the cell periphery and cross the PD to establish new infections in the adjacent cells (Kawakami, Watanabe et al. 2004). The replication and trafficking of PVX vRNA have been proposed to be coupled at the entrance of PD. This hypothesis derives from the observation that PVX MPs TGBp2 and TGBp3 proteins induce ER-derived membranous caps that contain vRNA and viral replicase components at PD orifices. TGBp1 protein then binds and directs PVX particles into PD (Tilsner, Linnik et al. 2013). In the case of TuMV, $6K_2$-tagged membrane-associated replication complexes have been observed by live-cell imaging to move from one cell to another (Grangeon, Jiang et al. 2013). In Chapter 2, it was shown that $6K_2$-tagged membrane-associated replication complexes end up in the vascular conducting tubes for long-distance movement, further supporting the notion that vRNA replication and movement are linked throughout the infection of the whole plant, whether it is intra-, inter- or long distance movement.

Viral particles and membrane-bound RNP complexes are formed to protect the viral genome during plant virus movement. Membranes provide shelters for plant viral components against host anti-viral responses during movement, and are thus a perfect media for connecting replication and movement. Moving as membrane-associated

replication complexes would also improve the efficiency of vRNA synthesis, since the progeny genomes do not have to leave the replication machinery while trafficking towards PDs. Finally, the entry of a complete viral replication complex in non-infected cells surely would speed up the infection process. Indeed, Agbeci *et al*. (Agbeci, Grangeon et al. 2013) showed that it takes three hours for TuMV to move from one cell layer to the next. Additionally, only one replication complex would be necessary to establish a successful infection. This notion is supported by the observation that the effective multiplicity of cellular infection (MOI, the number of viral genomes entering and replicating within a cell) for TuMV has been estimated to be close to one (Gutierrez, Michalakis et al. 2012).

3. Viral replication complexes are present in the apoplast

The apoplast, which includes cell walls, intercellular spaces and conducting dead cells of the xylem, is a dynamic compartment involved in plant signaling and communication. The intercellular fluids and xylem sap are connected, since a large number of xylem sap proteins have been found to originate from the proteins secreted in the intercellular fluids (Ligat, Lauber et al. 2011). Another important result of this thesis is thus the discovery of the presence of $6K_2$-tagged membrane-associated replication complexes (viral RNA, replication-associated viral and host proteins) in the xylem vessels and xylem sap of TuMV-infected plants, which suggests that they might be present in the intercellular fluids.

TEM studies have shown that paramural vesicles situated between the plasma membrane and the cell wall occur in various cell wall-associated processes, and are similar to exosomes both in location and in morphology (An, van Bel et al. 2007). Accumulating evidence suggests that exosome-like vesicles carry specific materials to be delivered into the paramural space of the plant to accomplish still undiscovered functions (An, Huckelhoven et al. 2006, Regente, Corti-Monzon et al. 2009, Wang, Ding et al. 2010). The exosome-like paramural vesicles may be released from the plasma membrane by at least two mechanisms. They could be released through a multivesiclular body-plasma membrane (MVB-PM) fusion, as shown for the pathogenic powdery mildew fungus (An, Huckelhoven et al. 2006) and for BSMV-induced cell wall-associated defense response (McMullen, Gardner et al. 1977). Alternatively, they could be released through an exocyst positive organelle (EXPO)-plasma membrane fusion, which is involved in non classical protein secretion (Wang, Ding et al. 2010).

Exosome-mediated transmission of human viruses have been reported. Non-enveloped *Hepatitis A virus* (HAV, *Picornaviridae*) has been shown to acquire an envelope by hijacking cellular membranes after it is released from cells to protect the virion from antibody-mediated neutralization (Feng, Hensley et al. 2013). Apart from classical transmission by free viral particles, enveloped HCV has also been shown to modify exosomes for transmission. For instance, purified exosomes from HCV-infected cells may contain virus particles, since they contain full-length vRNA, viral core protein

and E2, and can transmit HCV to establish a productive infection (Ramakrishnaiah, Thumann et al. 2013). Those exosomes are partially resistant to antibody neutralization (Ramakrishnaiah, Thumann et al. 2013). Furthermore, it also has been shown that HCV rewire the exosomes, which contain replication competent vRNA in complex with Ago2-miR122-HSP90, to mediate viral receptor-independent transmission (Bukong, Momen-Heravi et al. 2014). The miR-122, Ago2 and HSP90 have been demonstrated in enhancing HCV replication when bound to the 5'-UTR of HCV dsRNA (Wilson, Zhang et al. 2011). Could it also be the case for plant viruses, despite the presence of a thick surrounding cell wall that would act as a barrier for virus movement? Vesicular transport across the cell wall has been demonstrated in fungi (Casadevall, Nosanchuk et al. 2009). Could a similar situation be operating in plants? Alternatively, the exosome-like vesicles could spread throughout the paramural space and bypass the cell wall as depicted in Figure 1.

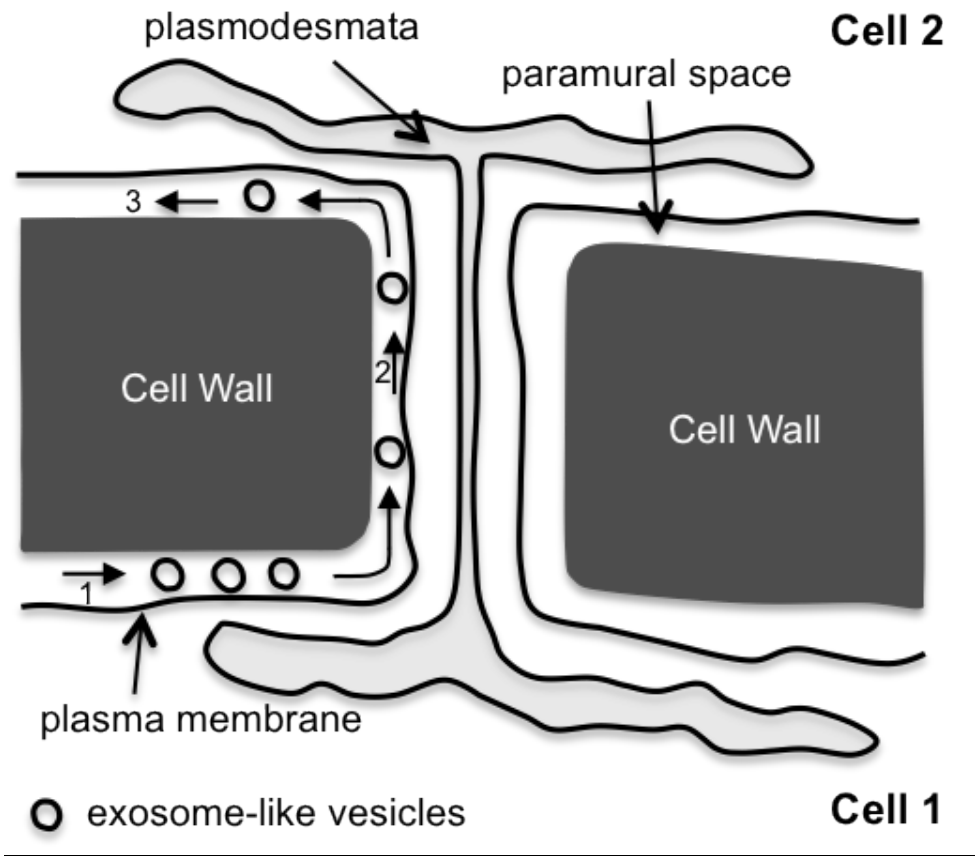

Figure 1. A model for exosome-like vesicle movement in the paramural space for bypassing the cell wall.

First, exosome-like vesicles from cell 1 are released in the paramural space (1), and then travel until they encounter the apoplastic face of a plasmodesmata (2) to cross over to the paramural space of cell 2 (3). Taken from (Wan and Laliberté 2015).

In support to the above hypothesis, numerous electron-translucent vesicles, which were morphologically similar to the paramural vesicles formed through MVB-PM fusion, were observed in the paramural space of TuMV-infected leaves (Fig. 2A, empty arrowheads). Some electron-dense vesicles, which appeared to pinch off from the plasma membrane into the paramural space, were also observed in TuMV-infected leaves (Fig. 2B, arrowheads). Only a few exosome-like paramural vesicles were observed in mock-infected leaves. In addition, The apoplastic fluid was collected from intact TuMV systemically infected *N. benthamiana* leaves by the infiltration-centrifugation method (Lohaus, Pennewiss et al. 2001). The preliminary results showed that $6K_2$ vesicles are present in the apoplastic fluid of TuMV-infected leaves (Fig. 3A, B). Western blot analysis also showed that apoplastic fluid from TuMV-infected leaves contains the replication associated vRdRp (data not shown) and host proteins (e.g. eIF4E, Fig. 3C). These observations suggest that there might indeed be an additional mechanism by which plant viruses exit cells. These results also indicate that the $6K_2$-tagged replication complexes end up in xylem vessels probably during the xylem vessel differentiation, or by trafficking from the intercellular space.

These studies thus present membrane-associated viral replication complexes that are located in the extracellular space of a plant. This contrasts with the general belief that viral replication complexes are found exclusively inside infected cells.

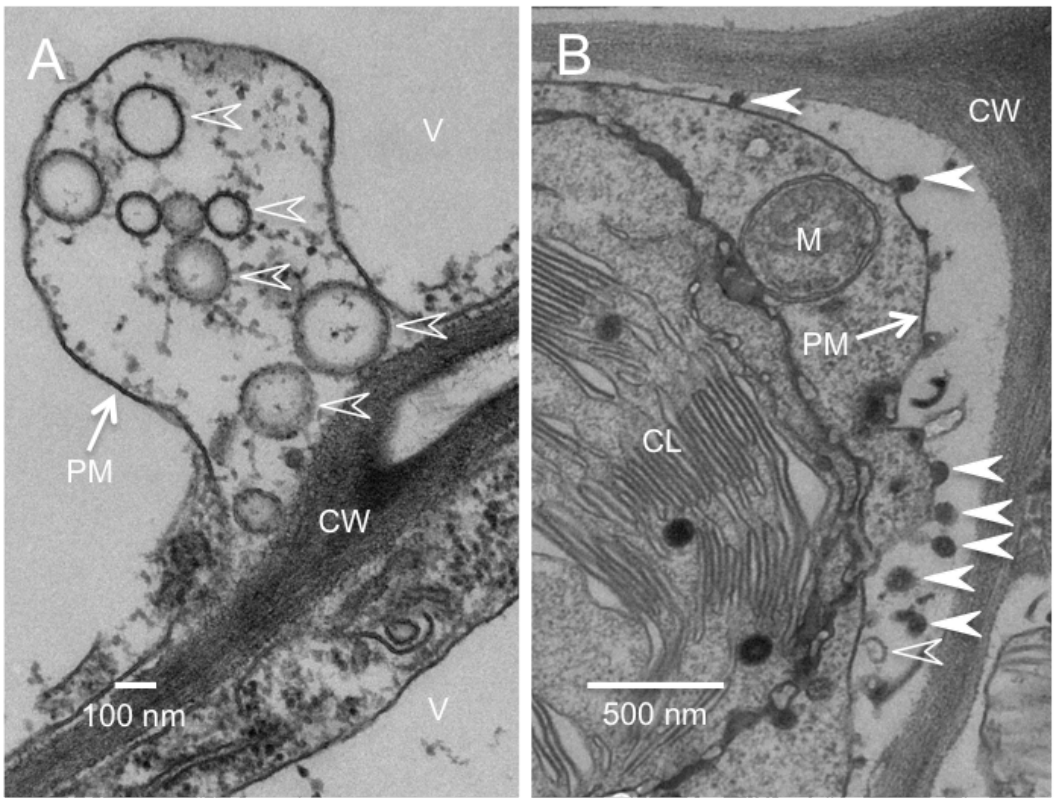

Figure 2. Exosome-like vesicles are present in the paramural space of TuMV-infected leaves.

Cross-sections of TuMV-infected *N. benthamiana* leaf were collected and observed by TEM. (A) shows the electron-translucent paramural vesicles (empty arrowheads) located between plasma membrane and cell wall. (B) shows both electron-translucent (empty arrowheads) and electron-dense paramural vesicles (arrowheads) located between plasma membrane and cell wall. V, vacuole; CL, chloroplast; M, mitochondria; CW, cell wall; PM, plasma membrane. Taken from (Wan and Laliberté 2015).

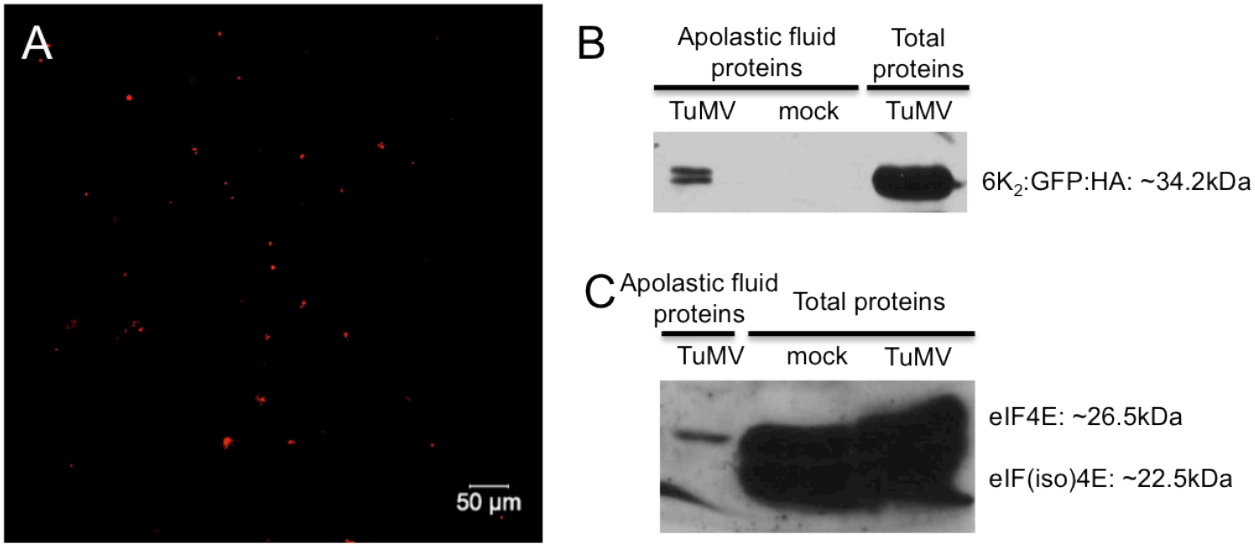

Figure 3. $6K_2$ vesicles are present in apoplastic fluid.

(A) $6K_2$:mCherry tagged vesicles observed in the apoplastic fluid, which was collected from TuMV/$6K_2$:mCherry systemically infected *N. benthamiana* leaves at 8 dpi. (B) Western blot analysis of apoplastic fluid with anti-HA and anti-eIF4E/eIF(iso)4E antibodies. Only eIF4E was detected in TuMV-infected apoplastic fluid.

4. Distinct organellar membranes are modified during TuMV infection

(+) RNA viruses remodel membranes of several organelles in the same cell during infection. For instance, HCV remodels ER membranes for vRNA synthesis (Romero-Brey, Merz et al. 2012) and exosomes for its transmission (Bukong, Momen-Heravi et al. 2014); the tobamovirus ToMV replication complexes are predominantly associated with both ER and vacuolar membranes (tonoplast) (Hagiwara, Komoda et al. 2003). In the case of TuMV, membrane modification of ER, chloroplasts and vacuoles was observed.

The TuMV $6K_2$-tagged irregular-shaped globular structure contains vesicle aggregates and ring-like structures associated with chloroplasts (Fig. 4A). The immunohistolocalization result showed that only vesicle aggregates contain the vRNA replication intermediate dsRNA (Fig. 4B). By TEM, ER-associated CM structures were detected in the vicinity of the chloroplast aggregates in the perinuclear region in TuMV-infected mesophyll cells at 6 dpi (Fig. 4C). The possible ultrastructure of the globular structure is consequently the $6K_2$-tagged ER-associated membranous aggregates plus chloroplast aggregates with $6K_2$ inserted into the outer membrane (Fig. 4D).

During TuMV infection, the ER-associated membranous aggregates undergo dynamic modifications for different functions as shown in Figure 4E. TuMV induced ER-connected CM structures may be for polyprotein translation and processing at 6 dpi (left panel), SMVs for replication at 7 dpi (middle panel), and DMVs may be involved in particles assembly at 8dpi (right panel) in mesophyll cells.

The ER-connected or -associated membranous aggregates are present in almost every cell of TuMV-infected leaf tissues, but are not present in mock-infected cells. On the other hand, the presence of vesicular-like inclusions, which are around 500 nm in diameter, in the chloroplast stroma (Fig. 4F), are observed in mock- and TuMV-infected cells. These are likely formed by invagination of the chloroplast double envelope membrane. Although the number of these inclusions in the chloroplast stroma increases during virus infection, still less than 10% of the chloroplasts contain such structures (Gao and Nassuth 1993). The dsRNA-specific gold particles did not decorate the

inclusions located in the chloroplast stroma (Fig. 4G). Thus, the function of these inclusions in virus replication still needs to be elucidated.

In addition, TuMV also modifies the tonoplast to form membrane-bound particles that accumulate in the central vacuole, as shown in Chapter 3. The volume of a central vacuole could occupy up to 95% of the total volume of a plant cell, thus the cytoplasm is limited. Instead of accumulating a high level of virus particles in the limited cytoplasm, which may induce immune defenses, or affect the cellular viability and integrity, the virus particles could be alternatively stored in the large central vacuole. In mature plant cells, the large central vacuoles are acidic with lysosome-like properties. To avoid virus particles degradation, they could subvert the tonoplast to form an envelope as a protective environment against the harsh conditions in the central vacuole. On the other hand, to test if the TuMV particles in vacuole are infectious, the purified vacuoles from TuMV-infected cells were mechanically applied on the healthy *N. benthamiana* plants, but no infection can be detected in the healthy plants. It could be due to the action of the degradative enzymes when the vacuoles were broken during the application process, or the low number of TuMV particles, which is not enough to establish the infection by mechanical inoculation.

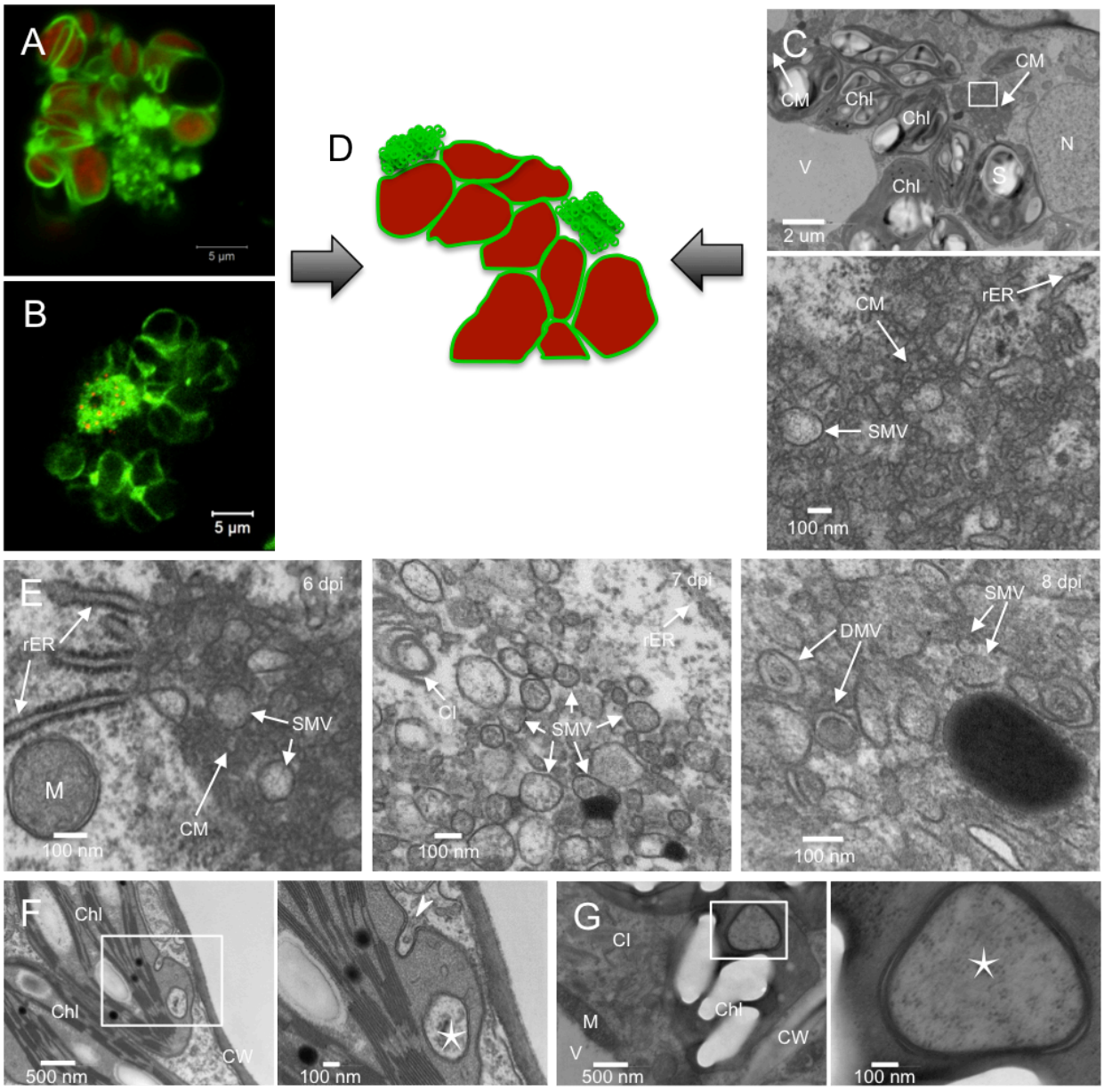
A
5 µm
B
5 µm
D
C
CM
CM
Chl
Chl
Chl
N
V
S
2 um
CM
rER
SMV
100 nm
E
6 dpi
rER
SMV
M
CM
100 nm
7 dpi
rER
Cl
SMV
100 nm
8 dpi
SMV
DMV
100 nm
F
Chl
Chl
CW
500 nm
100 nm
G
Cl
M
V
Chl
CW
500 nm
100 nm

Figure 4. Possible ultrastructure of $6K_2$:GFP-tagged globular structure.

(A and B) $6K_2$:GFP-tagged globular structures in TuMV-infected *N. benthamiana* leaf tissues were observed by confocal microscopy. (A) is taken from a live epidermal cell, (B) is taken from a fixed angular collenchyma cell. The green color indicates GFP signal, the red color in panel (A) indicates chlorophyll A autofluorescence and in panel (B) indicates punctate dsRNA signal. (C, E to G) Cross-sections of TuMV-infected *N. benthamiana* leaf tissues were collected and observed by TEM. White rectangles indicate the areas that are shown at higher magnification below (C) or on the right of (F, G) each subpanel. (C) TuMV-induced membranous aggregate and chloroplasts aggregate in the perinuclear region of a mesophyll cell at 6 dpi. (D) Schematic model for possible ultrastructure of $6K_2$:GFP-tagged globular structure. The green color indicates $6K_2$ proteins and the red color indicates chloroplasts. (E) Time course analysis of TuMV-induced membranous aggregate in mesophyll cells. Left: TuMV-induced CM structures, which amid with SMVs, were connected with several rER at 6 dpi. Middle: TuMV-induced SMVs aggregate close to the rER at 7 dpi. Right: TuMV-induced aggregate contains both SMVs and DMVs with an electron-dense core at 8 dpi. (F) Chloroplast envelope membrane invagination (arrowhead) results in DMVs (star) formation in chloroplast stroma. (G) Immuno-EM localization of dsRNA in TuMV-infected cells, no dsRNA-specific gold particles decorate DMVs (star) in chloroplast stroma. Chl, chloroplast; S, starch; V, vacuole; N, nucleus; rER, rough endoplasmic reticulum; CM, convoluted membranes; SMV, single-membrane vesicle; DMV, double-membrane vesicle; CI, cytoplasmic inclusion body; M, mitochondrion; CW, cell wall.

5. Several cellular pathways are hijacked during TuMV infection

This work has also highlighted that TuMV hijacks and remodels several different cellular pathways during the infectious cycle. This is reminiscent to what takes place during poliovirus infection. This virus belongs to the same superfamily (picorna-like viruses) as TuMV. Poliovirus infection has been shown to subvert the early secretory pathway (ER and/or Golgi apparatus) (Belov, Nair et al. 2012), the lipid synthesis pathway (Nchoutmboube, Viktorova et al. 2013) and autophagy pathway (Taylor and Kirkegaard 2008) for replication and maybe for transmission.

5.1 Secretory pathway

The plant secretory pathway is composed of a complex network of organelles including ER, Golgi apparatus, TGN, various endosomes and vacuoles (Bassham, Brandizzi et al. 2008). Many plant viruses remodel and utilize the host secretory pathway for their efficient replication and spread (reviewed in (Patarroyo, Laliberté et al. 2012)). In the case of TuMV, the confocal images have shown that the motile $6K_2$ vesicular compartments are ER-derived and are released at ERESs in a COPI- and COPII-dependent manner (Wei and Wang 2008). Recently, our lab reported that in *N. benthamiana* epidermal cells, TuMV infection induces the formation of a $6K_2$-tagged perinuclear globular structure, which contains ER, Golgi, and COPII markers, as well as chloroplasts (Grangeon, Agbeci et al. 2012). The exact mechanism of the globular structures formation is still not clear. Recent work has shown that vesicle formation depends on the N-terminal of $6K_2$, which is essential for $6K_2$ ER export (Jiang, Patarroyo et al. 2015). Additional determinants in the predicted transmembrane domain of $6K_2$ are also essential for $6K_2$ Golgi export (Jiang, personal communication).

The above conclusions are mainly based on confocal microscopy and molecular studies. My work complements these conclusions by offering ultrastructural information for the involvement of the secretory pathway during TuMV infection. ER-connected CM structures were detected at an early stage of infection (Fig. 4D, left panel), and ER was also located near the vesicle aggregates at mid (Fig. 4D, middle panel) and late stages of infection. This indicates that ER plays an essential role in the initiation and

development of TuMV factories. No obvious Golgi modification was detected under TEM, but the involvement of this organelle cannot be excluded, probably because of the remodeling process is too elusive to be detected. Besides the early secretory pathway (ER, Golgi apparatus), modifications of the late secretory pathway (vacuole) were also observed for TuMV particles accumulation. Linear arrays of TuMV particles were observed aligned along the cytoplasmic face of the tonoplast, and frequently protruding into the vacuole, finally forming an envelope around TuMV particles inside the central vacuole. During this process, TuMV particles must interact with the host proteins that located on the tonoplast, resulting in the tonoplast invagination. This interaction might be performed by some intermediate proteins, since the viral protein HCpro, which may function as a bridge protein linking potyvirus particles to the aphid stylet wall, was detected in purified vacuoles from TuMV-infected cells.

5.2 Lipid synthesis pathway

Accumulating data suggest that the simple remodeling of pre-existing membranes maybe insufficient to create the functional replication factories. Stimulating the *de novo* lipid synthesis pathway is essential to produce specific lipids for replication factory formation. For example, modulation of cholesterol biosynthesis can regulate DENV replication (Rothwell, Lebreton et al. 2009). Additionally, the fatty acid biosynthetic pathway is stimulated during both DENV (Heaton, Perera et al. 2010) and poliovirus (Nchoutmboube, Viktorova et al. 2013) infection to build the membrane replication complexes.

The replication of several plant (+) RNA viruses such as CPMV (Carette, Stuiver et al. 2000), *Grapevine fanleaf virus* (GFLV) (Ritzenthaler, Laporte et al. 2002) and PVX (Bamunusinghe, Hemenway et al. 2009) is strongly inhibited by the lipid synthesis inhibitor cerulenin, suggesting that plant virus replication depends on *de novo* lipid synthesis. The importance of some particular lipids for plant (+) RNA virus replication was obtained by using yeast as a surrogate host cell. Mutation of Δ9 fatty acid desaturase, which is the only enzyme for unsaturated fatty acid synthesis in yeast, inhibits BMV RNA replication (Lee, Ishikawa et al. 2001). TBSV replication complex formation is depended on phospholipids and sterols, since disruption of phospholipid

and sterols biosynthesis inhibited TBSV RNA accumulation (Sharma, Sasvari et al. 2010, Sharma, Sasvari et al. 2011).

To verify if the *de novo* lipid synthesis is also stimulated during TuMV infection, lipophilic dye $DiOC_6(3)$ staining was performed on the cross-sections of mock- and TuMV/$6K_2$:mCherry-infected *N. benthamiana* leaf midrib. Compared with mock-infected samples (Fig. 5A), I observed a strong signal for lipid staining in TuMV-infected samples (Fig. 5B), and this strong lipid staining colocalizes with the $6K_2$ replication factories (Fig. 5C). This result supports the hypothesis that TuMV replication factories formation and development depends on *de novo* lipid synthesis.

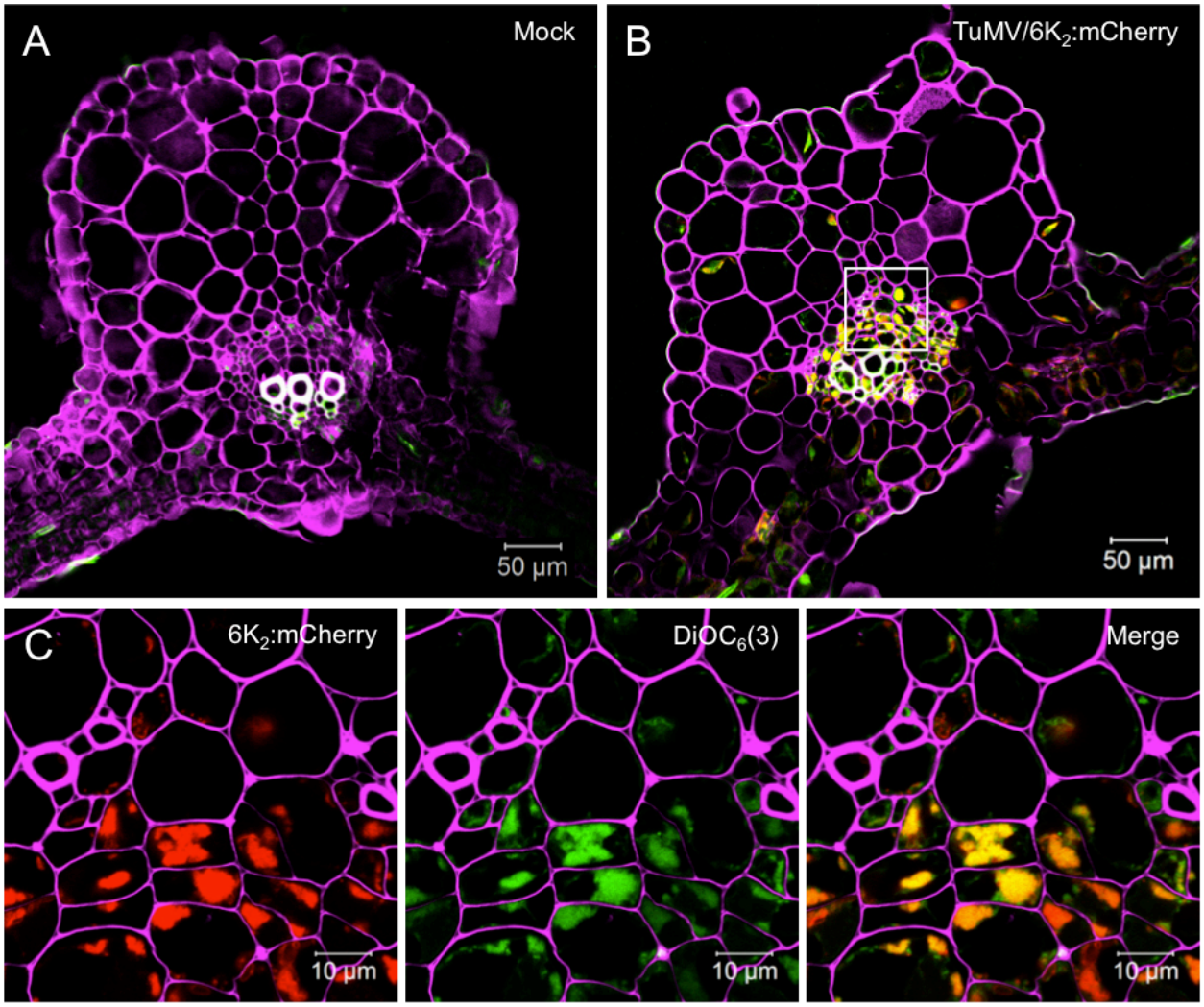

Figure 5. Lipid accumulation during TuMV infection.

(A and B) Cross-sections of mock- (A) and TuMV/6K_2:mCherry- systemically (B) infected *N. benthamiana* leaf midrib were observed by confocal microscopy. (C) A close up view of some vascular parenchyma cells from the White square area of panel (B). Fluorescent brightener 28-stained cell wall is shown in false-color magenta, 6K_2:mCherry-tagged vesicles are shown in red, and $DiOC_6$(3) stained membranes are shown in green. (C) is taken from (Laliberté and Zheng 2014).

In plants, lipid synthesis takes place in the ER, and may also in chloroplasts (Ohlrogge, Kuhn et al. 1979). The *de novo* fatty acids biosynthesis occurs inside the chloroplasts (Ohlrogge, Kuhn et al. 1979), then the fatty acids are either directly assembled into thylakoid lipids at the chloroplast envelope membrane, or are exported to the ER for lipid assembly. Only a fraction of lipid precursors assembled at the ER is reimported into the chloroplast for the synthesis of thylakoid lipids. Therefore, extensive lipid trafficking takes place between the ER and chloroplast envelope membranes (Wang and Benning 2012).

As shown in Figure 4, the ER-connected membranous aggregates are the TuMV replication factories, but the reason for the formation of chloroplast inclusions close to those replication factories is not clear. Since the *de novo* lipid synthesis is boosted during TuMV infection, the source (fatty acids) of *de novo* lipid synthesis may be produced inside chloroplasts, and there would be extensive lipids exchange between chloroplast and ER. I thus propose that chloroplasts are recruited close to the ER-associated replication factories for efficient fatty acids supplying and lipid assembly.

5.3 Other cellular pathways

1) Autophagy pathway

Autophagy is an intracellular degradation process that is important for the removal of damaged organelles and long-lived proteins for the maintenance of cellular homeostasis. It can also serve as innate immunity to destroy many intracellular pathogens. However, some viruses either suppress this pathway for their survival, or subvert this pathway to benefit their replication.

The hallmark of autophagy is the presence of DMVs with cytoplasmic contents that acidify and fuse with lysosomes to facilitate degradation of their contents (Xie and Klionsky 2007). It has been shown for several animal (+) RNA viruses, such as poliovirus, DENV and HCV that induce DMVs formation during infection, could modify the autophagy pathway to benefit their infectious cycle. Stimulation of autophagy increases the intracellular yield of poliovirus, and inhibition of autophagy reduces intracellular virus yield (Taylor and Kirkegaard 2008). It has been proposed that

poliovirus subverts the pathway of autophagosome formation and maybe blocks the subsequent maturation and degradation process, or provide a mechanism of virus particles secretion out of the infected cells (Taylor and Kirkegaard 2008, Richards and Jackson 2013). The autophagy pathway facilitates DENV RNA replication, and is also required for infectious virions maturation (Mateo, Nagamine et al. 2013). Inhibition of the autophagy machinery decreases the production of new HCV infectious particles (Tanida, Fukasawa et al. 2009).

TuMV DMVs with an electron-dense core were detected at the late stage of infection. The function of those DMVs is not clear. The DMVs are probably derived from the SMVs by enwrapping themselves with their cytoplasmic content. This possible transformation process is similar to autophagosome formation in the autophagy pathway, thus strongly indicating TuMV may also hijack this pathway.

2) Endosomal/MVB protein-sorting pathway

The ESCRT assemble into a multisubunit machinery that performs a topologically unique membrane bending and scission reaction away from the cytoplasm. The ESCRT machinery consists of four subcomplexes (ESCRT-0, -I, -II, -III) and a vacuolar protein sorting 4 complex (Wegner, Rodahl et al. 2011). TBSV replication protein p33 interacts with Vps4p and three other ESCRT-III proteins. Vps4p interacts with TBSV vRNA and is located in the replication complexes. Deletion of Vps4p in yeast leads to the formation of crescent-like membrane structures instead of the characteristic spherules (Barajas, Martin et al. 2014), suggesting Vps4p and the other ESCRT proteins are hijacked to build TBSV membrane-associated replication complexes.

Another important observation in this thesis is that TuMV particles acquire the tonoplast to form an envelope in the vacuole. The mechanism of this membrane structures formation is unclear. TuMV particles protruding tonoplast towards vacuole were observed, which is reminiscent to the endosomal/MVB protein-sorting pathway. Thus, it will be interesting to test if TuMV hijacks the ESCRT machinery for this loading process.

6. Perspectives and future direction

6.1 Identifying host factors present in $6K_2$ vesicles

Novel information on the host protein content of viral replication complexes could be obtained by collecting the xylem sap and the intercellular fluid of TuMV-infected plants, and then by analyzing the composition of $6K_2$ vesicles by mass spectrometry.

6.2 Understanding how $6K_2$ vesicles cross PDs and end up in the vascular conducting tubes

Previously, $6K_2$ vesicles have been shown to be adjacent to (Fig. 6A, arrows), in association with (Fig. 6A, white box) or colocalized with (Fig. 6B, arrows) the PD marker plasmodesmata located protein 1 (PDLP1) (Grangeon, Jiang et al. 2013). Aniline blue (Methyl Blue), which is a dye that stains callose (Evert 1977), could clearly show the sieve plate (dashed arrows) and PPUs (arrowheads) in the phloem sieve elements (Fig. 6C). By aniline blue staining, I observed that $6K_2$ vesicles are colocalized with the PPUs (Fig. 6D). The TEM data collected for this project mainly uncovered the ultrastructure and biogenesis of $6K_2$-tagged membranous aggregates, not the small motile $6K_2$ vesicles that traffic throughout TuMV-infected plants. Immunogold labeling is not a suitable method to study the small motile $6K_2$ vesicles, since almost no $6K_2$, dsRNA or vRdRp-specific gold particles are detected on the individual vesicles in TuMV infected cells. Therefore, it is not clear if the moving $6K_2$ vesicles are SMVs, DMVs or whether they may have additional other forms.

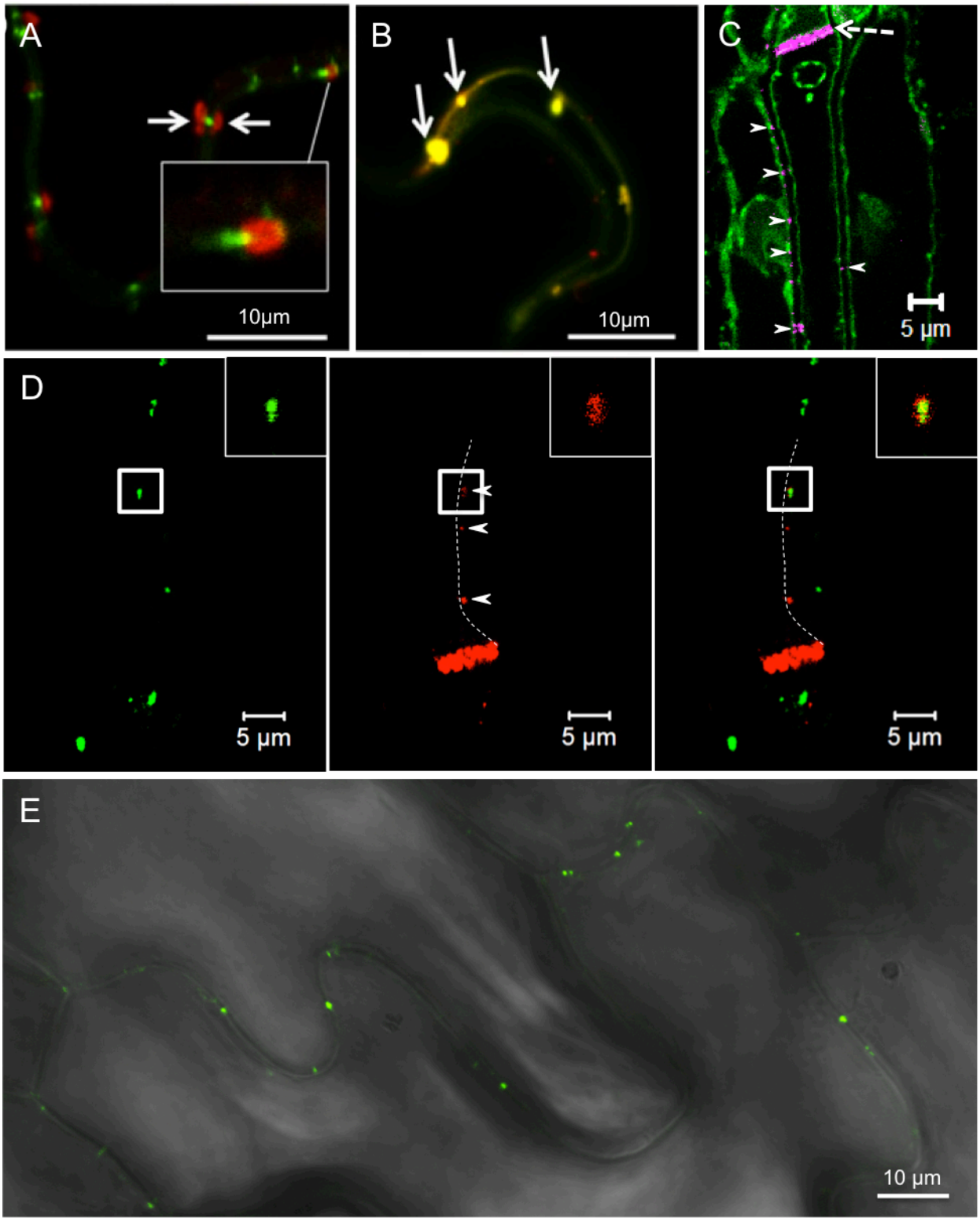
A
10μm
B
10μm
C
5 μm
D
5 μm
5 μm
5 μm
E
10 μm

Figure 6. $6K_2$ vesicles reach the PDs and PPUs.

(A and B) Confocal image of *N. benthamiana* epidermal cells expressing PDLP1:GFP and infected with TuMV producing $6K_2$:mCherry. (A) Arrows indicate $6K_2$ vesicles observed on either side of a PDLP1:GFP-labeled PD. White box is a close-up view of the structure indicated by white line. (B) Arrows indicate $6K_2$ vesicles located with PDLP1 within the intercellular wall space. (C and D) Confocal images of mock- (C) and TuMV/$6K_2$:GPF- (D) infected *N. benthamiana* stem cross-sections. The $DiOC_6(3)$ stained lipids are shown in green. The Aniline blue stained sieve plates and PPUs are shown in false color magenta in penal (C) and red in penal (D). (E) Confocal image of an epidermal cell from a transgenic *Arabidopsis thaliana* plants that express PDLP1:GFP. (A) and (B) are taken from (Grangeon, Jiang et al. 2013).

Correlative light electron microscopy (CLEM) can bridge the gap between light microscopy and electron microscopy. It involves the rapid sample imaging of fluorescently tagged proteins at the light microscope level, followed by retracing the same structure back in the electron microscope to show the protein localization in the specific structural space. There are many different CLEM techniques, each having its own special advantages but also its technical challenges. However in practice, not all approaches are equally well suited to plants. For instance, a genetically encoded fluorescent tag miniSOG (for mini singlet oxygen generator) has been generated for CLEM of mammalian cells and tissues, since miniSOG can generate electron-dense deposits through photoconversion that are visible by TEM (Shu, Lev-Ram et al. 2011). In this study, $6K_2$ was fused with miniSOG, and the photoconversion was performed in *N. benthamiana* leaf tissue, but it did not work.

To understand how the $6K_2$-tagged membrane-bound replication complexes move towards to the PD and then cross it, CLEM will be conducted to help us locate those small $6K_2$ vesicles on TEM samples, especially near or inside the PDs and PPUs. There are two types of CLEM that have been performed successfully in plant tissues. One is correlative imaging of fluorescent proteins in LR white resin-embedded plant material (Bell, Mitchell et al. 2013). Another one includes obtaining the ~50-μm-thick sections by cryosectioning, observing it under confocal microscope and then processing for TEM (Lee, Wang et al. 2011). The second methods will be tested in our case. The experiment will be performed with the transgenic *Arabidopsis thaliana* plants that express PDLP1:GFP to indicate the PDs and PPUs (Fig. 6E). The PDs association and localization of $6K_2$-tagged vesicles by CLEM will be done in collaboration with Dr. Jung-Youn Lee from the University of Delaware. To verify if $6K_2$ vesicles are released into the intercellular space as exosomes, the CLEM can be also conducted.

6.3 Locating viral and host proteins in TuMV-induced membrane structures

At the late stage of TuMV infection, TuMV particle bundles associate with electron-dense bodies, which may represent the particle assembly sites. These are located in close vicinity of vesicle aggregates. It is known that each TuMV particle contains a single (+) RNA, a 5’ terminal covalently linked VPg (Murphy, Klein et al.

1996, Oruetxebarria, Guo et al. 2001) and approximately 2 000 copies of CP (Shukla and Ward 1989). In addition, the viral protein HC-Pro and CI can physically interact with TuMV particles (Blanc, Lopez-Moya et al. 1997, Gabrenaite-Verkhovskaya, Andreev et al. 2008). Thus, at least the progeny vRNA and these viral proteins probably could be found in the electron-dense bodies. Immunogold labeling with anti-CP did not work well in this study. However instead of immunogold labeling, new techniques such as Metal-Tagging TEM (METTEM) (Risco, Sanmartin-Conesa et al. 2012) has been developed to identify proteins on TEM samples in yeast cells (Barajas, Martin et al. 2014). Whether they will be useful on plant tissue still need to be tested. To confirm the contents of the DMVs and electron-dense bodies, the CLEM can be also conducted.

7. Conclusion

The work in this thesis is based on the improvement and application of several crucial techniques: cryosectiong, immunohistolocalization, conventional TEM sample preparation, HPF/FS and ET.

To begin this project, the cryosectioning protocol to collect large cross- and longitudinal- sections of leaf and stem tissues, and the immunohistolocalization protocol on these sections were improved. Based on these techniques, it was shown that TuMV uses both phloem and xylem for its long-distance movement, and the moving entity is a membrane-associated replication complex.

Several steps of the TEM sample preparation were also optimized to give the best membrane structure contrast. The upper TuMV systemically infected leaf tissue was found better for the characterization of TuMV-induced cellular reorganization under TEM. Based on TEM and ET studies, this work also contributes to the overall understanding of the ultrastructure, biogenesis and functions of the TuMV-induced membrane structures. This work demonstrates that different TuMV-induced membrane structures, such as ER-connected CM structures maybe for polyprotein translation and processing, SMVs for vRNA replication, DMVs may be involved in viral particles assembly. The likely TuMV particles assembly site close to the vesicle aggregates was also uncovered. Finally, it was shwon that TuMV particles hijack the tonoplast to form enveloped structures for accumulation in the central vacuole.

This work then leads to a better understanding of the functions of membrane-associated viral structures during TuMV infection and may eventually contribute to develop plant cultivars that resist to virus infection.

REFERENCES

Achon, M. A., M. Pinner, V. Medina and G. Lomonossoff (1996). "Biological characteristics of maize dwarf mosaic potyvirus from Spain." European Journal of Plant Pathology **102**(7): 697-705.

Adams, M. J., J. F. Antoniw and F. Beaudoin (2005). "Overview and analysis of the polyprotein cleavage sites in the family Potyviridae." Mol Plant Pathol **6**(4): 471-487.

Agbeci, M., R. Grangeon, R. S. Nelson, H. Zheng and J. F. Laliberte (2013). "Contribution of host intracellular transport machineries to intercellular movement of turnip mosaic virus." PLoS Pathog **9**(10): e1003683.

An, Q., R. Huckelhoven, K. H. Kogel and A. J. van Bel (2006). "Multivesicular bodies participate in a cell wall-associated defence response in barley leaves attacked by the pathogenic powdery mildew fungus." Cell Microbiol **8**(6): 1009-1019.

An, Q., A. J. van Bel and R. Huckelhoven (2007). "Do plant cells secrete exosomes derived from multivesicular bodies?" Plant Signal Behav **2**(1): 4-7.

Angelini, M. M., M. Akhlaghpour, B. W. Neuman and M. J. Buchmeier (2013). "Severe acute respiratory syndrome coronavirus nonstructural proteins 3, 4, and 6 induce double-membrane vesicles." MBio **4**(4).

Anindya, R., S. Chittori and H. S. Savithri (2005). "Tyrosine 66 of Pepper vein banding virus genome-linked protein is uridylylated by RNA-dependent RNA polymerase." Virology **336**(2): 154-162.

Anindya, R. and H. S. Savithri (2003). "Surface-exposed amino- and carboxy-terminal residues are crucial for the initiation of assembly in Pepper vein banding virus: a flexuous rod-shaped virus." Virology **316**(2): 325-336.

Atreya, P. L., J. J. Lopez-Moya, M. Chu, C. D. Atreya and T. P. Pirone (1995). "Mutational analysis of the coat protein N-terminal amino acids involved in potyvirus transmission by aphids." J Gen Virol **76 (Pt 2)**: 265-270.

Bamunusinghe, D., C. L. Hemenway, R. S. Nelson, A. A. Sanderfoot, C. M. Ye, M. A. Silva, M. Payton and J. Verchot-Lubicz (2009). "Analysis of potato virus X replicase and TGBp3 subcellular locations." Virology **393**(2): 272-285.

Bamunusinghe, D., J. K. Seo and A. L. Rao (2011). "Subcellular localization and rearrangement of endoplasmic reticulum by Brome mosaic virus capsid protein." J Virol **85**(6): 2953-2963.

Barajas, D., I. F. Martin, J. Pogany, C. Risco and P. D. Nagy (2014). "Noncanonical role for the host Vps4 AAA+ ATPase ESCRT protein in the formation of Tomato bushy stunt virus replicase." PLoS Pathog **10**(4): e1004087.

Baratova, L. A., A. V. Efimov, E. N. Dobrov, N. V. Fedorova, R. Hunt, G. A. Badun, A. L. Ksenofontov, L. Torrance and L. Järvekülg (2001). "In Situ Spatial Organization of Potato Virus A Coat Protein Subunits as Assessed by Tritium Bombardment." Journal of Virology **75**(20): 9696-9702.

Barcena, M. and A. J. Koster (2009). "Electron tomography in life science." Semin Cell Dev Biol **20**(8): 920-930.

Bassham, D. C., F. Brandizzi, M. S. Otegui and A. A. Sanderfoot (2008). "The secretory system of Arabidopsis." Arabidopsis Book **6**: e0116.

Beauchemin, C., V. Bougie and J. F. Laliberte (2005). "Simultaneous production of two foreign proteins from a polyvirus-based vector." Virus Res **112**(1-2): 1-8.

Beauchemin, C., N. Boutet and J.-F. Laliberté (2007). "Visualization of the Interaction between the Precursors of VPg, the Viral Protein Linked to the Genome of Turnip Mosaic Virus, and the Translation Eukaryotic Initiation Factor iso 4E In Planta." Journal of Virology **81**(2): 775-782.
Beauchemin, C. and J.-F. Laliberté (2007). "The Poly(A) Binding Protein Is Internalized in Virus-Induced Vesicles or Redistributed to the Nucleolus during Turnip Mosaic Virus Infection." Journal of Virology **81**(20): 10905-10913.
Beauchemin, C. and J. F. Laliberte (2007). "The poly(A) binding protein is internalized in virus-induced vesicles or redistributed to the nucleolus during turnip mosaic virus infection." J Virol **81**(20): 10905-10913.
Bell, K., S. Mitchell, D. Paultre, M. Posch and K. Oparka (2013). "Correlative imaging of fluorescent proteins in resin-embedded plant material." Plant Physiol **161**(4): 1595-1603.
Belov, G. A., Q. Feng, K. Nikovics, C. L. Jackson and E. Ehrenfeld (2008). "A critical role of a cellular membrane traffic protein in poliovirus RNA replication." PLoS Pathog **4**(11): e1000216.
Belov, G. A., V. Nair, B. T. Hansen, F. H. Hoyt, E. R. Fischer and E. Ehrenfeld (2012). "Complex dynamic development of poliovirus membranous replication complexes." J Virol **86**(1): 302-312.
Belov, G. A., V. Nair, B. T. Hansen, F. H. Hoyt, E. R. Fischer and E. Ehrenfeld (2012). "Complex Dynamic Development of Poliovirus Membranous Replication Complexes." Journal of Virology **86**(1): 302-312.
Belov, G. A. and F. J. van Kuppeveld (2012). "(+)RNA viruses rewire cellular pathways to build replication organelles." Curr Opin Virol **2**(6): 740-747.
Betti, C., C. Lico, D. Maffi, S. D'Angeli, M. M. Altamura, E. Benvenuto, F. Faoro and S. Baschieri (2012). "Potato virus X movement in Nicotiana benthamiana: new details revealed by chimeric coat protein variants." Molecular Plant Pathology **13**(2): 198-203.
Bienz, K., D. Egger and L. Pasamontes (1987). "Association of polioviral proteins of the P2 genomic region with the viral replication complex and virus-induced membrane synthesis as visualized by electron microscopic immunocytochemistry and autoradiography." Virology **160**(1): 220-226.
Bienz, K., D. Egger, T. Pfister and M. Troxler (1992). "Structural and functional characterization of the poliovirus replication complex." J Virol **66**(5): 2740-2747.
Bienz, K., D. Egger, Y. Rasser and W. Bossart (1983). "Intracellular distribution of poliovirus proteins and the induction of virus-specific cytoplasmic structures." Virology **131**(1): 39-48.
Bilgin, D. D., Y. Liu, M. Schiff and S. P. Dinesh-Kumar (2003). "P58(IPK), a plant ortholog of double-stranded RNA-dependent protein kinase PKR inhibitor, functions in viral pathogenesis." Dev Cell **4**(5): 651-661.
Blackman, L. M., P. Boevink, S. S. Cruz, P. Palukaitis and K. J. Oparka (1998). "The movement protein of cucumber mosaic virus traffics into sieve elements in minor veins of nicotiana clevelandii." The Plant Cell Online **10**(4): 525-537.
Blanc, S., J. J. Lopez-Moya, R. Wang, S. Garcia-Lampasona, D. W. Thornbury and T. P. Pirone (1997). "A specific interaction between coat protein and helper component correlates with aphid transmission of a potyvirus." Virology **231**(1): 141-147.
Bragg, J. N., D. M. Lawrence and A. O. Jackson (2004). "The N-terminal 85 amino acids of the barley stripe mosaic virus gammab pathogenesis protein contain three zinc-binding motifs." J Virol **78**(14): 7379-7391.
Brandizzi, F. and C. Barlowe (2013). "Organization of the ER-Golgi interface for membrane traffic control." Nat Rev Mol Cell Biol **14**(6): 382-392.

Brault, V., M. Bergdoll, J. Mutterer, V. Prasad, S. Pfeffer, M. Erdinger, K. E. Richards and V. Ziegler-Graff (2003). "Effects of point mutations in the major capsid protein of beet western yellows virus on capsid formation, virus accumulation, and aphid transmission." Journal of Virology **77**(5): 3247-3256.
Brugidou, C., N. Opalka, M. Yeager, R. N. Beachy and C. Fauquet (2002). "Stability of rice yellow mottle virus and cellular compartmentalization during the infection process in Oryza sativa (L.)." Virology **297**(1): 98-108.
Bui, Q. T., M. P. Golinelli-Cohen and C. L. Jackson (2009). "Large Arf1 guanine nucleotide exchange factors: evolution, domain structure, and roles in membrane trafficking and human disease." Mol Genet Genomics **282**(4): 329-350.
Bukong, T. N., F. Momen-Heravi, K. Kodys, S. Bala and G. Szabo (2014). "Exosomes from Hepatitis C Infected Patients Transmit HCV Infection and Contain Replication Competent Viral RNA in Complex with Ago2-miR122-HSP90." PLoS Pathog **10**(10): e1004424.
Canto, T., D. A. Prior, K. H. Hellwald, K. J. Oparka and P. Palukaitis (1997). "Characterization of cucumber mosaic virus. IV. Movement protein and coat protein are both essential for cell-to-cell movement of cucumber mosaic virus." Virology **237**(2): 237-248.
Cao, X., X. Jin, X. Zhang, Y. Li, C. Wang, X. Wang, J. Hong, X. Wang, D. Li and Y. Zhang (2015). "Morphogenesis of the ER membrane-invaginated vesicles during Beet black scorch virus infection: The role of auxiliary replication protein and new implications of three-dimensional architecture." J Virol.
Carette, J. E., M. Stuiver, J. Van Lent, J. Wellink and A. Van Kammen (2000). "Cowpea mosaic virus infection induces a massive proliferation of endoplasmic reticulum but not Golgi membranes and is dependent on de novo membrane synthesis." J Virol **74**(14): 6556-6563.
Carrington, J. C., D. D. Freed and T. C. Sanders (1989). "Autocatalytic processing of the potyvirus helper component proteinase in Escherichia coli and in vitro." J Virol **63**(10): 4459-4463.
Carrington, J. C., P. E. Jensen and M. C. Schaad (1998). "Genetic evidence for an essential role for potyvirus CI protein in cell-to-cell movement." Plant J **14**(4): 393-400.
Carrington, J. C., K. D. Kasschau, S. K. Mahajan and M. C. Schaad (1996). "Cell-to-Cell and Long-Distance Transport of Viruses in Plants." Plant Cell **8**(10): 1669-1681.
Casadevall, A., J. D. Nosanchuk, P. Williamson and M. L. Rodrigues (2009). "Vesicular transport across the fungal cell wall." Trends Microbiol **17**(4): 158-162.
Chen, D., S. Juarez, L. Hartweck, J. M. Alamillo, C. Simon-Mateo, J. J. Perez, M. R. Fernandez-Fernandez, N. E. Olszewski and J. A. Garcia (2005). "Identification of secret agent as the O-GlcNAc transferase that participates in Plum pox virus infection." J Virol **79**(15): 9381-9387.
Chen, J., C. Doyle, X. Qi and H. Zheng (2012). "The endoplasmic reticulum: a social network in plant cells." J Integr Plant Biol **54**(11): 840-850.
Cheng, N. H., C. L. Su, S. A. Carter and R. S. Nelson (2000). "Vascular invasion routes and systemic accumulation patterns of tobacco mosaic virus in Nicotiana benthamiana." Plant J **23**(3): 349-362.
Choi, I. R., D. C. Stenger and R. French (2000). "Multiple interactions among proteins encoded by the mite-transmitted wheat streak mosaic tritimovirus." Virology **267**(2): 185-198.
Cosgrove, D. J. (2005). "Growth of the plant cell wall." Nat Rev Mol Cell Biol **6**(11): 850-861.
Cotton, S., R. Grangeon, K. Thivierge, I. Mathieu, C. Ide, T. Wei, A. Wang and J.-F. Laliberté (2009). "Turnip Mosaic Virus RNA Replication Complex Vesicles Are Mobile, Align with

Microfilaments, and Are Each Derived from a Single Viral Genome." Journal of Virology **83**(20): 10460-10471.
Crawford, K. M. and P. C. Zambryski (2001). "Non-targeted and targeted protein movement through plasmodesmata in leaves in different developmental and physiological states." Plant Physiol **125**(4): 1802-1812.
Cronin, S., J. Verchot, R. Haldemancahill, M. C. Schaad and J. C. Carrington (1995). "Long-distance movement factor - a transport function of the potyvirus helper component proteinase." Plant Cell **7**(5): 549-559.
de Mejia, M. V., E. Hiebert, D. E. Purcifull, D. W. Thornbury and T. P. Pirone (1985). "Identification of potyviral amorphous inclusion protein as a nonstructural, virus-specific protein related to helper component." Virology **142**(1): 34-43.
Derrick, P. M., H. Barker and K. J. Oparka (1990). "Effect of virus infection on symplastic transport of fluorescent tracers in Nicotiana clevelandii leaf epidermis." Planta **181**(4): 555-559.
Di Franco, A., M. Russo and G. P. Martelli (1984). "Ultrastructure and Origin of Cytoplasmic Multivesicular Bodies Induced by Carnation Italian Ringspot Virus." Journal of General Virology **65**(7): 1233-1237.
Diaz, A., X. Wang and P. Ahlquist (2010). "Membrane-shaping host reticulon proteins play crucial roles in viral RNA replication compartment formation and function." Proc Natl Acad Sci U S A **107**(37): 16291-16296.
Dinant, S., J. L. Bonnemain, C. Girousse and J. Kehr (2010). "Phloem sap intricacy and interplay with aphid feeding." C R Biol **333**(6-7): 504-515.
Ding, B., Q. Li, L. Nguyen, P. Palukaitis and W. J. Lucas (1995). "Cucumber mosaic virus 3a protein potentiates cell-to-cell trafficking of CMV RNA in tobacco plants." Virology **207**(2): 345-353.
Ding, X. S., C. M. Boydston and R. S. Nelson (2001). "Presence of brome mosaic virus in barley guttation fluid and its association with localized cell death response." Phytopathology **91**(5): 440-448.
Dolja, V. V., R. Haldeman, N. L. Robertson, W. G. Dougherty and J. C. Carrington (1994). "Distinct functions of capsid protein in assembly and movement of tobacco etch potyvirus in plants." The EMBO journal **13**(6): 1482-1491.
Dolja, V. V., R. Haldeman-Cahill, A. E. Montgomery, K. A. Vandenbosch and J. C. Carrington (1995). "Capsid Protein Determinants Involved in Cell-to-Cell and Long Distance Movement of Tobacco Etch Potyvirus." Virology **206**(2): 1007-1016.
Domier, L. L., J. G. Shaw and R. E. Rhoads (1987). "Potyviral proteins share amino acid sequence homology with picorna-, como-, and caulimoviral proteins." Virology **158**(1): 20-27.
Donald, R. G. and A. O. Jackson (1996). "RNA-binding activities of barley stripe mosaic virus gamma b fusion proteins." J Gen Virol **77 (Pt 5)**: 879-888.
Dufresne, P. J., K. Thivierge, S. Cotton, C. Beauchemin, C. Ide, E. Ubalijoro, J.-F. Laliberté and M. G. Fortin (2008). "Heat shock 70 protein interaction with Turnip mosaic virus RNA-dependent RNA polymerase within virus-induced membrane vesicles." Virology **374**(1): 217-227.
Dufresne, P. J., K. Thivierge, S. Cotton, C. Beauchemin, C. Ide, E. Ubalijoro, J. F. Laliberte and M. G. Fortin (2008). "Heat shock 70 protein interaction with Turnip mosaic virus RNA-dependent RNA polymerase within virus-induced membrane vesicles." Virology **374**(1): 217-227.

Eagles, R. M., E. Balmori-Melian, D. L. Beck, R. C. Gardner and R. L. Forster (1994). "Characterization of NTPase, RNA-binding and RNA-helicase activities of the cytoplasmic inclusion protein of tamarillo mosaic potyvirus." Eur J Biochem **224**(2): 677-684.
Edwardson, J. R., R. G. Christie and N. J. Ko (1984). "Potyvirus Cylindrical Inclusions—Subdivision—IV." phytopathology **74**: 1111-1114.
Egger, D., B. Wolk, R. Gosert, L. Bianchi, H. E. Blum, D. Moradpour and K. Bienz (2002). "Expression of hepatitis C virus proteins induces distinct membrane alterations including a candidate viral replication complex." J Virol **76**(12): 5974-5984.
Elena, S. F. and G. Rodrigo (2012). "Towards an integrated molecular model of plant-virus interactions." Curr Opin Virol **2**(6): 719-724.
Evert, R. F. (1977). "Phloem Structure and Histochemistry." Annual Review of Plant Physiology **28**(1): 199-222.
Feki, S., M. J. Loukili, R. Triki-Marrakchi, G. Karimova, I. Old, H. Ounouna, A. Nato, F. Nato, J. L. Guesdon, P. Lafaye and A. B. Elgaaied (2005). "Interaction between tobacco Ribulose-l,5-biphosphate Carboxylase/Oxygenase large subunit (RubisCO-LSU) and the PVY Coat Protein (PVY-CP)." European Journal of Plant Pathology **112**(3): 221-234.
Fellers, J., J. Wan, Y. Hong, G. B. Collins and A. G. Hunt (1998). "In vitro interactions between a potyvirus-encoded, genome-linked protein and RNA-dependent RNA polymerase." J Gen Virol **79 (Pt 8)**: 2043-2049.
Feng, Z., L. Hensley, K. L. McKnight, F. Hu, V. Madden, L. Ping, S. H. Jeong, C. Walker, R. E. Lanford and S. M. Lemon (2013). "A pathogenic picornavirus acquires an envelope by hijacking cellular membranes." Nature **496**(7445): 367-371.
Fernandez, A., H. S. Guo, P. Saenz, L. Simon-Buela, M. Gomez de Cedron and J. A. Garcia (1997). "The motif V of plum pox potyvirus CI RNA helicase is involved in NTP hydrolysis and is essential for virus RNA replication." Nucleic Acids Res **25**(22): 4474-4480.
Fisher, D. B., Y. Wu and M. S. B. Ku (1992). "Turnover of soluble proteins in the wheat sieve tube." Plant Physiology **100**(3): 1433-1441.
French, C. J. and M. Elder (1999). "Virus particles in guttate and xylem of infected cucumber (Cucumis sativus L.)." Annals of Applied Biology **134**(1): 81-87.
French, C. J., M. Elder and F. Skelton (1993). "Recovering and identifying infectious plant viruses in guttation fluid." HortScience **28**(7): 746-747.
Froelich, D. R., D. L. Mullendore, K. H. Jensen, T. J. Ross-Elliott, J. A. Anstead, G. A. Thompson, H. C. Pelissier and M. Knoblauch (2011). "Phloem ultrastructure and pressure flow: Sieve-Element-Occlusion-Related agglomerations do not affect translocation." Plant Cell **23**(12): 4428-4445.
Gabrenaite-Verkhovskaya, R., I. A. Andreev, N. O. Kalinina, L. Torrance, M. E. Taliansky and K. Makinen (2008). "Cylindrical inclusion protein of potato virus A is associated with a subpopulation of particles isolated from infected plants." J Gen Virol **89**(Pt 3): 829-838.
Gao, J. G. and A. Nassuth (1993). "Alteration of major cellular organelles in wheat leaf infected with wheat streak mosaic rymovirus (Potyviridae)." Phytopathology **83**(2): 206-213.
Gibbs, A. (1976). Viruses and Plasmodesmata. Intercellular Communication in Plants: Studies on Plasmodesmata. B. E. S. Gunning and A. W. Robards, Springer Berlin Heidelberg**:** 149-164.
Gibbs, A. J., K. Ohshima, M. J. Phillips and M. J. Gibbs (2008). "The prehistory of potyviruses: their initial radiation was during the dawn of agriculture." PLoS One **3**(6): e2523.
Gilkey, J. C. and L. A. Staehelin (1986). "Advances in ultrarapid freezing for the preservation of cellular ultrastructure." Journal of Electron Microscopy Technique **3**(2): 177-210.

Gomez-Aix, C., M. Garcia-Garcia, M. A. Aranda and M. A. Sanchez Pina (2014). "Melon necrotic spot virus replication occurs in association with altered mitochondria." Mol Plant Microbe Interact.
Gopinath, K. and C. C. Kao (2007). "Replication-Independent Long-Distance Trafficking by Viral RNAs in Nicotiana benthamiana." The Plant Cell Online **19**(4): 1179-1191.
Goueslain, L., K. Alsaleh, P. Horellou, P. Roingeard, V. Descamps, G. Duverlie, Y. Ciczora, C. Wychowski, J. Dubuisson and Y. Rouille (2010). "Identification of GBF1 as a cellular factor required for hepatitis C virus RNA replication." J Virol **84**(2): 773-787.
Govier, D. A., B. Kassanis and T. P. Pirone (1977). "Partial purification and characterization of the potato virus Y helper component." Virology **78**(1): 306-314.
Grangeon, R., M. Agbeci, J. Chen, G. Grondin, H. Zheng and J. F. Laliberte (2012). "Impact on the endoplasmic reticulum and Golgi apparatus of turnip mosaic virus infection." J Virol **86**(17): 9255-9265.
Grangeon, R., J. Jiang, J. Wan, M. Agbeci, H. Zheng and J. F. Laliberte (2013). "6K2-induced vesicles can move cell to cell during turnip mosaic virus infection." Front Microbiol **4**: 351.
Guo, D., M. L. Rajamaki, M. Saarma and J. P. Valkonen (2001). "Towards a protein interaction map of potyviruses: protein interaction matrixes of two potyviruses based on the yeast two-hybrid system." J Gen Virol **82**(Pt 4): 935-939.
Gutierrez, S., Y. Michalakis and S. Blanc (2012). "Virus population bottlenecks during within-host progression and host-to-host transmission." Curr Opin Virol **2**(5): 546-555.
Hafren, A., D. Hofius, G. Ronnholm, U. Sonnewald and K. Makinen (2010). "HSP70 and its cochaperone CPIP promote potyvirus infection in Nicotiana benthamiana by regulating viral coat protein functions." Plant Cell **22**(2): 523-535.
Hagiwara, Y., K. Komoda, T. Yamanaka, A. Tamai, T. Meshi, R. Funada, T. Tsuchiya, S. Naito and M. Ishikawa (2003). "Subcellular localization of host and viral proteins associated with tobamovirus RNA replication." EMBO J **22**(2): 344-353.
Halk, E. L. and J. M. McGuire (1973). "Translocation of tobacco ringspot virus in soybean." Phytopathology **63**: 1291-1300.
Hanton, S. L., L. Chatre, L. A. Matheson, M. Rossi, M. A. Held and F. Brandizzi (2008). "Plant Sar1 isoforms with near-identical protein sequences exhibit different localisations and effects on secretion." Plant Mol Biol **67**(3): 283-294.
Harlow, M. L., D. Ress, A. Stoschek, R. M. Marshall and U. J. McMahan (2001). "The architecture of active zone material at the frog's neuromuscular junction." Nature **409**(6819): 479-484.
Hatta, T., S. Bullivant and R. E. Matthews (1973). "Fine structure of vesicles induced in chloroplasts of Chinese cabbage leaves by infection with turnip yellow mosaic virus." J Gen Virol **20**(1): 37-50.
Hatta, T. and R. I. B. Francki (1981). "Cytopathic Structures Associated with Tonoplasts of Plant Cells Infected with Cucumber Mosaic and Tomato Aspermy Viruses." Journal of General Virology **53**(2): 343-346.
Hatta, T. and R. E. Matthews (1974). "The sequence of early cytological changes in Chinese cabbage leaf cells following systemic infection with turnip yellow mosaic virus." Virology **59**(2): 383-396.
Hatta, T. and R. E. Matthews (1976). "Sites of coat protein accumulation in turnip yellow mosaic virus-infected cells." Virology **73**(1): 1-16.

Heaton, N. S., R. Perera, K. L. Berger, S. Khadka, D. J. Lacount, R. J. Kuhn and G. Randall (2010). "Dengue virus nonstructural protein 3 redistributes fatty acid synthase to sites of viral replication and increases cellular fatty acid synthesis." Proc Natl Acad Sci U S A **107**(40): 17345-17350.
Heinlein, M. and B. L. Epel (2004). "Macromolecular transport and signaling through plasmodesmata." Int Rev Cytol **235**: 93-164.
Hess, M. and M. Hesse (1994). "Ultrastructural observations on anther tapetum development of freeze-fixed Ledebouria socialis Roth (Hyacinthaceae)." Planta **192**(3): 421-430.
Hess, M. W. (2003). "Of plants and other pets: practical aspects of freeze-substitution and resin embedding." J Microsc **212**(Pt 1): 44-52.
Hewer, A., A. Becker and A. J. van Bel (2011). "An aphid's Odyssey--the cortical quest for the vascular bundle." J Exp Biol **214**(Pt 22): 3868-3879.
Hipper, C., V. Brault, V. Ziegler-Graff and F. Revers (2013). "Viral and cellular factors involved in phloem transport of plant viruses." Frontiers in Plant Science **4**.
Hipper, C., B. Monsion, D. Bortolamiol-Bécet, V. Ziegler-Graff and V. Brault (2014). "Formation of virions is strictly required for turnip yellows virus long-distance movement in plants." Journal of General Virology **95**(Pt 2): 496-505.
Hoenger, A. and J. R. McIntosh (2009). "Probing the macromolecular organization of cells by electron tomography." Curr Opin Cell Biol **21**(1): 89-96.
Hong, Y. and A. G. Hunt (1996). "RNA polymerase activity catalyzed by a potyvirus-encoded RNA-dependent RNA polymerase." Virology **226**(1): 146-151.
Hong, Y., K. Levay, J. F. Murphy, P. G. Klein, J. G. Shaw and A. G. Hunt (1995). "A potyvirus polymerase interacts with the viral coat protein and VPg in yeast cells." Virology **214**(1): 159-166.
Hu, J., Y. Shibata, C. Voss, T. Shemesh, Z. Li, M. Coughlin, M. M. Kozlov, T. A. Rapoport and W. A. Prinz (2008). "Membrane proteins of the endoplasmic reticulum induce high-curvature tubules." Science **319**(5867): 1247-1250.
Hull, R. (2002). Chapter 2 - Nomenclature and Classification of Plant Viruses. Matthews' Plant Virology (Fourth Edition). R. Hull. London, Academic Press**:** 13-45.
Hwang, Y. T., A. W. McCartney, S. K. Gidda and R. T. Mullen (2008). "Localization of the Carnation Italian ringspot virus replication protein p36 to the mitochondrial outer membrane is mediated by an internal targeting signal and the TOM complex." BMC Cell Biol **9**: 54.
Hyodo, K., A. Mine, T. Taniguchi, M. Kaido, K. Mise, H. Taniguchi and T. Okuno (2013). "ADP ribosylation factor 1 plays an essential role in the replication of a plant RNA virus." J Virol **87**(1): 163-176.
Ibrahim, A., H. M. Hutchens, R. H. Berg and L. S. Loesch-Fries (2012). "Alfalfa mosaic virus replicase proteins, P1 and P2, localize to the tonoplast in the presence of virus RNA." Virology **433**(2): 449-461.
Ivanov, K. I., P. Puustinen, A. Merits, M. Saarma and K. Makinen (2001). "Phosphorylation down-regulates the RNA binding function of the coat protein of potato virus A." J Biol Chem **276**(17): 13530-13540.
Jiang, J. and J. F. Laliberte (2011). "The genome-linked protein VPg of plant viruses-a protein with many partners." Curr Opin Virol **1**(5): 347-354.
Jiang, J., C. Patarroyo, D. G. Cabanillas, H. Zheng and J. F. Laliberte (2015). "The vesicle-forming 6K2 protein of turnip mosaic virus interacts with the COPII coatomer Sec24a for viral systemic infection." J Virol.

Jimenez, I., L. Lopez, J. M. Alamillo, A. Valli and J. A. Garcia (2006). "Identification of a plum pox virus CI-interacting protein from chloroplast that has a negative effect in virus infection." Mol Plant Microbe Interact **19**(3): 350-358.
Jimenez, N., K. Vocking, E. G. van Donselaar, B. M. Humbel, J. A. Post and A. J. Verkleij (2009). "Tannic acid-mediated osmium impregnation after freeze-substitution: a strategy to enhance membrane contrast for electron tomography." J Struct Biol **166**(1): 103-106.
Jonczyk, M., K. B. Pathak, M. Sharma and P. D. Nagy (2007). "Exploiting alternative subcellular location for replication: tombusvirus replication switches to the endoplasmic reticulum in the absence of peroxisomes." Virology **362**(2): 320-330.
Kalina, M. and D. C. Pease (1977). "The probable role of phosphatidyl cholines in the tannic acid enhancement of cytomembrane electron contrast." J Cell Biol **74**(3): 742-746.
Kang, S. H., W. S. Lim, S. H. Hwang, J. W. Park, H. S. Choi and K. H. Kim (2006). "Importance of the C-terminal domain of soybean mosaic virus coat protein for subunit interactions." J Gen Virol **87**(Pt 1): 225-229.
Kaplan, I. B., L. Zhang and P. Palukaitis (1998). "Characterization of cucumber mosaic virus. V. Cell-to-cell movement requires capsid protein but not virions." Virology **246**(2): 221-231.
Kasschau, K. D. and J. C. Carrington (2001). "Long-distance movement and replication maintenance functions correlate with silencing suppression activity of potyviral HC-Pro." Virology **285**(1): 71-81.
Kawakami, S., Y. Watanabe and R. N. Beachy (2004). "Tobacco mosaic virus infection spreads cell to cell as intact replication complexes." Proc Natl Acad Sci U S A **101**(16): 6291-6296.
Kemball, C. C., M. Alirezaei, C. T. Flynn, M. R. Wood, S. Harkins, W. B. Kiosses and J. L. Whitton (2010). "Coxsackievirus infection induces autophagy-like vesicles and megaphagosomes in pancreatic acinar cells in vivo." J Virol **84**(23): 12110-12124.
Kempers, R. and A. E. Bel (1997). "Symplasmic connections between sieve element and companion cell in the stem phloem ofVicia faba L. have a molecular exclusion limit of at least 10 kDa." Planta **201**(2): 195-201.
Kendall, A., M. McDonald, W. Bian, T. Bowles, S. C. Baumgarten, J. Shi, P. L. Stewart, E. Bullitt, D. Gore, T. C. Irving, W. M. Havens, S. A. Ghabrial, J. S. Wall and G. Stubbs (2008). "Structure of flexible filamentous plant viruses." J Virol **82**(19): 9546-9554.
Kim, K. S. and J. P. Fulton (1969). "Electron microscopy of pokeweed leaf cells infected with pokeweed mosaic virus." Virology **37**(3): 297-308.
Kim, S. H., N. O. Kalinina, I. Andreev, E. V. Ryabov, A. G. Fitzgerald, M. E. Taliansky and P. Palukaitis (2004). "The C-terminal 33 amino acids of the cucumber mosaic virus 3a protein affect virus movement, RNA binding and inhibition of infection and translation." J Gen Virol **85**(Pt 1): 221-230.
Knapp, E., R. Flores, D. Scheiblin, D. Scheiblin, S. Modla, K. Czymmek, K. Czymmek and V. Yusibov (2012). "A cryohistological protocol for preparation of large plant tissue sections for screening intracellular fluorescent protein expression." Biotechniques **52**(1): 31-37.
Knoblauch, M. and W. S. Peters (2010). "Munch, morphology, microfluidics - our structural problem with the phloem." Plant Cell Environ **33**(9): 1439-1452.
Knoops, K., M. Kikkert, S. H. Worm, J. C. Zevenhoven-Dobbe, Y. van der Meer, A. J. Koster, A. M. Mommaas and E. J. Snijder (2008). "SARS-coronavirus replication is supported by a reticulovesicular network of modified endoplasmic reticulum." PLoS Biol **6**(9): e226.
Knuhtsen, H., E. Hiebert and D. E. Purcifull (1974). "Partial purification and some properties of tobacco etch virus induced intranuclear inclusions." Virology **61**(1): 200-209.

Kopek, B. G., G. Perkins, D. J. Miller, M. H. Ellisman and P. Ahlquist (2007). "Three-dimensional analysis of a viral RNA replication complex reveals a virus-induced mini-organelle." PLoS Biol **5**(9): e220.
Kopek, B. G., E. W. Settles, P. D. Friesen and P. Ahlquist (2010). "Nodavirus-induced membrane rearrangement in replication complex assembly requires replicase protein a, RNA templates, and polymerase activity." J Virol **84**(24): 12492-12503.
Kremer, J. R., D. N. Mastronarde and J. R. McIntosh (1996). "Computer visualization of three-dimensional image data using IMOD." J Struct Biol **116**(1): 71-76.
Ladinsky, M. S., J. R. Kremer, P. S. Furcinitti, J. R. McIntosh and K. E. Howell (1994). "HVEM tomography of the trans-Golgi network: structural insights and identification of a lace-like vesicle coat." J Cell Biol **127**(1): 29-38.
Laliberté, J.-F. and H. Zheng (2014). "Viral Manipulation of Plant Host Membranes." Annual Review of Virology **1**(1): 237-259.
Laliberte, J. F. and H. Sanfacon (2010). "Cellular remodeling during plant virus infection." Annu Rev Phytopathol **48**: 69-91.
Lanke, K. H., H. M. van der Schaar, G. A. Belov, Q. Feng, D. Duijsings, C. L. Jackson, E. Ehrenfeld and F. J. van Kuppeveld (2009). "GBF1, a guanine nucleotide exchange factor for Arf, is crucial for coxsackievirus B3 RNA replication." J Virol **83**(22): 11940-11949.
Lee, J. Y. and H. Lu (2011). "Plasmodesmata: the battleground against intruders." Trends Plant Sci **16**(4): 201-210.
Lee, J. Y., X. Wang, W. Cui, R. Sager, S. Modla, K. Czymmek, B. Zybaliov, K. van Wijk, C. Zhang, H. Lu and V. Lakshmanan (2011). "A plasmodesmata-localized protein mediates crosstalk between cell-to-cell communication and innate immunity in Arabidopsis." Plant Cell **23**(9): 3353-3373.
Lee, W. M. and P. Ahlquist (2003). "Membrane synthesis, specific lipid requirements, and localized lipid composition changes associated with a positive-strand RNA virus RNA replication protein." J Virol **77**(23): 12819-12828.
Lee, W. M., M. Ishikawa and P. Ahlquist (2001). "Mutation of host delta9 fatty acid desaturase inhibits brome mosaic virus RNA replication between template recognition and RNA synthesis." J Virol **75**(5): 2097-2106.
Li, Q. and P. Palukaitis (1996). "Comparison of the nucleic acid- and NTP-binding properties of the movement protein of cucumber mosaic cucumovirus and tobacco mosaic tobamovirus." Virology **216**(1): 71-79.
Li, X. H., P. Valdez, R. E. Olvera and J. C. Carrington (1997). "Functions of the tobacco etch virus RNA polymerase (NIb): subcellular transport and protein-protein interaction with VPg/proteinase (NIa)." J Virol **71**(2): 1598-1607.
Ligat, L., E. Lauber, C. Albenne, H. San Clemente, B. Valot, M. Zivy, R. Pont-Lezica, M. Arlat and E. Jamet (2011). "Analysis of the xylem sap proteome of Brassica oleracea reveals a high content in secreted proteins." Proteomics **11**(9): 1798-1813.
Limpens, R. W., H. M. van der Schaar, D. Kumar, A. J. Koster, E. J. Snijder, F. J. van Kuppeveld and M. Barcena (2011). "The transformation of enterovirus replication structures: a three-dimensional study of single- and double-membrane compartments." MBio **2**(5).
Lin, N. S. and W. G. Langenberg (1985). "Peripheral vesicles in proplastids of barley stripe mosaic virus-infected wheat cells contain double-stranded RNA." Virology **142**(2): 291-298.

Llave, C., K. D. Kasschau and J. C. Carrington (2000). "Virus-encoded suppressor of posttranscriptional gene silencing targets a maintenance step in the silencing pathway." Proc Natl Acad Sci U S A **97**(24): 13401-13406.
Lohaus, G., K. Pennewiss, B. Sattelmacher, M. Hussmann and K. Hermann Muehling (2001). "Is the infiltration-centrifugation technique appropriate for the isolation of apoplastic fluid? A critical evaluation with different plant species." Physiol Plant **111**(4): 457-465.
Lopez, L., A. Urzainqui, E. Dominguez and J. A. Garcia (2001). "Identification of an N-terminal domain of the plum pox potyvirus CI RNA helicase involved in self-interaction in a yeast two-hybrid system." J Gen Virol **82**(Pt 3): 677-686.
Lucas, W. J., B. K. Ham and J. Y. Kim (2009). "Plasmodesmata - bridging the gap between neighboring plant cells." Trends Cell Biol **19**(10): 495-503.
Lucocq, J. M., A. Habermann, S. Watt, J. M. Backer, T. M. Mayhew and G. Griffiths (2004). "A rapid method for assessing the distribution of gold labeling on thin sections." J Histochem Cytochem **52**(8): 991-1000.
Mackenzie, J. M., M. K. Jones and P. R. Young (1996). "Immunolocalization of the dengue virus nonstructural glycoprotein NS1 suggests a role in viral RNA replication." Virology **220**(1): 232-240.
Maia, I. G., A. Haenni and F. Bernardi (1996). "Potyviral HC-Pro: a multifunctional protein." J Gen Virol **77 (Pt 7)**: 1335-1341.
Manabayeva, S. A., M. Shamekova, J.-W. Park, X. S. Ding, R. S. Nelson, Y.-C. Hsieh, R. T. Omarov and H. B. Scholthof (2013). "Differential requirements for Tombusvirus coat protein and P19 in plants following leaf versus root inoculation." Virology **439**(2): 89-96.
Martelli, G. and M. Russo (1985). Virus-Host Relationships. The Plant Viruses. R. I. B. Francki, Springer US**:** 163-205.
Marty, F. (1999). "Plant Vacuoles." The Plant Cell **11**(4): 587-599.
Mateo, R., C. M. Nagamine, J. Spagnolo, E. Mendez, M. Rahe, M. Gale, Jr., J. Yuan and K. Kirkegaard (2013). "Inhibition of cellular autophagy deranges dengue virion maturation." J Virol **87**(3): 1312-1321.
Maule, A. J. (2008). "Plasmodesmata: structure, function and biogenesis." Curr Opin Plant Biol **11**(6): 680-686.
Maule, A. J., Y. Benitez-Alfonso and C. Faulkner (2011). "Plasmodesmata - membrane tunnels with attitude." Curr Opin Plant Biol **14**(6): 683-690.
McCartney, A. W., J. S. Greenwood, M. R. Fabian, K. A. White and R. T. Mullen (2005). "Localization of the tomato bushy stunt virus replication protein p33 reveals a peroxisome-to-endoplasmic reticulum sorting pathway." Plant Cell **17**(12): 3513-3531.
McDonald, J. G. and J. B. Bancroft (1977). "Assembly Studies on Potato Virus Y and its Coat Protein." Journal of General Virology **35**(2): 251-263.
McDonald, K. and M. K. Morphew (1993). "Improved preservation of ultrastructure in difficult-to-fix organisms by high pressure freezing and freeze substitution: I. Drosophila melanogaster and Strongylocentrotus purpuratus embryos." Microsc Res Tech **24**(6): 465-473.
McEwen, B. F., M. Radermacher, C. L. Rieder and J. Frank (1986). "Tomographic three-dimensional reconstruction of cilia ultrastructure from thick sections." Proc Natl Acad Sci U S A **83**(23): 9040-9044.
McIntosh, R., D. Nicastro and D. Mastronarde (2005). "New views of cells in 3D: an introduction to electron tomography." Trends Cell Biol **15**(1): 43-51.

McMullen, C. R., W. S. Gardner and G. A. Myers (1977). "Ultrastructure of cell-wall thickenings and paramural bodies induced by barley stripe mosaic virus." Phytopathology **67**: 462–467.
McMullen, C. R., W. S. Gardner and G. A. Myers (1978). "Aberrant Plastids in Barley Leaf Tissue Infected with Barley Stripe Mosaic Virus." Phytopathology **68**: 317-325.
Merits, A., D. Guo, L. Jarvekulg and M. Saarma (1999). "Biochemical and genetic evidence for interactions between potato A potyvirus-encoded proteins P1 and P3 and proteins of the putative replication complex." Virology **263**(1): 15-22.
Meshi, T., Y. Watanabe, T. Saito, A. Sugimoto, T. Maeda and Y. Okada (1987). "Function of the 30 kd protein of tobacco mosaic virus: involvement in cell-to-cell movement and dispensability for replication." EMBO J **6**(9): 2557-2563.
Miller, S. and J. Krijnse-Locker (2008). "Modification of intracellular membrane structures for virus replication." Nat Rev Microbiol **6**(5): 363-374.
Milne, J. L. and S. Subramaniam (2009). "Cryo-electron tomography of bacteria: progress, challenges and future prospects." Nat Rev Microbiol **7**(9): 666-675.
Mitra, R., K. Krishnamurthy, E. Blancaflor, M. Payton, R. S. Nelson and J. Verchot-Lubicz (2003). "The potato virus X TGBp2 protein association with the endoplasmic reticulum plays a role in but is not sufficient for viral cell-to-cell movement." Virology **312**(1): 35-48.
Murant, A. F. and I. M. Roberts (1979). "Virus-like particles in phloem tissue of chervil (Anthriscus cerefolium) infected with carrot red leaf virus." Annals of Applied Biology **92**(3): 343-346.
Murphy, J. F., P. G. Klein, A. G. Hunt and J. G. Shaw (1996). "Replacement of the tyrosine residue that links a potyviral VPg to the viral RNA is lethal." Virology **220**(2): 535-538.
Nchoutmboube, J. A., E. G. Viktorova, A. J. Scott, L. A. Ford, Z. Pei, P. A. Watkins, R. K. Ernst and G. A. Belov (2013). "Increased long chain acyl-Coa synthetase activity and fatty acid import is linked to membrane synthesis for development of picornavirus replication organelles." PLoS Pathog **9**(6): e1003401.
Netherton, C. L. and T. Wileman (2011). "Virus factories, double membrane vesicles and viroplasm generated in animal cells." Curr Opin Virol **1**(5): 381-387.
Ng, J. C. and B. W. Falk (2006). "Virus-vector interactions mediating nonpersistent and semipersistent transmission of plant viruses." Annu Rev Phytopathol **44**: 183-212.
Nickell, S., C. Kofler, A. P. Leis and W. Baumeister (2006). "A visual approach to proteomics." Nat Rev Mol Cell Biol **7**(3): 225-230.
Oda, Y., T. Higaki, S. Hasezawa and N. Kutsuna (2009). "Chapter 3. New insights into plant vacuolar structure and dynamics." Int Rev Cell Mol Biol **277**: 103-135.
Ohlrogge, J. B., D. N. Kuhn and P. K. Stumpf (1979). "Subcellular localization of acyl carrier protein in leaf protoplasts of Spinacia oleracea." Proc Natl Acad Sci U S A **76**(3): 1194-1198.
Opalka, N., C. Brugidou, C. Bonneau, M. Nicole, R. N. Beachy, M. Yeager and C. Fauquet (1998). "Movement of rice yellow mottle virus between xylem cells through pit membranes." Proceedings of the National Academy of Sciences **95**(6): 3323-3328.
Opalka, N., C. Brugidou, C. Bonneau, M. Nicole, R. N. Beachy, M. Yeager and C. Fauquet (1998). "Movement of rice yellow mottle virus between xylem cells through pit membranes." Proc Natl Acad Sci U S A **95**(6): 3323-3328.
Oparka, K. J. and R. Turgeon (1999). "Sieve elements and companion cells—traffic control centers of the phloem." The Plant Cell **11**(4): 739-750.

Oruetxebarria, I., D. Guo, A. Merits, K. Makinen, M. Saarma and J. P. Valkonen (2001). "Identification of the genome-linked protein in virions of Potato virus A, with comparison to other members in genus Potyvirus." Virus Res **73**(2): 103-112.
Otulak, K. and G. Garbaczewska (2010). "Ultrastructural events during hypersensitive response of potato cv. Rywal infected with necrotic strains of potato virus Y." Acta Physiologiae Plantarum **32**(4): 635-644.
Otulak, K. and G. Garbaczewska (2012). "Cytopathological potato virus Y structures during Solanaceous plants infection." Micron **43**(7): 839-850.
Patarroyo, C., J. F. Laliberte and H. Zheng (2012). "Hijack it, change it: how do plant viruses utilize the host secretory pathway for efficient viral replication and spread?" Front Plant Sci **3**: 308.
Paul, D. and R. Bartenschlager (2013). "Architecture and biogenesis of plus-strand RNA virus replication factories." World J Virol **2**(2): 32-48.
Perez Jde, J., N. D. Udeshi, J. Shabanowitz, S. Ciordia, S. Juarez, C. L. Scott, N. E. Olszewski, D. F. Hunt and J. A. Garcia (2013). "O-GlcNAc modification of the coat protein of the potyvirus Plum pox virus enhances viral infection." Virology **442**(2): 122-131.
Plisson, C., M. Drucker, S. Blanc, S. German-Retana, O. Le Gall, D. Thomas and P. Bron (2003). "Structural characterization of HC-Pro, a plant virus multifunctional protein." J Biol Chem **278**(26): 23753-23761.
Powell, G. (1991). "Cell membrane punctures during epidermal penetrations by aphids: consequences for the transmission of two potyviruses." Annals of Applied Biology **119**(2): 313-321.
Prod'homme, D., S. Le Panse, G. Drugeon and I. Jupin (2001). "Detection and subcellular localization of the turnip yellow mosaic virus 66K replication protein in infected cells." Virology **281**(1): 88-101.
Pruss, G., X. Ge, X. M. Shi, J. C. Carrington and V. Bowman Vance (1997). "Plant viral synergism: the potyviral genome encodes a broad-range pathogenicity enhancer that transactivates replication of heterologous viruses." Plant Cell **9**(6): 859-868.
Puurand, U., K. Makinen, M. Baumann and M. Saarma (1992). "Nucleotide sequence of the 3'-terminal region of potato virus A RNA." Virus Res **23**(1-2): 99-105.
Rajamaki, M. L. and J. P. Valkonen (1999). "The 6K2 protein and the VPg of potato virus A are determinants of systemic infection in Nicandra physaloides." Mol Plant Microbe Interact **12**(12): 1074-1081.
Rajamaki, M. L. and J. P. T. Valkonen (2002). "Viral genome-linked protein (VPg) controls accumulation and phloem-loading of a potyvirus in inoculated potato leaves." Molecular Plant-Microbe Interactions **15**(2): 138-149.
Ramakrishnaiah, V., C. Thumann, I. Fofana, F. Habersetzer, Q. Pan, P. E. de Ruiter, R. Willemsen, J. A. Demmers, V. Stalin Raj, G. Jenster, J. Kwekkeboom, H. W. Tilanus, B. L. Haagmans, T. F. Baumert and L. J. van der Laan (2013). "Exosome-mediated transmission of hepatitis C virus between human hepatoma Huh7.5 cells." Proc Natl Acad Sci U S A **110**(32): 13109-13113.
Ravelonandro, M., O. Peyruchaud, L. Garrigue, G. de Marcillac and J. Dunez (1993). "Immunodetection of the plum pox virus helper component in infected plants and expression of its gene in transgenic plants." Arch Virol **130**(3-4): 251-268.
Rawsthorne, S. (2002). "Carbon flux and fatty acid synthesis in plants." Prog Lipid Res **41**(2): 182-196.

Redondo, E., R. Krause-Sakate, S. J. Yang, H. Lot, O. Le Gall and T. Candresse (2001). "Lettuce mosaic virus pathogenicity determinants in susceptible and tolerant lettuce cultivars map to different regions of the viral genome." Mol Plant Microbe Interact **14**(6): 804-810.
Regente, M., G. Corti-Monzon, A. M. Maldonado, M. Pinedo, J. Jorrin and L. de la Canal (2009). "Vesicular fractions of sunflower apoplastic fluids are associated with potential exosome marker proteins." FEBS Lett **583**(20): 3363-3366.
Requena, A., L. Simón-Buela, G. Salcedo and F. García-Arenal (2006). "Potential involvement of a cucumber homolog of phloem protein 1 in the long-distance movement of cucumber mosaic virus particles." Molecular Plant-Microbe Interactions **19**(7): 734-746.
Revers, F. and J. A. Garcia (2015). "Molecular biology of potyviruses." Adv Virus Res **92**: 101-199.
Richards, A. L. and W. T. Jackson (2013). "Behind closed membranes: the secret lives of picornaviruses?" PLoS Pathog **9**(5): e1003262.
Risco, C., E. Sanmartin-Conesa, W. P. Tzeng, T. K. Frey, V. Seybold and R. J. de Groot (2012). "Specific, sensitive, high-resolution detection of protein molecules in eukaryotic cells using metal-tagging transmission electron microscopy." Structure **20**(5): 759-766.
Ritzenthaler, C., C. Laporte, F. Gaire, P. Dunoyer, C. Schmitt, S. Duval, A. Piequet, A. M. Loudes, O. Rohfritsch, C. Stussi-Garaud and P. Pfeiffer (2002). "Grapevine fanleaf virus replication occurs on endoplasmic reticulum-derived membranes." J Virol **76**(17): 8808-8819.
Ritzenthaler, C., A.-C. Schmit, P. M. Michler, C. Stussi-Garaud and P. Lothaire (1995). "Grapevine Fanleaf Nepovirus P38 Putative Movement Protein Is Located on Tubules In Vivo." Molecular Plant-Microbe Interactions Journal **8**: 379-387.
Robert, S., J. Zouhar, C. Carter and N. Raikhel (2007). "Isolation of intact vacuoles from Arabidopsis rosette leaf-derived protoplasts." Nat Protoc **2**(2): 259-262.
Roberts, A. G., S. S. Cruz, I. M. Roberts, D. Prior, R. Turgeon and K. J. Oparka (1997). "Phloem Unloading in Sink Leaves of Nicotiana benthamiana: Comparison of a Fluorescent Solute with a Fluorescent Virus." Plant Cell **9**(8): 1381-1396.
Roberts, K. and M. C. McCann (2000). "Xylogenesis: the birth of a corpse." Current Opinion in Plant Biology **3**(6): 517-522.
Rojas, M. R., F. M. Zerbini, R. F. Allison, R. L. Gilbertson and W. J. Lucas (1997). "Capsid protein and helper component-proteinase function as potyvirus cell-to-cell movement proteins." Virology **237**(2): 283-295.
Romero-Brey, I. and R. Bartenschlager (2014). "Membranous replication factories induced by plus-strand RNA viruses." Viruses **6**(7): 2826-2857.
Romero-Brey, I., A. Merz, A. Chiramel, J. Y. Lee, P. Chlanda, U. Haselman, R. Santarella-Mellwig, A. Habermann, S. Hoppe, S. Kallis, P. Walther, C. Antony, J. Krijnse-Locker and R. Bartenschlager (2012). "Three-dimensional architecture and biogenesis of membrane structures associated with hepatitis C virus replication." PLoS Pathog **8**(12): e1003056.
Rothwell, C., A. Lebreton, C. Young Ng, J. Y. Lim, W. Liu, S. Vasudevan, M. Labow, F. Gu and L. A. Gaither (2009). "Cholesterol biosynthesis modulation regulates dengue viral replication." Virology **389**(1-2): 8-19.
Roudet-Tavert, G., S. German-Retana, T. Delaunay, B. Delecolle, T. Candresse and O. Le Gall (2002). "Interaction between potyvirus helper component-proteinase and capsid protein in infected plants." J Gen Virol **83**(Pt 7): 1765-1770.

Saenz, P., B. Salvador, C. Simon-Mateo, K. D. Kasschau, J. C. Carrington and J. A. Garcia (2002). "Host-specific involvement of the HC protein in the long-distance movement of potyviruses." J Virol **76**(4): 1922-1931.
Sahana, N., H. Kaur, R. K. Jain, P. Palukaitis, T. Canto and S. Praveen (2014). "The asparagine residue in the FRNK box of potyviral helper-component protease is critical for its small RNA binding and subcellular localization." J Gen Virol **95**(Pt 5): 1167-1177.
Savenkov, E. I., A. Germundsson, A. A. Zamyatnin, M. Sandgren and J. P. T. Valkonen (2003). "Potato mop-top virus: the coat protein-encoding RNA and the gene for cysteine-rich protein are dispensable for systemic virus movement in Nicotiana benthamiana." Journal of General Virology **84**(4): 1001-1005.
Schaad, M. C., P. E. Jensen and J. C. Carrington (1997). "Formation of plant RNA virus replication complexes on membranes: role of an endoplasmic reticulum-targeted viral protein." EMBO J **16**(13): 4049-4059.
Schaad, M. C., A. D. Lellis and J. C. Carrington (1997). "VPg of tobacco etch potyvirus is a host genotype-specific determinant for long-distance movement." Journal of Virology **71**(11): 8624-8631.
Schattat, M., K. Barton, B. Baudisch, R. B. Klosgen and J. Mathur (2011). "Plastid stromule branching coincides with contiguous endoplasmic reticulum dynamics." Plant Physiol **155**(4): 1667-1677.
Schlegel, A., T. H. Giddings, Jr., M. S. Ladinsky and K. Kirkegaard (1996). "Cellular origin and ultrastructure of membranes induced during poliovirus infection." J Virol **70**(10): 6576-6588.
Scholthof, K. B., H. B. Scholthof and A. O. Jackson (1995). "The tomato bushy stunt virus replicase proteins are coordinately expressed and membrane associated." Virology **208**(1): 365-369.
Schuetz, M., R. Smith and B. Ellis (2013). "Xylem tissue specification, patterning, and differentiation mechanisms." J Exp Bot **64**(1): 11-31.
Schwartz, M., J. Chen, M. Janda, M. Sullivan, J. den Boon and P. Ahlquist (2002). "A positive-strand RNA virus replication complex parallels form and function of retrovirus capsids." Mol Cell **9**(3): 505-514.
Sharma, M., Z. Sasvari and P. D. Nagy (2010). "Inhibition of sterol biosynthesis reduces tombusvirus replication in yeast and plants." J Virol **84**(5): 2270-2281.
Sharma, M., Z. Sasvari and P. D. Nagy (2011). "Inhibition of phospholipid biosynthesis decreases the activity of the tombusvirus replicase and alters the subcellular localization of replication proteins." Virology **415**(2): 141-152.
Shu, X., V. Lev-Ram, T. J. Deerinck, Y. Qi, E. B. Ramko, M. W. Davidson, Y. Jin, M. H. Ellisman and R. Y. Tsien (2011). "A genetically encoded tag for correlated light and electron microscopy of intact cells, tissues, and organisms." PLoS Biol **9**(4): e1001041.
Shukla, D. D. and C. W. Ward (1989). "Structure of potyvirus coat proteins and its application in the taxonomy of the potyvirus group." Adv Virus Res **36**: 273-314.
Shukla, D. D., C. W. Ward and A. A. Brunt (1994). The Potyviridae. Wallingford, United kingdom, CAB international.
Siaw, M. F., M. Shahabuddin, S. Ballard, J. G. Shaw and R. E. Rhoads (1985). "Identification of a protein covalently linked to the 5' terminus of tobacco vein mottling virus RNA." Virology **142**(1): 134-143.
Silva, M. S., J. Wellink, R. W. Goldbach and J. W. van Lent (2002). "Phloem loading and unloading of Cowpea mosaic virus in Vigna unguiculata." J Gen Virol **83**(Pt 6): 1493-1504.

Simón-Buela, L. and F. García-Arenal (1999). "Virus particles of cucumber green mottle mosaic tobamovirus move systemically in the phloem of infected cucumber plants." Molecular Plant-Microbe Interactions **12**(2): 112-118.
Snijder, E. J., Y. van der Meer, J. Zevenhoven-Dobbe, J. J. Onderwater, J. van der Meulen, H. K. Koerten and A. M. Mommaas (2006). "Ultrastructure and origin of membrane vesicles associated with the severe acute respiratory syndrome coronavirus replication complex." J Virol **80**(12): 5927-5940.
Snijder, E. J., H. van Tol, N. Roos and K. W. Pedersen (2001). "Non-structural proteins 2 and 3 interact to modify host cell membranes during the formation of the arterivirus replication complex." J Gen Virol **82**(Pt 5): 985-994.
Sochor, J., P. Babula, V. Adam, B. Krska and R. Kizek (2012). "Sharka: the past, the present and the future." Viruses **4**(11): 2853-2901.
Sorel, M., J. A. Garcia and S. German-Retana (2014). "The Potyviridae cylindrical inclusion helicase: a key multipartner and multifunctional protein." Mol Plant Microbe Interact **27**(3): 215-226.
Spetz, C. and J. P. Valkonen (2004). "Potyviral 6K2 protein long-distance movement and symptom-induction functions are independent and host-specific." Mol Plant Microbe Interact **17**(5): 502-510.
Studer, D., M. Michel and M. Muller (1989). "High pressure freezing comes of age." Scanning Microsc Suppl **3**: 253-268; discussion 268-259.
Swanson, M., H. Barker and S. A. Macfarlane (2002). "Rapid vascular movement of tobraviruses does not require coat protein: evidence from mutated and wild-type viruses." Annals of Applied Biology **141**(3): 259-266.
Syller, J. (2005). "The roles and mechanisms of helper component proteins encoded by potyviruses and caulimoviruses." Physiological and Molecular Plant Pathology **67**(3–5): 119-130.
Tang, W. F., S. Y. Yang, B. W. Wu, J. R. Jheng, Y. L. Chen, C. H. Shih, K. H. Lin, H. C. Lai, P. Tang and J. T. Horng (2007). "Reticulon 3 binds the 2C protein of enterovirus 71 and is required for viral replication." J Biol Chem **282**(8): 5888-5898.
Tanida, I., M. Fukasawa, T. Ueno, E. Kominami, T. Wakita and K. Hanada (2009). "Knockdown of autophagy-related gene decreases the production of infectious hepatitis C virus particles." Autophagy **5**(7): 937-945.
Tavert-Roudet, G., A. Abdul-Razzak, B. Doublet, J. Walter, T. Delaunay, S. German-Retana, T. Michon, O. Le Gall and T. Candresse (2012). "The C terminus of lettuce mosaic potyvirus cylindrical inclusion helicase interacts with the viral VPg and with lettuce translation eukaryotic initiation factor 4E." J Gen Virol **93**(Pt 1): 184-193.
Taylor, M. P. and K. Kirkegaard (2008). "Potential subversion of autophagosomal pathway by picornaviruses." Autophagy **4**(3): 286-289.
Thivierge, K., S. Cotton, P. J. Dufresne, I. Mathieu, C. Beauchemin, C. Ide, M. G. Fortin and J.-F. Laliberté (2008). "Eukaryotic elongation factor 1A interacts with Turnip mosaic virus RNA-dependent RNA polymerase and VPg-Pro in virus-induced vesicles." Virology **377**(1): 216-225.
Thivierge, K., S. Cotton, P. J. Dufresne, I. Mathieu, C. Beauchemin, C. Ide, M. G. Fortin and J. F. Laliberte (2008). "Eukaryotic elongation factor 1A interacts with Turnip mosaic virus RNA-dependent RNA polymerase and VPg-Pro in virus-induced vesicles." Virology **377**(1): 216-225.

Thompson, J. R., G. Leone, J. L. Lindner, W. Jelkmann and C. D. Schoen (2002). "Characterization and complete nucleotide sequence of Strawberry mottle virus: a tentative member of a new family of bipartite plant picorna-like viruses." J Gen Virol **83**(Pt 1): 229-239.
Tilsner, J., O. Linnik, M. Louveaux, I. M. Roberts, S. N. Chapman and K. J. Oparka (2013). "Replication and trafficking of a plant virus are coupled at the entrances of plasmodesmata." The Journal of Cell Biology **201**(7): 981-995.
Torrance, L., I. A. Andreev, R. Gabrenaite-Verhovskaya, G. Cowan, K. Makinen and M. E. Taliansky (2006). "An unusual structure at one end of potato potyvirus particles." J Mol Biol **357**(1): 1-8.
Torrance, L., G. H. Cowan, T. Gillespie, A. Ziegler and C. Lacomme (2006). "Barley stripe mosaic virus-encoded proteins triple-gene block 2 and gammab localize to chloroplasts in virus-infected monocot and dicot plants, revealing hitherto-unknown roles in virus replication." J Gen Virol **87**(Pt 8): 2403-2411.
Valli, A., A. Gallo, M. Calvo, J. de Jesus Perez and J. A. Garcia (2014). "A novel role of the potyviral helper component proteinase contributes to enhance the yield of viral particles." J Virol **88**(17): 9808-9818.
Vanhecke, D., W. Graber and D. Studer (2008). "Close-to-native ultrastructural preservation by high pressure freezing." Methods Cell Biol **88**: 151-164.
Varma, A., A. J. Gibbs, R. D. Woods and J. T. Finch (1968). "Some Observations on the Structure of the Filamentous Particles of Several Plant Viruses." Journal of General Virology **2**(1): 107-114,NP-NP.
Verchot, J., B. A. Driskel, Y. Zhu, R. M. Hunger and L. J. Littlefield (2001). "Evidence that soilborne wheat mosaic virus moves long distance through the xylem in wheat." Protoplasma **218**(1-2): 57-66.
Verchot, J., E. V. Koonin and J. C. Carrington (1991). "The 35-kDa protein from the N-terminus of the potyviral polyprotein functions as a third virus-encoded proteinase." Virology **185**(2): 527-535.
Verheije, M. H., M. Raaben, M. Mari, E. G. Te Lintelo, F. Reggiori, F. J. van Kuppeveld, P. J. Rottier and C. A. de Haan (2008). "Mouse hepatitis coronavirus RNA replication depends on GBF1-mediated ARF1 activation." PLoS Pathog **4**(6): e1000088.
Voeltz, G. K., W. A. Prinz, Y. Shibata, J. M. Rist and T. A. Rapoport (2006). "A class of membrane proteins shaping the tubular endoplasmic reticulum." Cell **124**(3): 573-586.
Walther, P. and A. Ziegler (2002). "Freeze substitution of high-pressure frozen samples: the visibility of biological membranes is improved when the substitution medium contains water." J Microsc **208**(Pt 1): 3-10.
Wan, J., D. G. Cabanillas, H. Zheng and J. F. Laliberte (2015). "Turnip mosaic virus Moves Systemically through Both Phloem and Xylem as Membrane-Associated Complexes." Plant Physiol **167**(4): 1374-1388.
Wan, J. and J. F. Laliberte (2015). "Membrane-associated virus replication complexes locate to plant conducting tubes." Plant Signal Behav: 0.
Wang, J., Y. Ding, J. Wang, S. Hillmer, Y. Miao, S. W. Lo, X. Wang, D. G. Robinson and L. Jiang (2010). "EXPO, an exocyst-positive organelle distinct from multivesicular endosomes and autophagosomes, mediates cytosol to cell wall exocytosis in Arabidopsis and tobacco cells." Plant Cell **22**(12): 4009-4030.
Wang, Z. and C. Benning (2012). "Chloroplast lipid synthesis and lipid trafficking through ER-plastid membrane contact sites." Biochem Soc Trans **40**(2): 457-463.

Wegner, C. S., L. M. Rodahl and H. Stenmark (2011). "ESCRT proteins and cell signalling." Traffic **12**(10): 1291-1297.
Wei, T., T. S. Huang, J. McNeil, J. F. Laliberte, J. Hong, R. S. Nelson and A. Wang (2010). "Sequential recruitment of the endoplasmic reticulum and chloroplasts for plant potyvirus replication." J Virol **84**(2): 799-809.
Wei, T. and A. Wang (2008). "Biogenesis of cytoplasmic membranous vesicles for plant potyvirus replication occurs at endoplasmic reticulum exit sites in a COPI- and COPII-dependent manner." J Virol **82**(24): 12252-12264.
Wei, T., C. Zhang, J. Hong, R. Xiong, K. D. Kasschau, X. Zhou, J. C. Carrington and A. Wang (2010). "Formation of complexes at plasmodesmata for potyvirus intercellular movement is mediated by the viral protein P3N-PIPO." PLoS Pathog **6**(6): e1000962.
Wei, T., C. Zhang, X. Hou, H. Sanfacon and A. Wang (2013). "The SNARE protein Syp71 is essential for turnip mosaic virus infection by mediating fusion of virus-induced vesicles with chloroplasts." PLoS Pathog **9**(5): e1003378.
Weintraub, M. and H. W. Ragetli (1970). "Distribution of viruslike particles in leaf cells of Dianthus barbatus infected with carnation vein mottle virus." Virology **40**(4): 868-881.
Wellink, J., J. W. van Lent, J. Verver, T. Sijen, R. W. Goldbach and A. van Kammen (1993). "The cowpea mosaic virus M RNA-encoded 48-kilodalton protein is responsible for induction of tubular structures in protoplasts." J Virol **67**(6): 3660-3664.
Welsch, S., S. Miller, I. Romero-Brey, A. Merz, C. K. Bleck, P. Walther, S. D. Fuller, C. Antony, J. Krijnse-Locker and R. Bartenschlager (2009). "Composition and three-dimensional architecture of the dengue virus replication and assembly sites." Cell Host Microbe **5**(4): 365-375.
Wilson, J. A., C. Zhang, A. Huys and C. D. Richardson (2011). "Human Ago2 is required for efficient microRNA 122 regulation of hepatitis C virus RNA accumulation and translation." J Virol **85**(5): 2342-2350.
Wolf, S., C. M. Deom, R. N. Beachy and W. J. Lucas (1989). "Movement protein of tobacco mosaic virus modifies plasmodesmatal size exclusion limit." Science **246**(4928): 377-379.
Wolf, S., W. J. Lucas, C. M. Deom and R. N. Beachy (1989). "Movement protein of tobacco mosaic virus modifies plasmodesmatal size exclusion limit." Science **246**(4928): 377-379.
Wong, J., J. Zhang, X. Si, G. Gao, I. Mao, B. M. McManus and H. Luo (2008). "Autophagosome supports coxsackievirus B3 replication in host cells." J Virol **82**(18): 9143-9153.
Wu, S., T. I. Baskin and K. L. Gallagher (2012). "Mechanical fixation techniques for processing and orienting delicate samples, such as the root of Arabidopsis thaliana, for light or electron microscopy." Nat Protoc **7**(6): 1113-1124.
Xie, Z. and D. J. Klionsky (2007). "Autophagosome formation: core machinery and adaptations." Nat Cell Biol **9**(10): 1102-1109.
Xiong, R. and A. Wang (2013). "SCE1, the SUMO-conjugating enzyme in plants that interacts with NIb, the RNA-dependent RNA polymerase of Turnip mosaic virus, is required for viral infection." J Virol **87**(8): 4704-4715.
Xu, C., J. Fan, A. J. Cornish and C. Benning (2008). "Lipid trafficking between the endoplasmic reticulum and the plastid in Arabidopsis requires the extraplastidic TGD4 protein." Plant Cell **20**(8): 2190-2204.
Xu, K. and P. D. Nagy (2014). "Expanding use of multi-origin subcellular membranes by positive-strand RNA viruses during replication." Curr Opin Virol **9**: 119-126.

Xu, X. M. and D. Jackson (2010). "Lights at the end of the tunnel: new views of plasmodesmal structure and function." Curr Opin Plant Biol **13**(6): 684-692.
Yambao, M. L., C. Masuta, K. Nakahara and I. Uyeda (2003). "The central and C-terminal domains of VPg of Clover yellow vein virus are important for VPg-HCPro and VPg-VPg interactions." J Gen Virol **84**(Pt 10): 2861-2869.
Yang, Y. S. and S. M. Strittmatter (2007). "The reticulons: a family of proteins with diverse functions." Genome Biol **8**(12): 234.
Zechmann, B., M. Muller and G. Zellnig (2005). "Effects of different fixation and freeze substitution methods on the ultrastructural preservation of ZYMV-infected Cucurbita pepo (L.) leaves." J Electron Microsc (Tokyo) **54**(4): 393-402.
Zhang, X., X. Zhao, Y. Zhang, S. Niu, F. Qu, Y. Zhang, C. Han, J. Yu and D. Li (2013). "N-terminal basic amino acid residues of Beet black scorch virus capsid protein play a critical role in virion assembly and systemic movement." Virol J **10**: 200.

CHAPTER 5: OTHER CONTRIBUTIONS

PUBLICATION NO. 3

Membrane-associated virus replication complexes locate to plant conducting tubes

Plant Signaling & Behavior

May 2015, Vol.8

Addendum to: Wan J, Garcia Cabanillas D, Zheng H, Laliberté JF. Turnip mosaic virus moves systemically through both phloem and xylem as membrane-associated complexes. 2015. Plant Physiology 167, pp. 1374–1388.

Juan Wan[a] and Jean-François Laliberté[a*]

a. INRS-Institut Armand-Frappier, Laval, Québec, Canada

*** Author for correspondence**: Prof. Jean-François Laliberté

Address : INRS-Institut Armand Frappier

531, boulevard des Prairies, Laval, Québec, Canada, H7V 1B7

Tel: 1.450.687.5010

Email: jean-francois.laliberte@iaf.inrs.ca

Contribution

This article addendum has been published in *Plant Signaling & Behavior*. I wrote the the first draft of this article addendum, and Jean-Francois Laliberté helped me improve the writing.

Résumé

Il est généralement admis que les virus se déplacent depuis une première cellule infectée ver les tissus vasculaires par un mouvement dit de cellule-à-cellule au travers des plasmodesmes (PD) pour être chargés dans les tubes conducteurs (i.e. les tubes criblés du phloème et les vaisseaux du xylème) et se déplacer sur de longues distances pour établir une infection systémique dans la plante. L'entité virale impliquée dans ces mouvements peut être un virion ou un complexe ribonucléoprotéique (RNP) qui demande encore à être défini. Auparavant, notre laboratoire a démontré par "live-cell imaging" que les complexes de réplication associés aux membranes du *Turnip mosaic virus* (TuMV) pouvaient se déplacer de cellule à cellule au cours de l'infection. Notre récente étude montre que ces derniers se retrouvent dans les vaisseaux vasculaires, ce qui est vraisemblablement aussi le cas du *Potato virus X* (PVX). La présence des complexes membranaires induits par le TuMV dans les vaisseaux du xylème suggère que des entités virales pourraient être retrouvées dans l'espace intercellulaire tel que l'apoplaste. Cette possibilité pourrait avoir un impact sur notre façon de concevoir ce qu'est l'immunité innée contre les virus chez les plantes.

Abstract

It is generally accepted that in order to establish a systemic infection in a plant, viruses move from the initially infected cell to the vascular tissues by cell-to-cell movement through plasmodesmata (PD), and load into the vascular conducting tubes (i.e. phloem sieve elements and xylem vessel elements) for long-distance movement. The viral unit in these movements can be a virion or a yet-to-be-defined ribonucleic protein (RNP) complex. Using live-cell imaging, our laboratory has previously demonstrated that membrane-bound replication complexes move cell-to-cell during *Turnip mosaic virus* (TuMV) infection. Our recent study shows that these membrane-bound replication complexes end up in the vascular conducting tubes, which is likely the case for *Potato virus X* (PVX) also. The presence of TuMV-induced membrane complexes in xylem vessels suggests that viral components could also be found in other apoplastic regions of the plant, such as the intercellular space. This possibility may have implications regarding how we approach the study of plant innate immune responses against viruses.

Introduction

Plant viral spread throughout a plant involves short distance, cell-to-cell, movement through plasmodesmata (PD) and long-distance trafficking through vascular tissues. The moving entities are thought to be viral particles or ribonucleic protein (RNP) complexes. However, the exact nature of the trafficking RNP complexes has not been defined. An emerging concept is that viral RNA replication and movement are tightly linked processes. For example, it has been proposed that *Tobacco mosaic virus* (TMV) moves from cell to cell as intact replication complexes [1]. Replication and trafficking of *Potato virus X* (PVX) have also been shown to be coupled at the entrances of PD [2]. Furthermore, *Turnip mosaic virus* (TuMV) -induced membrane-bound replication complexes have been observed by live-cell imaging to move from one cell to another [3]. Thus, the plant virus life cycle may not be easily separated into several distinct stages.

Most plant viruses move systemically through the phloem along the source-to-sink flow of photoassimilates for long-distance movement (reviewed in [4]). The viral entity loads into phloem sieve elements through pore-plasmodesmata units (PPUs) that connect the sieve elements (SE) and companion cells (CC) in all vein classes of source leaves [5, 6]. The viral phloem unloading pattern is similar to the phloem-mobile dye 5(6)-carboxyfluorescein diacetate (CFDA), which is limited to major veins of sink leaves [5-7]. Some viruses have also been observed in xylem vessels. It has been proposed that viruses enter into immature xylem vessel elements. Upon apoptosis, these become hollow vessels, thereby releasing viruses into the water flow [8]. Viral uploading into xylem parenchymal cells would then take place through pit membranes [8, 9]. Both virus particles and yet-to-be-defined RNP complexes have been implicated as the unit for plant virus long-distance movement. Virus particles have been detected in phloem sieve elements [10-13] and phloem sap [14, 15], as well as in the xylem vessel elements and guttation fluid [16-18]. Alternatively, some viruses are believed to move as RNP complexes since systemic movement was observed in coat protein (CP) deletion mutants [19-22].

Brief summary of the recently published manuscript

TuMV is a positive strand RNA virus belonging to the family Potyviridae. TuMV remodels cellular membranes into viral factories, which are intracellular compartments involved in viral replication as well as in intra- and intercellular movements. These compartments take the form of vesicles of ~100 nm in diameter originating from the endoplasmic reticulum (ER). These vesicles contain viral RNA (vRNA) and viral and host proteins involved in vRNA replication. The viral membrane $6K_2$ protein is involved in the membrane alterations and vesicle production, and is thus a marker for the presence of the membrane-bound replication complex. In our recent publication [23], we analyzed the distribution of $6K_2$ vesicles in vascular tissues during TuMV infection to test whether membrane-bound replication complexes are involved in long-distance movement. Through cryohistological observations of TuMV-infected plants, $6K_2$ vesicle aggregates were found in both phloem sieve elements and in xylem vessels (Fig. 1A, B). Moreover, $6K_2$ vesicles were observed in TuMV-infected xylem sap (Fig. 1C). Stem girdling experiments, which leave xylem vessels intact but destroy the surrounding tissues, confirmed that TuMV could move long-distance through xylem vessels. Hence, we showed that membrane-bound replication complexes might be the viral entity for TuMV long-distance movement. Interestingly, the presence of membrane-associated replication complexes in the phloem and xylem may not be limited to TuMV, since PVX-induced membrane-associated double-stranded viral RNA complexes were also observed in both phloem sieve elements and xylem vessels. In other words, we observed membrane-associated viral replication complexes that were located in the extracellular space of a plant. This contrasts with the general belief that viral replication complexes are found exclusively inside infected cells.

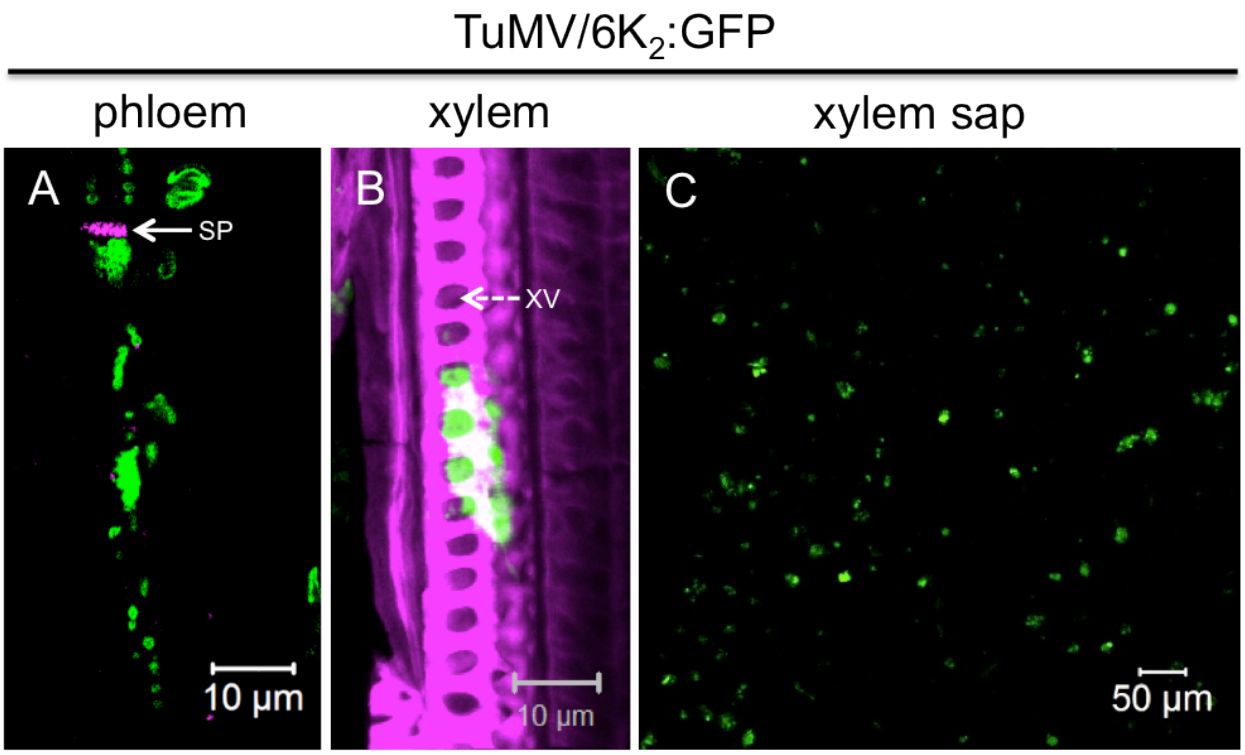

Figure 1. TuMV membrane-bound complexes are present in phloem sieve elements, xylem vessels and xylem sap.

(A and B) Longitudinal-sections of $6K_2$:GFP-producing TuMV-infected *N. benthamiana* stem internodes above the inoculated leaf, were observed with a Zeiss LSM-780 confocal microscope using a 63× objective. Aniline blue-stained sieve plate (A) and Fluorescent brightener 28-stained cell wall (B) are shown in false-color magenta. $6K_2$:GFP is shown in green. Panel (A) is a single optical slice, and Panel (B) is a three-dimensional image. (C) shows xylem sap collected from $6K_2$:GFP-producing TuMV-infected *N. benthamiana* plants observed with a Zeiss LSM-780 confocal microscope using a 20× objective. SP, sieve plate; XV, xylem vessel.

Change of paradigm?

The apoplast, which includes cell walls, intercellular spaces and conducting dead cells of the xylem, is a dynamic compartment involved in plant signaling and communication. The intercellular fluids and xylem sap are connected, since a large number of xylem sap proteins have been found to originate from the proteins secreted in the intercellular fluids [24]. Transmission electron microscopy (TEM) studies have shown that paramural vesicles situated between the plasma membrane and the cell wall occur in various cell wall-associated processes, and are similar to exosomes both in location and in morphology [25]. Accumulating evidence suggests that exosome-like vesicles carry specific materials to be delivered into the paramural space of the plant to accomplish still undiscovered functions [26-28]. The exosome-like paramural vesicles may be released from the plasma membrane by at least two mechanisms. They could be released through a multivesiclular body-plasma membrane (MVB-PM) fusion, as shown for the pathogenic powdery mildew fungus [27] and BSMV [29] induced cell wall-associated defense response. Alternatively, they could be released through an exocyst positive organelle (EXPO)-plasma membrane fusion, which is involved in non classical protein secretion [28].

Exosome-mediated transmission of human viruses have been reported [30, 31]. Could it also be the case for plant viruses, despite the presence of a thick surrounding cell wall that would act as a barrier for virus movement? Vesicular transport across the cell wall has been demonstrated in fungi [32]. Could a similar situation be operating in plants? Alternatively, the exosome-like vesicles could spread throughout the paramural space and bypass the cell wall as depicted in Fig. 2.

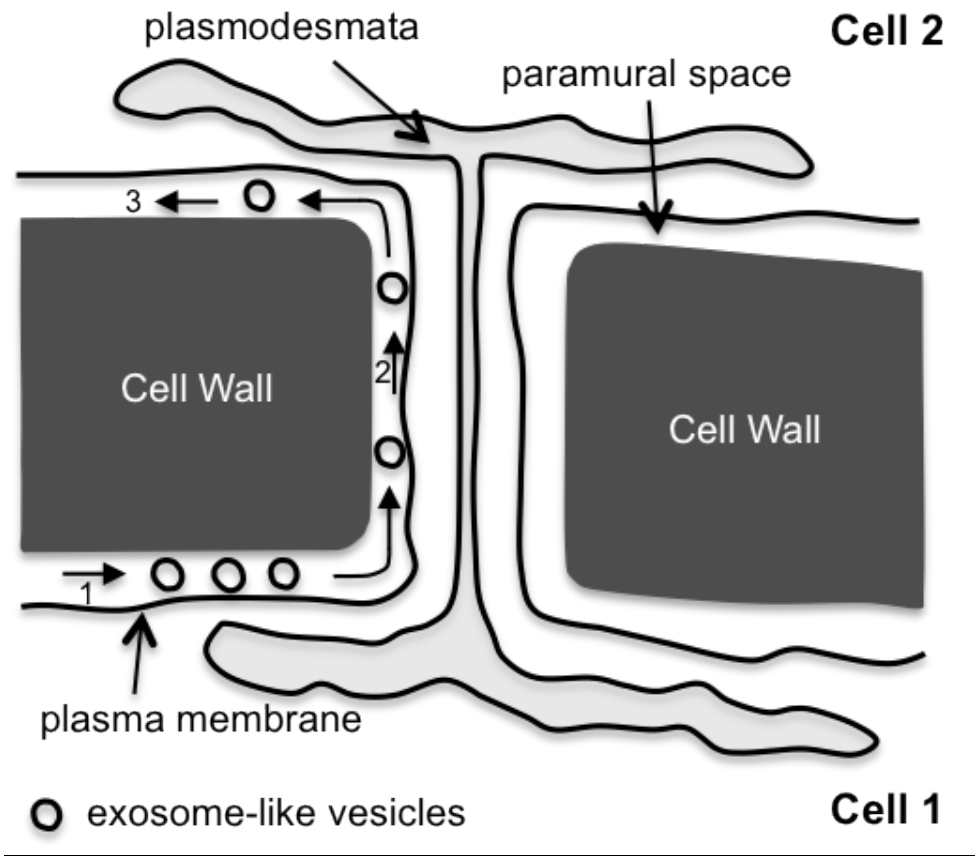

Figure 2. A model for exosome-like vesicle movement in the paramural space for bypassing the cell wall.

First, exosome-like vesicles from cell 1 are released in the paramural space (1), and then travel until they encounter the apoplastic face of a plasmodesmata (2) to cross over to the paramural space of cell 2 (3).

In support to the above hypothesis, we observed numerous electron-translucent vesicles that are morphologically similar to the paramural vesicles formed through MVB-PM fusion in the paramural space of TuMV-infected leaves (Fig. 3A, empty arrowheads). We also observed some electron-dense vesicles that appeared to pinch out from the plasma membrane into the paramural space (Fig. 3B, arrowheads). Only a few exosome-like paramural vesicles were observed in mock-infected leaves. Additionally, $6K_2$:GFP in the form of aggregates were collected from the apoplast. These observations suggest that there might indeed be an additional mechanism by which plant viruses exit cells.

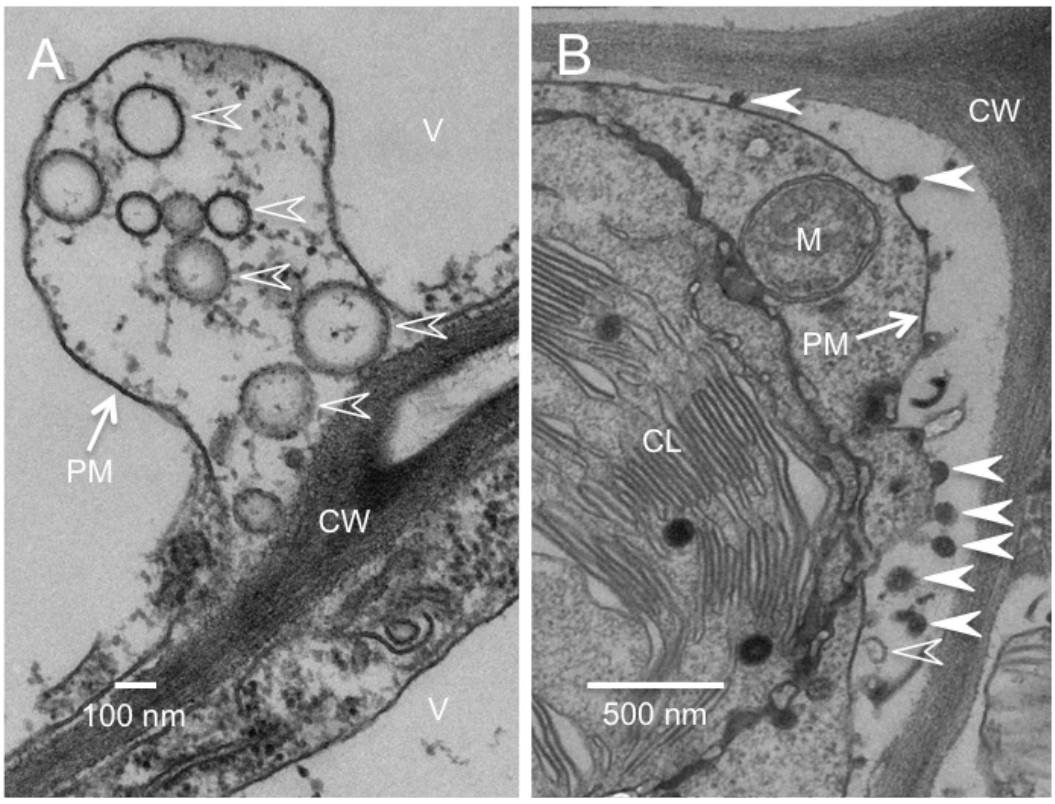

Figure 3. Exosome-like vesicles are present in the paramural space of TuMV-infected leaves.

Cross-sections of TuMV-infected *N. benthamiana* leaf were collected and observed by TEM. (A) shows the electron-translucent paramural vesicles (empty arrowheads) located between plasma membrane and cell wall. (B) shows both electron-translucent (empty arrowheads) and electron-dense paramural vesicles (arrowheads) located between plasma membrane and cell wall. V, vacuole; CL, chloroplast; M, mitochondria; CW, cell wall; PM, plasma membrane.

Virus components located in the apoplast and their relationship with plant innate immune responses

The presence of intricate membrane structures containing viral replication complexes in the xylem vessels may also change our way of looking at plant immunity against viruses. Pathogen perception of the plant innate immune system is mediated by microbe/danger-associated molecular patterns (MAMPs/DAMPs) that are recognized by pattern recognition receptors (PRRs) on the plasma membrane [33]. Ligand binding to PRRs for non-viral pathogens takes place on the apoplastic side of the membrane. Although the recognition of MAMPs/DAMPs is believed to occur intracellularly in the case of viruses [34], a recent study reported on the possible involvement of receptor-like kinases in MAMP recognition by PRRs in plant-virus interactions [35]. This finding indirectly suggests the presence of some viral components in apoplast. Thus, it will be interesting to see if any of the components of TuMV structures found in xylem vessels could act as apoplastic MAMPs/DAMPs.

Acknowledgements

The authors thank Dr. Peter Moffett for his helpful comments.

References

1. Kawakami S, Watanabe Y, Beachy RN. Tobacco mosaic virus infection spreads cell to cell as intact replication complexes. Proc Natl Acad Sci U S A 2004; 101:6291-6.

2. Tilsner J, Linnik O, Louveaux M, Roberts IM, Chapman SN, Oparka KJ. Replication and trafficking of a plant virus are coupled at the entrances of plasmodesmata. The Journal of Cell Biology 2013; 201:981-95.

3. Grangeon R, Jiang J, Wan J, Agbeci M, Zheng H, Laliberte JF. 6K2-induced vesicles can move cell to cell during turnip mosaic virus infection. Frontiers in microbiology 2013; 4:351.

4. Hipper C, Brault V, Ziegler-Graff V, Revers F. Viral and cellular factors involved in phloem transport of plant viruses. Frontiers in Plant Science 2013; 4.

5. Silva MS, Wellink J, Goldbach RW, van Lent JW. Phloem loading and unloading of Cowpea mosaic virus in Vigna unguiculata. J Gen Virol 2002; 83:1493-504.

6. Cheng NH, Su CL, Carter SA, Nelson RS. Vascular invasion routes and systemic accumulation patterns of tobacco mosaic virus in Nicotiana benthamiana. Plant J 2000; 23:349-62.

7. Roberts AG, Cruz SS, Roberts IM, Prior D, Turgeon R, Oparka KJ. Phloem Unloading in Sink Leaves of Nicotiana benthamiana: Comparison of a Fluorescent Solute with a Fluorescent Virus. Plant Cell 1997; 9:1381-96.

8. Opalka N, Brugidou C, Bonneau C, Nicole M, Beachy RN, Yeager M, Fauquet C. Movement of rice yellow mottle virus between xylem cells through pit membranes. Proceedings of the National Academy of Sciences 1998; 95:3323-8.

9. Verchot J, Driskel BA, Zhu Y, Hunger RM, Littlefield LJ. Evidence that soilborne wheat mosaic virus moves long distance through the xylem in wheat. Protoplasma 2001; 218:57-66.

10. McGuire ELHJM. Translocation of Tobacco Ringspot Virus in Soybean. Phytopathology 1973; 63:1291-300.

11. Murant AF, Roberts IM. Virus-like particles in phloem tissue of chervil (Anthriscus cerefolium) infected with carrot red leaf virus. Annals of Applied Biology 1979; 92:343-6.

12. Shepardson S, Esau K, McCrum R. Ultrastructure of potato leaf phloem infected with potato leafroll virus. Virology 1980; 105:379-92.

13. Hoefert LL. Beet western yellows virus in phloem of pennycress. Journal of Ultrastructure Research 1984; 88:44-54.

14. Requena A, Simón-Buela L, Salcedo G, García-Arenal F. Potential Involvement of a Cucumber Homolog of Phloem Protein 1 in the Long-Distance Movement of Cucumber mosaic virus Particles. Molecular Plant-Microbe Interactions 2006; 19:734-46.

15. Simón-Buela L, García-Arenal F. Virus Particles of Cucumber Green Mottle Mosaic Tobamovirus Move Systemically in the Phloem of Infected Cucumber Plants. Molecular Plant-Microbe Interactions 1999; 12:112-8.

16. French CJ, Elder M. Virus particles in guttate and xylem of infected cucumber (Cucumis sativus L.). Annals of Applied Biology 1999; 134:81-7.

17. Ding XS, Boydston CM, Nelson RS. Presence of Brome mosaic virus in Barley Guttation Fluid and Its Association with Localized Cell Death Response. Phytopathology 2001; 91:440-8.

18. French CJ, Elder M, Skelton F. Recovering and Identifying Infectious Plant Viruses in Guttation Fluid. HortScience 1993; 28:746-7.

19. Swanson M, Barker H, Macfarlane SA. Rapid vascular movement of tobraviruses does not require coat protein: evidence from mutated and wild-type viruses. Annals of Applied Biology 2002; 141:259-66.

20. Savenkov EI, Germundsson A, Zamyatnin AA, Sandgren M, Valkonen JPT. Potato mop-top virus: the coat protein-encoding RNA and the gene for cysteine-rich protein are dispensable for systemic virus movement in Nicotiana benthamiana. Journal of General Virology 2003; 84:1001-5.

21. Gopinath K, Kao CC. Replication-Independent Long-Distance Trafficking by Viral RNAs in Nicotiana benthamiana. The Plant Cell Online 2007; 19:1179-91.

22. Manabayeva SA, Shamekova M, Park J-W, Ding XS, Nelson RS, Hsieh Y-C, Omarov RT, Scholthof HB. Differential requirements for Tombusvirus coat protein and P19 in plants following leaf versus root inoculation. Virology 2013; 439:89-96.

23. Wan J, Garcia Cabanillas D, Zheng H, Laliberte JF. Turnip mosaic virus moves systemically through both phloem and xylem as membrane-associated complexes. Plant Physiol 2015; 167:1374-88.

24. Ligat L, Lauber E, Albenne C, San Clemente H, Valot B, Zivy M, Pont-Lezica R, Arlat M, Jamet E. Analysis of the xylem sap proteome of Brassica oleracea reveals a high content in secreted proteins. Proteomics 2011; 11:1798-813.

25. An Q, van Bel AJ, Huckelhoven R. Do plant cells secrete exosomes derived from multivesicular bodies? Plant Signal Behav 2007; 2:4-7.

26. Regente M, Corti-Monzon G, Maldonado AM, Pinedo M, Jorrin J, de la Canal L. Vesicular fractions of sunflower apoplastic fluids are associated with potential exosome marker proteins. FEBS Lett 2009; 583:3363-6.

27. An Q, Huckelhoven R, Kogel KH, van Bel AJ. Multivesicular bodies participate in a cell wall-associated defence response in barley leaves attacked by the pathogenic powdery mildew fungus. Cell Microbiol 2006; 8:1009-19.

28. Wang J, Ding Y, Wang J, Hillmer S, Miao Y, Lo SW, Wang X, Robinson DG, Jiang L. EXPO, an exocyst-positive organelle distinct from multivesicular endosomes and autophagosomes, mediates cytosol to cell wall exocytosis in Arabidopsis and tobacco cells. Plant Cell 2010; 22:4009-30.

29. McMullen CR, Gardner WS, Myers GA. Ultrastructure of cell-wall thickenings and paramural bodies induced by barley stripe mosaic virus. Phytopathology 1977; 67:462–7.

30. Ramakrishnaiah V, Thumann C, Fofana I, Habersetzer F, Pan Q, de Ruiter PE, Willemsen R, Demmers JA, Stalin Raj V, Jenster G, et al. Exosome-mediated

transmission of hepatitis C virus between human hepatoma Huh7.5 cells. Proc Natl Acad Sci U S A 2013; 110:13109-13.

31. Feng Z, Hensley L, McKnight KL, Hu F, Madden V, Ping L, Jeong SH, Walker C, Lanford RE, Lemon SM. A pathogenic picornavirus acquires an envelope by hijacking cellular membranes. Nature 2013; 496:367-71.

32. Casadevall A, Nosanchuk JD, Williamson P, Rodrigues ML. Vesicular transport across the fungal cell wall. Trends Microbiol 2009; 17:158-62.

33. Macho Alberto P, Zipfel C. Plant PRRs and the Activation of Innate Immune Signaling. Molecular Cell 2014; 54:263-72.

34. Ding SW, Voinnet O. Antiviral immunity directed by small RNAs. Cell 2007; 130:413-26.

35. Korner CJ, Klauser D, Niehl A, Dominguez-Ferreras A, Chinchilla D, Boller T, Heinlein M, Hann DR. The immunity regulator BAK1 contributes to resistance against diverse RNA viruses. Molecular plant-microbe interactions : MPMI 2013; 26:1271-80.

PUBLICATION NO. 4

$6K_2$-induced vesicles can move cell to cell during turnip mosaic virus infection

Frontiers in Microbiology

December 2013, Volume 4, Article 351.

Romain Grangeon[1], Jun Jiang[1], Juan Wan[1], Maxime Agbeci[1], Huanquan Zheng[2] and Jean-François Laliberté[1*]

1. Institut national de la recherche scientifique, INRS-Institut Armand-Frappier, Laval, QC, Canada
2. Department of Biology, McGill University, Montréal, QC, Canada

*** Author for correspondence**: Prof. Jean-François Laliberté

Email: jean-francois.laliberte@iaf.inrs.ca

Contribution

This manuscript has been published in *Frontiers in Microbiology*. I did the immunohistolocalization experiments to detect the dsRNA (a replication intermediate) signal in $6K_2$-tagged small vesicles, and wrote the relative information in this manuscript.

APPENDIX: LIST OF PUBLICATIONS AND COMMUNICATIONS

Publications

1. **Wan J**, Mui J, Vali H, Zheng H, Laliberté JF. Ultrastructural characterization of Turnip mosaic virus induced cellular rearrangements reveal membrane-bound viral particles accumulating in vacuoles. Submitted.
2. **Wan J**, Laliberté JF. Membrane-associated virus replication complexes locate to plant conducting tubes. *Plant Signal Behav*. 2015 May 8:0.
3. **Wan J**, Cabanillas DG, Zheng H, Laliberté JF. Turnip mosaic virus Moves Systemically through Both Phloem and Xylem as Membrane-Associated Complexes. *Plant Physiol*. 2015 Apr;167(4):1374-88.
4. Grangeon R, Jiang J, **Wan J**, Agbeci M, Zheng H, Laliberté JF. 6K2-induced vesicles can move cell to cell during turnip mosaic virus infection. *Front Microbiol*. 2013 Dec 4;4:351.

Communications

Oral

1. **Juan Wan**, Daniel Garcia, Romain Grangeon, Hojatollah Vali and Jean-François Laliberté. Potyvirus move systemically through xylem vessel as membrane associated structures. IUMS- XVIth International Congress of Virology 2014, Montréal, Québec.

Poster

1. **Juan Wan (invited)**, Jeannie Mui, Mihnea Bostina, Hojatollah Vali and Jean-François Laliberté. Structural perspective of Turnip mosaic virus factories. McGill University Department of Anatomy and Cell Biology research symposium 2013, Orford, Québec. (I was invited by Dr. H. Vali, Director of Electron Microscopy Research Facility at McGill University)
2. **Juan Wan**, Daniel Garcia, Romain Grangeon, Hojatollah Vali, Jean-François Laliberté. Ultrastructure des usines virales du virus de la mosaïque du navet. Congrès Armand-Frappier 2013, Orford, Québec.

3. **Juan Wan**, Romain Grangeon, Jun Jiang, Maxime Agbeci, Huanquan Zheng and Jean-François Laliberté. Turnip mosaic virus factories – an ultrastructural perspective. American Society for Virology, 32nd Annual Meeting 2013, Penn State University, USA.